

Department of Physics and Astronomy

University of Heidelberg

Master thesis in Physics

submitted by

Tobias Haas

born in Wermelskirchen, Germany

Heidelberg, October 25, 2018

Higher derivative quantum gravity
in
different approximations

This Master thesis has been carried out by

Tobias Haas

at the

Institute for Theoretical Physics

under the supervision of

Herrn Prof. Dr. Jan Martin Pawlowski

Higher derivative quantum gravity in different approximations

An asymptotically safe theory of quantum gravity which includes Einstein-Hilbert and the higher order tensor structures R^2 and $R_{\mu\nu}^2$ in a self-consistent vertex expansion is formulated and investigated in various approximations. To that end methods from the functional renormalization group (FRG) are employed within a background flow approximation to obtain closed flow equations for theory parameters. Different scenarios for attractive ultraviolet (UV) fixed points are observed: Many but not all approximations adhere one or more UV fixed points. Furthermore non-trivial solutions which either are known from the Einstein-Hilbert truncation or only stem from the newly introduced higher order tensor structures can be found. Moreover the graviton 2- and 3-point functions are studied with respect to their behaviour in momentum space. This contains a breakdown of their polynomial momentum dependence for $p^2 \in [0, k^2]$ which reveals to be of low order, s.t. higher orders are non-trivially suppressed, and an extended check of their flows concerning momentum locality where S-projected and higher order flows turned out to be non-local. Finally all presented results are analyzed related to their physical implications in order to be able to suggest potential directions for successive research.

Quantengravitation mit höheren Ableitungen in verschiedenen Approximationen

Es wird eine asymptotisch sichere Theorie der Quantengravitation, welche Einstein-Hilbert und die höheren Ordnungen R^2 und $R_{\mu\nu}^2$ in einer selbstkonsistenten Vertexentwicklung beinhaltet, formuliert und in diversen Approximationen untersucht. Dazu werden Methoden der funktionalen Renormierungsgruppe (FRG) innerhalb einer Hintergrundfeldnäherung angewandt, um geschlossene Flussgleichungen für Theorieparameter zu erhalten. Es werden verschiedene Szenarien für attraktive ultraviolett (UV) Fixpunkte beobachtet: Viele, aber nicht alle Approximationen, weisen einen oder mehrere UV Fixpunkte auf. Weiterhin findet man nicht triviale Lösungen, welche entweder von der Einstein-Hilbert Trunkierung bekannt sind, oder allein von den neu eingeführten höheren Ordnungen stammen. Außerdem werden die 2- und 3-Punkt Funktionen des Gravitons in Bezug auf ihr Verhalten im Impulsraum untersucht. Dies beinhaltet eine Analyse der polynomiellen Impulsabhängigkeit für $p^2 \in [0, k^2]$, welche nur niedrige Ordnungen hervorbringt, so dass höhere Ordnungen nicht trivial unterdrückt werden, und ein erweiterter Test der Flüsse bezüglich ihrer Lokalität im Impulsraum, wobei sich S-projizierte Flüsse und Flüsse mit höheren Ordnungen als nicht-lokal herausstellen. Zuletzt werden alle vorliegenden Resultate entsprechend ihrer physikalischen Implikationen ausgewertet, um potentielle Richtungen für weitere Forschungen aufzeigen zu können.

Contents

1	Introduction and outline	6
I	Basic concepts and underlying theories	9
2	Quantum Field Theory	10
2.1	Feynman's Path integral formulation	11
2.2	Gauge theories	17
3	General Relativity	21
3.1	Principles and conventions	21
3.2	The Einstein equations	25
3.3	The Einstein-Hilbert action	26
3.4	General covariance and diffeomorphism invariance	27
4	The Functional Renormalization Group	30
4.1	Ideas behind renormalization	30
4.2	The Wetterich Equation	33
4.3	Regulator and shape function	40
4.4	Truncation schemes	42
5	Quantum Gravity	43
5.1	Houston, we've got a problem	43
5.2	Asymptotic Safety	45
5.3	Asymptotic Safety in pure gravity	49
II	Setup for pure gravity at higher orders	53
6	Approximations and flow equations	54
6.1	Vertex expansion and flow diagrams of the n -point functions	54
6.2	Vertex construction	60
6.3	Flows of the n -point functions	68
6.3.1	Flow of the graviton 2-point function	69
6.3.2	Flow of the ghost 2-point function	74
6.3.3	Flow of the graviton 3-point function	75

7	Computational details	80
7.1	General workflow	80
7.2	Some more details	83
7.2.1	Pure propagators and propagators with regulator insertions	83
7.2.2	Momentum derivatives and analytical integrals	90
7.2.3	Numerical checks of analytically performed integrals	91
7.2.4	Numerical integration and interpolation procedure	93
III	Results	99
8	Results and discussion	100
8.1	Einstein-Hilbert truncation	100
8.1.1	Checking the Einstein-Hilbert limit	100
8.1.2	Einstein-Hilbert truncation with diverse TT- and S-projected couplings and anomalous dimensions	104
8.2	Momentum locality of the graviton flows	106
8.2.1	Locality of the graviton 2-point function	107
8.2.2	Locality of the graviton 3-point function	116
8.2.3	Summary	119
8.3	Approximation 1: Einstein-Hilbert and $R_{\mu\nu}^2$	120
8.3.1	Fixed points analysis	120
8.3.2	Polynomial behaviour of the flows	124
8.4	Approximation 2: Einstein-Hilbert, R^2 and $R_{\mu\nu}^2$	128
8.4.1	Fixed points analysis	128
8.4.2	Polynomial behaviour of the flows	130
9	Conclusion and outlook	134
IV	Appendix	137
A	Fixed point solutions for approximation 1 with η_{ϕ_i}	138
B	Lists	139
B.1	List of Figures	139
B.2	List of Tables	141
C	Bibliography	143

1 Introduction and outline

To study and describe gravity is one of the disciplines within physics with the longest history. The milestone with the largest influence in the modern spirit was marked by Einstein's theory of *General Relativity* (GR) [1, 2]: Classical gravitational forces between massive objects were reinvented as geometrical effects of unified space-time itself, s.t. also massless objects as e.g. photons were detected to be sensible to gravitational effects [3]. Nowadays general relativity has passed several tests [2, 4] and was never falsified. However nature provides phenomena which are out of reach within the theoretical framework of general relativity, e.g. black holes or the early stage of cosmic inflation. More generally speaking, it is not clear how gravity behaves at a very high energy scale (roughly the Planck scale $m_P = \sqrt{\hbar c/G} \approx 10^{19} \text{ GeV}/c^2$) or, in other words, at a very small length scale (Planck length $l_P = \sqrt{\hbar G/c^3} \approx 10^{-35} \text{ m}$).

Naturally small length scales are the playground of another modern paradigm in physics, namely *Quantum Field Theory* (QFT). These types of theories are used to describe the remaining three of the four known fundamental forces, i.e. the strong, the weak and the electromagnetic force. More precisely all three are described within the *Standard Model of Elementary Particle Physics*, which was perfected recently with the discovery of the last missing particle, the Higgs boson [5]. As a matter of course an unification of the two corner stones of modern physics is desired, but unfortunately none of the plenty attempts was able to answer all open questions. A classical, i.e. canonical, quantization of gravity within a perturbative expansion of the metric $g_{\mu\nu} = \delta_{\mu\nu} + \epsilon h_{\mu\nu}$ (small $\epsilon > 0$) around a flat background leads to a physically very impractical situation: Renormalizability requires infinitely experiments to set all parameters appearing in counter terms to certain values [6]. Such a theory is simply ill-defined and consequently many different theories were proposed to solve the quantum gravity puzzle. The two most popular ideas are *String Theory* and *Loop Quantum Gravity*, which both try to dispense this and other problems from more fundamental first principles. In contrast the approach pursued in this thesis is a more conservative one. The understanding of the renormalization procedure changed a lot with time, which allowed for other ways to think about a quantized version of gravity.

In the early days of QFT's renormalization was considered as a dubious necessity to gain finite results, but around the 1970s that view changed. Kenneth G. Wilson established the notion of effective field theories, which is mathematically based on the *Renormalization Group* (RG) [7]. This tool allowed to assign a specific energy scale to a field theory and to investigate its behaviour under a change of that scale. In particular such a change can be achieved by iteratively integrating out small momentum shells, which leads to a new effective version of the prior Lagrangian after each iteration step. Every effective Lagrangian is accompanied with its own coupling constants, s.t. couplings

gain a scale-dependence. The renormalization group allows to trace their flows and to make statements about their influence on the renormalizability of an underlying physical theory, even beyond perturbation theory: Besides the so-called *Gaussian fixed point*, which corresponds to vanishing couplings, other non-trivial fixed points can appear.

At this point the *Asymptotic Safety (AS)* scenario comes into play [8]: The breakdown of a perturbative treatment of general relativity is rooted in the negative mass dimension of the Newton coupling ($[G_N] = -2$), s.t. it will diverge for high energy scales. But to protect Newton's coupling from diverging, it only has to attain a non-trivial ultraviolet (UV) fixed point (which is not reachable by perturbative calculations). The crucial difference to the Gaussian fixed point is that couplings can take finite values. Furthermore an ultraviolet fixed point provides physical predictions: Couplings, which are not attracted by the non-trivial ultraviolet fixed point, keep their value in the infrared (IR). Therefore the predictive power of a theory depends on the existence of an ultraviolet fixed point and the number of repulsed couplings at this fixed point.

To access the flows of the couplings one needs an equation, which accounts for the scale-dependence of a theory. This can be achieved by introducing a scale-dependent effective action constructed from the usual effective action and a scale-dependent cutoff-term, whose evolution is covered by the *Wetterich equation* [9]. With this tool by hand quantum gravity in the asymptotic safety scenario became technically accessible. The corresponding flow equations in an Einstein-Hilbert truncation were set up at first by Martin Reuter [10] in 1998 and numerically solved on year later [11]. A non-trivial UV fixed point was observed and the rush about asymptotically safe quantum gravity started. In the last twenty years several improvements and more precise truncations were investigated which widely support the existence of a physical ultraviolet fixed point [12, 13, 14].

Despite the progress of the last years several conceptual problems remain. The most debated questions concern the metric split which is needed for a gauge-fixed Einstein-Hilbert action. The background and the fluctuating metric are related by very non-trivial relations that require approximations when it comes to actual computations. Examples are the geometrical flow equation [15] and the far developed vertex expansion [16, 17, 18], which is used in this thesis. Vertices will be constructed not only from Einstein-Hilbert tensor structures, but also from the four-derivative operators R^2 and $R_{\mu\nu}^2$, which possess marginal couplings. Key features of the investigated system are perturbative renormalizability [19], a distinction of parameters appearing in the spin 2 and spin 0 components of the graviton propagator, momentum dependent anomalous dimensions, the running of Newton's coupling extracted from the graviton 3-point function and the running of the higher order parameters leached from different tensor projections of the graviton 2-point function. Several physically important properties observed within the Einstein-Hilbert truncation in a vertex expansion will be analyzed: At first the system should feature a non-trivial UV fixed point. Furthermore the n -point functions should be local in momentum space since otherwise a small change of scale in the UV would affect the IR and vice versa. For Einstein-Hilbert vertices this was confirmed for the graviton 2- and 3-point function [16, 17, 20]. Besides the graviton flows behave like low-order polynomials in the important momentum range $p^2 \in [0, k^2]$ within an Einstein-Hilbert

truncation, where higher order polynomials are non-trivially suppressed. It is believed that diffeomorphism invariance is in charge for this behaviour and it is expected that including higher order tensor structures in the vertices doesn't destroy this characteristics but maybe slightly increases the highest order of the polynomials [18].

At last some words about the outline of this thesis: **Part I** is fully dedicated to the fundamentals. The two great theories, i.e. quantum field theory and general relativity, are presented in **chapter 2** and **chapter 3**, respectively. The focus lies on a path integral approach to the effective action and gauge theories in **chapter 2**. The latter is a connection to diffeomorphism invariance, which is discussed after having introduced the physical concepts and mathematical foundations of general relativity in **chapter 3**. In **chapter 4** the basics of the functional renormalization group, including a deviation of Wetterich's equation, are explained, beginning with the renormalization procedure itself. The subsequent **chapter 5** is about quantum gravity, i.e. the failure of a perturbative treatment and the methods of asymptotic safety for pure gravity systems. **Part II** includes the setup for the presented approximations. The starting point is **chapter 6**, where the vertex expansion is used to derive diagrammatic flow equations for the n -point functions. Afterwards the vertices are constructed from Einstein-Hilbert and higher order tensor structures. Implementing the latter into the flow diagrams leads to closed flow equations for all involved theory parameters and anomalous dimensions. Then **chapter 7** contains an insight into the computational details, in particular the working routine, used programs, analytical forms of the building blocks, the numerical integration and interpolation procedure and further technical challenges. The results are presented and discussed in **Part III, chapter 8**. The findings within an Einstein-Hilbert truncation are checked and developed. Then momentum locality of the graviton 2- and 3-point function for higher order systems is investigated. At last fixed points and momentum dependence are studied for two approximations: The 1st approximation only contains Einstein-Hilbert and $R_{\mu\nu}^2$ tensor structures, while the 2nd approximation also includes the R^2 tensor structure. Finally all results are summarized in **chapter 9** and used to provide an outlook for reasonable investigations in the future.

Part I

Basic concepts and underlying theories

2 Quantum Field Theory

Quantum Field Theory (QFT) plays a crucial role in understanding the fundamental bricks of the universe. It is useful to describe elementary particles and quasiparticles as field excitations in a quantum mechanical and relativistic way. A characteristic example for a QFT is the Standard Model of Elementary Particle Physics.

In contrast to General Relativity (GR) the development of the first QFT, Quantum Electrodynamics (QED), took many years and was affected by several publications, which also led to a couple of Nobel Prizes for the authors. The beginning of QED was marked in 1927 with a publication by Paul A. M. Dirac where he described photons as quanta of the electromagnetic field [21]. One year later Wolfgang Pauli and Pascual Jordan incorporated special relativity [22] and Paul Dirac found the equation named after him which describes spin $\frac{1}{2}$ particles as e.g. the electron [23]. Another important step was made in 1934 by Enrico Fermi and his theory of the β -decay [24] which matched with the property of a QFT to describe the creation and annihilation processes of particles during interactions. The main problem of QED were certain infinities which occurred when using perturbative methods. In the years 1946-1949 Richard P. Feynman [25, 26, 27], Julian Schwinger [28, 29, 30, 31] and Shin'ichirō Tomonaga¹ [33, 34, 35, 36, 37, 38, 39] presented the new method renormalization to tackle the infinities. This was done by adding specific counterterms in the Lagrangian which cancel the infinities at every order in perturbation theory. Theory parameters (e.g. the electric charge of the electron e) are then divided into bare parameters (e_0) in the Lagrangian and physical quantities ($e_{\text{phys}} = Ze_0$) after the renormalization procedure with some corresponding artefacts (renormalization constant Z) at a specific order in perturbation theory.

Further progress was made by Chen-Ning Yang and Robert Mills who noticed that QED belongs to a more general group of QFT's, namely gauge theories, and more precisely to abelian gauge theories. Yang and Mills also gave the first non-abelian gauge theory, Yang-Mills theory, which was named after them [40]. In the following more complex ideas entered new theories to gain an understanding of the weak interaction. Most importantly spontaneous symmetry breaking proposed by Yōichirō Nambu² in 1960 (allows the description of physical theories with a symmetry in the Lagrangian which is broken when the system takes its vacuum state) [42] and the Higgs Mechanism (explains how gauge bosons can gain a mass term by interacting with the Higgs field which spontaneously breaks the symmetry of the underlying Lagrangian but doesn't spoil its gauge invariance) introduced by a couple of theoretical physicists³ in 1964. This led to

¹The three theoretical physicists won the Nobel Prize in Physics in 1965 "for their fundamental work in quantum electrodynamics (QED) [...]" [32]

²Nambu got the Nobel Prize in Physics in 2008 "for the discovery of the mechanism of spontaneous symmetry breaking [...]" [41]

³Most prominently François Englert [43] and Peter Ware Higgs [44] who obtained the Nobel

the unification of electromagnetic and weak force to the electroweak interaction in 1959 founded by Sheldon Lee Glashow [46], Abdus Salam [47] and Steven Weinberg,⁴ [49] who incorporated the Higgs mechanism in 1967.

In parallel another fundamental theory came to several breakthroughs: Quantum Chromodynamics (QCD). In 1961 Murray Gell-Mann⁵ found a scheme (the eightfold way) to organize the multiple hadrons found till then [51]. He also postulated the quarks as the constituents of hadrons in 1964 [52]. One of the two key ingredients of QCD, asymptotic freedom (interaction strength decreases asymptotically for an increasing energy scale), was postulated by David Gross, Frank Wilczek [53] and David Politzer⁶ (independently) [55] in 1973.

QCD and the electroweak interaction build up the Standard Model. Its last building block, the Higgs boson, was found in 2013 at LHC (at CERN) [5]. Today important questions among many others concern the unification of the weak and the strong interaction, which is called a Grand Unified Theory (GUT), and the quantization of gravity (Quantum Gravity, see [chapter 5](#)).

A more comprehensive view on the history of QFT can be found in [56, pp. 1 - 48] (with early mathematical ideas) and [57]. The following two sections recap the main points of QFT which are necessary to continue. They are mainly taken from [56, 58, 59, 60].

2.1 Feynman's Path integral formulation

As usual in physics there are several possibilities to access a physical problem. In QFT one can mainly choose between two popular approaches: Firstly the canonical formalism, which quantizes classical fields in the Hamiltonian by promoting these classical fields to field operators with help of the known canonical commutations relations from Quantum Mechanics (QM). This technique is more intuitive from a technical point of view but a more profound insight in physics at high energy scales is denied. The second approach is the path integral formalism. Its central idea applies not only to QFT but already to QM.

Consider a particle moving from a point A to a point B. In classical mechanics its Equation of Motion (E.o.M.) can be found with the principle of stationary action. The simplest case, a freely moving particle, leads to the motion along a straight line which connects A and B (cf. [Figure 2.1](#)).

In Quantum Mechanics the situation is a bit more complicated. A quantum particle can take every possible trajectory which connects A and B (cf. [Figure 2.2](#)). The description

Prize in Physics in 2015 "for the theoretical discovery of a mechanism that contributes to our understanding of the origin of mass of subatomic particles [...]" [45]

⁴All three gained the Nobel Prize in Physics in 1979 "for their contributions to the theory of the unified weak and electromagnetic interaction between elementary particles [...]" [48]

⁵Gell-Mann gathered the Nobel Prize in Physics in 1969 "for his contributions and discoveries concerning the classification of elementary particles and their interactions" [50]

⁶The three shared the Nobel Prize in Physics in 2004 "for the discovery of asymptotic freedom in the theory of the strong interaction" [54]

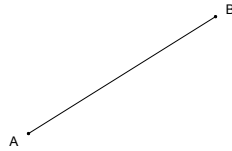


Figure 2.1: Movement of a classical particle

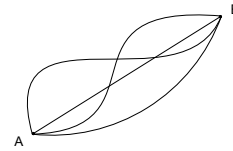


Figure 2.2: Movement of a quantum particle

of the quantum particle doesn't assume a sharp trajectory $\vec{r}(t)$ anymore, this concept gets replaced by a probability density $\rho(\vec{r}, t)$ which gives the probability to find a particle at $B \equiv \vec{r}(t_2)$ when it started at $A \equiv \vec{r}(t_1)$. This probability density is constructed from some complex amplitude $\mathcal{A}(\vec{r}, t)$ via $\rho(\vec{r}, t) = |\mathcal{A}(\vec{r}, t)|^2$. The amplitude then follows by summing over all possible paths where each path is weighted with a phase factor containing the usual action S divided by the reduced Planck constant \hbar

$$\mathcal{A}(\vec{r}, t) = \sum_{\text{paths}} e^{\frac{i}{\hbar} S}. \quad (2.1)$$

This suppresses paths which strongly differ from the classical path in the following way: In the complex plane $\frac{S}{\hbar}$ is the argument (polar angle) of each complex amplitude. For paths far away from the classical one (cf. path B in Figure 2.3) the action strongly varies for variation paths (paths A and C) s.t. the angles of this variations average out and result in a small amplitude \mathcal{A}_1 which doesn't contribute. In contrast for paths near the classical path (cf. path B in Figure 2.4) the phases are small for variations (paths A and C) since the action S takes its extremum in this region and the amplitudes add up. Therefore \mathcal{A}_2 strongly contributes to the particle motion.

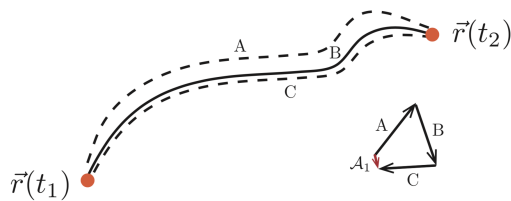


Figure 2.3: Paths away from the classical path: Amplitudes cancel each other out; from [61, p. 9]

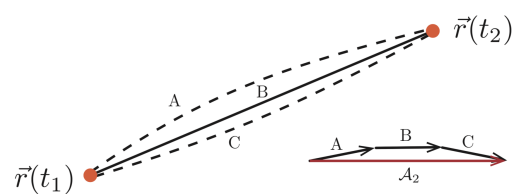


Figure 2.4: Paths near the classical path: Amplitudes get added up; from [61, p. 9]

Altogether this leads to a generalization of the principle of stationary action: The path integral. The main advantage of this approach is its simplicity when it comes to calculations. Coordinate transforms (important for relativistic computations) can be done directly and the Lagrangian instead of the Hamiltonian enters the path integral. Also deep connections between QFT and statistical field theory can be found. The prize to pay is that the path integral is mathematically not well-defined.

Although both formulations of QFT are equivalent the convergence of the path integral is not proven in a strict manner. From a mathematical point of view the path integral therefore has more a heuristic character. Anyway its importance for physics is unquestioned. Therefore we proceed with presenting the main concepts. Note that from now on all calculations are done in natural units $\hbar = c = 1$.

The path integral in QM and QFT

In QM the main question is how one can write the transition amplitude from an initial state $|x_i\rangle$ at t_i to a final state $|x_f\rangle$ at t_f , where $|x\rangle$ is an eigenstate of the position operator \hat{x} with corresponding eigenvalue x . By using the time evolution operator \hat{U} follows (cf. eq. (2.1))

$$\langle x_f | \hat{U}(t_f, t_i) | x_i \rangle = \frac{1}{N} \int \mathcal{D}x e^{iS[x]} \quad (2.2)$$

where N is some normalization constant. This can be directly generalized for further inserted position operators ($t_n \geq t_{n-1} \geq \dots \geq t_1$) by switching to Heisenberg picture

$$\langle x_f, t_f | \hat{x}(t_n) \dots \hat{x}(t_1) | x_i, t_i \rangle = \frac{1}{N} \int \mathcal{D}x x(t_n) \dots x(t_1) e^{iS[x]}. \quad (2.3)$$

Of special interest are vacuum amplitudes s.t. one needs to project this on the vacuum denoted by $|0\rangle$. When including time ordering \hat{T} and normalization w.r.t. the vacuum (N drops out) one will end up with

$$\langle \hat{T} \hat{x}(t_1) \dots \hat{x}(t_n) \rangle \equiv \frac{\langle 0 | \hat{T} \hat{x}(t_1) \dots \hat{x}(t_n) | 0 \rangle}{\langle 0 | 0 \rangle} = \frac{\int \mathcal{D}x x(t_1) \dots x(t_n) e^{iS[x]}}{\int \mathcal{D}x e^{iS[x]}}, \quad (2.4)$$

where S needs an additional ϵ -term which comes from the projection procedure and the measure has to be read as

$$\mathcal{D}x = \prod_i dx_i. \quad (2.5)$$

The QFT version of eq. (2.4) with fields φ instead of coordinates follows straightforwardly to be

$$\begin{aligned} \langle \hat{T} \hat{\varphi}(x_1) \dots \hat{\varphi}(x_n) \rangle &\equiv \frac{\langle 0 | \hat{T} \hat{\varphi}(x_1) \dots \hat{\varphi}(x_n) | 0 \rangle}{\langle 0 | 0 \rangle} \\ &= \frac{\int \mathcal{D}\varphi \varphi(x_1) \dots \varphi(x_n) e^{iS[\varphi]}}{\int \mathcal{D}\varphi e^{iS[\varphi]}}. \end{aligned} \quad (2.6)$$

A detailed derivation (the so-called time slicing method) of the path integral can be found in [58, pp. 275 - 282]. Note that the operator hats will be dropped from now on to improve readability.

Wick rotation

All functional integrals from before are defined with complex measures $d\varphi e^{iS[\varphi]}$. This can be brought from Minkowskian space into Euclidean space by performing a so-called Wick rotation for the time component x_0 . The latter is defined as

$$(x_0)_M \rightarrow -i(x_0)_E, \quad (2.7)$$

which is nothing but a rotation in the complex plane (cf. blue arrows in Figure 2.5).

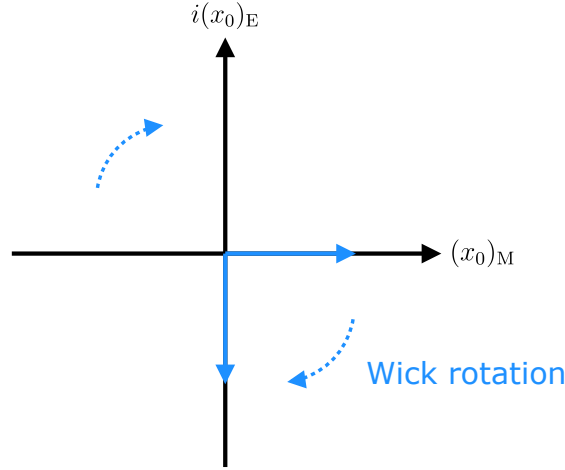


Figure 2.5: Wick rotation

After some mathematical intermediate steps this causes

$$i(S[\varphi])_M \rightarrow -(S[\varphi])_E \quad (2.8)$$

in the exponent of the path integral and converts all complex measures into statistical ones. Henceforth only Wick rotated quantities are used.

Functional calculus

The mathematical tool in use for all further computations is functional calculus, which is nothing but infinite dimensional vector calculus. Every physical field $\varphi(x)$ with a d dimensional continuous parameter $x = (x_1, \dots, x_d)$ lives in an infinite dimensional vector space. Inner products are defined as

$$J \cdot \varphi := \int d^d x J(x) \varphi(x), \quad (2.9)$$

where the former will be used as shorthand notation in the whole thesis (note that in most cases $d = 4$). Furthermore a linear operator $K(x, y)$ needs an additional integration to act on a field $\varphi(x)$ as

$$(K \cdot \varphi)(x) := \int d^d y K(x, y) \varphi(y). \quad (2.10)$$

From this one can derive two useful rules for functional differentiation.

1. Functional derivatives of fields:

$$\frac{\delta\varphi(x)}{\delta\varphi(y)} = \delta^d(x - y) \quad (2.11)$$

2. Functional derivatives of inner products:

$$\frac{\delta}{\delta\varphi(x)}(\varphi \cdot \psi) \stackrel{(2.9)}{=} \frac{\delta}{\delta\varphi(x)} \int d^d y \varphi(y)\psi(y) \stackrel{(2.11)}{=} \psi(x) \quad (2.12)$$

Generating functional and Schwinger functional

The generating functional is defined as:

$$Z[J] := \int \mathcal{D}\varphi e^{-S[\varphi] + J \cdot \varphi} \quad \text{Generating functional} \quad (2.13)$$

There the shorthand notation was already used. From this expression all n -point correlation functions can be calculated by taking functional derivatives w.r.t. the source term $J(x)$ at vanishing sources

$$\langle \varphi(x_1) \dots \varphi(x_n) \rangle = \frac{1}{Z[0]} \frac{\delta^n Z[J]}{\delta J(x_1) \dots \delta J(x_n)} \Big|_{J=0}, \quad (2.14)$$

where the prefactor ensures that vacuum contributions don't appear in the correlation functions.

To exclude all disconnected correlation functions another quantity can be defined, the Schwinger functional. It is related to the generating functional via a logarithm:

$$W[J] := \ln Z[J] \quad \text{Schwinger functional} \quad (2.15)$$

One only gets connected correlation functions since e.g. for the 2-point correlation function follows

$$\begin{aligned} \frac{\delta^2 W[J]}{\delta J(x_1) \delta J(x_2)} \Big|_{J=0} &\stackrel{(2.15)}{=} \left(\frac{1}{Z[0]} \frac{\delta^2 Z[J]}{\delta J(x_1) \delta J(x_2)} - \frac{1}{Z[0]} \frac{\delta Z[J]}{\delta J(x_1)} \frac{1}{Z[0]} \frac{\delta Z[J]}{\delta J(x_2)} \right) \Big|_{J=0} \\ &\stackrel{(2.14)}{=} \underbrace{\langle \varphi(x_1) \varphi(x_2) \rangle}_{\text{full 2-point function}} - \underbrace{\langle \varphi(x_1) \rangle \langle \varphi(x_2) \rangle}_{\text{disconnected 2-point function}} \end{aligned} \quad (2.16)$$

This comes handy because the propagator is nothing but the connected 2-point function.

Effective action and Quantum E.o.M.

After having introduced the generating functional for general n -point correlation functions and the Schwinger functional for connected correlation functions a third quantity can be defined: The effective action which generates one particle irreducible (1PI) correlation functions. It is defined as the Legendre transform of the Schwinger functional:

$$\Gamma[\phi] := \sup_J (J \cdot \phi - W[J]) \quad \text{Effective action} \quad (2.17)$$

2.1. Feynman's Path integral formulation

To understand the meaning of the new field ϕ let's evaluate eq. (2.17) at the supremum $J = J_{\text{sup}}$, s.t. the "sup" in eq. (2.17) can be dropped. Taking a functional derivative w.r.t. J then leads to

$$\begin{aligned} \left. \frac{\delta \Gamma[\phi]}{\delta J} \right|_{J=J_{\text{sup}}} &= \frac{\delta}{\delta J} (J \cdot \phi - W[J]) \Leftrightarrow 0 = \phi - \frac{\delta W[J]}{\delta J} \\ &\Leftrightarrow \phi = \frac{\delta W[J]}{\delta J} \stackrel{(2.16)}{=} \langle \varphi \rangle_J. \end{aligned} \quad (2.18)$$

Therefore the field ϕ is equal to the expectation value of the field φ when an external source J is present. One can also take a functional derivative of eq. (2.17) w.r.t. ϕ which leads to:

$$\boxed{\frac{\delta \Gamma[\phi]}{\delta \phi} = J \quad \text{Quantum E.o.M.}} \quad (2.19)$$

This reveals the crucial role of the effective action $\Gamma[\phi]$ in QFT: It describes the evolution of the field ϕ while encountering all quantum effects. Its relation to the action $S[\varphi]$ is rather fundamental than technical. The derivation begins with using eq. (2.18) to interpret ϕ as a background field. Therefore φ can be treated as a fluctuation around this background field ϕ which can be implemented by shifting $\varphi \rightarrow \phi + \varphi$. After various steps and using eq. (2.19) one finds

$$e^{-\Gamma[\phi]} = \int \mathcal{D}\varphi e^{-S[\phi+\varphi] + \frac{\delta \Gamma[\phi]}{\delta \phi} \cdot \phi}. \quad (2.20)$$

In principle eq. (2.20) is a closed equation for the effective action $\Gamma[\phi]$. Finding a solution is limited due to its complexity. Thus an approximation scheme is needed: A convenient ansatz is to use a saddlepoint expansion for the action $S[\phi + \varphi]$ around $S[\phi]$ in loop-orders

$$\begin{aligned} S[\phi + \varphi] &= S[\phi] + \int d^d x \frac{\delta S}{\delta \phi}(x) \varphi(x) \\ &\quad + \frac{1}{2} \int d^d x d^d y \varphi(x) S^{(2)}(x, y) \varphi(y) + \dots, \end{aligned} \quad (2.21)$$

wherein

$$S^{(2)}(x, y) = \frac{\delta^2 S}{\delta \phi(x) \delta \phi(y)}. \quad (2.22)$$

In the end one obtains

$$\Gamma[\phi] \Big|_{1\text{-loop}} = S[\phi] + \frac{1}{2} \text{Tr} \ln S^{(2)}[\phi] \quad (2.23)$$

as a 1-loop approximation. Therefore one gets back the classical E.o.M. from eq. (2.19) at lowest order ($\Gamma[\phi] = S[\phi]$) and vanishing sources ($J = 0$).

2.2 Gauge theories

A special case of QFT's are gauge theories which play a crucial role in elementary particle physics, e.g. QED is a gauge theory. In general the fundamental equations of physical theories involve several mathematical setups that describe one and the same physical setting.

Classical analogue

As an intuitive illustration consider an electron e^- at rest in classical electrodynamics. This electron is surrounded by his electrical field (cf. Figure 2.6)

$$\vec{E}(\vec{r}) = \frac{1}{4\pi\epsilon_0} \frac{e}{r^3} \vec{r}, \quad (2.24)$$

with $r = |\vec{r}|$, which can be translated into an electric potential $V(r)$ (cf. Figure 2.7) via

$$\vec{E}(\vec{r}) = -\vec{\nabla} V(r). \quad (2.25)$$

Obviously the electric potential $V(r)$ follows from some integration procedure

$$V(r) = \frac{1}{4\pi\epsilon_0} \frac{e}{r} + a, \quad (2.26)$$

s.t. an arbitrary integration constant a appears that can be regarded as an additional gauge degree of freedom. Of course all physical situations are completely independent of the actual value of a . It can be fixed by choosing a reference point \vec{x} where the electric potential vanishes⁷ $V(r = x) = 0$.

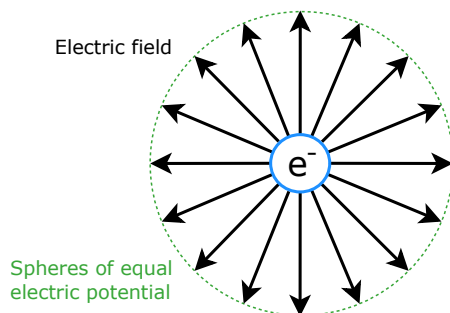


Figure 2.6: Electric field $\vec{E}(\vec{r})$ of an electron

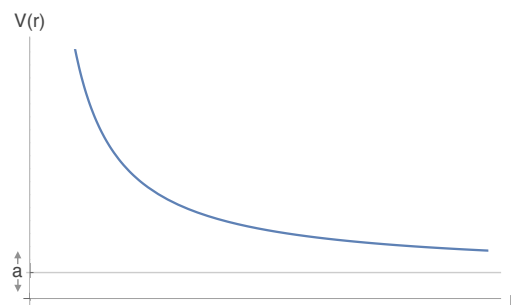


Figure 2.7: Electric potential $V(r)$ of an electron with a gauge parameter a

⁷The common literature mostly uses $V(r \rightarrow \infty) = 0$ s.t. $a = 0$

Mathematical background

Mathematically gauge theories are constructed as follows: The Lagrangian \mathcal{L} of a gauge theory is invariant under some local⁸ gauge transformation $U(x)$. These transformations form a Lie group \mathcal{G} with dimension $\dim(\mathcal{G})$ that is the symmetry group of the underlying theory. The group generators T^a of the Lie group naturally fulfill a corresponding Lie algebra \mathfrak{g} , i.e. the algebra of infinitesimal gauge transformations $\omega(x)$. One can determine the Lie algebra by a Lie bracket, which is in this case the well-known commutator

$$[T^a, T^b] = i f^{abc} T^c, \quad (2.27)$$

where f^{abc} are the so-called structure constants. In addition each group element $g \in \mathcal{G}$ can be written as

$$g = \exp \left(-ig \sum_{a=1}^{\dim(\mathcal{G})} \alpha^a T^a \right). \quad (2.28)$$

For every group generator T^a one can find an associated gauge field $A^\mu(x)$ (in most cases a vector field) which describes a gauge boson. In the Standard Model gauge bosons mediate fundamental forces between matter particles. Mathematically this is achieved by coupling gauge bosons to matter fermions in the Lagrangian \mathcal{L} . Depending on the values of the structure constants f^{abc} one can distinct between two types of gauge theories:

1. **Abelian gauge theories:** $f^{abc} = 0 \forall \{abc\}$ s.t. in eq. (2.27) follows $[T, T] = 0$. The most prominent example is QED where $\mathcal{G} = U(1)$ which implies $\dim(\mathcal{G}) = 1$ and $T^a \equiv T \in \mathbb{R}$. The gauge boson is the photon γ and the gauge field is the electromagnetic 4-potential $A^\mu(x)$.
2. **Non-Abelian gauge theories:** $f^{abc} \neq 0$ for some $\{abc\}$. E.g. in QCD the symmetry group is $\mathcal{G} = SU(3)$. The structure constants follow as $f^{abc} = \epsilon^{abc}$ which is the usual fully antisymmetric ϵ -tensor and the generators are related to the Gell-Mann matrices λ^a via $T^a = \frac{1}{2}\lambda^a$. Finally one gets out 8 gluons g as gauge bosons.

All considerations culminate in the Standard Model of Elementary Particle Physics with an underlying symmetry group $U(1) \times SU(2) \times SU(3)$ which leads to a total of 12 gauge bosons (1 photon γ + 3 weak bosons W^\pm, Z^0 + 8 gluons g).

Yang-Mills theory and Faddeev-Popov procedure

Of special interest in this thesis are non-abelian gauge theories since the quantization procedure of gravity refers to the symmetry group of GR, which is of the non-abelian type. To describe their behaviour more precisely consider the generalization of QCD

⁸In this case *local* designates a space-time dependent gauge parameter, in contrast *global* denotes a constant gauge parameter

(SU(3)) and the weak interaction (SU(2)): Yang-Mills theory (SU(N) with $N \in \mathbb{N}$). The Lagrangian \mathcal{L}_{YM} is in general given by:

$$\mathcal{L}_{\text{YM}} = -\frac{1}{4} F_{\mu\nu}^a F^{a,\mu\nu} \quad \text{Yang-Mills Lagrangian} \quad (2.29)$$

There a denotes a group index, $\mu\nu$ represent space-time indices and $F_{\mu\nu}^a$ is the field-strength tensor which is defined as

$$F_{\mu\nu}^a(A) := \partial_\mu A_\nu^a - \partial_\nu A_\mu^a + g f^{abc} A_\mu^b A_\nu^c. \quad (2.30)$$

Note the appearance of the structure constants in eq. (2.30) which signals the possible non-abelian behaviour. The Lagrangian \mathcal{L}_{YM} is invariant under the following local gauge transformation $U(x)$ for the 4-potential

$$A_\mu(x) \xrightarrow{U} A_\mu^U(x) = -U(x)A_\mu(x)U^\dagger(x) + \frac{i}{g}U(x)\partial_\mu U^\dagger(x). \quad (2.31)$$

In a naive way a generating functional should be obtainable as usual with only one slight correction: Since the gauge field $A_\mu^a(x)$ carries a group index a the corresponding source must also possess one. Therefore should follow

$$Z[J] = \int \mathcal{D}A e^{-S_{\text{YM}} + J_\mu^a \cdot A^{a,\mu}}. \quad (2.32)$$

But now the key ingredient of gauge theories comes into play and complicates the whole situation: Gauge transformations connect different gauge fields in such a way that they lead to the same physics. Therefore eq. (2.32) overcounts these gauge field configurations. To cure this problem consider the space of all gauge fields M (cf. green oval in Figure 2.8). Gauge fields, which are equivalent under gauge transformations, lie in

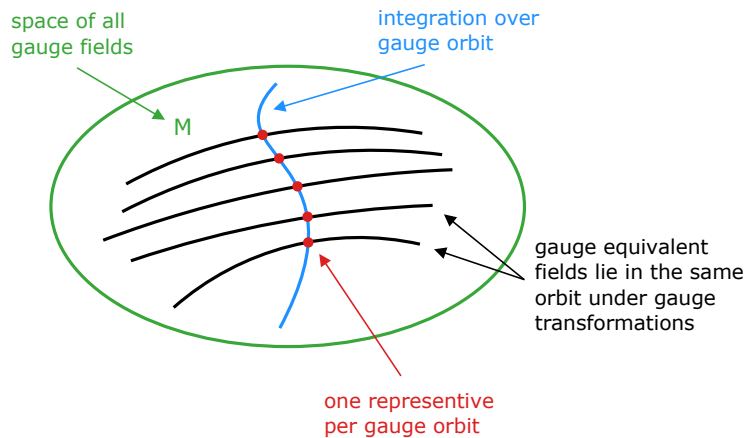


Figure 2.8: Integration over one representation per gauge orbit

the same orbit s.t. M consists of many orbits (black lines). The integration procedure

(blue line) should pick only one gauge field per gauge orbit (red dots)⁹. Therefore the gauge has to be fixed which can be achieved by a gauge fixing condition: For a given $A \in M$ should hold

$$F^a[A^g] = 0 \quad \text{for some unique } g \in \mathcal{G}. \quad (2.33)$$

To implement this one can include a "1" in (2.32) in the following way

$$\mathbb{1} = \int_{\mathcal{G}} d\mu[g] \delta[F(A^g)] L(A^g) \quad (2.34)$$

where $L(A^g) = \det\left(\frac{\delta F^a(A^g)}{\delta g}\right)$ is the Jacobian, $d\mu[g]$ is the measure on \mathcal{G} (integration goes over all group elements g) and A^g indicates a gauge transformation on a gauge field. Inserting eq. (2.34) in eq. (2.32) and using eq. (2.33) and the gauge invariance of the action S and the measure \mathcal{D}_A leads to

$$Z[J] = \int \mathcal{D}A \delta[F(A)] \det \Delta_{\text{FP}} e^{-S_{\text{YM}} + J_{\mu}^a A^{a,\mu}}, \quad (2.35)$$

wherein

$$\det \Delta_{\text{FP}} = \det \left(-\frac{\delta F^a(A)}{\delta A_{\mu}^b} \cdot D_{\mu}^{bc} \right) \quad (2.36)$$

is the so-called Faddeev-Popov determinant. Now the two factors in the integrand can be converted into additional actions:

1. Introduce the so-called (grassmannian) ghost fields $c^a(x)$ and $\bar{c}^a(x)$ with sources $\bar{\eta}^a(x)$ and $\eta^a(x)$ to rewrite the Faddeev-Popov determinant as

$$\det \Delta_{\text{FP}} = \int \mathcal{D}\bar{c} \mathcal{D}c e^{-S_{\text{gh}}[c, \bar{c}]}, \quad (2.37)$$

where $S_{\text{gh}}[c, \bar{c}]$ denotes the ghost action

$$S_{\text{gh}}[c, \bar{c}] = - \int d^d x \bar{c}^a(x) (\Delta_{\text{FP}} c(x))^a. \quad (2.38)$$

2. The δ -functional can also be translated into a gaussian exponential when introducing the so-called gauge-fixing parameter ξ . After some mathematical steps one can use the replacement

$$\delta[F^a(A)] \rightarrow e^{-S_{\text{gf}}[A]} \quad (2.39)$$

with the gauge-fixing action

$$S_{\text{gf}}[A] = \frac{1}{2\xi} \int d^d x F^a(A) F^a(A). \quad (2.40)$$

Putting all together finally leads to the gauge-fixed generating functional

$$Z[J, \eta, \bar{\eta}] = \int \mathcal{D}A \mathcal{D}\bar{c} \mathcal{D}c e^{-S_{\text{YM}} - S_{\text{gf}} - S_{\text{gh}} + J_{\mu}^a A^{a,\mu} + \bar{\eta}^b \cdot c^b - \bar{c}^c \cdot \eta^c}. \quad (2.41)$$

⁹This is not always true (known as the Gribov-Problem), for more details see [62]

3 General Relativity

General Relativity (GR) is one of the pillars in modern physics. Its key ingredient is the description of gravity as a geometric property of unified space-time. After years of work on this subject¹ and a stunning battle of wits against David Hilbert², Albert Einstein found the equations of GR in November 1915 [1]. A first review article was published a half year later by Einstein too [2].

Up to date GR is one of the best tested theories of mankind. It did not only passed the three classical tests³ proposed by Einstein himself, but also implicated theoretically the existence of gravitational waves which were found after almost 100 years of research in 2015 at LIGO [4].

The four sections below are mostly taken from [68, 69, 70, 71, 72] and can be seen as a quick reminder of GR which is essential to proceed.

3.1 Principles and conventions

According to Einstein GR is based on three principles [73]:

1. **General principle of relativity:** All physical laws are the same for all reference systems, i.e. all physical laws are covariant.
2. **Equivalence principle:** Gravitational and inertial mass are identically the same, i.e. the metric $g_{\mu\nu}$ determines the gravitational and the inertial behaviours in the same way.
3. **Mach's principle:** The gravitational field is only determined by the stress energy tensor $T_{\mu\nu}$.

The first two principles are definitely fulfilled by GR since they are implemented mathematically. In contrast the question if Mach's principle is fulfilled in GR is more a philosophical one and is discussed since then⁴.

The mathematical basis for GR are Pseudo-Riemannian manifolds⁵ which represent curved space-time and generalize the well-known Euclidean space, i.e. the flat space. Thereupon physical observables can be linked to certain mathematical objects from

¹Einstein published four more articles about his ideas concerning general relativity [3, 63, 64, 65]

²For a historical point of view and a decision in the priority dispute see [66, 67]

³1. Gravitational redshift of light [2, p. 820], 2. Deviation of light by massive objects, e.g. the sun [2, p. 822], 3. Perihelion precession of mercury [2, p. 822]

⁴An overview over recent positions can be found in the first chapter of [74]

⁵ ds^2 doesn't need to be positive-definite

differential geometry. In the following all needed mathematical expressions will be introduced and shortly explained. Additionally certain conventions which naturally differ in the wide field of literature will be fixed.

1. **Metric** $g_{\mu\nu}$: Symmetric tensor which describes the space-time geometry. It can be linked to the Newtonian gravitational potential $\vec{F}_g = -\vec{\nabla}\phi$ by using the weak-field approximation. Also it is employed to raise and lower indices. Here it is used with the sign convention $g_{\mu\nu} = \text{diag}(-1, 1, 1, 1)$.
2. **Contravariant 4-vector**: Vector with 4 (1 time + 3 space) components which transforms under Lorentz transformation Λ from a coordinate system S to another coordinate system S' as

$$x^\mu \rightarrow x'^\mu = \Lambda^\mu_\nu x^\nu. \quad (3.1)$$

It can be linked to a covariant vector via the metric

$$x_\mu = g^{\mu\nu} x_\nu. \quad (3.2)$$

The notation is given by $x^\mu = (x^0, x^1, x^2, x^3) = (ct, x, y, z)$.

3. **Christoffel symbols**: The role of an affine connection is played by the Christoffel symbols which allow to measure distances on a curved manifold. A Christoffel symbol $\Gamma^\mu_{\alpha\beta}$ is not a tensor and can be thought as the projection of $\partial_\beta e_\mu$ on e^α (change of an unit vector in one direction projected onto another direction). It can locally be written in terms of the metric as

$$\Gamma^\mu_{\alpha\beta} = \frac{g^{\mu\nu}}{2} (\partial_\alpha g_{\beta\nu} + \partial_\beta g_{\nu\alpha} - \partial_\nu g_{\alpha\beta}). \quad (3.3)$$

If the manifold is torsion-free the Christoffel symbols are symmetric in the lower two indices. The analogon in Newtonian gravity is the gravitational acceleration $g^i = -\partial^i\phi$.

4. **Covariant derivative**: The partial derivative ∂_μ doesn't transform covariantly under a general coordinate transform. This is due to the fact that a derivative of a vector field $v(x)$ on a curved space-time has 2 contributions: First the change of the vector components themselves (the usual partial derivative) and second the modification of the basis system, which can be written in terms of the Christoffel symbols as

$$\mathcal{D}_\mu x^\nu = \partial_\mu x^\nu + \Gamma^\nu_{\mu\gamma} x^\gamma, \quad (3.4)$$

where the order of the two lower indices is only important for manifolds including torsion.

5. **Riemann curvature tensor:** Describes the curvature of a manifold which can't be transformed away by coordinate transforms. It can be characterized as the commutator of covariant derivatives acting on a contravariant 4-vector

$$R^{\beta\alpha}_{\mu\nu} x^\beta = [\mathcal{D}_\mu, \mathcal{D}_\nu] x^\alpha = (\mathcal{D}_\mu \mathcal{D}_\nu - \mathcal{D}_\nu \mathcal{D}_\mu) x^\alpha. \quad (3.5)$$

The Riemann curvature tensor obeys some symmetry relations and the two Bianchi identities s.t. it has 20 independent tensorial components in 4 dimensions. In Newtonian gravity it is connected to the tidal field $\partial^i \partial^j \phi$ and it is possible to express it with the Christoffel symbols as

$$R^\alpha_{\beta\gamma\delta} = \partial_\gamma \Gamma^\alpha_{\delta\beta} - \partial_\delta \Gamma^\alpha_{\gamma\beta} + \Gamma^\nu_{\delta\beta} \Gamma^\alpha_{\gamma\nu} - \Gamma^\nu_{\gamma\beta} \Gamma^\alpha_{\delta\nu}. \quad (3.6)$$

6. **Ricci curvature tensor:** Measures the deviation of the volume of a sphere on a curved manifold compared to the normal sphere in Euclidean space. In GR it contains the full information about space-time curvature and is related to matter via the Einstein equations. The Ricci curvature tensor is simply the contraction of the Riemann curvature tensor with the metric

$$R_{\mu\nu} = g^{\lambda\alpha} R_{\alpha\mu\lambda\nu} = R^\lambda_{\mu\lambda\nu}. \quad (3.7)$$

In addition it has 10 independent tensorial components in 4 dimensions and is symmetric in the lower to indices. It can be linked to the Laplacian of the gravitational potential $\Delta\phi$ in the Newtonian case.

7. **Ricci curvature scalar:** One can get the Ricci curvature scalar by contracting the Ricci curvature tensor with the metric again

$$R = g^{\mu\nu} R_{\mu\nu} = R^\nu_{\nu}. \quad (3.8)$$

This gives a number which indicates in which way the manifold is curved: $R = 0$ is valid for Euclidean space, $R > 0$ for manifolds with positive curvature, e.g. the 2-sphere and $R < 0$ for manifolds with negative curvature, e.g. a saddle.

8. **Diffeomorphism:** Let's begin with the general definition of a diffeomorphism. Let M and M' be two manifolds and $\phi : M \rightarrow M'$ with $\phi \in C^\infty$ a map between them. ϕ is a diffeomorphism, if ϕ is a one-to-one bijection and its inverse $\phi^{-1} : M' \rightarrow M$ with $\phi^{-1} \in C^\infty$ exists. Accordingly the two manifolds M and M' are called diffeomorphic, if there exists a diffeomorphism between them. Thinking in geometry a diffeomorphism does the following: A tensor $T(p)$ which is evaluated at the point $p \in M$ is pushed forward to $T'(p') := \phi T(p)$ with $p' \in M'$, while the coordinate *values* won't change (= coordinate basis is pulled back accordingly), s.t. $x'^\mu(p') = x^\mu(p)$ holds. Hence a diffeomorphism is an *active* coordinate transformation since spatial points change but coordinates do not.

In the case of GR the group of diffeomorphisms is a one parameter group (the parameter is usually denoted by λ , the pushforward map by ϕ_λ) and has a very

important meaning: It forms the gauge group of GR. More details about the implications will be given in [section 3.4](#).

If the infinitesimal version of a diffeomorphism has a pushforward (up to 1st order)

$$x^\mu \rightarrow y^\mu = x^\mu + \eta^\mu d\lambda, \quad (3.9)$$

where $\eta^\mu(x) = \frac{\partial x^\mu}{\partial \lambda}$ is the tangent vector field of x^μ along changes in λ then the coordinates x^μ have to change accordingly as

$$x^\mu \rightarrow x'^\mu = x^\mu - \eta^\mu d\lambda, \quad (3.10)$$

s.t. $x'^\mu(p') = x^\mu(p)$ is fulfilled.

9. **Lie derivative:** Asking how an infinitesimal diffeomorphism acts on tensor, e.g. on the metric, directly leads to the idea of the Lie derivative. As before but now infinitesimally a tensor T transforms under a diffeomorphism as

$$T \rightarrow T' = \phi_{\Delta\lambda} T, \quad (3.11)$$

wherein a finite $\Delta\lambda$ is used for the following definition of the Lie derivative. One can now define a linear quantity which measures the absolute difference between the transformed tensor T' and the untransformed tensor T for small group parameter changes $\Delta\lambda$, i.e. different particular diffeomorphisms, which is the so-called Lie derivative. In full analogy to the classical differential quotient it is defined as

$$\mathcal{L}_\eta T := \lim_{\Delta\lambda \rightarrow 0} \frac{\phi_{\Delta\lambda} T(x) - T(x)}{\Delta\lambda}, \quad (3.12)$$

where the shorthand notation $T = T_{\nu_1, \dots, \nu_j}^{\mu_1, \dots, \mu_i}$ was used. Obviously a (i, j) tensor is mapped to a (i, j) tensor. The lower index η of the Lie derivative \mathcal{L}_η denotes that a tensor T is pushed forward along the tangent vector field $\eta^\mu(x)$. As maybe already suggested by the previous procedure an infinitesimal diffeomorphism is generated by a Lie derivative. Assuming the same pushforward as before (given in eq. (3.9)) one therefore finds for the transformation behaviour of a tensor T

$$T \rightarrow T' = T + \mathcal{L}_\eta T d\lambda. \quad (3.13)$$

It is possible to write out a Lie derivative locally which entails a deeper insight on its functionality. E.g. for the metric $g_{\mu\nu}$ holds

$$\mathcal{L}_\eta g_{\mu\nu} = \underbrace{\eta^\gamma \partial_\gamma g_{\mu\nu}}_{\sim \text{pushforward}} + \underbrace{g_{\sigma\nu} \partial_\mu \eta^\sigma + g_{\mu\delta} \partial_\nu \eta^\delta}_{\sim \text{pullback co. trafo.}}. \quad (3.14)$$

Here one can see that the contrast between covariant and Lie derivative: While the former uses the affine connection ($\nabla \sim \partial g$) the latter uses the tangent vector field ($\mathcal{L} \sim \partial \eta$), s.t. the Lie derivative is truly coordinate independent.

3.2 The Einstein equations

The heart of GR are the Einstein equations. They are designed to fulfill in principle 5 properties⁶:

1. **2nd order differential equation:** 2nd derivatives of the metric, i.e. some type of curvature, are linked to the source (as the Poisson equation does in the Newtonian case).
2. **Divergence-free:** Energy-momentum must be covariantly conserved (\Leftrightarrow Covariant derivative of the Einstein equations must vanish).
3. **Local field equation:** Only parts of the curvature, i.e. Ricci curvature, can be constrained by the source.
4. **4 space-time dimensions:** Enough degrees of freedom are needed for gravity to propagate.
5. **One dynamical field:** The metric is the only dynamical field.

Only two tensors besides the stress-energy tensor fulfill the requirement of vanishing divergence: The metric $g_{\mu\nu}$ and the so-called Einstein tensor which is defined as

$$G_{\mu\nu} := R_{\mu\nu} - \frac{1}{2}Rg_{\mu\nu}. \quad (3.15)$$

After respecting all demands the result is:

$$\boxed{G_{\mu\nu} + \Lambda g_{\mu\nu} = \frac{8\pi G}{c^4} T_{\mu\nu} \quad \text{Einstein equations}} \quad (3.16)$$

Therein Λ is the cosmological constant, G Newton's gravitational constant and c the speed of light.

The set of 10 equations relate symmetric 4x4 tensors to describe the behaviour of space-time geometry, but to find trajectories of particles in a particular geometry another equation is needed: The geodesic equation. A geodesic is defined as a curve which parallel transports its own tangent vector along the curve. In Euclidean space this would be a straight line, in curved spaces more complex curves arise. Freely falling motion proceeds exactly on such a geodesic and is depicted by

$$\dot{x}^\mu + \Gamma^\mu_{\alpha\beta} \dot{x}^\alpha \dot{x}^\beta = 0. \quad (3.17)$$

Of course one gets back Newton's law in the non-relativistic limit $v \ll c$ and for weak fields.

⁶It can be shown that the Einstein equations are general under these assumptions, cf. [75]

3.3 The Einstein-Hilbert action

To arrive at the Einstein equations one can also start from a proper chosen action and use the principle of stationary action, which can be generalized from classical field theory to GR, to find the Einstein equations as the corresponding equations of motion. Finding a convenient action requires the integral measure to be covariant which is generated by a factor of $\sqrt{-g}$ where $g = \det(g_{\mu\nu})$. Also all terms are either proportional to $\int d^4x \sqrt{-g}$ or proportional to the only possible scalar which involves 2nd derivatives of the metric: the Ricci scalar $\int d^4x \sqrt{-g} R$. The right action to start with is the so-called Einstein-Hilbert action which is a composition of a gravitational action

$$S_G = \frac{1}{2\kappa} \int d^4x \sqrt{-g} R \quad (3.18)$$

where $\kappa = \frac{8\pi G}{c^4}$, an action which involves all matter fields denoted by the Matter Lagrangian \mathcal{L}_M

$$S_M = \int d^4x \sqrt{-g} \mathcal{L}_M \quad (3.19)$$

and a term for the cosmological constant

$$S_\Lambda = -\frac{1}{\kappa} \int d^4x \sqrt{-g} \Lambda. \quad (3.20)$$

The Matter Lagrangian defines also the stress-energy tensor as the response of the system to a variation in the metric via

$$T_{\mu\nu} := \frac{-2}{\sqrt{-g}} \frac{\delta(\sqrt{-g} \mathcal{L}_M)}{\delta g^{\mu\nu}}. \quad (3.21)$$

In addition follows:

$$\boxed{S_{\text{EH}} = \int d^4x \sqrt{-g} \left[\frac{1}{2\kappa} (R - 2\Lambda) + \mathcal{L}_M \right] \quad \text{Einstein-Hilbert action}} \quad (3.22)$$

Intuitively the gravitational action alone leads to the vacuum field equations with $T_{\mu\nu} = 0$. To get the full Einstein equations one needs to start with the whole Einstein-Hilbert action, vary with respect to the inverse of the metric and force this to be zero

$$\frac{\delta S_{\text{EH}}}{\delta g^{\mu\nu}} \stackrel{!}{=} 0 \Leftrightarrow \frac{\delta S_G}{\delta g^{\mu\nu}} + \frac{\delta S_M}{\delta g^{\mu\nu}} + \frac{\delta S_\Lambda}{\delta g^{\mu\nu}} \stackrel{!}{=} 0. \quad (3.23)$$

3.4 General covariance and diffeomorphism invariance

Transferring the deeply physical general principle of relativity to mathematics leads to the concepts of general covariance and diffeomorphism invariance. Both are key properties of GR and are used *synonymously*. For a better understanding of the mathematical basis of GR a detailed overview is given in the following section.

General coordinate transformations and general covariance

The term *general covariance* denotes the circumstance that GR is invariant under *general* coordinate transformations, i.e. that there doesn't exist a favored coordinate system for describing physical processes. It is very important to be precise at this point: The outstanding feature of GR is *not* coordinate invariance. The latter is already implemented in special relativity and even in classical mechanics. Essential is that GR goes one step further, i.e. that the prior concept of coordinates, namely geometry in terms of the metric, doesn't need to be fixed at all. In other words: GR doesn't need preset geometry. Therefore a *general* coordinate transformation, i.e. a transformation which can include changes in the metric, leaves GR invariant and special relativity or classical mechanics not.

Although the statement that GR is generally covariant seems to be very clear and appealing from a physical point of view a more mathematical treatment is indispensable. A general coordinate transformation is simply given by

$$x^\mu \rightarrow x'^\mu(x), \quad (3.24)$$

which is as general as possible. To write down the transformation rules for all classes of mathematical objects let's introduce the Jacobian J_ν^μ and its inverse J_μ^ν as usually

$$J_\nu^\mu := \frac{\partial x'^\mu}{\partial x^\nu} \quad \text{and} \quad J_\mu^\nu = \frac{\partial x^\mu}{\partial x'^\nu}. \quad (3.25)$$

The following transformation rules for scalars, vectors and tensors are listed below.

1. **Scalars:** These are genuinely invariant under general coordinate transformations,

$$S(x) \rightarrow S'(x') = S(x). \quad (3.26)$$

2. **Vectors:** Covariant and contravariant vectors transform likewise but with different Jacobians

$$V^\mu(x) \rightarrow V'^\mu(x') = V^\alpha(x) J_\alpha^\mu \quad \text{and} \quad V_\mu(x) \rightarrow V'_\mu(x') = V_\alpha(x) J_\mu^\alpha. \quad (3.27)$$

3. **Tensors:** Obviously each upper/lower index transforms with a normal/inverse Jacobian s.t. for a (i, j) tensor holds

$$T_{\nu_1, \dots, \nu_j}^{\mu_1, \dots, \mu_i}(x) \rightarrow T_{\nu'_1, \dots, \nu'_j}^{\mu'_1, \dots, \mu'_i}(x') = T_{\beta_1, \dots, \beta_j}^{\alpha_1, \dots, \alpha_i}(x) J_{\alpha_1, \dots, \alpha_i}^{\mu'_1, \dots, \mu'_i} J_{\nu'_1, \dots, \nu'_j}^{\beta_1, \dots, \beta_j}. \quad (3.28)$$

For later use the explicit transformation behaviour of the metric $g_{\mu\nu}$ is given here

$$g_{\mu\nu}(x) \rightarrow g'_{\mu\nu}(x') = g_{\alpha\beta}(x) J_\mu^\alpha J_\nu^\beta. \quad (3.29)$$

To argue that GR is invariant under general coordinate transformations one can pursue the following two ways:

At first a short analysis of Einstein's equations eq. (3.16): Involved quantities are scalars (Λ, G and c^4) and rank four tensors ($G_{\mu\nu}, g_{\mu\nu}$ and $T_{\mu\nu}$). The former don't transform and the latter transform identically s.t. the two appearing Jacobian's (normal and inverse) can be factored out which gives Einstein's equations in the new coordinates x' again.

Second a check of the Einstein-Hilbert action eq. (3.22). Here one has two quantities:

- As mentioned before the 4D volume element d^4x alone isn't invariant. A transformation of a volume element always acquires a determinant of the corresponding Jacobian matrix. With this fact and using eq. (3.29) follows that the integral measure

$$\begin{aligned}
 \int d^4x \sqrt{-g} &\rightarrow \int d^4x \sqrt{-\det(g'_{\mu\nu})} \left| \det \left(\frac{\partial x'^{\sigma}}{\partial x^{\gamma}} \right) \right| \\
 &= \int d^4x \sqrt{-\det(g_{\alpha\beta} J_{\mu}^{\alpha} J_{\nu}^{\beta})} \sqrt{\det(J'_{\gamma}{}^{\sigma})^2} \\
 &= \int d^4x \sqrt{-\det(g_{\alpha\beta} J_{\mu}^{\alpha} J_{\nu}^{\beta})} \sqrt{\det(J'_{\rho}{}^{\sigma} J'_{\gamma}{}^{\rho})} \\
 &= \int d^4x \sqrt{-g} \underbrace{\sqrt{\det(J_{\mu}^{\alpha}) \det(J'_{\rho}{}^{\sigma})}}_{=1} \underbrace{\sqrt{\det(J_{\nu}^{\beta}) \det(J'_{\gamma}{}^{\rho})}}_{=1} \\
 &= \int d^4x \sqrt{-g}
 \end{aligned} \tag{3.30}$$

is in total invariant.

- The integrand $\frac{1}{2\kappa}(R - 2\Lambda)$ only consists of scalars and is therefore invariant.

Therefore the Einstein-Hilbert action is also invariant under general coordinate transformations.

Diffeomorphism invariance

Another possibility of expressing the absence of prior geometry in GR is diffeomorphism invariance. The advantage of this representation is the facility of a more clear treatment of mathematical implications. Also the real key feature of GR seems to be more apparent. To that end let's begin with a qualitative perspective: Suppose a physical system is described by a manifold M endowed with a metric $g_{\mu\nu}$ and some matter denoted by a matter field Ψ . Then diffeomorphism invariance means that given a group of diffeomorphisms ϕ_{λ} with pushforwards ϕ_{λ}^* one gets two representations of the system, namely $(M, g_{\mu\nu}, \Psi)$ and $(M, \phi_{\lambda}^* g_{\mu\nu}, \phi_{\lambda}^* \Psi)$, which are *physically equivalent*. This is exactly the idea behind a gauge symmetry and not surprisingly the one-parameter group of diffeomorphisms is the gauge group of GR. As seen in section 2.2 this entails a very careful treatment when quantizing gravity: Gauge equivalent configurations must be sorted out

in the path integral using the Faddeev-Popov procedure, i.e. a gauge-fixing and a ghost action have to be introduced. This will be done in [section 5.3](#).

In a final step the diffeomorphism invariance of GR is shown. For this reason have a look on the Einstein-Hilbert action eq. (3.22) again. Interestingly the integral measure isn't invariant under diffeomorphisms, but indeed the 4D volume element is, since the coordinates don't change. The integrand is a composition of scalars which can be abbreviated as $S := \frac{1}{2\kappa}(R - 2\Lambda)$. According to eq. (3.13) an infinitesimal diffeomorphism changes the metric as

$$g_{\mu\nu} \rightarrow g'_{\mu\nu} = g_{\mu\nu} + \delta g_{\mu\nu} \quad (3.31)$$

with $\delta g_{\mu\nu} = \mathcal{L}_\eta g_{\mu\nu}$. Therefore diffeomorphism invariance is encoded in demanding

$$\delta S_{\text{EH}} = \mathcal{L}_\eta S_{\text{EH}} \stackrel{!}{=} 0. \quad (3.32)$$

Since the Lie derivative satisfies Leibniz' rule on gets

$$\delta S_{\text{EH}} = \int d^4x \mathcal{L}_\eta (\sqrt{-g}S) = \int d^4x \left((\mathcal{L}_\eta \sqrt{-g})S + \sqrt{-g}(\mathcal{L}_\eta S) \right). \quad (3.33)$$

For the 1st term holds using $\delta\sqrt{-g} = \frac{1}{2}\sqrt{-g}g^{\mu\nu}\delta g_{\mu\nu}$ and $\delta g_{\mu\nu} = \mathcal{L}_\eta g_{\mu\nu}$

$$\mathcal{L}_\eta \sqrt{-g} = \frac{\sqrt{-g}}{2}g^{\mu\nu}\mathcal{L}_\eta g_{\mu\nu}. \quad (3.34)$$

The Lie derivative of the metric (given in eq. (3.14)) can be expressed with covariant derivatives if the underlying manifold is torsion-free ($T_{\mu\nu}^\alpha = 0$) and has an affine connection ($\mathcal{D}_\alpha g_{\mu\nu} = 0$), which is justified for GR, as $\mathcal{L}_\eta g_{\mu\nu} = \mathcal{D}_\mu \eta_\nu + \mathcal{D}_\nu \eta_\mu$, s.t.

$$\mathcal{L}_\eta \sqrt{-g} = \frac{\sqrt{-g}}{2}(g^{\mu\nu}\mathcal{D}_\mu \eta_\nu + g^{\mu\nu}\mathcal{D}_\nu \eta_\mu) = \sqrt{-g}(\mathcal{D}_\mu \eta^\mu) \quad (3.35)$$

holds. The 2nd term in eq. (3.33) can be obtained by considering the Lie derivative of a scalar field which is simply

$$\mathcal{L}_\eta S = (\eta^\mu \mathcal{D}_\mu)S. \quad (3.36)$$

Combining eqs. (3.35), (3.36) and (3.33) and using the covariant Gauss' law leads to

$$\begin{aligned} \delta S_{\text{EH}} &= \int d^4x \sqrt{-g} \left(\eta^\mu \mathcal{D}_\mu S + S \mathcal{D}_\mu \eta^\mu \right) = \int d^4x \sqrt{-g} \mathcal{D}_\mu (S \eta^\mu) \\ &= \int d^3A_\mu (S \eta^\mu), \end{aligned} \quad (3.37)$$

wherein d^3A_μ is the 3D surface element. The boundary condition $\eta^\mu = 0$, i.e. a shift along η^μ on the boundary vanishes, finally entails the desired result $\delta S_{\text{EH}} = 0$.

4 The Functional Renormalization Group

This chapter is dedicated to the Functional renormalization group (FRG). In principle FRG is a continuation of Wilson's idea of the renormalization group (RG) which presumes the known functional methods of QFT (c.f. [section 2.1](#)). The result is a method which allows to construct a smooth flow from the quantum laws on a microscopic scale to physically observable phenomenons on macroscopic scales. The mathematical cornerstone of FRG is the Wetterich equation, named after the german physicist Christof Wetterich who found this equation in 1993 [9]. It describes the flow of a scale-dependent effective action between two (micro- and macroscopic) scales. All introductory physical and mathematical ideas are presented in the next four sections. The primarily sources are [58, 60, 76, 77].

4.1 Ideas behind renormalization

Basically there two ways of approaching the renormalization procedure: The somehow technical and a bit mysterious way or the more intuitive and physical way. Both ideas are shown in this section, where the ordering is historically oriented.

Technical approach

In perturbation theory the problem of infinities arises when going beyond tree-level Feynman diagrams. Consider a crucial example in QED: Evaluating the photon propagator at 1-loop order gives diagrammatically¹

$$\mu \text{---} \text{---} \text{---} \nu \Big|_{1\text{-loop}} = \mu \text{---} \text{---} \text{---} \nu + \mu \text{---} \text{---} \text{---} \nu \quad (4.1)$$

Obviously the photon propagator $G_{\mu\nu}(p)$ gets modified by an additional electron/positron pair

$$G_{\mu\nu}(p) \rightarrow G'_{\mu\nu}(p) = G_{\mu\nu}(p) + G_{\mu\lambda}(p) \Pi^{\lambda\sigma}(p) G_{\sigma\nu}(p), \quad (4.2)$$

¹This Feynman diagram was created with the TikZ-Feynman package for L^AT_EX [78], all others were made using the TikZ package itself.

with the vacuum polarization tensor

$$\Pi^{\lambda\sigma}(p) = e^2 \int \frac{d^4k}{(2\pi)^4} \text{Tr} \left(\gamma^\lambda \frac{1}{\not{k} - m + i\epsilon} \gamma^\sigma \frac{1}{\not{k} - \not{p} - m - i\epsilon} \right). \quad (4.3)$$

Therein the integral over the loop momentum k produces a divergence for high momenta k (= in the UV) and unfortunately these infinities occur in all QFT's. At this point only a total realignment can rescue QFT as a theoretical concept. The first step after hitting rock bottom is to notice that the parameters (mass m and charge e) in the Lagrangian \mathcal{L} do not equal the observable parameters in measurements. For this consider again the photon propagator at 1-loop: It consists out of an electron/positron pair, s.t. the vacuum gets polarized, which makes it impossible to observe the naked elementary charge e . To distinguish the two types of parameters call quantities in the Lagrangian *bare* (m_0 and e_0) and observable ones *physical* (m and e) parameters.

Now renormalization comes into play: It connects bare and physical parameters in an analytic way to control UV divergencies. The procedure starts with incorporating counterterms (e.g. δm for the mass) in the original Lagrangian \mathcal{L} which compensate for identifying $m = m_0$ at the energy scale where experiments are done. The latter is called a renormalization condition which fixes a physical parameter to its measured value at a certain renormalization scale. This also applies to the so-called wave function renormalization constant Z which arises due to the arbitrariness of the wave function normalization. If a theory is in principle renormalizable this procedure leads to relations between bare and physical quantities and preserves finite results for the latter ones. Finiteness is also ensured by a method called regularization: UV-divergent integrals gain a cut-off Λ s.t. the cut-off dependence replaces a divergence. In this fashion the above diagram leads to $e = \sqrt{Z_3} e_0$ where $Z_3 = 1 - \frac{e^2}{3\pi} \ln \frac{\Lambda^2}{m^2}$ (note that also other diagrams contribute).

At this point have a closer look on the renormalizability of theories. To measure the degree of divergence the so-called superficial degree of divergence D is defined as

$$D = d - [\lambda_0^{(n)}] V - \frac{d-2}{2} E, \quad (4.4)$$

where d is the dimension, $[\lambda_0^{(n)}]$ the mass dimension of the bare coupling λ at order n , V the number of vertices and E is the number of external lines in a certain Feynman diagram for a scalar theory. If additionally all momentum integrals are regularized with a cut-off Λ one can distinct between three cases which concern the behaviour of the amplitude \mathcal{M} of a Feynman diagram (note that there exist exceptions for these rules, which are not discussed here):

1. Superficially divergent: $D > 0 : \mathcal{M} \sim \Lambda^D$
2. Superficially log-divergent: $D = 0 : \mathcal{M} \sim \ln(\Lambda)$
3. Superficially finite: $D < 0 : \mathcal{M} \sim \Lambda^{-|D|}$

Renormalizability	Diagrams/Amplitudes	$[\lambda_0^{(n)}]$
Renormalizable	Number of superficially divergent amplitudes is finite, but they emerge at every order in perturbation theory	$= 0$
Super-renormalizable	Number of superficially divergent Feynman diagrams is finite	> 0
Non-renormalizable	Number of superficially divergent amplitudes is infinite	< 0

Table 4.1: Three classes of theories concerning their renormalizability

This classification can be generalized to other theories. One ends up with three classes of theories which are listed in Table 4.1. Therein the differentiation via $[\lambda_0^{(n)}]$ will play a crucial role when it comes to Quantum Gravity.

Wilson's approach

In contrast to before Wilson's approach is not only a more meaningful way to interpret the somehow cryptic renormalization procedure, but also a rearrangement of the mathematical background. The corresponding formalism is named after Kenneth Geddes Wilson² who supplied several fundamental contributions to what is called the renormalization group (RG) [7, 80, 81, 82, 83, 84, 85, 86].

The procedure begins with restricting the momentum degrees of freedom of some field $\phi(p)$. This can be achieved by only considering momenta smaller than an arbitrary momentum cutoff Λ , s.t. $p^2 \leq \Lambda^2$ holds. Note that Λ is a sharp cutoff, which is the simplest but not the general case (of course the cutoff can also be smooth). Then the generating functional reads

$$Z_\Lambda = \int \mathcal{D}\phi|_\Lambda e^{-S_\Lambda[\phi]}, \quad \text{where } \mathcal{D}\phi|_\Lambda = \prod_{p^2 \leq \Lambda^2} d\phi(p). \quad (4.5)$$

The latter is equivalent to $\phi(p^2 > \Lambda^2) = 0$. After that the cutoff Λ is lowered by an iteration step $\Lambda \rightarrow \Lambda' = b\Lambda$ with $b < 1$. In analog to eq. (4.5) follows for the new generating functional

$$Z_{\Lambda'} = \int \mathcal{D}\phi|_{\Lambda'} e^{-S_{\Lambda'}[\phi]}. \quad (4.6)$$

By performing the iteration step the momentum shell $\Lambda'^2 < p^2 < \Lambda^2$ was integrated out. Also this leads to an effective action $S_{\text{eff},1} = S_{\Lambda'}$ with correction terms for theory parameters (couplings, masses etc.) which compensate the missing high momentum modes. Repeating this iteration step several times and thinking it in a continuous

²Wilson got the Nobel Prize in Physics in 1982 "for his theory for critical phenomena in connection with phase transitions" [79] where he established RG methods

fashion can be used to define the RG. Demonstratively the RG gives a trajectory in the so-called theory space, i.e. the space which is spanned by all operators in the action. The starting point of this trajectory is e.g. given by the high energy scale Λ whereas the endpoint represents the fully renormalized theory. Mathematically the RG is defined via a group equation for the effective action at every iteration step

$$b \frac{d}{db} S_{\text{eff}, \Lambda} = 0. \quad (4.7)$$

To study the scaling behaviour (running) of the coupling constants λ_i one can define the so-called β -functions

$$\beta_i(\lambda) := \Lambda \frac{d}{d\Lambda} \lambda_i, \quad (4.8)$$

which will play an important role for Asymptotic Safety in Quantum Gravity. All considerations up to here can be linked to the renormalizability of a given theory: Consider a coupling constant $\lambda_{n,m}$ in the action S_Λ as prefactor of an operator with $\phi^n(p)$ fields and ∂^m derivatives. For on iteration step $\Lambda \rightarrow b\Lambda$ this coupling scales as

$$\lambda_{n,m} \rightarrow b^{n(\frac{d}{2}-1)+m-d} \lambda_{n,m}. \quad (4.9)$$

Defining $d_{n,m} := n(\frac{d}{2} - 1) + m$ allows to identify three possible cases (cf. [Table 4.2](#)), where the mass dimension of the coupling plays again a crucial role.

$d - d_{n,m}$	Operator	RG behaviour	$[\lambda_{n,m}]$
> 0	relevant	grows for $\Lambda \rightarrow \infty$	> 0
$= 0$	marginal	runs logarithmically for $\Lambda \rightarrow \infty$	$= 0$
< 0	irrelevant	decays for $\Lambda \rightarrow \infty$	< 0

Table 4.2: Three classes of operators under RG transformations

Obviously $[\lambda_{n,m}]$ mediates between the renormalizability of a theory and its behaviour under the RG: A testable theory (at some high energy scale) has to include relevant and marginal couplings, whereas irrelevant couplings must have decayed.

4.2 The Wetterich Equation

To gain an understanding of the FRG one has to internalize Wilson's thought: The transition between two scales arises from integrating over momentum shells. Therefore the core question is how can one make the usual quantities in QFT (effective action Γ etc.) scale-dependent in a way that lowering the scale is equivalent to integrating out momentum shells. A possible answer follows below.

Scale dependence by a cutoff-term

The basic idea is to find an effective action Γ_k which interpolates between two points: On one side the bare unquantized action S_{bare} at some high energy scale $k \rightarrow \Lambda$ and on the other side the full quantum action Γ at a low energy scale $k \rightarrow 0$. A wise starting point is to make all quantities scale-dependent: The action S gains a dependence on the momentum scale k by adding a cutoff-term ΔS_k , s.t. the action gets modified

$$S \rightarrow S + \Delta S_k. \quad (4.10)$$

Let's specify ΔS_k further: For $k \rightarrow 0$ (in the IR) one should regain the effective action Γ . Thus ΔS_k can be understood as a mass term which suppresses the IR modes. This can be generalized to a scale dependent mass term s.t. ΔS_k has to be quadratic in the fields. A quadratic behaviour allows an operator in between the fields to be present, the so-called regulator R_k . To write ΔS_k explicitly consider two properties of R_k : Firstly R_k is assumed to be diagonal in momentum space. Secondly one has to be careful in case of gauge theories: For a background field ϕ and a dynamical field φ the regulator should depend on the background field $R_k = R_k(\phi)$ while the quadratic part consists of φ 's. In addition one ends up with

$$\Delta S_k[\varphi] = \frac{1}{2} \int \frac{d^d q}{(2\pi)^d} \varphi(-q) R_k(\phi)(q) \varphi(q). \quad (4.11)$$

With the modification $S \rightarrow S + \Delta S_k$ all derived quantities gain a k -dependence. For the k -dependent generating and Schwinger functionals follows (cf. eq. (2.13) and eq. (2.15))

$$Z_k[J] = e^{W_k[J]} = \int \mathcal{D}\varphi e^{-S[\varphi] - \Delta S_k[\varphi] + J \cdot \varphi} = \exp\left(-\Delta S_k\left[\frac{\delta}{\delta J}\right]\right) Z[J]. \quad (4.12)$$

Scale-dependent effective action

To actually define a scale-dependent effective action³ Γ_k one can start in analogy to the definition of the effective action (cf. eq. (2.17)), but now the scale-dependence has to be incorporated: The Schwinger functional gains a k -dependence as shown in eq. (4.12). After building the Legendre transform the cutoff-term ΔS_k is subtracted to regain the usual effective action Γ in the limit $k \rightarrow 0$ (= on a microscopic level). Therefore follows

$$\Gamma_k[\phi] := \sup_J (J \cdot \phi - W_k[J]) - \Delta S_k[\phi]. \quad (4.13)$$

From this a modified Quantum E.o.M. can be computed by taking a functional derivative w.r.t. ϕ

$$\frac{\delta \Gamma_k[\phi]}{\delta \phi(x)} \stackrel{(4.13)}{=} J(x) - (R_k \phi)(x), \quad (4.14)$$

³This is also called the *average* effective action

s.t. the regulator R_k comes into play. When proceeding as mentioned in [section 2.1](#) one gets the analogue of eq. (2.20)

$$e^{-\Gamma_k[\phi]} = \int \mathcal{D}\varphi e^{-S[\phi+\varphi] + \frac{\delta\Gamma[\phi]}{\delta\phi} \cdot \phi - \Delta S_k[\varphi]}. \quad (4.15)$$

From this one might extract some high energy scale Λ , at which $\Gamma_{k \rightarrow \Lambda} = S_{\text{bare}}$ holds, by a saddle point approximation. Having Γ_Λ as an initial value one only needs Wetterich's equation to describe the flow of Γ_k .

Regulator $R_k(q)$

To really connect the new scale dependencies to integrating out momentum shells the regulator has to be designed in a certain way. The previous considerations imply three properties which must be fulfilled by the regulator:

1. At a high momentum scale $k \rightarrow \Lambda$ (= on a macroscopic level) the scale-dependent effective action Γ_k should approach the bare classical action S_{bare}

$$\lim_{k \rightarrow \Lambda} \Gamma_k = S_{\text{bare}}. \quad (4.16)$$

Since the regulator term in the modified action is a gaussian integral this can be translated into condition **no. 1**:

$$\lim_{k \rightarrow \Lambda} R_k(q) \rightarrow \infty \quad \text{for } \Lambda \rightarrow \infty, \quad (4.17)$$

because then follows

$$\lim_{k \rightarrow \Lambda} e^{-\Delta S_k[\varphi]} = \delta^d[\varphi] \quad \text{for } \Lambda \rightarrow \infty. \quad (4.18)$$

Additionally this guarantees the saddle point approximation to be reasonable since $\Gamma_{k \rightarrow \Lambda} \rightarrow S + \text{const.}$

2. As mentioned before Γ_k should match Γ for $k \rightarrow 0$,

$$\lim_{k \rightarrow 0} \Gamma_k = \Gamma, \quad (4.19)$$

i.e. when all momentum shells are integrated out the physics is described by a quantum effective action Γ . When looking on eq. (4.11) and eq. (4.13) this can obviously be achieved for condition **no. 2**

$$\lim_{k^2/q^2 \rightarrow 0} R_k(q) = 0. \quad (4.20)$$

Note that $k \rightarrow 0$ in eq. (4.20) is not sufficient since then it would be possible that $R_k(q) > 0$ for $k \rightarrow 0$ and $q \rightarrow \infty$.

3. In the IR the cutoff-term ΔS_k acts like a suppressing mass term and therefore should stay finite. An IR limit must be again constructed by the momentum scale k and the momentum q . Then one obtains as condition **no. 3**

$$\lim_{q^2/k^2 \rightarrow 0} R_k(q) > 0, \quad (4.21)$$

which is a regularisation for IR divergencies.

More details concerning the regulator $R_k(q)$ are presented in [section 4.3](#).

RG-time t

The momentum scale k can be converted into a dimensionless scale which is extremely useful to simplify calculations. The result is called the RG-time t . For this take the fixed momentum scale Λ and define

$$t := \ln \left(\frac{k}{\Lambda} \right). \quad (4.22)$$

For the partial derivative w.r.t. the RG-time follows

$$\frac{\partial}{\partial t} \equiv \partial_t = \frac{\partial k}{\partial t} \frac{\partial}{\partial k} \stackrel{(4.22)}{=} k \frac{\partial}{\partial k}. \quad (4.23)$$

However a dot over a quantity denotes a partial derivative w.r.t. the RG-time, e.g. $\dot{R}_k = \partial_t R_k$.

Derivation of Wetterich's equation

The Wetterich equation is a flow equation for the scale-dependent effective action Γ_k , which determines the behaviour of Γ_k when changing the dimensionless momentum scale t . At first let's fix some notation. For a scalar field ϕ in d dimensions call

$$\Gamma_k^{(n)}(x_1, \dots, x_n) := \frac{\delta^n \Gamma_k[\phi]}{\delta \phi(x_1) \dots \delta \phi(x_n)} \quad (4.24)$$

the n -th vertex. Hence let's start with the computation of the connected 2-point function, i.e. the propagator (cf. eq. (2.16))

$$G_k(x, y) \equiv W_k^{(2)}(x, y) = \frac{\delta^2 W_k}{\delta J(x) \delta J(y)} = -\phi(x) \phi(y) + \langle \varphi(x) \varphi(y) \rangle_J, \quad (4.25)$$

where again

$$\frac{\delta W_k[J]}{\delta J(x)} = \langle \varphi(x) \rangle_J = \phi(x). \quad (4.26)$$

Now calculate the partial derivative of Γ_k w.r.t. the RG-time t . For this assume again that the evaluation is made at $J = J_{\text{sup}}$ and for fixed fields ϕ . Also note that all RG-time

derivatives ∂_t only hit k -dependent quantities. Thus

$$\begin{aligned}
 \partial_t \Gamma_k[\phi] &= \phi \cdot (\partial_t J) + J \cdot \underbrace{(\partial_t \phi)}_{=0} - \partial_t W_k[J] \Big|_{\phi} - \partial_t (\Delta S_k[\phi]) \\
 &= \phi \cdot (\partial_t J) - \underbrace{\frac{\delta W_k[J]}{\delta J} \cdot (\partial_t J)}_{\stackrel{(4.26)}{=} 0} - \partial_t W_k[J] \Big|_J - \partial_t (\Delta S_k[\phi]) \\
 &= -\partial_t W_k[J] \Big|_J - \partial_t (\Delta S_k[\phi]).
 \end{aligned} \tag{4.27}$$

The scale derivative of $W_k[J]$ can be obtained with the help of eq. (4.12)

$$\partial_t W_k[J] = \partial_t \ln(Z_k[J]) \stackrel{(4.12)}{=} -\frac{1}{Z_k[J]} \int \mathcal{D}\varphi \partial_t (\Delta S_k[\varphi]) e^{W_k[J]}. \tag{4.28}$$

Plugging in eq. (4.11) and using eq. (4.25) leads to

$$\begin{aligned}
 \partial_t W_k[J] &= -\frac{1}{2} \int \frac{d^d q}{(2\pi)^d} (\partial_t R_k(q)) \underbrace{\left(\frac{1}{Z_k[J]} \int \mathcal{D}\varphi \varphi(-q) \varphi(q) e^{W_k[J]} \right)}_{=\langle \varphi \varphi \rangle} \\
 &= -\frac{1}{2} \int \frac{d^d q}{(2\pi)^d} (\partial_t R_k(q)) G_k(q) - \partial_t \underbrace{\left(\frac{1}{2} \int \frac{d^d q}{(2\pi)^d} \phi R_k \phi \right)}_{\stackrel{(4.11)}{=} \Delta S_k[\phi]} \\
 &= -\frac{1}{2} \int \frac{d^d q}{(2\pi)^d} (\partial_t R_k(q)) G_k(q) - \partial_t (\Delta S_k[\phi]),
 \end{aligned} \tag{4.29}$$

where $G_k(q)$ is the propagator in momentum space. When inserting eq. (4.29) into eq. (4.27) the cutoff-terms cancel out and one is left over with

$$\partial_t \Gamma_k[\phi] = \frac{1}{2} \int \frac{d^d q}{(2\pi)^d} (\partial_t R_k(q)) G_k(q). \tag{4.30}$$

In purpose to eliminate the propagator $G_k(q)$ one needs two functional derivative identities. Deriving them in position space yields:

1. Take the Quantum E.o.M. (4.14) and build a functional derivative w.r.t. ϕ

$$\frac{\delta J(x)}{\delta \phi(y)} = \frac{\delta^2 \Gamma_k[\phi]}{\delta \phi(x) \delta \phi(y)} + R_k(x, y) = \Gamma_k^{(2)}[\phi] + R_k(x, y) \tag{4.31}$$

2. Begin with eq. (4.26) and take now a functional derivative w.r.t. J

$$\frac{\delta \phi(y)}{\delta J(z)} = \frac{\delta^2 W_k[J]}{\delta J(y) \delta J(z)} \stackrel{(4.25)}{=} G_k(y, z). \tag{4.32}$$

Combining eq. (4.31) and eq. (4.32) leads to

$$\begin{aligned}\delta^d(x-z) &= \frac{\delta J(x)}{\delta J(z)} = \int d^d y \frac{\delta J(x)}{\delta \phi(y)} \frac{\delta \phi(y)}{\delta J(z)} \\ &= \int d^d y (\Gamma_k^{(2)}[\phi] + R_k)(x, y) G_k(y, z),\end{aligned}\quad (4.33)$$

which implies the operator equation

$$\mathbb{1} = (\Gamma_k^{(2)} + R_k) G_k. \quad (4.34)$$

The latter can be easily translated into momentum space

$$G_k(q) = (\Gamma_k^{(2)}(q) + R_k(q))^{-1}. \quad (4.35)$$

Inserting eq. (4.35) into eq. (4.30) finally leads to:

$$\partial_t \Gamma_k[\phi] = \frac{1}{2} \text{STr} \left(\partial_t R_k \frac{1}{\Gamma_k^{(2)}[\phi] + R_k} \right) \quad \textbf{Wetterich equation} \quad (4.36)$$

Therein the supertrace STr denotes an integral over the loop momentum combined with a trace over all open indices.

Key properties of Wetterich's equation

After having derived the Wetterich equation let's discuss some of its important properties:

1. **It is exact:** The deviation was made without any approximations. Only finding a solution requires an approximation scheme in non-trivial cases.
2. **It is a functional differential equation:** In contrast to many cases in QFT Wetterich's equation doesn't contain any functional integrals.
3. **Solution = Trajectory in theory space:** The theory space is the space of action functionals spanned by all (in principle infinite) field operator invariants. Every operator is dressed with a corresponding (dimensionless) coupling c_i . Therefore the infinite dimensional theory space is spanned by all these couplings c_i . A truncated system has a finite dimensional theory space $\{c_1, \dots, c_n\}$ (cf. coordinate system in Figure 4.1). The solution of Wetterich's equation is nothing but the RG trajectory in this theory space with the fixed endpoints defined in eq. (4.16) and eq. (4.19) (cf. Figure 4.1: blue and red points).
4. **Endpoints of RG trajectory are regulator-independent:** Per definition of the regulator the endpoints of the RG trajectory are fixed. The evident regulator dependence of the Wetterich equation only causes different trajectories for different regulators (cf. Figure 4.1: black and grey lines). Again a truncated system behaves differently: The endpoint $\Gamma_{k \rightarrow 0}$ then depends on the chosen regulator and one has to be careful to distinguish between physical results and computational artefacts.

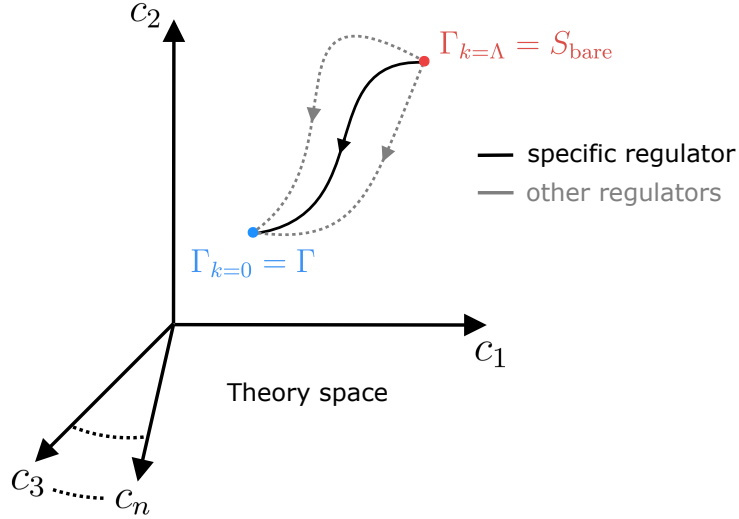


Figure 4.1: RG trajectories in the theory space $\{c_1, \dots, c_n\}$ with the starting point $\Gamma_{k=\Lambda} = S_{\text{bare}}$ and the endpoint $\Gamma_{k=0} = \Gamma$ for several regulators

5. **Perturbation theory is retrievable:** As hopefully expected one can regain perturbation theory out of Wetterich's equation by supposing a loop expansion

$$\Gamma_k = S + \Gamma_{k,1\text{-loop}} + \mathcal{O}(2\text{-loop}). \quad (4.37)$$

Plugging in eq. (4.37) into the Wetterich equation gives at 1-loop order

$$\partial_t \Gamma_{k,1\text{-loop}} = \frac{1}{2} \text{Tr} \left(\partial_t R_k \frac{1}{S^{(2)} + R_k} \right) = \frac{1}{2} \partial_t \text{Tr} \ln(S^{(2)} + R_k), \quad (4.38)$$

since on the RHS the 1-loop nature of Wetterich's equation demands to replace $\Gamma_k^{(2)}$ by $S^{(2)}$. This directly implies

$$\Gamma_{k,1\text{-loop}} = S + \frac{1}{2} \text{Tr} \ln S^{(2)} + \text{const.}, \quad (4.39)$$

which is the usual approximation for the 1-loop effective action (cf. eq. (2.23)).

Diagrammatic Wetterich equation

To create a diagrammatic representation of Wetterich's equation in Feynman's fashion one has to define the building blocks at first:

1. The *full* propagator $G_k \stackrel{(4.34)}{=} (\Gamma_k^{(2)} + R_k)^{-1}$ is depicted by a single line with the common filled dot which will be dropped later (to improve readability):

$$G_k = \text{---} \bullet \text{---} \quad (4.40)$$

2. A supertrace STr connects origin and tail of a full propagator to a loop:

$$\text{STr}(G_k) = \text{---} \bullet \text{---} \text{---} \bullet \text{---} \quad (4.41)$$

3. Any regulator insertion $\partial_t R_k$ is illustrated by a crossed dot:

$$\partial_t R_k = \otimes \tag{4.42}$$

Altogether one obtains:

$$\partial_t \Gamma_k[\phi] = \frac{1}{2} \text{ (diagram of a loop with a crossed dot at the top and an orange dot at the bottom) } \quad \text{Diagrammatic Wetterich equation} \tag{4.43}$$

4.3 Regulator and shape function

In this section a more profound insight into the regulator and its technical details is given.

More properties of the regulator

To get a feeling for what the regulator really does consider two of its properties:

1. As already seen in eq. (4.21) the regulator $R_k(q)$ provides an IR regularisation. Thus all momentum modes with $q^2 < k^2$ get suppressed and the regulator $R_k(q)$ has to be positive in this regime. When approaching $q^2 \approx k^2$ its value turns and then tends to zero for $q^2 > k^2$ which ensures that high momentum modes are not integrated out (cf. green curve Figure 4.2 and blue curve Figure 4.3).
2. In the Wetterich equation one always gets a $\partial_t R_k(q)$ insertion. This quantity features a peak at $q^2 \approx k^2$ (cf. red curve in Figure 4.2 and yellow curve in Figure 4.3). At exactly this point Wilson's idea is contained: In the neighbourhood of $q^2 \approx k^2$ momentum shells are integrated out.

Introducing the shape function

When it comes to actual calculations one can once again simplify all computations by rendering quantities dimensionless (as e.g. the RG-time t). In case of the regulator $R_k(q)$ this can be done by introducing the so-called shape function

$$r = r\left(\frac{q^2}{k^2}\right) \tag{4.44}$$

with a dimensionless argument. The simplest way of connecting the shape function r with the regulator R_k is

$$R_k(q^2) = q^2 r\left(\frac{q^2}{k^2}\right), \tag{4.45}$$

which only ensures the right dimension of R_k . In our case a more efficient choice for computations is made with

$$R_k(q^2) \propto \Gamma_k^{(2)}(q^2) r\left(\frac{q^2}{k^2}\right), \tag{4.46}$$

since the denominator of Wetterich's equation contains $\Gamma_k^{(2)} + R_k$. Independently of the explicit connection between regulator and shape function all conditions for the regulator transfer completely to the shape function.

Different shape functions

Depending on how the calculation is explicitly done, i.e. analytically or numerically, a wise choice for the shape function has to be made. In the following two reasonable shape functions are listed:

1. **Litim regulator**⁴ [87]: For analytic calculations a good choice is

$$r_{\text{Litim}}(s) = \left(\frac{1}{s} - 1 \right) \Theta(1 - s). \quad (4.47)$$

wherein $s = q^2/k^2$ is an abbreviation (cf. Figure 4.2). But the non-analytic Θ -function spoils the usefulness for numerical computations.

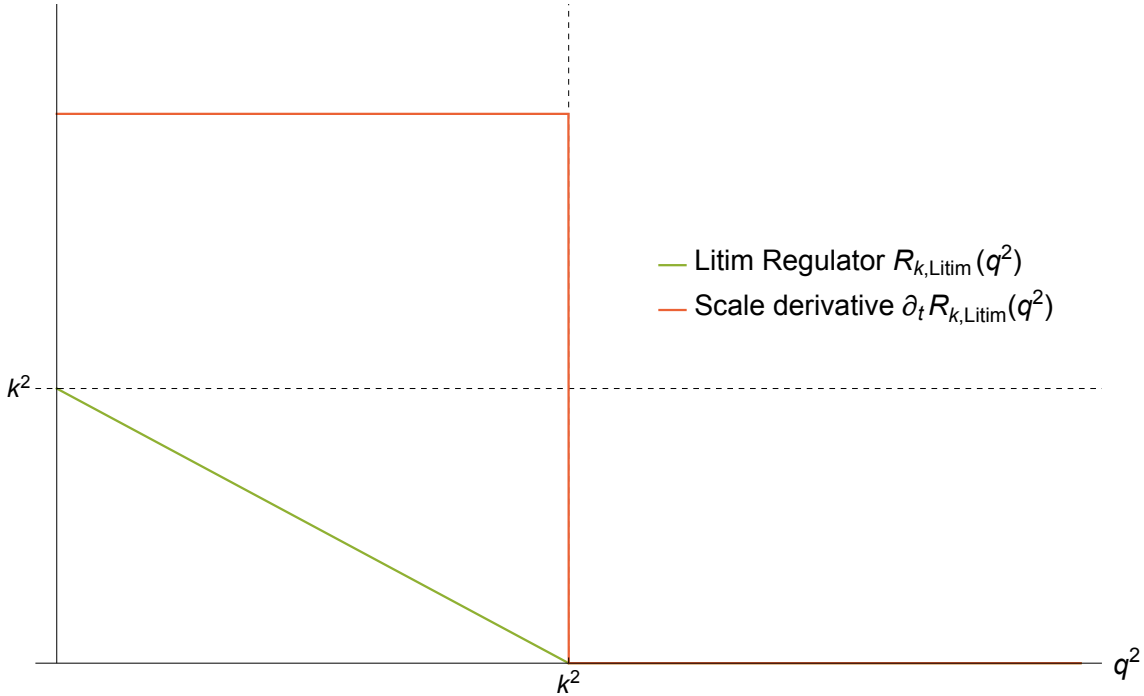


Figure 4.2: Litim Regulator $R_{k,\text{Litim}}(q)$ and its scale derivative $\partial_t R_{k,\text{Litim}}(q)$

2. **Exponential regulator:**

$$r_{\text{exp}}(s) = \frac{1}{s(2e^{s^a} - 1)}, \quad (4.48)$$

with $a \in \mathbb{R}^+$ (cf. Figure 4.3). In contrast to the Litim regulator this ansatz is more efficient for numerical calculations.

⁴The Litim regulator is also often called the *optimized* regulator

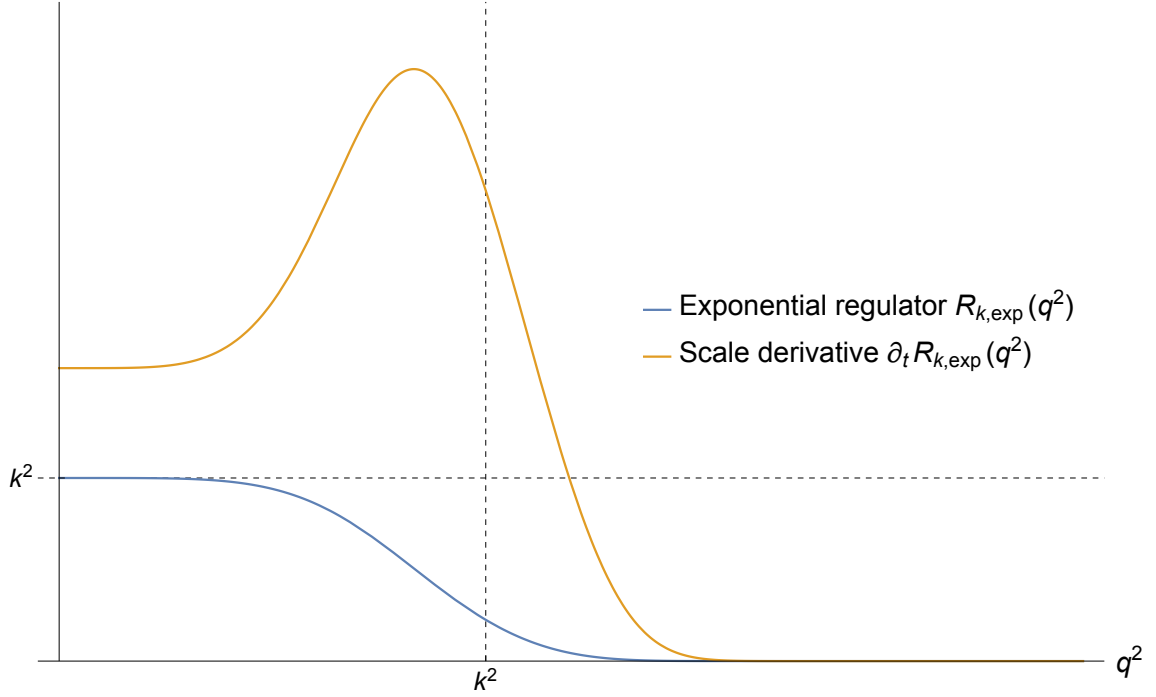


Figure 4.3: Exponential Regulator $R_{k,\text{exp}}(q)$ and its scale derivative $\partial_t R_{k,\text{exp}}(q)$

4.4 Truncation schemes

Since analytic solutions of Wetterich's equation rarely exist one has to think about approximation schemes. The basic idea is to define a systematic expansion which is truncated at some point. Therefore these schemes are also often called *truncations*. Note that it is necessary to relate all arose quantities up to the last order which is not truncated. This ensures the consistency of flow equations, i.e. all expansion terms will contribute in the flow equations. The so-called vertex expansion will be used in this thesis.

Vertex expansion

The scale-dependent action $\Gamma_k[\phi]$ is expanded in powers of field derivatives of itself, i.e. in vertices $\Gamma_k^{(n)}$. Of course this idea comes from the usual Taylor expansion. Again for one real scalar field ϕ in d dimensions one gets

$$\Gamma_k[\phi] = \sum_{n=0}^{\infty} \frac{1}{n!} \int \mathbf{d}^d x_1 \dots \mathbf{d}^d x_n \Gamma_k^{(n)}(x_1, \dots, x_n) \phi(x_1) \dots \phi(x_n). \quad (4.49)$$

Plugging in eq. (4.49) into the Wetterich equation leads to flow equations for the vertices $\Gamma_k^{(n)}$. Note that since the Wetterich equation is a closed loop equation every vertex $\Gamma_k^{(n)}$ depends on the set of vertices $\{\Gamma_k^{(2)}, \dots, \Gamma_k^{(n+2)}\}$.

5 Quantum Gravity

Having introduced QFT as *the* theoretical concept for particles and their fundamental interactions (physics at small length scales) and GR as *the* theory for gravity (at high length scales) one can directly ask if there exists a way to describe GR's gravity on a fundamental level, i.e. if gravity can be quantized. This question is not only important from a theoretical point of view, but also from a physical sight: E.g. the Schwarzschild solutions of Einstein's equations (uncharged and non-rotating black holes) describe highly dense regions of space-time where effects at small length scales hopefully will clear things up. Today many physicists all over the world investigate this unsolved problem. Hence there exists a plenty of approaches and fully new theoretical concepts, which evolved side by side over the years. In this thesis the path of Asymptotic Safety (AS) is pursued. Before introducing AS on a mathematical basis a short overview over the difficulty of quantizing gravity is given. The cardinal reference for the following three sections are [6, 13, 88, 89, 90].

5.1 Houston, we've got a problem

To understand what causes the problem consider at first the Einstein-Hilbert action and look on the mass dimension of Newton's coupling.

Illustration with the mass dimension of G

In the case of gravity the coupling constant is the gravitational constant. To analyze renormalizability compute the mass dimension of the gravitational constant $[G]$ and use Table 4.1. In natural units ($\hbar = c = 1$) one has $[m] = [E] = [\frac{1}{t}] = [\frac{1}{x}] = 1$. Thus follows $[g] = 0$, $[R] \sim [\partial_\mu^2 g] \sim [\frac{1}{x^2}] = +2$ and $[\int d^4x] \sim [x^4] = -4$. Looking on eq. (3.18) and demanding $[S_G] = 0$ finally leads to

$$\begin{aligned} [S_G] &= \left[\frac{1}{16\pi} \right] \left[\frac{1}{G} \right] \left[\int d^4x \right] [\sqrt{-g}] [R] \\ \Rightarrow 0 &= 0 + \left[\frac{1}{G} \right] - 4 + 0 + 2 \Leftrightarrow [G] = -2. \end{aligned} \quad (5.1)$$

Obviously $[G] = -2$ corresponds to an irrelevant coupling (cf. Table 4.2) and a non-renormalizable theory (cf. Table 4.1).

Perturbative analysis

Since perturbation theory is usually the preferred concept in QFT the first intuitive attempt to quantize gravity is perturbatively. For this take the pure gravitational action

(cf. eq. (3.18)), add a gauge-fixing and a ghost term and perturb the metric $g_{\mu\nu}$ around an Euclidean background $g_{\mu\nu} = \delta_{\mu\nu} + \epsilon h_{\mu\nu}$ with $h_{\mu\nu}$ being small and $\epsilon^2 \sim G$. After implementing counter terms $\Delta\mathcal{L}$ into the Lagrangian one finds:

1. At 1-loop pure gravity is perturbatively renormalizable.
2. At 2-loop one additional new fundamental constant, i.e. one counter term, is needed to guarantee renormalizability.
3. The perturbation series in G for pure gravity is divergent.
4. Including matter reduces the renormalizability with a new parameter to 1-loop.

The conclusions (2) and (3) uncover the problem: At every order in perturbation theory new counter terms are needed to control the divergencies. Therefore the number of the associated parameters is in total infinite. In principle it is possible to fix the values of infinitely many parameters to construct a renormalizable theory, but practically this is impossible: Every value must be taken from some experiment and of course the claim to conduct infinitely many experiments is senseless.

In addition all considerations lead to a very important (and similarly frustrating) statement: *Perturbatively* Quantum Gravity is non-renormalizable [6, 91]. This directly raises the question if a non-perturbative treatment will keep a satisfying solution, which is one way to begin thinking about Asymptotic Safety.

Two most popular approaches for solving the riddle

Besides many other approaches there are two of them which gain the highest public perception and try to solve other fundamental problems (e.g. grand unification or the hierarchy problem) simultaneously:

1. **String theory:** Instead of point-like particles as fundamental objects one assumes one-dimensional strings (and high dimensional branes on which strings begin and end) to be fundamental. Key features are extra dimensions ($d = 26$ for bosonic and $d = 10$ for fermionic strings), dualities between different string theory types and M-theory as generalization. It's starting point are concepts from QFT, while GR is added afterwards. A very extensive introduction is [92].
2. **Loop quantum gravity:** Beginning with Einstein's interpretation of gravity as deformed space-time geometry space-time itself is assumed to be quantized at the Planck length ($\sim 10^{-35}$ m). In contrast to String theory Loop quantum gravity preserves diffeomorphism invariance and background independence. However there exists no explicit Hamiltonian. Here the 2nd part of [93] can be recommended as a comprehensive and open-source introduction.

Nevertheless and knowing that up to now all approaches didn't solve the problem the route in this thesis is a different one, i.e. the Asymptotic Safety scenario.

5.2 Asymptotic Safety

In this section the Asymptotic Safety (AS) scenario is introduced as an ansatz to solve the quantum gravity problem. It was firstly proposed by Steven Weinberg in 1979 [8].

Why Asymptotic Safety?

Quantum Gravity should make predictions at some high energy scale Λ , i.e. in the UV regime. In this case a quantum theory should in general preserve a coupling λ which tends to a constant value. In QCD one finds $\lambda \rightarrow 0$ for $k \rightarrow \infty$. Hence QCD is an asymptotic free theory. Thereby AS can be thought as an generalization: $\lambda \rightarrow \alpha$ with $\alpha > 0$ for $k \rightarrow \infty$ (in both cases holds $\beta(\lambda) = 0$ for $k \rightarrow \infty$). Then all physical observables don't contain any divergencies. In contrast to perturbation theory all couplings are not necessarily small or striving to zero for $k \rightarrow \infty$. The only requirement is their finiteness for $k \rightarrow \infty$. Consequently non-perturbative methods are needed, which directly leads to the FRG as *the* central mathematical tool of AS.

Fixed point analysis: Fixed point types and stability

In general a fixed point is defined as follows: Let's consider n coupling constants λ_i with $i \in \{1, \dots, n\}$ in some theory. A corresponding non-perturbative β -function $\beta_i(\lambda_1, \dots, \lambda_n) = k \frac{\partial}{\partial k} \lambda_i = \partial_t \lambda_i$ preserves a fixed point $\vec{\lambda}^* = (\lambda_1^*, \dots, \lambda_n^*)^T$ if

$$\beta_i(\lambda_1^*, \dots, \lambda_n^*) = 0 \text{ for all } i \in \{1, \dots, n\}. \quad (5.2)$$

More precisely a fixed point $\vec{\lambda}^*$ is called an

1. **UV fixed point**, if $\vec{\beta}(\vec{\lambda}) \rightarrow \vec{\beta}(\vec{\lambda}^*) = \vec{0}$ for $k \rightarrow \infty$, or an
2. **IR fixed point**, if $\vec{\beta}(\vec{\lambda}) \rightarrow \vec{\beta}(\vec{\lambda}^*) = \vec{0}$ for $k \rightarrow 0$.

Obviously AS is mostly investigating UV fixed points. In perturbation theory one always considers a perturbation series which converges for small couplings λ . This corresponds to the so-called Gaussian fixed point, at which all couplings vanish. In contrast a non-gaussian fixed point can't be reached by perturbation theory and belongs to a non-zero value of the coupling in the UV. Both fixed point types are listed in [Table 5.1](#).

Fixed point type	Coupling behaviour	Coupling type
Gaussian	$\lambda \rightarrow 0$ for $k \rightarrow \infty$	asymptotically free
Non-Gaussian	$\lambda \rightarrow \alpha$ with $\alpha > 0$ for $k \rightarrow \infty$	asymptotically safe

Table 5.1: Two types of fixed points (gaussian and non-gaussian) and their key properties

Having found fixed points λ_i^* doesn't answer all questions. Additionally one has to investigate their stability. Let's exemplify this for two couplings λ_1 and λ_2 with fixed points λ_1^* and λ_2^* . The latter can be thought as extremum values, s.t. a stability analysis

will lead to some matrix similar to the Hessian matrix. Begin with considering small variations $\delta\lambda_1$ and $\delta\lambda_2$ around the fixed points

$$\lambda_1 = \lambda_1^* + \delta\lambda_1, \quad (5.3)$$

$$\lambda_2 = \lambda_2^* + \delta\lambda_2. \quad (5.4)$$

Plugging this into the β -functions, which can be merged into a two component vector $\vec{\beta} = (\beta_1, \beta_2)^T$, gives up to first order in the variations

$$\begin{pmatrix} \beta_1(\lambda_1, \lambda_2) \\ \beta_2(\lambda_1, \lambda_2) \end{pmatrix} = \begin{pmatrix} \beta_1(\lambda_1^*, \lambda_2^*) \\ \beta_2(\lambda_1^*, \lambda_2^*) \end{pmatrix} + \begin{pmatrix} \frac{\partial\beta_1}{\partial\lambda_1} & \frac{\partial\beta_1}{\partial\lambda_2} \\ \frac{\partial\beta_2}{\partial\lambda_1} & \frac{\partial\beta_2}{\partial\lambda_2} \end{pmatrix} \Big|_{\lambda_1^*, \lambda_2^*} \cdot \begin{pmatrix} \delta\lambda_1 \\ \delta\lambda_2 \end{pmatrix} + \mathcal{O}(\delta\lambda_i^2). \quad (5.5)$$

Therein only the 2nd term survives since the 1st term vanishes due to eq. (5.2). The matrix in eq. (5.5) is called the stability matrix B , which is evaluated at the fixed points λ_i^* . In components B is defined as

$$B_{ij} := \frac{\partial\beta_i}{\partial\lambda_j} \Big|_{\lambda_i=\lambda_i^*}. \quad (5.6)$$

As the name suggests the stability matrix allows to determine the stability behaviour of a given fixed point. In that purpose one has to find the eigenvalues b_k of B by solving the eigenvalue equation

$$B \vec{e}_k = b_k \vec{e}_k. \quad (5.7)$$

In general the eigenvalues b_k can be complex, i.e. $b_k = \text{Re}(b_k) + i \text{Im}(b_k)$. Depending on the signs of the real parts of the eigenvalues $\text{Re}(b_k)$ one can distinct three cases which are listed in Table 5.2.

Sign of $\text{Re}(b_k)$	Direction in Theory Space	Flow in Theory Space
$\exists k$ s.t. $\text{Re}(b_k) > 0$	irrelevant	away from UV fixed point
$\exists k$ s.t. $\text{Re}(b_k) < 0$	relevant	towards UV fixed point
$\exists k$ s.t. $\text{Re}(b_k) = 0$	marginal	parallel to UV fixed point

Table 5.2: Three types of signs of $\text{Re}(b_k)$

Therefore the stability matrix is directly related to the three operator classes of RG transformations, which are associated to the couplings (cf. Table 4.2). The last open question concerns the interplay of all eigenvalues b_k , or more precisely the signs of their real parts $\text{Re}(b_k)$: Under which conditions is a fixed point stable? The three possibilities are itemized in Table 5.3.

Signs of $\text{Re}(b_k)$	Fixed point stability
$\text{Re}(b_k) > 0 \forall k$	fully UV repulsive & IR attractive
$\text{Re}(b_k) < 0 \forall k$	fully UV attractive & IR repulsive
$\text{Re}(b_{k_i}) > 0, \text{Re}(b_{k_j}) < 0$	metastable or saddle point

Table 5.3: Three cases for the stability of a fixed point

To ensure a theory with a metastable UV fixed point it is necessary to have at least one attractive direction. But does AS really correspond to the 2nd case in Table 5.3 where all directions are attractive? The answer to this question is: not always. Since irrelevant and marginal directions are associated with decaying operators when taking the UV limit $k \rightarrow \infty$ they can't contribute to the full quantum theory on a fundamental level, but of course a specific truncated action can lead to irrelevant or marginal directions. Thus a metastable fixed point is also a possibility.

Let's discuss this a bit further: Consider a theory space (cf. Figure 5.1¹: blue background) which is spanned by n couplings $\{\lambda_1, \dots, \lambda_n\}$. Assuming that the eigenvalues b_k of the stability matrix B are not degenerated one will get n eigenvalues b_k with $k \in \{1, \dots, n\}$. Now suppose that $i < n$ (with $i > 0$) of them have a negative real part and the remaining $n - i$ have a positive real part. Then one has a metastable fixed point with i relevant directions which are UV attractive (cf. Figure 5.1: Blue, orange and magenta trajectories). The flow of the i relevant directions form a hypersurface in the theory space, the so-called UV critical surface (cf. Figure 5.1: grey surface).

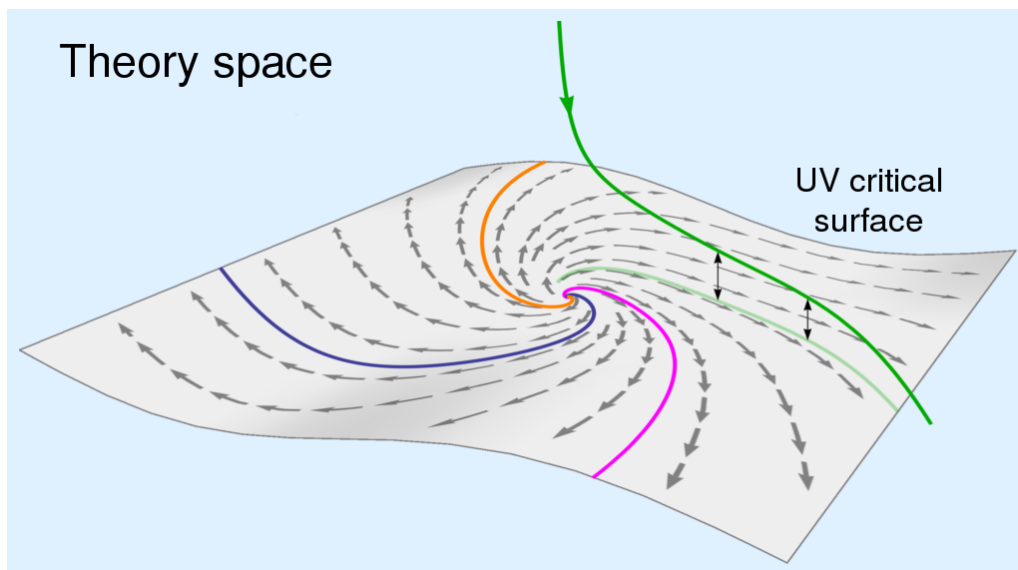


Figure 5.1: UV critical surface in a Theory Space with attractive and repulsive flows; from [94]

¹Note that all arrows indicate the flow from the UV to the IR, s.t. UV attractive directions point away from the fixed point

Therein one can find all renormalizable trajectories, which start from an UV fixed point. Obviously the dimension d of the UV critical surface equals the number of relevant directions $i = d$. The irrelevant and marginal directions (cf. Figure 5.1: green trajectory) flow away from the UV critical surface for $k \rightarrow \infty$, but the projections of them onto the UV critical surface flow towards the fixed point (cf. Figure 5.1: lime green trajectory on the UV critical surface).

The importance of the UV critical surface is even higher: Since each relevant direction corresponds to a coupling, which can be seen as an input parameter and has to be determined by an experiment, the dimension d of the UV critical surface equals the number of experiments that must be done to set up the theory. To avoid the problem of infinitely many measurements which occurred in section 5.1 one has to claim that the dimension of the UV critical surface remains finite. In addition one can conclude that a lower dimension of the UV critical surface increases the predictive power of the underlying theory. Note that mostly a truncated theory contains a finite number of directions by construction, s.t. the finiteness of the UV critical surface is ensured in a trivial sense. Nevertheless there exist approaches as e.g. theories with the usual Einstein-Hilbert action and additional terms which contain powers of the curvature $f(R)$ where the UV critical surface remains finite because only low powers of R lead to relevant directions.

AS paradigm and predictions

In a nutshell the AS program is based on two assumptions which can be summarized in only one sentence:

AS searches for a non-gaussian and attractive UV fixed point with a finite dimensional UV critical surface.

This sentence should be in mind during the whole following analysis. Also it must be checked if the presented model achieves all demands.

The last question one can ask is what does AS predict? To that end look once again on Table 5.2 and Table 5.3: A coupling corresponding to an irrelevant operator is attracted by an IR fixed point, s.t. its value in the IR is *fixed*. So having found an asymptotic safe UV fixed point sets the value of an irrelevant coupling in the UV and flowing on a renormalizable trajectory towards the IR prevents it from changing its value, therefore the exact value is *predicted* by the underlying model. Since the IR, i.e. the low-energy scale, should be accessible within experiments there exists some space for comparing a model with experiments. Examples are the predictions of the top quark mass [95] and the Higgs mass [96] from asymptotically safe theories.

5.3 Asymptotic Safety in pure gravity

The last introductory section is dedicated to the asymptotic safety scenario for pure gravity. After losing a few words about the gauge-fixing and ghost action the basic ideas of the background flow method based on the fundamental contributions made in [88, 10, 11] are presented. From now on the metric signature is changed to the Euclidean signature $g_{\mu\nu} = \text{diag}(+1, +1, +1, +1)$.

Introducing a gauge-fixing condition and action

In gravity the underlying bare action, i.e. the Einstein-Hilbert action (or with higher order tensor structures), is diffeomorphism invariant (cf. eq. (3.32)), which is nothing but the gauge symmetry of the theory. Therefore a clear treatment in the framework of a QFT has to respect the over counting of gauge equivalent field configurations (cf. section 2.2). A convenient ansatz is to split the full metric $g_{\mu\nu}$ into a fixed background metric $\bar{g}_{\mu\nu}$ and a fluctuating metric $h_{\mu\nu}$ (cf. background field procedure, in particular eq. (2.20)). Please note that the fluctuating metric is not necessarily small or does correspond to a perturbative expansion of the full metric, it is just the part of the full metric which fluctuates in some sense. The easiest choice is a linear split, i.e.

$$g_{\mu\nu} = \bar{g}_{\mu\nu} + h_{\mu\nu}. \quad (5.8)$$

Then the fixed background metric instead of the full metric is used for the gauge-fixing and the ghost action. Most commonly the gauge-fixing action reads

$$S_{\text{gf}} = \frac{1}{2\alpha} \int d^4x \sqrt{\bar{g}} \bar{g}^{\mu\nu} \mathcal{F}_\mu \mathcal{F}_\nu, \quad (5.9)$$

where the gauge fixing condition is given by

$$\mathcal{F}_\mu = \bar{D}^\alpha h_{\alpha\mu} - \frac{1}{2} \bar{D}_\mu \bar{g}^{\beta\gamma} h_{\beta\gamma}. \quad (5.10)$$

Therein the gauge fixing parameter α has to be fixed during computations. In [97] it was shown that choosing an axial gauge, i.e. $\alpha \rightarrow 0$, corresponds to a fixed point of the flow. Therefore $\alpha \rightarrow 0$ will be implemented as soon as possible. In the present case $\alpha \rightarrow 0$ only plays a role for the graviton propagator. It can be applied directly after executing the inversion (cf. eq. (4.35)).

A little side note for an actual derivation: To lower and raise indices of 'bar' quantities one needs the background metric \bar{g} .

Deducing the ghost action

To get an expression for the ghost action one has to compute the Faddeev-Popov operator $\mathcal{M}_{\mu\nu}$. Translating the knowledge from section 2.2 to the case of gravity with the metric split where the gauge transformation, i.e. a diffeomorphism generated by a Lie derivative, acts on the full metric and the gauge fixing condition is varied w.r.t. to the fluctuating

field gives

$$S_{\text{gh}} = \int d^4x \sqrt{\bar{g}} \bar{c}^\mu \mathcal{M}_{\mu\nu} c^\nu, \quad (5.11)$$

wherein the Faddeev-Popov operator is now defined via

$$\mathcal{M}_{\mu\nu} c^\nu := \frac{\delta F^\mu}{\delta h_{\alpha\beta}} \mathcal{L}_c(\bar{g}_{\alpha\beta} + h_{\alpha\beta}). \quad (5.12)$$

Note that the Lie derivative acts on the full metric along the tangent vector field which is in this case given by the ghost field c^μ . Since $F \propto h$ the derivative in eq. (5.12) can be executed easily. One only has to symmetrize when taking functional derivatives of metrics w.r.t. metrics, i.e.

$$\frac{\delta g_{\mu\nu}(x_1)}{\delta g_{\alpha\beta}(x_2)} = \frac{1}{2} (\delta_\mu^\alpha \delta_\nu^\beta + \delta_\nu^\alpha \delta_\mu^\beta) \delta(x_1 - x_2). \quad (5.13)$$

Taking a Lie derivative of a fixed tensor gives zero, i.e. $\mathcal{L}_c \bar{g}_{\alpha\beta} = 0$, s.t. in total follows for the 2nd term in eq. (5.12)

$$\mathcal{L}_c(\bar{g}_{\alpha\beta} + h_{\alpha\beta}) = \mathcal{L}_c h_{\alpha\beta} = \mathcal{D}_\alpha c_\beta + \mathcal{D}_\beta c_\alpha. \quad (5.14)$$

Combining both latter statements and doing some math finally leads to

$$\mathcal{M}_{\mu\nu} = \bar{\mathcal{D}}^\alpha (g_{\mu\nu} \mathcal{D}_\alpha + g_{\alpha\nu} \mathcal{D}_\mu) - \bar{\mathcal{D}}_\mu \mathcal{D}_\nu. \quad (5.15)$$

From eq. (5.15) one can directly deduce that the only graviton-ghost interaction vertex is $\Gamma_k^{(hc\bar{c})}$ since $S_{\text{gh}} \propto \bar{c} h c$ and all vertices are derived by taking functional derivatives w.r.t. $h_{\mu\nu}$ at vanishing fields $h = 0$. Furthermore this statement is independent of the concrete chosen gravitational action, i.e. including higher orders does *not* influence this.

Background flow method: Basic ideas and challenges

In principle the theory space of pure gravity is spanned by infinitely many operators (the ones from the Einstein-Hilbert action and higher order terms). Of course a system consisting out of infinitely many terms is incomputable. Therefore one has to truncate the theory space by only considering a few generating tensor structures. The simplest choice is the so-called Einstein-Hilbert truncation where only the cosmological constant and the Ricci scalar are included. Then the two coupling constants Λ and G are converted into scale-dependent couplings Λ_k and G_k . One ends up with

$$S_{\text{EH}} \rightarrow \Gamma_{k,\text{EH}} = \frac{1}{16\pi G_k} \int d^4x \sqrt{g} (2\Lambda_k - R). \quad (5.16)$$

To compute the running of the two theory parameters one should introduce dimensionless couplings by defining

$$g := k^2 G_k \quad \text{and} \quad \lambda := \frac{1}{k^2} \Lambda_k. \quad (5.17)$$

As a next step the wave function renormalization constant of the graviton fluctuating field Z_h is introduced. Its flow is encoded in the graviton anomalous dimension

$$\eta_h := -\frac{\dot{Z}_h}{Z_h}. \quad (5.18)$$

Using eq. (5.16) on both sides of Wetterich's equation (cf. eq. (4.36)) and evaluating at vanishing fields $g = \bar{g}$ leads to flow equations for g , λ and to an equation for η_h . For a sharp-cutoff the former flow equation is simply given by

$$\dot{g} = (2 - \eta_h)g. \quad (5.19)$$

In this system one can find two fixed points:

- Trivial Gaussian fixed point: $(g^*, \lambda^*) = (0, 0)$
- Non-trivial and fully attractive UV fixed point: $(g^*, \lambda^*) \approx (0.3, 0.3)$

However no IR fixed point corresponding to GR can be found. Furthermore it is possible to compute flow trajectories in the two-dimensional theory space by integrating the flow equations numerically. The resulting phase diagram is shown in Figure 5.2.

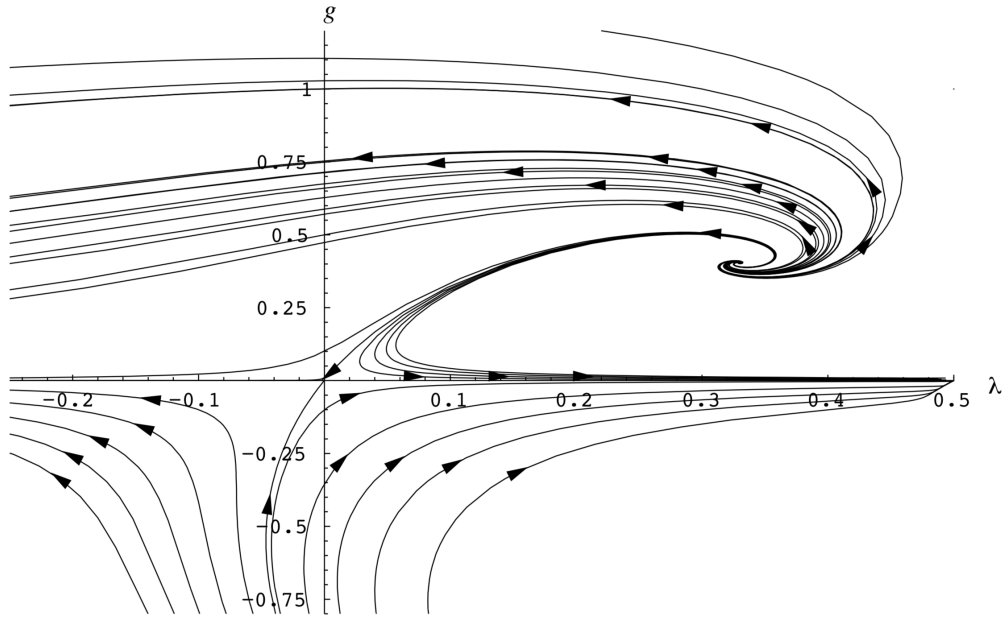


Figure 5.2: Phase diagram of the two dimensional theory space within the Einstein-Hilbert truncation. The arrows point along the RG flow, i.e. in the IR; from [88, p. 32]

At last one word about the dependence of certain quantities on the different metrics g , \bar{g} and h . As usually the symmetry of an underlying QFT is encoded in the effective action as it generates all 1PI diagrams. Unfortunately the metric split complicates the

whole situation: For the gauge-fixing and ghost terms and the regulator the background metric \bar{g} is treated as a constant but at the same time evaluating functional derivatives of the scale-dependent effective action at vanishing fields gives the background metric a scale-dependence. The different dependencies on the metrics are already included in the effective action itself: Unintuitively it is only a functional of two metrics separately, namely the background metric \bar{g} and the fluctuating metric h , s.t. $\Gamma_k = \Gamma_k[\bar{g}, h] \neq \Gamma_k[g = \bar{g} + h]$ holds. These statements can be summed up in the so-called Nielsen or split-Ward identities [10, 15, 98]. They can only be given in a schematic manner due to their highly non-trivial nature, but nevertheless one can extract simple relations to exemplify why the background flow method is basically an approximation. Without respecting the ghost sector one can e.g. write

$$\frac{\delta^2 \Gamma_k[\bar{g}, 0]}{\delta^2 \bar{g}_{\mu\nu}} \approx \left. \frac{\delta^2 \Gamma_k[\bar{g}, h]}{\delta^2 h_{\mu\nu}} \right|_{h=0}, \quad (5.20)$$

where the equality can't be reached due to the statements made so far. These relations should always be in mind when analyzing the impact of diffeomorphism invariance on the investigated system.

Part II

Setup for pure gravity at higher orders

6 Approximations and flow equations

In this chapter the approximations are built up step by step. After having motivated the metric split and its difficulties the vertex expansion is employed to express the scale-dependent effective action Γ_k in terms of vertices. Using this ansatz in Wetterich's equation leads to diagrammatic expressions for the flows of the different n -point vertices. Constructing vertices out of tensor structures and building suitable projectors then allows to extract flow equations for theory parameters.

6.1 Vertex expansion and flow diagrams of the n -point functions

The central tool of the presented approximations is the vertex expansion as an ansatz for Γ_k . Implications and resulting flow diagrams are discussed in this section.

Exploiting the metric split

To use the metric split in actual computations it is necessary to choose a specific background metric. Of course the simplest possible choice is the flat metric, s.t. the identification $\bar{g}_{\mu\nu} = \delta_{\mu\nu}$ can be made and the full metric reads

$$g_{\mu\nu} = \delta_{\mu\nu} + \sqrt{G} h_{\mu\nu}. \quad (6.1)$$

One can ask if choosing a flat background instead of a Minkowskian background, i.e. $\bar{g}_{\mu\nu} = \eta_{\mu\nu}$ is reasonable, particularly in comparison with the Minkowskian nature of special and general relativity. The usual argument in QFT would be that all involved quantities can be Wick rotated from Euclidean to Minkowski space (cf. [section 2.1](#)). However it is not strictly proven that this holds in the case of QG. Research on this question was done in [\[99\]](#). Therein the RG flows of Einstein-Hilbert gravity for an Euclidean and a Minkowskian metric (connected by a Wick rotation) were compared. The result was quite convincing: Both lead to similar UV fixed points and might lie in the same universality class in the UV. Therefore it is expected that the analysis with an Euclidean metric can be extended to a Minkowskian one.

One could also wonder about the \sqrt{G} prefactor in eq. (6.1) for the fluctuating field $h_{\mu\nu}$. Since $[\sqrt{G}] = -1$ the mass dimension of $h_{\mu\nu}$ has to be $[h_{\mu\nu}] = +1$, which appears to be a natural choice due to its bosonic nature.

Setting conventions and diagrammatic representations

At this stage the quantum version of gravity in the background field approximation contains three fields: The fluctuating metric $h_{\mu\nu}$ on one hand and the two ghost field,

i.e. ghosts c and anti-ghosts \bar{c} , on the other hand. To write all following equations in a more readable manner let's define a super-field vector

$$\Phi = (h, c, \bar{c}) \tag{6.2}$$

which unifies all three fields (indices are left out). With this by hand one can write

$$\Gamma_k = \Gamma_k[\bar{g}, \Phi]. \tag{6.3}$$

Thanks to Feynman quite a lot calculations can be done in a diagrammatic way. Since one has to deal with several types of fields and according propagators or vertices a distinction based on the type of a line (permanent, doubled, dashed) and the color (black, blue, red) is made. A full list of involved building blocks is given in Table 6.1. Please note that the sum over the superfield Φ in Wetterich's equation requires a kind of redundant definition for the general vertex.

Building block	Math symbol	Diagrammatic form
• Propagators:		
Superfield	$G_\Phi = (\Gamma_k^{(\Phi\Phi)} + R_k^\Phi)^{-1}$	
Graviton	$G_h = (\Gamma_k^{(2h)} + R_k^h)^{-1}$	
Ghost	$G_{c\bar{c}} = (\Gamma_k^{(c\bar{c})} + R_k^c)^{-1}$	
• Vertices:		
General vertex	$\Gamma_k^{(n \cdot \Phi \ m \cdot c, \bar{c} \ s \cdot h)}$	
• Scale derivatives of regulators:		
In all cases	$\partial_t R_k^\Phi, \partial_t R_k^h$ or $\partial_t R_k^c$	

Table 6.1: Building blocks of flow diagrams

Vertex expansion

As suggested in section 4.4 a reasonable ansatz for the scale-dependent effective action is to expand it in powers of vertices. Since the idea comes from the usual Taylor expansion the result will be a polynomial in Φ as Φ contains the fluctuating fields of Γ_k . As expansion point one should choose the origin, which corresponds to vanishing fields. Thus one is able to write [20]

$$\Gamma_k[\bar{g}, \Phi] = \sum_{i=0}^{\infty} \frac{1}{n!} \Gamma_k^{(n)}[\bar{g}, 0] \Phi^n. \tag{6.4}$$

This identification already tells that the whole following computation must be an approximation since it's impossible to account for arbitrary high powers of Φ .

The sum in eq. (6.4) can be carried out if an ansatz from tensor structures for all needed vertices (for a n level approximation the vertices up to level $(n+2)$ are needed) is made, s.t. some vertices will vanish immediately. For a gauge fixed gravitational theory in the background field approximation the specific form of the vertex generators, i.e. if considering tensor structures from the Einstein-Hilbert action or even higher orders, is unnecessary, s.t. the non-vanishing vertices will be (cf. section 5.3):

1. Arbitrary derivatives w.r.t. the fluctuating metric $h_{\mu\nu}$: $\Gamma_k^{(n-h)} \neq 0 \forall n \in \mathbb{N}$.
2. 2nd derivative w.r.t. the ghost/anti-ghost fields c and \bar{c} : $\Gamma_k^{(c\bar{c})} \neq 0$, which guarantees the existence of a ghost propagator.
3. Graviton/ghost/anti-ghost interaction vertex: $\Gamma_k^{(hc\bar{c})} \neq 0$, which is a desired property of a gauge theory.

All other vertices vanish, s.t. eq. (6.4) can be exploited to

$$\begin{aligned}
 \Gamma_k[\bar{g}, \Phi] &= \Gamma_k[\bar{g}, 0] && \sim \text{graviton background field} \\
 &+ \Gamma_k^{(h)}[\bar{g}, 0] h + \frac{1}{2} \Gamma_k^{(2h)}[\bar{g}, 0] h^2 + \dots && \sim \text{graviton fluctuation field} \\
 &+ \frac{1}{2} \Gamma_k^{(c\bar{c})}[\bar{g}, 0] c\bar{c} && \sim \text{ghost propagator} \\
 &+ \frac{1}{6} \Gamma_k^{(hc\bar{c})}[\bar{g}, 0] h c\bar{c}. && \sim \text{graviton/ghost vertex} \quad (6.5)
 \end{aligned}$$

The precise vertex expansion found in eq. (6.5) can be combined with Wetterich's equation in the following way: For each vertex Wetterich's equation holds and vertices follow from the scale-dependent effective action by taking functional derivatives at vanishing fields. Since all functional derivatives commute with the partial derivative w.r.t. RG time t , i.e.

$$\left[\frac{\delta}{\delta\Phi}, \partial_t \right] \Gamma_k^{(n\Phi)} = 0, \quad (6.6)$$

it is possible to simply take functional derivatives of the whole Wetterich equation to obtain flow equations for all vertices separately. This procedure should be done in a diagrammatic manner, therefore all needed rules are presented below.

Cooking recipe for taking functional derivatives diagrammatically

If one wants to take functional derivatives w.r.t. some field of Wetterich's equation one needs to know which quantities can depend on the fields Φ . To that end look again on Wetterich's equation

$$\partial_t \Gamma_k[\Phi] = \frac{1}{2} \sum_{\Phi} \text{STr} \left(\frac{\partial_t R_k^{\Phi}}{\Gamma_k^{(2\Phi)}[\Phi] + R_k^{\Phi}} \right), \quad (6.7)$$

were now a sum over the superfield is understood, since the regulator is diagonal in this space. Obviously only all n -point functions $\Gamma_k^{(n\Phi)}[\Phi]$ depend on the fields, s.t. only they will be affected when taking functional derivatives.

In all following cases consider quantities which depend on a superfield Φ (denoted by a straight line) and take derivatives w.r.t. another superfield Φ' (denoted by a dashed line).

- Hitting a m -point vertex with n Φ vertices and $s = (m - n)$ Φ' vertices:

– Mathematically:

$$\frac{\delta}{\delta\Phi'} \Gamma_k^{(n\Phi s\Phi')} = \Gamma_k^{(n\Phi (s+1)\Phi')} \quad (6.8)$$

– Diagrammatically:

$$\frac{\delta}{\delta\Phi'} \begin{array}{c} n \\ \diagup \quad \diagdown \\ \cdots \quad \cdots \\ \bullet \\ \diagdown \quad \diagup \\ \Phi' \quad \cdots \\ s \end{array} = \begin{array}{c} n \\ \diagup \quad \diagdown \\ \cdots \quad \cdots \\ \bullet \\ \diagdown \quad \diagup \\ \Phi' \quad \cdots \\ s+1 \end{array} \quad (6.9)$$

- Hitting a propagator:

– Mathematically:

$$\begin{aligned} \frac{\delta}{\delta\Phi'} G_\Phi &= \frac{\delta}{\delta\Phi'} (\Gamma_k^{(2\Phi)}[\Phi] + R_k^\Phi)^{-1} \\ &= -(\Gamma_k^{(2\Phi)}[\Phi] + R_k^\Phi)^{-1} \left[\frac{\delta}{\delta\Phi'} (\Gamma_k^{(2\Phi)}[\Phi] + R_k^\Phi) \right] (\Gamma_k^{(2\Phi)}[\Phi] + R_k^\Phi)^{-1} \\ &= -G_\Phi \Gamma_k^{(2\Phi\Phi')} G_\Phi \end{aligned} \quad (6.10)$$

– Diagrammatically this translates into:

$$\frac{\delta}{\delta\Phi'} \begin{array}{c} \Phi \quad \bullet \quad \Phi \\ \hline \end{array} = - \begin{array}{c} \Phi' \\ \vdots \\ \bullet \\ \hline \Phi \quad \bullet \quad \Phi \end{array} \quad (6.11)$$

- Hitting a scale derivative of the regulator:

– Mathematically:

$$\frac{\delta}{\delta\Phi'} (\partial_t R_k^\Phi) = \partial_t \left(\frac{\delta}{\delta\Phi'} R_k^\Phi \right) = 0 \quad \forall \Phi' \quad (6.12)$$

– Diagrammatically:

$$\frac{\delta}{\delta\Phi'} \otimes^\Phi = 0 \quad \forall \Phi' \quad (6.13)$$

Having this by hand the flow diagrams of n -point functions can be derived. In this thesis all involved theory parameters are extracted from the flows of the 2-point flow diagrams (graviton and ghost) and the 3-point flow diagram (graviton). Of course this is an approximation and incorporating higher levels would improve the model, but the computational costs for the 4-point flow diagram are significantly higher and even then closing the flow equations is approximative.


To exemplify the procedure of deriving n -point flow diagrams the graviton 2-point function is computed below. The other flow diagrams can be computed in exactly the same manner and are therefore presented without a detailed derivation.

Derivation of the flow diagrams of the graviton 2-point function

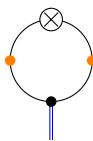
Begin with the diagrammatic representation of Wetterich's equation with a sum over the superfield $\Phi = (h, c, \bar{c})$:

$$\partial_t \Gamma_k = \frac{1}{2} \sum_{\Phi} \text{Diagram} \quad (6.14)$$

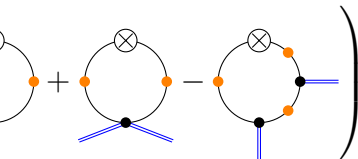

Then take two functional derivatives w.r.t. the graviton field h on both sides. On the LHS one directly gets:

$$\frac{\delta}{\delta h} \frac{\delta}{\delta h} (\partial_t \Gamma_k) = \partial_t \Gamma_k^{(2h)} = \partial_t (\text{Diagram})^{-1} \quad (6.15)$$


The RHS is a bit more complex. Taking the 1st derivative is still quite simple:

$$\frac{\delta}{\delta h} \left(\frac{1}{2} \sum_{\Phi} \text{Diagram} \right) = -\frac{1}{2} \sum_{\Phi} \text{Diagram} \quad (6.16)$$


Now the 2nd derivative: One can hit the left propagator, the vertex or the right propagator:

$$\frac{\delta}{\delta h} \left(-\frac{1}{2} \sum_{\Phi} \text{Diagram} \right) = -\frac{1}{2} \sum_{\Phi} \left(\text{Diagram 1} + \text{Diagram 2} + \text{Diagram 3} \right) \quad (6.17)$$


Of course the 1st and the 3rd diagrams are equal s.t. they can be summed up. Also the diagrams can be graphically rearranged to highlight their belonging to the flow equation of the 2-point function ($\sim \text{propagator}^{-1}$). At last drop the orange dot which signals a full propagator s.t. all lines connecting two vertices or a vertex and a regulator insertion are propagators. Applying all this gives:

$$\frac{\delta^2}{\delta h^2} \left(\frac{1}{2} \sum_{\Phi} \text{Diagram} \right) = -\frac{1}{2} \sum_{\Phi} \text{Diagram 1} + \sum_{\Phi} \text{Diagram 2} \quad (6.18)$$

To evaluate the remaining sums over the superfield Φ one has to consider eq. (6.5) again to cancel out vanishing vertices: The sum over the 1st diagram gives only one contribution, namely that one with a graviton loop and the 2nd diagram gives both contributions, that with a graviton and that with a ghost loop. The latter case has a special feature: Due to the Grassmanian nature of fermions the ghost loop gets a factor of (-1) and additionally a factor of $(+2)$ which takes the exchange symmetry (ghost \leftrightarrow anti-ghost) into account. Therefore in total a factor of (-2) has to be implemented and one ends up with:

$$\frac{\delta^2}{\delta h^2} \left(\frac{1}{2} \sum_{\Phi} \text{circle with } \otimes \right) = -\frac{1}{2} \text{circle with } \otimes \text{ and } \bullet \text{ on bottom} + \text{circle with } \otimes \text{ and } \bullet \text{ on left and right} - 2 \text{circle with } \otimes \text{ and } \bullet \text{ on left and right, dashed red} \quad (6.19)$$

Finally both sides can be combined to obtain the flow of the graviton 2-point function (Flow^(2h) simply denotes the RHS of Wetterich's equation):

$$\partial_t (\text{blue line})^{-1} = -\frac{1}{2} \text{circle with } \otimes \text{ and } \bullet \text{ on bottom} + \text{circle with } \otimes \text{ and } \bullet \text{ on left and right} - 2 \text{circle with } \otimes \text{ and } \bullet \text{ on left and right, dashed red} \equiv \text{Flow}^{(2h)} \quad (6.20)$$

Flow diagrams of the graviton 3-point function

Without further comments the flow diagrams of the graviton 3-point function are presented below:

$$\partial_t \text{3-point vertex} = -\frac{1}{2} \text{circle with } \otimes \text{ and } \bullet \text{ on bottom, 3 lines} + 3 \text{circle with } \otimes \text{ and } \bullet \text{ on left and right, 3 lines} - 3 \text{circle with } \otimes \text{ and } \bullet \text{ on left and right, 3 lines} + 6 \text{circle with } \otimes \text{ and } \bullet \text{ on left and right, 3 lines, dashed red} \equiv \text{Flow}^{(3h)} \quad (6.21)$$

Flow diagrams of the ghost 2-point function

Last but not least the flow diagrams of the ghost 2-point function:

$$\partial_t (\text{dashed red line})^{-1} = \text{circle with } \otimes \text{ and } \bullet \text{ on left and right, dashed red} + \text{circle with } \otimes \text{ and } \bullet \text{ on left and right, solid blue} \equiv \text{Flow}^{(c\bar{c})} \quad (6.22)$$

6.2 Vertex construction

The last missing piece for defining the full theory is an ansatz for each vertex appearing in the vertex expansion. It is of special interest how higher order curvature invariants influence the flows and the fixed points. Therefore one should ask at first why to include them and which of them will be worthwhile.

Why higher order curvature invariants?

In principle there are three main arguments for investigating higher order curvature invariants as input tensor structures in a vertex expansion of Γ_k :

- Investigating a perturbatively renormalizable theory:** The couplings of four-derivative curvature invariants (e.g. R^2 and $R_{\mu\nu}^2$) have mass dimension zero. Therefore the underlying theory is perturbatively renormalizable (cf. Table 4.1 [19]). Furthermore the flows of these couplings are 1-loop universal, i.e. independent of the chosen regulator. In general these types of theories were already analyzed in AS besides the vertex expansion [100, 101, 102].
- Improving on the tensor structures used in the vertex expansion:** In the last couple of years the vertex expansion was upgraded several times and in several directions. In pure gravity this included the investigation of the graviton 2-point flow [16], the graviton 3-point flow [17] and later the graviton 4-point flow [18] within the Einstein-Hilbert truncation, where also the momentum dependence of the involved theory parameters and anomalous dimensions was partly respected. Besides the fact that in all cases an attractive UV fixed point was found a whole slew of other non-trivial results were accomplished: E.g. momentum locality of the graviton 2-point and 3-point flows and effective universality for the avatars of the dynamical version of Newton's coupling G at quantum level [103]. Especially in [18] some research in the direction of higher orders was adjoined: Without including higher order terms directly in the vertices one could expect that they are generated in e.g. the flow of the graviton 4-point vertex, which has an overlap with all higher order terms (testable by possible p^{2n} contributions with $n \geq 2$). Non-trivially only the R^2 tensor structure contributes while all other terms are suppressed (= the highest power of the graviton 4-point flow is p^4 , but a contribution of a $R_{\mu\nu}^2$ term could be excluded due to the p^2 behaviour of the graviton 3-point flow, c.f. [18, pp. 7-8]). Of course a reasonable improvement is to directly include higher order terms in the vertices and again investigate the polynomial structure of the flows.
- Computing beyond graviton 2-point flow:** Within the vertex expansion higher order curvature invariants were already investigated up to the graviton 2-point flow in [104], but not beyond and only with momentum independent couplings and anomalous dimensions. Therein an attractive UV fixed point with only two relevant directions was found. In contrast the 1-loop coefficient of the $R_{\mu\nu}^2$ coupling deviated from the known perturbative result by a factor of ≈ 1.1 and the regulator dependence was not tested, which has to be inquired further.

Including higher order curvature invariants

In general curvature invariants are scalars which are constructed out of curvature tensors like the Riemann tensor $R_{\alpha\beta\gamma\delta}$ (or tensors deduced from it, e.g. the Ricci tensor $R_{\mu\nu}$) or the Weyl tensor $C_{\alpha\beta\gamma\delta}$. By definition curvature invariants are always invariant under diffeomorphisms as they are scalars. The Einstein-Hilbert action comprises the Ricci scalar R as a tensor structure which possesses curvature. As is well-known R includes two derivatives of the metric. Therefore higher order curvature invariants are curvature invariants which exhibit terms with at least four derivatives of the metric.

There are several possibilities of including higher order curvature invariants in the graviton vertices in four space-time dimensions. A decision for a specific ansatz is conditioned by two questions: The first question is how many orders, i.e. how many derivatives of the metric, one wants to include. Of course the main limitation here is given by technical feasibility as each new order comes with exponentially more terms (and taking functional derivatives makes this even worse). In this thesis only tensor structures with at the most four derivatives of the metric are included which is the natural extension of the tensor structures in the Einstein-Hilbert action. At this stage one is left with the following classes of terms:

1. Ricci scalar/tensor squared: $R^2, R_{\mu\nu}^2 = R_{\mu\nu}R^{\mu\nu}$.
2. Riemann tensor squared: $R_{\alpha\beta\gamma\delta}^2 = R_{\alpha\beta\gamma\delta}R^{\alpha\beta\gamma\delta}$.
3. Weyl tensor squared: $C_{\alpha\beta\gamma\delta}^2 = C_{\alpha\beta\gamma\delta}C^{\alpha\beta\gamma\delta}$.
4. Derivative operators acting on scalars, e.g. ΔR .
5. In principle more complicated terms like $R \cdot \ln(\frac{\Delta}{R})$ can be constructed, but won't be considered in this thesis.

In contrast terms with even higher derivatives of the metric, like e.g. R^3 or $R\Delta R$, are excluded. Note that this step is an approximation.

The second question is which of the remaining terms are physically and mathematically relevant. The fourth class of terms, i.e. terms with derivative operators, don't affect the equations of motions since they are total derivatives which will lead to boundary terms. Hence they don't influence physics locally and can be dropped. A closer look on the third class reveals that C^2 can be written as a linear combination of the remaining three terms. After a long calculation one finds in four space-time dimensions that

$$C_{\alpha\beta\gamma\delta}^2 = R_{\epsilon\sigma\rho\eta}^2 - 2R_{\mu\nu}^2 + \frac{1}{3}R^2 \quad (6.23)$$

holds. The two remaining classes are connected via the so-called Gauss-Bonnet term G which is in four space-time dimensions given by

$$G = R^2 - 4R_{\mu\nu}R^{\mu\nu} + R_{\alpha\beta\gamma\delta}R^{\alpha\beta\gamma\delta}. \quad (6.24)$$

The Gauss-Bonnet term G has a very striking feature: Due to the Gauss-Bonnet theorem on a four dimensional manifold M the Gauss-Bonnet term G will lead to a topologically invariant surface term if its included in an action s.t.

$$\int d^4x \sqrt{g} G = f(M) \quad (6.25)$$

holds. Therefore it is possible to represent $R_{\alpha\beta\gamma\delta}^2$ by a linear combination of R^2 , $R_{\mu\nu}^2$ and a topological invariant. Of course it would also be an option to eliminate R^2 or $R_{\mu\nu}^2$ instead of $R_{\alpha\beta\gamma\delta}^2$ but technically all computations are way more easy if one gets rid of complicated tensor structures, i.e. $R_{\alpha\beta\gamma\delta}^2$. Summing up all statements made so far leads to the very general conclusion

$$\begin{aligned} S &= \int d^4x \sqrt{g} (c_1 R^2 + c_2 R_{\mu\nu}^2 + c_3 R_{\alpha\beta\gamma\delta}^2 + c_4 C_{\epsilon\sigma\rho\eta}^2 + c_5 \Delta R) \\ &= \int d^4x \sqrt{g} (c'_1 R^2 + c'_2 R_{\mu\nu}^2) + \text{topological inv.} + \text{boundary term,} \end{aligned} \quad (6.26)$$

with general coefficients $c_1, c_2, c_3, c_4, c_5, c'_1, c'_2$. Thus the tensor structures R^2 and $R_{\mu\nu}^2$ span the space of local curvature invariants with four derivatives of the metric and are the only ones which will additionally be included in the graviton vertices.

About projections and tensor bases

The biggest technical challenge when doing computations in quantum gravity originates from the fact that general relativity features very complex tensor structures. Therefore inverting the graviton 2-point function to obtain the graviton propagator is a complicated task. It is somehow indispensable to decompose the graviton vertices in complete sets of tensor structures. Consider e.g. the flow of the graviton 2-point function: Therein the 3-graviton and 4-graviton vertices are needed which are rank 6 and rank 8 tensors, respectively, with symmetric pairs of indices. Unfortunately there is no known full tensor basis for both of them or even higher order vertices. Only for the graviton 2-point function such a decomposition into a full basis of tensor structures is known: The so-called Stelle decomposition [19], which is closely related to the York decomposition [105]. One can think of the York decomposition as the generalization of the transversal/longitudinal decomposition of vector fields, which is explicitly given by

$$v^\mu = v_\perp^\mu + \mathcal{D}^\mu \phi_L, \quad (6.27)$$

wherein v^μ is a vector field and ϕ_L is a scalar field. In momentum space the decomposition can be expressed via the two projectors (which are rank 2 tensors)

$$\mathcal{P}_{\mu\nu}^T = \delta_{\mu\nu} - \frac{p_\mu p_\nu}{p^2}, \quad \sim \text{transversal projector} \quad (6.28)$$

$$\mathcal{P}_{\mu\nu}^L = \frac{p_\mu p_\nu}{p^2}. \quad \sim \text{longitudinal projector} \quad (6.29)$$

The York decomposition does the same for symmetric rank two tensor fields, in particular the fluctuating metric $h_{\mu\nu}$. One gets out four different modes: A transverse traceless

mode $h_{\mu\nu}^{\text{TT}}$ (= spin two mode), a longitudinal traceless mode h_{μ}^{LT} (= spin one mode), the longitudinal mode h^{LL} and the trace mode h^{Tr} (both = spin zero mode). In analog to eq. (6.27) the decomposition reads (in four space-time dimensions)

$$h_{\mu\nu} = h_{\mu\nu}^{\text{TT}} + \bar{\mathcal{D}}_{\mu} h_{\nu}^{\text{LT}} + \bar{\mathcal{D}}_{\nu} h_{\mu}^{\text{LT}} + \left(\bar{\mathcal{D}}_{\mu} \bar{\mathcal{D}}_{\nu} - \frac{\bar{g}_{\mu\nu}}{4} \bar{\mathcal{D}}_{\alpha} \bar{\mathcal{D}}^{\alpha} \right) h^{\text{LL}} + \frac{\bar{g}_{\mu\nu}}{4} h^{\text{Tr}}, \quad (6.30)$$

where again $\bar{\mathcal{D}}_{\mu}$ denotes the background covariant derivative. Alternatively one can use appropriate projectors, which can be constructed out of the transversal and longitudinal projectors for vectors. They are given by (again only in four space-time dimensions)

$$\mathcal{P}_{\mu\nu\alpha\beta}^{\text{TT}} = \frac{1}{2} (\mathcal{P}_{\mu\alpha}^{\text{T}} \mathcal{P}_{\nu\beta}^{\text{T}} + \mathcal{P}_{\mu\beta}^{\text{T}} \mathcal{P}_{\nu\alpha}^{\text{T}}) - \frac{1}{3} \mathcal{P}_{\mu\nu}^{\text{T}} \mathcal{P}_{\alpha\beta}^{\text{T}}, \quad \sim \text{spin } 2 \quad (6.31)$$

$$\mathcal{P}_{\mu\nu\alpha\beta}^{\text{V}} = \frac{1}{2} (\mathcal{P}_{\mu\alpha}^{\text{T}} \mathcal{P}_{\nu\beta}^{\text{L}} + \mathcal{P}_{\mu\beta}^{\text{T}} \mathcal{P}_{\nu\alpha}^{\text{L}} + \mathcal{P}_{\nu\alpha}^{\text{T}} \mathcal{P}_{\mu\beta}^{\text{L}} + \mathcal{P}_{\nu\beta}^{\text{T}} \mathcal{P}_{\mu\alpha}^{\text{L}}), \quad \sim \text{spin } 1 \quad (6.32)$$

$$\mathcal{P}_{\mu\nu\alpha\beta}^{\text{S}_1} = \frac{1}{3} \mathcal{P}_{\mu\nu}^{\text{T}} \mathcal{P}_{\alpha\beta}^{\text{T}}, \quad \sim \text{spin } 0 \quad (6.33)$$

$$\mathcal{P}_{\mu\nu\alpha\beta}^{\text{S}_2} = \mathcal{P}_{\mu\nu}^{\text{L}} \mathcal{P}_{\alpha\beta}^{\text{L}}. \quad \sim \text{spin } \bar{0} \quad (6.34)$$

As these four projectors span the space of symmetric rank two tensors they fulfill a completeness relation, i.e. for a symmetric rank two tensor $z^{\mu\nu} = z^{\nu\mu}$ follows

$$(\mathcal{P}_{\mu\nu\alpha\beta}^{\text{TT}} + \mathcal{P}_{\mu\nu\alpha\beta}^{\text{V}} + \mathcal{P}_{\mu\nu\alpha\beta}^{\text{S}_1} + \mathcal{P}_{\mu\nu\alpha\beta}^{\text{S}_2})^{\mu\nu}{}_{\alpha\beta} z^{\alpha\beta} = \frac{1}{2} (z^{\mu\nu} + z^{\nu\mu}) = z^{\mu\nu}. \quad (6.35)$$

In principle this is fine and up to here the Stelle and York decompositions are identical. But what if one wants to decompose an operator, which acts on a symmetric rank two tensor, s.t. each of its components acts only on the corresponding spin mode? Since the spin zero sector has two different modes one will get a mixing of both of them. This is exactly where the Stelle decomposition comes into play: Two new projection operators are defined, the so-called spin zero transfer operators, which describe the transition between both spin zero modes

$$\mathcal{P}_{\mu\nu\alpha\beta}^{\text{S}_3} = \frac{1}{\sqrt{3}} \mathcal{P}_{\mu\nu}^{\text{T}} \mathcal{P}_{\alpha\beta}^{\text{L}}, \quad (6.36)$$

$$\mathcal{P}_{\mu\nu\alpha\beta}^{\text{S}_4} = \frac{1}{\sqrt{3}} \mathcal{P}_{\mu\nu}^{\text{L}} \mathcal{P}_{\alpha\beta}^{\text{T}}. \quad (6.37)$$

With this six projectors by hand one is now able to fully decompose symmetric rank two tensors in scalar components. Furthermore the graviton 2-point function can be written in a full basis. In matrix form the first four components are aligned along the diagonal of a 4×4 matrix while the two spin zero transfer components are the off-diagonal elements in the lower right 2×2 block matrix (cf. eq. (7.11)).

For later use one last projector is defined: One will discover that the propagator only has a TT and four scalar components (no vector component) after gauge-fixing (cf. eqs. (7.25) and (7.26)). The four scalar components can then be merged to one scalar component by defining a scalar projector $\mathcal{P}_{\mu\nu\alpha\beta}^{\text{S}}$ as the linear combination of all four

scalar components weighted by their factors appearing in the propagator. Forestalling eq. (7.26) leads to the definition

$$\mathcal{P}_{\mu\nu\alpha\beta}^S := \mathcal{P}_{\mu\nu\alpha\beta}^{S_1} + 3\mathcal{P}_{\mu\nu\alpha\beta}^{S_2} + \sqrt{3}\mathcal{P}_{\mu\nu\alpha\beta}^{S_3} + \sqrt{3}\mathcal{P}_{\mu\nu\alpha\beta}^{S_4} \quad (6.38)$$

$$= \frac{1}{3} (3\mathcal{P}_{\mu\nu}^L + \mathcal{P}_{\alpha\beta}^T) (3\mathcal{P}_{\alpha\beta}^L + \mathcal{P}_{\mu\nu}^T). \quad (6.39)$$

Constructing general undressed vertices from tensor structures

As motivated before only the TT and S component of the graviton propagator will play a role. Since diagrams are computed by contracting the indices of all building blocks pairwise and each vertex is contracted with at least one propagator (cf. eqs. (6.20), (6.21) and (6.22)) one can deduce that also for vertices only the TT and S components don't vanish during the computation. E.g. for the 3-graviton vertex this statement can diagrammatically be translated into

$$\begin{aligned} & \text{Vertex} = \text{TT} \text{---} \text{TT} \text{---} \text{TT} + 3 \text{Sc} \text{---} \text{TT} \text{---} \text{TT} + 3 \text{Sc} \text{---} \text{Sc} \text{---} \text{Sc} \\ & + (\text{longitudinal terms} \equiv 0). \end{aligned} \quad (6.40)$$

Therefore it is reasonable to define a new super-field ϕ which separates the graviton fluctuating field $h_{\mu\nu}$ into its two important components $h_{\mu\nu}^{\text{TT}}$ and $h_{\mu\nu}^{\text{S}}$ as

$$\phi := (h^{\text{TT}}, h^{\text{S}}, c, \bar{c}). \quad (6.41)$$

In principle it would also be possible to differentiate between c_μ^{T} and c_μ^{L} , but since the ghost field is only associated to the ghost anomalous dimension and not to a coupling this distinction is omitted.

Now everything is prepared to write down a self-consistent vertex construction, which is a straight forward extension of the Einstein-Hilbert case (e.g. used in [18]): In this thesis the truncated theory space is spanned by four diffeomorphism invariant tensor structures. This set is given by

$$\mathcal{T}_{\text{Diff}} := \left\{ \int d^4x \sqrt{g}, \int d^4x \sqrt{g} R, \int d^4x \sqrt{g} R^2, \int d^4x \sqrt{g} R_{\mu\nu}^2 \right\}. \quad (6.42)$$

It is very important to always have in mind that this definition is exactly the approximation which is investigated in this thesis. As seen before the Faddeev-Popov procedure generated the two non diffeomorphism invariant tensor structures S_{gf} (cf. eq. (5.9)) and S_{gh} (cf. eq. (5.11)), which are summarized in the set

$$\mathcal{T}_{\text{FP}} := \{S_{\text{gf}}, S_{\text{gh}}\}. \quad (6.43)$$

Altogether the set of input tensor structures is then defined as the union of both, i.e.

$$\mathcal{T} := \mathcal{T}_{\text{Diff}} \cup \mathcal{T}_{\text{FP}}. \quad (6.44)$$

Each undressed vertex $\bar{\Gamma}_k^{(\phi_1, \dots, \phi_n)}$ can be computed by taking functional derivatives of all elements in \mathcal{T} w.r.t. to the split super-field ϕ , where each contribution gets its own (in general momentum and scale dependent) coupling constant \tilde{g} . As formula this statement reads

$$\bar{\Gamma}_k^{(\phi_1, \dots, \phi_n)}(p_1, \dots, p_n) := \sum_{\mathcal{T}_i \in \mathcal{T}} \tilde{g}_{\mathcal{T}_i, \phi_1, \dots, \phi_n}(k, p_1, \dots, p_n) \mathcal{T}_i^{(\phi_1, \dots, \phi_n)}(p_1, \dots, p_n). \quad (6.45)$$

This definition ensures that a coupling $\tilde{g}_{\mathcal{T}_i, \phi_1, \dots, \phi_n}$ is not only associated to a tensor structure \mathcal{T}_i , but also to the number and type of functional derivatives $\frac{\delta}{\delta \phi_1} \dots \frac{\delta}{\delta \phi_n}$. Accordingly some couplings are connected to TT components, e.g. $\tilde{g}_{R, h_{\text{TT}}^2}$, some to S components, e.g. \tilde{g}_{R, h_S^2} , and some to mixed components, e.g. $\tilde{g}_{R, h_{\text{TT}} h_S}$.

Up to now everything is very general: The couplings are in principle all different (but related via very complicated Slavnov-Taylor identities) and eq. (6.45) contains both sectors, the gravity and the ghost sector. Let's focus a bit more on the gravity sector. To that end one can define a gravity super-field $\phi' := \{h^{\text{TT}}, h^{\text{S}}\}$. According to eq. (6.45) an undressed graviton n -point function then can be written as (to improve readability the explicit momentum dependencies are dropped from now on)

$$\bar{\Gamma}_k^{(nh)} = \sum_{\phi'_1, \dots, \phi'_n} \sum_{\mathcal{T}_i \in \mathcal{T}} \tilde{g}_{\mathcal{T}_i, \phi'_1, \dots, \phi'_n} \mathcal{T}_i^{(\phi'_1, \dots, \phi'_n)}. \quad (6.46)$$

One could ask where the additional sum over the gravity super-field in eq. (6.46) compared to eq. (6.45) stems from. The answer is already visible in eq. (6.40): While eq. (6.45) describes all vertices with differently projected legs at one specific order (= RHS of eq. (6.40)), eq. (6.46) depicts the full vertex at the same order (= LHS of eq. (6.40)).

Before dressing the vertices one last general comment about the graviton n -point functions: Only for the graviton 2-point function a full basis exists (the Stelle basis) for higher order vertices not. Therefore the four input tensor structures are always an approximation.

Dressing the vertices

As usual in QFTs each field is combined with a wave function renormalization constant Z , which is generally momentum dependent $Z = Z(p^2)$. Commonly each leg of a vertex is attached with a factor of $Z^{\frac{1}{2}}(p^2)$. Here one has to distinct three cases:

- A ghost or anti-ghost leg gets a factor $Z_c^{\frac{1}{2}}(p^2)$,
- A TT-projected graviton leg gets a factor $Z_{h_{\text{TT}}}^{\frac{1}{2}}(p^2)$,
- A S-projected graviton leg gets a factor $Z_{h_S}^{\frac{1}{2}}(p^2)$.

The distinction in the gravity sector is another improvement which is implemented for the first time in this thesis. In total each ϕ_i leg of a vertex is dressed with a factor $Z_{\phi_i}^{\frac{1}{2}}(p^2)$.

The 2nd part of the dressing procedure concerns the \sqrt{G} prefactor in the metric split (cf. eq. (6.1)): Taking a functional derivative w.r.t. $h_{\mu\nu}$ actually has to include this factor, which was missed out up to now. Hence n functional derivatives have to be accompanied with a factor $G_n^{\frac{n}{2}}$, where the lower index specifies that each vertex level has its own Newton's coupling. To align the presented vertex construction with previous works one should identify Newton's coupling with the TT-projected inverse of the coupling originating from the Ricci scalar tensor structure, i.e.

$$G_n \equiv \tilde{g}_{R,h_{\text{TT}}^n}^{-1}. \quad (6.47)$$

Finally the dressed version of eq. (6.46) reads

$$\Gamma_k^{(nh)} = \frac{\tilde{g}_{R,h_{\text{TT}}^n}^{-\frac{n}{2}}}{16\pi} \sum_{\phi'_1, \dots, \phi'_n} \left(\prod_{i=1}^n Z_{\phi'_i}^{\frac{1}{2}}(p_i^2) \right) \sum_{\mathcal{T}_i \in \mathcal{T}} \tilde{g}_{\mathcal{T}_i, \phi'_1, \dots, \phi'_n} \mathcal{T}_i^{(\phi'_1, \dots, \phi'_n)}, \quad (6.48)$$

where the overall $\frac{1}{16\pi}$ prefactors ensures that the vertex construction matches with the tensor structures from the Einstein-Hilbert action. Following the common procedure it is only left to factor out the coupling which is associated to the Ricci scalar R . This corresponds to a total rescaling of all involved couplings and therefore rescaled couplings are introduced via

$$g'_{\mathcal{T}_i, \phi'_1, \dots, \phi'_n} \equiv \tilde{g}_{R,h_{\text{TT}}^n}^{-1} \tilde{g}_{\mathcal{T}_i, \phi'_1, \dots, \phi'_n}. \quad (6.49)$$

Note that the mass dimensions of the new couplings are different since $[\tilde{g}_{R,h_{\text{TT}}^n}^{-1}] = -2$. Using eq. (6.49) in eq. (6.48) then leads to

$$\Gamma_k^{(nh)} = \frac{\tilde{g}_{R,h_{\text{TT}}^n}^{-\frac{n}{2}+1}}{16\pi} \sum_{\phi'_1, \dots, \phi'_n} \left(\prod_{i=1}^n Z_{\phi'_i}^{\frac{1}{2}}(p_i^2) \right) \sum_{\mathcal{T}_i \in \mathcal{T}} g'_{\mathcal{T}_i, \phi'_1, \dots, \phi'_n} \mathcal{T}_i^{(\phi'_1, \dots, \phi'_n)}. \quad (6.50)$$

Further approximations for the graviton vertices

Of course the latter formula is far too general for actual computations, s.t. more approximations have to be implemented. This is best done by writing down the 2-graviton and 3-graviton vertices explicitly (higher order graviton vertices can be constructed analogously to the 3-graviton vertex, only the 2-graviton vertex behaves differently due to a full basis being available) and introducing the well-known dimensionless couplings from previous works (without a tilde or a dash). First of all TT-projected and S-projected Ricci scalar couplings are identified, i.e. $\tilde{g}_{R, \phi'_1, \dots, \phi'_n} \equiv \tilde{g}_{R, h_{\text{TT}}^n} \forall n$, s.t. they are general prefactors at each order with $n > 2$. Furthermore $\tilde{g}_{R, h_{\text{TT}}^n}$ has mass dimension $+2$. Accordingly one should define a corresponding dimensionless coupling as

$$g_{R, h_{\text{TT}}^n} := \tilde{g}_{R, h_{\text{TT}}^n}^{-1} k^2. \quad (6.51)$$

Let's start with the 2-graviton vertex: Executing eq. (6.50) for $n = 2$ yields

$$\begin{aligned} \Gamma_k^{(2h)} &= \frac{Z_{h_{\text{TT}}}}{16\pi} \left(g'_{\mathbb{1},h_{\text{TT}}^2} (\sqrt{g})^{(h_{\text{TT}},h_{\text{TT}})} + (\sqrt{g}R)^{(h_{\text{TT}},h_{\text{TT}})} + g'_{R_{\mu\nu}^2,h_{\text{TT}}^2} (\sqrt{g}R_{\mu\nu}^2)^{(h_{\text{TT}},h_{\text{TT}})} \right) \\ &+ \frac{Z_{h_{\text{S}}}}{16\pi} \left(g'_{\mathbb{1},h_{\text{S}}^2} (\sqrt{g})^{(h_{\text{S}},h_{\text{S}})} + (\sqrt{g}R)^{(h_{\text{S}},h_{\text{S}})} + g'_{R^2,h_{\text{S}}^2} (\sqrt{g}R^2)^{(h_{\text{S}},h_{\text{S}})} \right) \\ &+ g'_{R_{\mu\nu}^2,h_{\text{TT}}^2} (\sqrt{g}R_{\mu\nu}^2)^{(h_{\text{S}},h_{\text{S}})}, \end{aligned} \quad (6.52)$$

wherein $(\sqrt{g}R^2)^{(h_{\text{TT}},h_{\text{TT}})} = 0$ was implemented (the R^2 tensor structure has no overlap with the TT-mode) and the identification $g'_{R_{\mu\nu}^2,h_{\text{TT}}^2} \equiv g'_{R_{\mu\nu}^2,h_{\text{S}}^2}$ was performed. The next step is to convert the remaining four dimensionful couplings into dimensionless couplings (the notation is in common with previous works):

1. TT-projected graviton mass parameter: $\mu_{h_{\text{TT}}} := -\frac{2}{k^2} \Lambda_{2,h_{\text{TT}}} \equiv -\frac{1}{k^2} g'_{\mathbb{1},h_{\text{TT}}^2}$,
2. S-projected graviton mass parameter: $\mu_{h_{\text{S}}} := -\frac{2}{k^2} \Lambda_{2,h_{\text{S}}} \equiv -\frac{1}{k^2} g'_{\mathbb{1},h_{\text{S}}^2}$,
3. Level 2 S-projected R^2 coupling: $g_{R^2,h_{\text{S}}^2} \equiv g'_{R^2,h_{\text{S}}^2} k^2$,
4. Level 2 TT-projected $R_{\mu\nu}^2$ coupling: $g_{R_{\mu\nu}^2,h_{\text{TT}}^2} \equiv g'_{R_{\mu\nu}^2,h_{\text{TT}}^2} k^2$.

Using all four identifications in eq. (6.52) finally leads to

$$\begin{aligned} \Gamma_k^{(2h)} &= \frac{Z_{h_{\text{TT}}}}{16\pi} \left(-\mu_{h_{\text{TT}}} k^2 (\sqrt{g})^{(h_{\text{TT}},h_{\text{TT}})} + (\sqrt{g}R)^{(h_{\text{TT}},h_{\text{TT}})} \right. \\ &\quad \left. + \frac{g_{R_{\mu\nu}^2,h_{\text{TT}}^2}}{k^2} (\sqrt{g}R_{\mu\nu}^2)^{(h_{\text{TT}},h_{\text{TT}})} \right) \\ &+ \frac{Z_{h_{\text{S}}}}{16\pi} \left(-\mu_{h_{\text{S}}} k^2 (\sqrt{g})^{(h_{\text{S}},h_{\text{S}})} + (\sqrt{g}R)^{(h_{\text{S}},h_{\text{S}})} + \frac{g_{R^2,h_{\text{S}}^2}}{k^2} (\sqrt{g}R^2)^{(h_{\text{S}},h_{\text{S}})} \right. \\ &\quad \left. + \frac{g_{R_{\mu\nu}^2,h_{\text{TT}}^2}}{k^2} (\sqrt{g}R_{\mu\nu}^2)^{(h_{\text{S}},h_{\text{S}})} \right). \end{aligned} \quad (6.53)$$

Now the same for the 3-graviton vertex: Performing $n = 3$ in eq. (6.50) leads to four different contributions (cf. RHS of eq. (6.40)), where again the fully TT-projected R^2 terms are absent. Furthermore one gets mixed couplings like e.g. $g'_{R_{\mu\nu}^2,h_{\text{TT}}h_{\text{S}}^2}$, which are identified and made dimensionless as follows (here no distinction w.r.t. the projection as e.g. for the graviton mass parameter is made):

1. Level 3 TT-projected cosmological constant: $\lambda_3 := \Lambda_3 k^{-2} \equiv g'_{\mathbb{1},h_{\text{TT}}^3} k^{-2} \equiv g'_{\mathbb{1},i} k^{-2}$,
2. Level 3 S-projected R^2 coupling: $g_{R^2,h_{\text{S}}^3} \equiv g'_{R^2,h_{\text{S}}^3} k^2$,
3. Level 3 TT-projected $R_{\mu\nu}^2$ coupling: $g_{R_{\mu\nu}^2,h_{\text{TT}}^3} \equiv g'_{R_{\mu\nu}^2,h_{\text{TT}}^3} k^2 \equiv g'_{R_{\mu\nu}^2,i} k^2$.

These identifications are performed analogously for the 4-graviton and 5-graviton vertex. Afterwards all couplings at levels $n > 3$ are identified with the ones at level 3 to close the flow equations, i.e.

$$g'_{\mathcal{T}_i, \phi'_1, \dots, \phi'_n} \equiv g'_{\mathcal{T}_i, \phi'_1 \phi'_2 \phi'_3} \quad \forall n > 3. \quad (6.54)$$

Of course this step is again an approximation and a good point for later improvements. Applying all identifications to the 3-graviton vertex gives

$$\begin{aligned} \Gamma_k^{(3h)} = \frac{g_{R, h_{\text{TT}}}^{\frac{1}{2}}}{16\pi k} & \left[Z_{h_{\text{TT}}}^{\frac{3}{2}} \left(\lambda_3 k^2 (\sqrt{g})^{(h_{\text{TT}}, h_{\text{TT}}, h_{\text{TT}})} + (\sqrt{g}R)^{(h_{\text{TT}}, h_{\text{TT}}, h_{\text{TT}})} \right. \right. \\ & \left. \left. + \frac{g_{R_{\mu\nu}, h_{\text{TT}}}^2}{k^2} (\sqrt{g}R_{\mu\nu}^2)^{(h_{\text{TT}}, h_{\text{TT}}, h_{\text{TT}})} \right) \right. \\ & Z_{h_{\text{TT}}} Z_{h_S}^{\frac{1}{2}} \left(\lambda_3 k^2 (\sqrt{g})^{(h_{\text{TT}}, h_{\text{TT}}, h_S)} + (\sqrt{g}R)^{(h_{\text{TT}}, h_{\text{TT}}, h_S)} + \frac{g_{R^2, h_S^3}}{k^2} \right. \\ & \left. \cdot (\sqrt{g}R^2)^{(h_{\text{TT}}, h_{\text{TT}}, h_S)} + \frac{g_{R_{\mu\nu}, h_{\text{TT}}}^2}{k^2} (\sqrt{g}R_{\mu\nu}^2)^{(h_{\text{TT}}, h_{\text{TT}}, h_S)} \right) \\ & Z_{h_{\text{TT}}}^{\frac{1}{2}} Z_{h_S} \left(\lambda_3 k^2 (\sqrt{g})^{(h_{\text{TT}}, h_S, h_S)} + (\sqrt{g}R)^{(h_{\text{TT}}, h_S, h_S)} + \frac{g_{R^2, h_S^3}}{k^2} \right. \\ & \left. \cdot (\sqrt{g}R^2)^{(h_{\text{TT}}, h_S, h_S)} + \frac{g_{R_{\mu\nu}, h_{\text{TT}}}^2}{k^2} (\sqrt{g}R_{\mu\nu}^2)^{(h_{\text{TT}}, h_S, h_S)} \right) \\ & Z_{h_S}^{\frac{3}{2}} \left(\lambda_3 k^2 (\sqrt{g})^{(h_S, h_S, h_S)} + (\sqrt{g}R)^{(h_S, h_S, h_S)} + \frac{g_{R^2, h_S^3}}{k^2} (\sqrt{g}R^2)^{(h_S, h_S, h_S)} \right. \\ & \left. \left. + \frac{g_{R_{\mu\nu}, h_{\text{TT}}}^2}{k^2} (\sqrt{g}R_{\mu\nu}^2)^{(h_S, h_S, h_S)} \right) \right]. \quad (6.55) \end{aligned}$$

In summary the following couplings are investigated in this thesis

$$\text{Theory space} \equiv \{ \mu_{h_{\text{TT}}}, \mu_{h_S}, \lambda_3, g_{R^2, h_S^2}, g_{R_{\mu\nu}, h_{\text{TT}}}^2, g_{R^2, h_S^3}, g_{R_{\mu\nu}, h_{\text{TT}}}^3 \}. \quad (6.56)$$

Additionally one has the three anomalous dimensions

$$\{ \eta_{h_{\text{TT}}}, \eta_{h_S}, \eta_c \}, \quad (6.57)$$

which are as usually defined via

$$\eta_{\phi_i}(p^2) := - \frac{\dot{Z}_{\phi_i}(p^2)}{Z_{\phi_i}(p^2)}. \quad (6.58)$$

6.3 Flows of the n -point functions

Now one can set up the flows of the n -point functions and extract the flows of the theory parameters. This is best done by projecting the flow of an n -point function onto all occurring theory parameters in two steps: At first each n -level flow is partially or fully projected onto its TT or S component. Then the resulting equations are either projected

out with a finite lattice derivative at some reasonable values for the outer momentum p^2 (bi-local and tri-local projection scheme) or are extracted by partial derivatives w.r.t. the momentum p^2 evaluated at $p^2 = 0$ (derivative projection scheme). Both projection schemes were used and investigated in numerous previous works [16, 17, 18, 20] and seem to have common pros and cons: The derivative projection scheme allows for analytic flow equations, which are exact in some sense and can be handled easily. Contrariwise the momentum dependence of the flows is essentially ignored, especially in the important momentum range $p^2 \in [0, k^2]$. For the bi- and tri-local projection scheme its the other way round: The momentum dependence of the flows is covered but the flow equations can only be solved with numerical integration methods. Taken as a whole the bi- and tri-local projection is well suited for a momentum dependent analysis whereas the derivative projection could be used as an approximation to find fixed points more quickly.

At this stage one should note that none of the following projection schemes are unique in some sense or enforced by first principles. There are a plenty of ways on projecting onto theory parameters and all schemes will lead to more or less different results. Of course the goal of the projections presented below is to keep the errors due to approximations as small as possible. The main reason to pursue this way is that the former studies led to nice and physically reasonable results which somewhat justifies the procedure.

Besides a comment on the Einstein-Hilbert limit: Already the vertices were constructed in full agreement to previous works, s.t. identifying TT and S components and taking the limits $g_{R^2, h_\xi^2} \rightarrow 0$ and $g_{R_{\mu\nu}^2, h_{\text{TT}}^2} \rightarrow 0$ allows to retrieve the former results in [17, 18, 20]. Of course this property must be entailed to the flow equations and is a consistency check which should always be performed. Also all flow equations obtained at $p^2 = 0$ have to be identical to the Einstein-Hilbert ones as the higher order contributions vanish due to their higher power in p^2 .

Finally a very important remark which concerns all considered flows: In the flow equations of the theory parameters one will never find any wavefunction renormalization constants Z_{ϕ_i} but only anomalous dimensions η_{ϕ_i} . This is due to the fact that all n -level flows will naturally be divided by the appropriate Z_{ϕ_i} s.t. the Z_{ϕ_i} will cancel out. Therefore each flow is only a functional of all anomalous dimensions.

6.3.1 Flow of the graviton 2-point function

The flow of the graviton 2-point function contains the running of several theory parameters ($\mu_{h_{\text{TT}}}, \mu_{h_\xi}, g_{R^2, h_\xi^2}, g_{R_{\mu\nu}^2, h_{\text{TT}}^2}$) and both graviton anomalous dimensions ($\eta_{h_{\text{TT}}}, \eta_{h_\xi}$). Since $\Gamma_k^{(2h)}$ has four open indices it can be fully contracted with either the TT-projector or the S-projector. In the following detailed steps for the TT-projected flow are presented and flow equations are explicitly derived. The results for the S-projected flows follow along the same lines and are given afterwards with less details.

Projecting the flow on its TT-component

Begin with projecting the graviton 2-point function onto its TT-component using the corresponding Stelle projector (cf. eq. (6.31)). With the help of *Mathematica* one finds

(remind that the overlap of the R^2 tensor structure with the TT-projector is 0)

$$\Gamma_{\text{TT}}^{(2h)}(p^2) = \frac{Z_{h_{\text{TT}}}(p^2)}{32\pi} \left(\mu_{h_{\text{TT}}} k^2 + p^2 + g_{R_{\mu\nu}, h_{\text{TT}}^2} \frac{p^4}{k^2} \right). \quad (6.59)$$

As a next step take a scale derivative on both sides to access the flow of the 2-point function. Remember that $\dot{f} = \partial_t f = k \partial_k f$ holds and that all theory parameters are scale-dependent. Therefore follows

$$\begin{aligned} \text{Flow}_{\text{TT}}^{(2h)}(p^2) &\equiv \dot{\Gamma}_{\text{TT}}^{(2h)}(p^2) \\ &= \frac{1}{32\pi} \partial_t \left[Z_{h_{\text{TT}}}(p^2) \left(\mu_{h_{\text{TT}}} k^2 + p^2 + g_{R_{\mu\nu}, h_{\text{TT}}^2} \frac{p^4}{k^2} \right) \right] \\ &= \frac{1}{32\pi} \left[\dot{Z}_{h_{\text{TT}}}(p^2) \left(\mu_{h_{\text{TT}}} k^2 + p^2 + g_{R_{\mu\nu}, h_{\text{TT}}^2} \frac{p^4}{k^2} \right) + Z_{h_{\text{TT}}}(p^2) \right. \\ &\quad \left. \cdot \left((\dot{\mu}_{h_{\text{TT}}} + 2\mu_{h_{\text{TT}}}) k^2 + \left(\dot{g}_{R_{\mu\nu}, h_{\text{TT}}^2} - 2g_{R_{\mu\nu}, h_{\text{TT}}^2} \right) \frac{p^4}{k^2} \right) \right]. \end{aligned} \quad (6.60)$$

Extracting flows of the theory parameters $\mu_{h_{\text{TT}}}$, $g_{R_{\mu\nu}, h_{\text{TT}}^2}$ and the TT-projected graviton anomalous dimension $\eta_{h_{\text{TT}}}$

Since $\mu_{h_{\text{TT}}}$ represents the momentum independent part of the TT-projected graviton 2-point function simply evaluate the latter equation at $p^2 = 0$

$$\begin{aligned} \text{Flow}_{\text{TT}}^{(2h)}(p^2 = 0) &\stackrel{(6.60)}{=} \frac{1}{32\pi} \left(\dot{Z}_{h_{\text{TT}}}(0) \mu_{h_{\text{TT}}} k^2 \right. \\ &\quad \left. + Z_{h_{\text{TT}}}(0) (\dot{\mu}_{h_{\text{TT}}} + 2\mu_{h_{\text{TT}}}) k^2 \right) \end{aligned} \quad (6.61)$$

and solve for $\dot{\mu}_{h_{\text{TT}}}$ by using eq. (6.58) to obtain

$$\dot{\mu}_{h_{\text{TT}}} = (\eta_{h_{\text{TT}}}(0) - 2)\mu_{h_{\text{TT}}} + \frac{32\pi}{k^2 Z_{h_{\text{TT}}}} \text{Flow}_{\text{TT}}^{(2h)}(p^2 = 0). \quad (6.62)$$

For the momentum dependent $\eta_{h_{\text{TT}}}$ start once again with eq. (6.60) and evaluate it at $p^2 = -\mu_{h_{\text{TT}}} k^2$. Then follows

$$\begin{aligned} \text{Flow}_{\text{TT}}^{(2h)}(p^2 = -\mu_{h_{\text{TT}}} k^2) &= \frac{1}{32\pi} \left[\dot{Z}_{h_{\text{TT}}}(-\mu_{h_{\text{TT}}} k^2) g_{R_{\mu\nu}, h_{\text{TT}}^2} \mu_{h_{\text{TT}}}^2 k^2 \right. \\ &\quad \left. + Z_{h_{\text{TT}}}(-\mu_{h_{\text{TT}}} k^2) \left((\dot{\mu}_{h_{\text{TT}}} + 2\mu_{h_{\text{TT}}}) k^2 \right. \right. \\ &\quad \left. \left. + (\dot{g}_{R_{\mu\nu}, h_{\text{TT}}^2} - 2g_{R_{\mu\nu}, h_{\text{TT}}^2}) \mu_{h_{\text{TT}}}^2 k^2 \right) \right]. \end{aligned} \quad (6.63)$$

Now subtract eq. (6.60) from eq. (6.63) in the following fashion

$$\begin{aligned}
 & \frac{\text{Flow}_{\text{TT}}^{(2h)}(p^2 = -\mu_{h_{\text{TT}}}k^2)}{k^2 Z_{h_{\text{TT}}}(-\mu_{h_{\text{TT}}}k^2)} - \frac{\text{Flow}_{\text{TT}}^{(2h)}(p^2)}{k^2 Z_{h_{\text{TT}}}(p^2)} \\
 &= \frac{1}{32\pi} \left[\left(\dot{g}_{R_{\mu\nu}^2, h_{\text{TT}}^2} - 2g_{R_{\mu\nu}^2, h_{\text{TT}}^2} \right) \left(\mu_{h_{\text{TT}}}^2 - \frac{p^4}{k^4} \right) \right. \\
 & \left. - \frac{\dot{Z}_{h_{\text{TT}}}(p^2)}{Z_{h_{\text{TT}}}(p^2)} \cdot \left(\mu_{h_{\text{TT}}} + \frac{p^2}{k^2} + g_{R_{\mu\nu}^2, h_{\text{TT}}^2} \left(\frac{p^4}{k^4} - \mu_{h_{\text{TT}}}^2 \right) \right) \right]. \tag{6.64}
 \end{aligned}$$

Therein one can use eq. (6.58) once again and solve for the fully momentum dependent TT-projected anomalous dimension

$$\begin{aligned}
 \eta_{h_{\text{TT}}}(p^2) &= \frac{1}{\mu_{h_{\text{TT}}} + \frac{p^2}{k^2} + g_{R_{\mu\nu}^2, h_{\text{TT}}^2} \left(\frac{p^4}{k^4} - \mu_{h_{\text{TT}}}^2 \right)} \left[\left(\dot{g}_{R_{\mu\nu}^2, h_{\text{TT}}^2} - 2g_{R_{\mu\nu}^2, h_{\text{TT}}^2} \right) \left(\frac{p^4}{k^4} - \mu_{h_{\text{TT}}}^2 \right) \right. \\
 & \left. + 32\pi \left(\frac{\text{Flow}_{\text{TT}}^{(2h)}(p^2 = -\mu_{h_{\text{TT}}}k^2)}{k^2 Z_{h_{\text{TT}}}(-\mu_{h_{\text{TT}}}k^2)} - \frac{\text{Flow}_{\text{TT}}^{(2h)}(p^2)}{k^2 Z_{h_{\text{TT}}}(p^2)} \right) \right]. \tag{6.65}
 \end{aligned}$$

The equation for $\eta_{h_{\text{TT}}}$ is a so-called Fredholm equation, i.e. a self-consistent integral equation. To solve such an equation with the full momentum dependence one has to compute iteratively (cf. [106, Appendix C]). Alternatively one can use only the specific values at $p^2 = 0$, $p^2 = k^2$ and $p^2 = \frac{k^2}{2}$ (these are the only ones appearing in the flow equations of the theory parameters). In this case one has to solve the self-consistent equation for $\eta_{h_{\text{TT}}}(k^2)$ at first and use the result to compute $\eta_{h_{\text{TT}}}(0)$ and $\eta_{h_{\text{TT}}}\left(\frac{k^2}{2}\right)$. All three remaining equations are only functionals of theory parameters and can therefore be inserted into the flow equations without further ambiguities.

Furthermore it is possible to handle the anomalous dimension as a momentum independent object. In this case taking a derivative of eq. (6.60) w.r.t. p^2 evaluated at $p^2 = 0$ is a suitable projection scheme. All terms except for one vanish and one gets out

$$\eta_{h_{\text{TT}}} = -\frac{32\pi}{Z_{h_{\text{TT}}}} \left(\partial_{p^2} \text{Flow}_{\text{TT}}^{(2h)} \Big|_{p^2=0} \right). \tag{6.66}$$

Of course one can also take two partial derivatives w.r.t. p and evaluate at $p = 0$, the only difference is a factor two

$$\partial_p^2 f(p^2) \Big|_{p=0} = 2 \cdot \partial_{p^2} f(p^2) \Big|_{p^2=0}. \tag{6.67}$$

The last flow equation which can be extracted here is the one for $g_{R_{\mu\nu}^2, h_{\text{TT}}^2}$. Since the $R_{\mu\nu}^2$ coupling at level 2 is associated with the p^4 behaviour of $\text{Flow}_{\text{TT}}^{(2h)}$ a tril-ocal momentum projection is suitable for extracting the flow of $g_{R_{\mu\nu}^2, h_{\text{TT}}^2}$. To that end choose three evaluation points s.t. the important momentum range $0 \leq p^2 \leq k^2$ is fully covered. A convenient choice is $p^2 = 0$, $p^2 = \frac{k^2}{2}$ and $p^2 = k^2$. As a next step match these

three points to $g_{R_{\mu\nu}, h_{\text{TT}}^2}$ in the following way: The graviton 2-point flow *behaves* (i.e. considering only contracted expressions) like

$$f(p^2) = c_0 k^2 + c_1 p^2 + c_2 \frac{p^4}{k^2}, \quad (6.68)$$

where c_0, c_1 and c_2 are coefficients (cf. eq. (6.59)). The tri-local momentum projection can then be used to derive equations for the three coefficients c_0, c_1 and c_2 in terms of the function $f(p^2)$ evaluated at the three points mentioned above. Evaluating eq. (6.68) at the three points simply gives

$$f(0) = k^2 \cdot c_0, \quad (6.69)$$

$$f\left(\frac{k^2}{2}\right) = k^2 \cdot \left(c_0 + \frac{c_1}{2} + \frac{c_2}{4}\right), \quad (6.70)$$

$$f(k^2) = k^2 \cdot (c_0 + c_1 + c_2), \quad (6.71)$$

and solving for c_0, c_1 and c_2 leads to

$$c_0 = \frac{1}{k^2} f(0), \quad (6.72)$$

$$c_1 = \frac{1}{k^2} \left(-3f(0) + 4f\left(\frac{k^2}{4}\right) - f(k^2)\right), \quad (6.73)$$

$$c_2 = \frac{2}{k^2} \left(f(0) - 2f\left(\frac{k^2}{4}\right) + f(k^2)\right). \quad (6.74)$$

Therein $g_{R_{\mu\nu}, h_{\text{TT}}^2}$ is hidden in the c_2 coefficient (they are *not* identical), s.t. the last of the three equations has to be used in order to get a flow equation for $g_{R_{\mu\nu}, h_{\text{TT}}^2}$. Therefore one can conclude: Eq. (6.60) has to be evaluated at the three points, the results must be combined as in eq. (6.74) and the resulting equation should be solved for $\dot{g}_{R_{\mu\nu}, h_{\text{TT}}^2}$. One can see that the whole RHS of eq. (6.60) is proportional to $\frac{1}{32\pi}$ and that some $Z_{h_{\text{TT}}}$ appear. This can be handled as already done e.g. for the TT-projected graviton anomalous dimension: Dividing the whole expression by $Z_{h_{\text{TT}}}(p^2)$ cancels out each $Z_{h_{\text{TT}}}$ s.t. only anomalous dimensions are left.

Let' starts with $p^2 = 0$, which was already computed in eq. (6.61). Applying the considerations made so far yields

$$\frac{32\pi}{k^2 Z_{h_{\text{TT}}}(0)} \text{Flow}_{\text{TT}}^{(2h)}(0) = (2 - \eta_{h_{\text{TT}}}(0)) \mu_{h_{\text{TT}}} + \dot{\mu}_{h_{\text{TT}}}. \quad (6.75)$$

Evaluating eq. (6.60) at $p^2 = \frac{k^2}{2}$ gives

$$\begin{aligned} \frac{32\pi}{k^2 Z_{h_{\text{TT}}}\left(\frac{k^2}{2}\right)} \text{Flow}_{\text{TT}}^{(2h)}\left(\frac{k^2}{2}\right) &= \left(2 - \eta_{h_{\text{TT}}}\left(\frac{k^2}{2}\right)\right) \mu_{h_{\text{TT}}} + \dot{\mu}_{h_{\text{TT}}} - \frac{1}{2} \eta_{h_{\text{TT}}}\left(\frac{k^2}{2}\right) \\ &\quad - \frac{1}{4} \left(2 + \eta_{h_{\text{TT}}}\left(\frac{k^2}{2}\right)\right) g_{R_{\mu\nu}, h_{\text{TT}}^2} + \frac{\dot{g}_{R_{\mu\nu}, h_{\text{TT}}^2}}{4}. \end{aligned} \quad (6.76)$$

Last but not least exploiting eq. (6.60) at $p^2 = k^2$ leads to

$$\begin{aligned} \frac{32\pi}{k^2 Z_{h_{\text{TT}}}(k^2)} \text{Flow}_{\text{TT}}^{(2h)}(k^2) &= (2 - \eta_{h_{\text{TT}}}(k^2)) \mu_{h_{\text{TT}}} + \dot{\mu}_{h_{\text{TT}}} - \eta_{h_{\text{TT}}}(k^2) \\ &\quad - (2 + \eta_{h_{\text{TT}}}(k^2)) g_{R^2_{\mu\nu}, h^2_{\text{TT}}} + \dot{g}_{R^2_{\mu\nu}, h^2_{\text{TT}}}. \end{aligned} \quad (6.77)$$

Combining the eqs. (6.75), (6.76) and (6.77) as suggested in eq. (6.74) and solving for $\dot{g}_{R^2_{\mu\nu}, h^2_{\text{TT}}}$ finally entails (note that $\dot{\mu}_{h_{\text{TT}}}$ and $\mu_{h_{\text{TT}}}$ both cancel out)

$$\begin{aligned} \dot{g}_{R^2_{\mu\nu}, h^2_{\text{TT}}} &= 2\mu_{h_{\text{TT}}} \left(\eta_{h_{\text{TT}}}(0) - 2\eta_{h_{\text{TT}}}\left(\frac{k^2}{2}\right) + \eta_{h_{\text{TT}}}(k^2) \right) \\ &\quad - (2 + g_{R^2_{\mu\nu}, h^2_{\text{TT}}}) \eta_{h_{\text{TT}}}\left(\frac{k^2}{2}\right) + 2(1 + g_{R^2_{\mu\nu}, h^2_{\text{TT}}}) \eta_{h_{\text{TT}}}(k^2) + 2g_{R^2_{\mu\nu}, h^2_{\text{TT}}} \\ &\quad + \frac{64\pi}{k^2} \left(\frac{\text{Flow}_{\text{TT}}^{(2h)}(0)}{Z_{h_{\text{TT}}}(0)} - 2 \frac{\text{Flow}_{\text{TT}}^{(2h)}\left(\frac{k^2}{2}\right)}{Z_{h_{\text{TT}}}\left(\frac{k^2}{2}\right)} + \frac{\text{Flow}_{\text{TT}}^{(2h)}(k^2)}{Z_{h_{\text{TT}}}(k^2)} \right). \end{aligned} \quad (6.78)$$

A derivative projection for the higher order couplings requires a derivative w.r.t. p^4 . Due to too high computational costs this wasn't investigated in this thesis.

Projecting the flow on its S-component

Essentially one has to repeat the same steps as before. Now both higher order tensor structures appear and the other theory parameters are the S-projected ones. Using *Mathematica* one gets

$$\Gamma_S^{(2h)}(p^2) = \frac{Z_{h_S}(p^2)}{256\pi} \left(\mu_{h_S} k^2 + p^2 - 2 \left(3g_{R^2, h^2_S} + g_{R^2_{\mu\nu}, h^2_{\text{TT}}} \right) \frac{p^4}{k^2} \right). \quad (6.79)$$

Taking a scale derivative gives

$$\begin{aligned} \text{Flow}_S^{(2h)}(p^2) &\equiv \dot{\Gamma}_S^{(2h)}(p^2) \\ &= \frac{1}{256\pi} \left[\dot{Z}_{h_S}(p^2) \left(\mu_{h_S} k^2 + p^2 - 2 \left(3g_{R^2, h^2_S} + g_{R^2_{\mu\nu}, h^2_{\text{TT}}} \right) \frac{p^4}{k^2} \right) \right. \\ &\quad + Z_{h_S}(p^2) \left((\dot{\mu}_{h_S} + 2\mu_{h_S}) k^2 - 2 \left(3\dot{g}_{R^2, h^2_S} + \dot{g}_{R^2_{\mu\nu}, h^2_{\text{TT}}} \right. \right. \\ &\quad \left. \left. - 6g_{R^2, h^2_S} - 2g_{R^2_{\mu\nu}, h^2_{\text{TT}}} \right) \frac{p^4}{k^2} \right) \left. \right]. \end{aligned} \quad (6.80)$$

A simple consistency check between the TT-projected and the S-projected flow equations of the theory parameters can be done with the replacements $\text{TT} \rightarrow \text{S}$ for all parameters, $32\pi \rightarrow 256\pi$ for the prefactor, $g_{R^2_{\mu\nu}, h^2_{\text{TT}}} \rightarrow -2(3g_{R^2, h^2_S} + g_{R^2_{\mu\nu}, h^2_{\text{TT}}})$ and $\dot{g}_{R^2_{\mu\nu}, h^2_{\text{TT}}} \rightarrow -2(3\dot{g}_{R^2, h^2_S} + \dot{g}_{R^2_{\mu\nu}, h^2_{\text{TT}}})$ for the higher order couplings at vertex level 2.

Extracting flows of the theory parameters μ_{h_S} , g_{R^2, h_S^2} and the S-projected graviton anomalous dimension η_{h_S}

With these little adjustments follows for $\dot{\mu}_{h_S}$

$$\dot{\mu}_{h_S} = (\eta_{h_S}(0) - 2)\mu_{h_S} + \frac{256\pi}{k^2 Z_{h_S}} \text{Flow}_S^{(2h)}(p^2 = 0). \quad (6.81)$$

For the S-projected momentum dependent anomalous dimension η_{h_S} follows

$$\begin{aligned} \eta_{h_S}(p^2) = & \frac{1}{\mu_{h_S} + \frac{p^2}{k^2} - 2(3g_{R^2, h_S^2} + g_{R_{\mu\nu}^2, h_{\uparrow\uparrow}^2})\left(\frac{p^4}{k^4} - \mu_{h_S}^2\right)} \\ & \cdot \left[- \left(3\dot{g}_{R^2, h_S^2} + \dot{g}_{R_{\mu\nu}^2, h_{\uparrow\uparrow}^2} - 6g_{R^2, h_S^2} - 2g_{R_{\mu\nu}^2, h_{\uparrow\uparrow}^2} \right) \left(\frac{p^4}{k^4} - \mu_{h_S}^2 \right) \right. \\ & \left. + 256\pi \left(\frac{\text{Flow}_S^{(2h)}(p^2 = -\mu_{h_S} k^2)}{k^2 Z_{h_S}(-\mu_{h_S} k^2)} - \frac{\text{Flow}_S^{(2h)}(p^2)}{k^2 Z_{h_S}(p^2)} \right) \right]. \end{aligned} \quad (6.82)$$

Its momentum independent counterpart reads

$$\eta_{h_S} = -\frac{256\pi}{Z_{h_S}} \left(\partial_{p^2} \text{Flow}_S^{(2h)} \Big|_{p^2=0} \right). \quad (6.83)$$

Last but not least the flow equation for the Ricci tensor squared coupling at vertex level 2 obtained from a tri-local momentum projection at the points $p^2 = 0$, $p^2 = \frac{k^2}{2}$ and $p^2 = k^2$ is given by

$$\begin{aligned} \dot{g}_{R^2, h_S^2} = & -\frac{\mu_{h_S}}{3} \left(\eta_{h_S}(0) - 2\eta_{h_S}\left(\frac{k^2}{2}\right) + \eta_{h_S}(k^2) \right) + 2 \left(g_{R^2, h_S^2} + \frac{g_{R_{\mu\nu}^2, h_{\uparrow\uparrow}^2}}{3} \right) \\ & - \frac{\dot{g}_{R_{\mu\nu}^2, h_{\uparrow\uparrow}^2}}{6} + \frac{1}{3} \left(1 - \left(3g_{R^2, h_S^2} + g_{R_{\mu\nu}^2, h_{\uparrow\uparrow}^2} \right) \right) \eta_{h_{Sc}} \left(\frac{k^2}{2} \right) - \frac{1}{3} \left(1 - 2 \left(3g_{R^2, h_S^2} \right. \right. \\ & \left. \left. + g_{R_{\mu\nu}^2, h_{\uparrow\uparrow}^2} \right) \right) \eta_{h_S}(k^2) - \frac{256\pi}{3k^2} \left(\frac{\text{Flow}_S^{(2h)}(0)}{Z_{h_S(0)}} - 2 \frac{\text{Flow}_S^{(2h)}\left(\frac{k^2}{2}\right)}{Z_{h_{Sc}}\left(\frac{k^2}{2}\right)} + \frac{\text{Flow}_S^{(2h)}(k^2)}{Z_{h_S}(k^2)} \right). \end{aligned} \quad (6.84)$$

6.3.2 Flow of the ghost 2-point function

The flow of the ghost 2-point function only reveals information about the flow of the ghost anomalous dimension η_c . To access η_c one can pursue the following path: The ghost 2-point function is a symmetric rank 2 tensor and can be fully decomposed using the transversal and the longitudinal projector. As suggested earlier a distinction between Z_{c_T} and Z_{c_L} is unnecessary, s.t. only one Z_c appears.

Projecting the flow on its T-component

To project onto η_c one can use the T-projected flow of the ghost 2-point function which is given by (thanks to *Mathematica* once again)

$$\Gamma_{\top}^{(c\bar{c})}(p^2) = \frac{1}{2} Z_c(p^2) p^2. \quad (6.85)$$

As usual take a scale-derivative which leads to

$$\text{Flow}_{\top}^{(c\bar{c})}(p^2) \equiv \dot{\Gamma}_{\top}^{(c\bar{c})}(p^2) = \frac{1}{2} \dot{Z}_c(p^2) p^2. \quad (6.86)$$

Extracting flow of the anomalous dimension η_c

The latter equation can simply be solved for η_c which was defined in eq. (6.58). One obtains for the fully momentum dependent ghost anomalous dimension

$$\eta_c(p^2) = -\frac{2 \text{Flow}_{\top}^{(c\bar{c})}(p^2)}{p^2 Z_c(p^2)}. \quad (6.87)$$

6.3.3 Flow of the graviton 3-point function

The flow of the graviton 3-point function comprises the flows of the theory parameters $\lambda_3, g_{R, h_{\top\top}^3}, g_{R^2, h_S^3}$ and $g_{R_{\mu\nu}^2, h_{\top\top}^3}$. Generally speaking the graviton 3-point function is by far the most complicated object in this thesis. To handle it carefully one has to build suitable projectors to project onto the involved theory parameters and one has to stick to a specific momentum configuration.

Constructing projectors

All vertices have one thing in common: Due to the generating tensor structure of the cosmological constant each vertex has a momentum independent part (cf. e.g. eq. (6.59)). Therefore it is possible to split the generating tensor structures at vertex level 3 in a momentum independent part (by setting all external momenta to zero, i.e. $p_1 = p_2 = p_3 = 0$) and a momentum dependent part (by setting the cosmological constant at vertex level 3 to zero, i.e. $\lambda_3 = 0$), s.t.

$$\begin{aligned} \Gamma_k^{(3h)}(p_1, p_2, p_3; \lambda_3) &= \Gamma_k^{(3h)}(p_1, p_2, p_3; \lambda_3 = 0) \\ &+ \Gamma_k^{(3h)}(p_1 = p_2 = p_3 = 0; \lambda_3) \end{aligned} \quad (6.88)$$

holds. The higher order and the Ricci scalar tensor structures are included in the momentum dependent part while the momentum independent part only contains the cosmological constant tensor structure. Orienting oneself at this splitting implicates the following projections:

As mentioned before $\Gamma_k^{(3h)}$ has 6 open indices. A possible way to project onto theory parameters is to contract indices pairwise (= each of the 3 legs) with three $\mathcal{P}_{\top\top}$ projectors (since the TT-parts are the numerically dominating ones) or with two $\mathcal{P}_{\top\top}$ projectors and one \mathcal{P}_S projector (as the overlap of the Ricci scalar squared tensor structure with the $\mathcal{P}_{\top\top}$

projector is zero) and contract this with appropriate parts of $\Gamma_{\text{EH}}^{(3h)}$. In principle it is also possible to contract with suitable parts of the full $\Gamma^{(3h)}$ but its unnecessary to include the higher order tensor structures in the projectors since the higher order couplings will already appear in the flows if one uses the Einstein-Hilbert tensor structures. Choosing this approach of course comes with much less computational costs. Let's begin with defining a projector which projects onto λ_3

$$\mathcal{P}_\lambda^{\alpha\beta\gamma\delta\mu\nu}(p_1, p_2, p_3) := \mathcal{P}_{\text{TT}}^{\alpha\beta\alpha'\beta'}(p_1) \mathcal{P}_{\text{TT}}^{\gamma\delta\gamma'\delta'}(p_2) \mathcal{P}_{\text{TT}}^{\mu\nu\mu'\nu'}(p_3) \Gamma_{\text{EH}, \alpha'\beta'\gamma'\delta'\mu'\nu'}^{(3h)}(p_1 = p_2 = p_3 = 0; \lambda_3). \quad (6.89)$$

Applying this projector on $\Gamma^{(3h)}$ gives symbolically

$$\Gamma_\lambda^{(3h)} = \lim_{p_1, p_2, p_3 \rightarrow 0} \mathcal{P}_\lambda^{\alpha\beta\gamma\delta\mu\nu} \Gamma_{\alpha\beta\gamma\delta\mu\nu}^{(3h)}, \quad (6.90)$$

where all external momenta have to be taken to zero to really catch the momentum independent part. To project onto g_{R, h_{TT}^3} and $g_{R_{\mu\nu}, h_{\text{TT}}^3}$ one can define

$$\mathcal{P}_G^{\alpha\beta\gamma\delta\mu\nu}(p_1, p_2, p_3) := \mathcal{P}_{\text{TT}}^{\alpha\beta\alpha'\beta'}(p_1) \mathcal{P}_{\text{TT}}^{\gamma\delta\gamma'\delta'}(p_2) \mathcal{P}_{\text{TT}}^{\mu\nu\mu'\nu'}(p_3) \Gamma_{\text{EH}, \alpha'\beta'\gamma'\delta'\mu'\nu'}^{(3h)}(p_1, p_2, p_3; \lambda_3 = 0). \quad (6.91)$$

The two projectors defined in eq. (6.89) and eq. (6.91) are exactly the same projectors as in the previous works which only included Einstein-Hilbert tensor structures in the vertices. For the projection on g_{R^2, h_S^3} one of the three \mathcal{P}_{TT} projectors is exchanged for a \mathcal{P}_S projector s.t. one obtains

$$\mathcal{P}_A^{\alpha\beta\gamma\delta\mu\nu}(p_1, p_2, p_3) := \mathcal{P}_S^{\alpha\beta\alpha'\beta'}(p_1) \mathcal{P}_{\text{TT}}^{\gamma\delta\gamma'\delta'}(p_2) \mathcal{P}_{\text{TT}}^{\mu\nu\mu'\nu'}(p_3) \Gamma_{\text{EH}, \alpha'\beta'\gamma'\delta'\mu'\nu'}^{(3h)}(p_1, p_2, p_3; \lambda_3 = 0). \quad (6.92)$$

Symmetric momentum configuration

Unfortunately having constructed suitable projectors isn't enough to start the computation. Technical feasibility is another time a limiting feature: Although its possible to express one external momentum, say p_3 , of the graviton 3-point function by the two others (p_1 and p_2) due to momentum conservation, i.e. $p_1 + p_2 + p_3 = 0$, it currently seems to be technically impossible to end up at reliable results without using further approximations for the configuration of the two remaining external momenta p_1 and p_2 . For the graviton 2-point function this won't lead to any problems since momentum conservation forces it to only depend on one single external momentum $p \equiv p_1$.

In former works the most reasonably used momentum configuration is the *symmetric* one which has the following key features: All three external momenta

- are aligned in a two-dimensional plane, e.g. in the (p^0, p^1) -plane, s.t. $p_i^3 = p_i^4 = 0$ holds for $i = 1, 2, 3$,
- have the absolute value p ,

- are arranged s.t. two of them surround an angle of $\frac{2\pi}{3}$.

If one chooses the coordinate system s.t. the external momentum p_1 runs parallel to the p^0 axis one gets the following configuration

$$\vec{p}_1 = p \begin{pmatrix} 1 \\ 0 \\ 0 \\ 0 \end{pmatrix}, \quad \vec{p}_2 = p \begin{pmatrix} -\frac{1}{2} \\ \frac{\sqrt{3}}{2} \\ 0 \\ 0 \end{pmatrix}, \quad \vec{p}_3 = p \begin{pmatrix} -\frac{1}{2} \\ -\frac{\sqrt{3}}{2} \\ 0 \\ 0 \end{pmatrix}, \quad (6.93)$$

which is also displayed in Figure 6.1. One can directly see that the absolute value of each

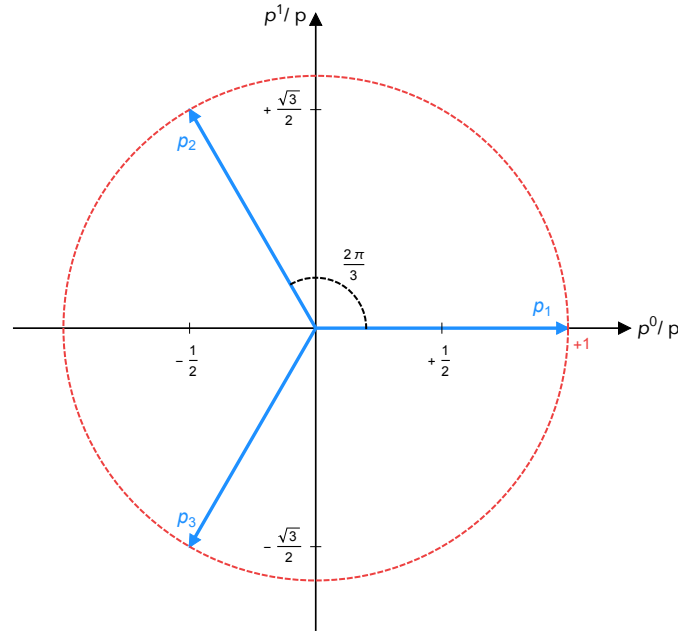


Figure 6.1: Symmetric momentum configuration in the (p^0, p^1) plane

external momentum is indeed p and that momentum conservation $p_1 + p_2 + p_3 = 0$ is valid. Also let's take a look on scalar products of two arbitrary momenta \vec{p}_i and \vec{p}_j with $i, j = 1, 2, 3$ since thousands of them will appear in the flows after the contractions with the respective projectors were executed: A scalar product of a momentum \vec{p}_i with itself will always give $\vec{p}_i \cdot \vec{p}_i = p^2$ for $i = j$. Otherwise one gets $\vec{p}_i \cdot \vec{p}_j = |\vec{p}_i| |\vec{p}_j| \cos\left(\frac{2\pi}{3}\right) = -\frac{1}{2}p^2$ for $i \neq j$. In addition one can write using the Kronecker delta δ_{ij}

$$\vec{p}_i \cdot \vec{p}_j = \frac{3\delta_{ij} - 1}{2} p^2. \quad (6.94)$$

Evaluating all graviton 3-point flows at the symmetric momentum configuration will therefore lead to expressions which are only functions of p^2 .

Projecting the flow on its momentum-independent part

Using the λ_3 projector \mathcal{P}_λ and after taking the limit $p \rightarrow 0$ only the one momentum independent term in $\Gamma_k^{(3h)}$ survives. With *Mathematica* one finds

$$\Gamma_\lambda^{(3h)} = \lim_{p \rightarrow 0} \left(\mathcal{P}_\lambda \circ \Gamma_k^{(3h)} \right) = \frac{35}{96\pi} Z_{h_{\text{TT}}}^{\frac{3}{2}} g_{R,h_{\text{TT}}}^{\frac{1}{2}} \lambda_3 k, \quad (6.95)$$

where \circ represents a full contraction of all six indices. Building the scale derivative gives

$$\begin{aligned} \text{Flow}_\lambda^{(3h)} &\equiv \dot{\Gamma}_\lambda^{(3h)} \\ &= \frac{35}{96\pi} \partial_t \left(Z_{h_{\text{TT}}}^{\frac{3}{2}} g_{R,h_{\text{TT}}}^{\frac{1}{2}} \lambda_3 k \right) \\ &= \frac{35}{96\pi} \left(\frac{3}{2} Z_{h_{\text{TT}}}^{\frac{1}{2}} \dot{Z}_{h_{\text{TT}}} g_{R,h_{\text{TT}}}^{\frac{1}{2}} \lambda_3 k + \frac{1}{2} Z_{h_{\text{TT}}}^{\frac{3}{2}} g_{R,h_{\text{TT}}}^{\frac{1}{2}} \dot{g}_{R,h_{\text{TT}}}^{\frac{1}{2}} \lambda_3 k \right. \\ &\quad \left. + Z_{h_{\text{TT}}}^{\frac{3}{2}} g_{R,h_{\text{TT}}}^{\frac{1}{2}} \dot{\lambda}_3 k + Z_{h_{\text{TT}}}^{\frac{3}{2}} g_{R,h_{\text{TT}}}^{\frac{1}{2}} \lambda_3 \dot{k} \right) \\ &= \frac{35k}{96\pi} Z_{h_{\text{TT}}}^{\frac{3}{2}} g_{R,h_{\text{TT}}}^{\frac{1}{2}} \lambda_3 \left(\frac{3}{2} \frac{\dot{Z}_{h_{\text{TT}}}}{Z_{h_{\text{TT}}}} + \frac{1}{2} \frac{\dot{g}_{R,h_{\text{TT}}}}{g_{R,h_{\text{TT}}}} + \frac{\dot{\lambda}_3}{\lambda_3} + 1 \right). \end{aligned} \quad (6.96)$$

Extracting flow of the theory parameter λ_3

The previous result can be dissolved for $\dot{\lambda}_3$ which leads to

$$\dot{\lambda}_3 = \left(-1 + \frac{3}{2} \eta_{h_{\text{TT}}}(0) - \frac{1}{2} \frac{\dot{g}_{R,h_{\text{TT}}}}{g_{R,h_{\text{TT}}}} \right) \lambda_3 + \frac{96\pi \text{Flow}_\lambda^{(3h)}(p^2 = 0)}{35k Z_{h_{\text{TT}}}^{\frac{3}{2}}(0) g_{R,h_{\text{TT}}}^{\frac{1}{2}}}. \quad (6.97)$$

Projecting the flow on its momentum-dependent part with three TT-projectors

A full contraction of $\Gamma_k^{(3h)}$ with the projector \mathcal{P}_G (where again *Mathematica* acts big) yields

$$\Gamma_G^{(3h)}(p^2) = \frac{1}{4096\pi^2} Z_{h_{\text{TT}}}^{\frac{3}{2}} g_{R,h_{\text{TT}}}^{\frac{1}{2}} \left(-9\lambda_3 k p^2 + \frac{171}{8} \frac{p^4}{k} + \frac{405}{8} g_{R_{\mu\nu},h_{\text{TT}}}^2 \frac{p^6}{k^3} \right), \quad (6.98)$$

Executing the scale derivative and dividing by $Z_{h_{\text{TT}}}(p^2) p^2$ (necessary for the projection scheme: a p^2 comes from \mathcal{P}_G) leads to

$$\begin{aligned} \frac{\text{Flow}_G^{(3h)}(p^2)}{Z_{h_{\text{TT}}}(p^2) p^2} &= \frac{g_{R,h_{\text{TT}}}^{\frac{1}{2}}}{4096\pi^2} \left[\left(-\frac{3}{2} \eta_{h_{\text{TT}}} + \frac{1}{2} \frac{\dot{g}_{R,h_{\text{TT}}}}{g_{R,h_{\text{TT}}}} \right) \cdot \left(-9\lambda_3 k + \frac{171}{8} \frac{p^2}{k} \right. \right. \\ &\quad \left. \left. + \frac{405}{8} g_{R_{\mu\nu},h_{\text{TT}}}^2 \frac{p^4}{k^3} \right) - 9k(\dot{\lambda}_3 + \lambda_3) - \frac{171}{8} \frac{p^2}{k} \right. \\ &\quad \left. + \frac{405}{8} \frac{p^4}{k^3} \left(\dot{g}_{R,h_{\text{TT}}} - 3g_{R,h_{\text{TT}}} \right) \right]. \end{aligned} \quad (6.99)$$

Extracting flow of the theory parameter $g_{R,h_{\text{TT}}}^3$

The flow of $g_{R,h_{\text{TT}}}^3$ can be derived using a bi-local projection at the two points $p^2 = 0$ and $p^2 = k^2$. As the expressions became very large at this stage only the resulting flow equation is presented. The computation follows along the same lines as before, one should only notice that the LHS of eq. (6.99) is indeed well defined for $p^2 \rightarrow 0$. Without further comments one ends up with

$$\begin{aligned} \dot{g}_{R,h_{\text{TT}}}^3 = \frac{16}{171 + 405g_{R,h_{\text{TT}}}^3} & \left[\frac{3}{2}\eta_{h_{\text{TT}}}(k^2) \left(\frac{171}{8} - 9\lambda_3 + \frac{405}{8}g_{R,h_{\text{TT}}}^3 \right) g_{R,h_{\text{TT}}}^3 \right. \\ & + \frac{27}{2}\eta_{h_{\text{TT}}}(0)\lambda_3 g_{R,h_{\text{TT}}}^3 + \frac{1}{8}(171 - 405(\dot{g}_{R,h_{\text{TT}}}^3 \\ & - 3g_{R,h_{\text{TT}}}^3)) g_{R,h_{\text{TT}}}^3 + \frac{4096\pi^2}{k} g_{R,h_{\text{TT}}}^{\frac{1}{2}} \\ & \left. \cdot \left(\frac{\text{Flow}_{\text{G}}^{(3h)}(k^2)}{Z_{h_{\text{TT}}}(k^2)k^2} - \lim_{p^2 \rightarrow 0} \frac{\text{Flow}_{\text{G}}^{(3h)}(p^2)}{Z_{h_{\text{TT}}}(p^2)p^2} \right) \right]. \end{aligned} \quad (6.100)$$

A bi-local momentum projection comes always with much more computational costs than a derivative projection. Additionally the graviton flow at level 3 are in general tremendously complicated compared to the 2-graviton flow. Therefore the corresponding flow equation obtained by a derivative projection at $p^2 = 0$ is also investigated. Taking a derivative w.r.t. p^2 of eq. (6.100) evaluated at $p^2 = 0$ yields

$$\dot{g}_{R,h_{\text{TT}}}^3 = (2 + 3\eta_{h_{\text{TT}}}) g_{R,h_{\text{TT}}}^3 + \frac{8 \cdot 4096\pi^2 k^{\frac{1}{2}}}{171} g_{R,h_{\text{TT}}}^{\frac{1}{2}} \left(\partial_{p^2} \frac{\text{Flow}_{\text{G}}^{(3h)}(p^2)}{Z_{h_{\text{TT}}} p^2} \Big|_{p^2=0} \right). \quad (6.101)$$

Extracting flows of the higher order couplings

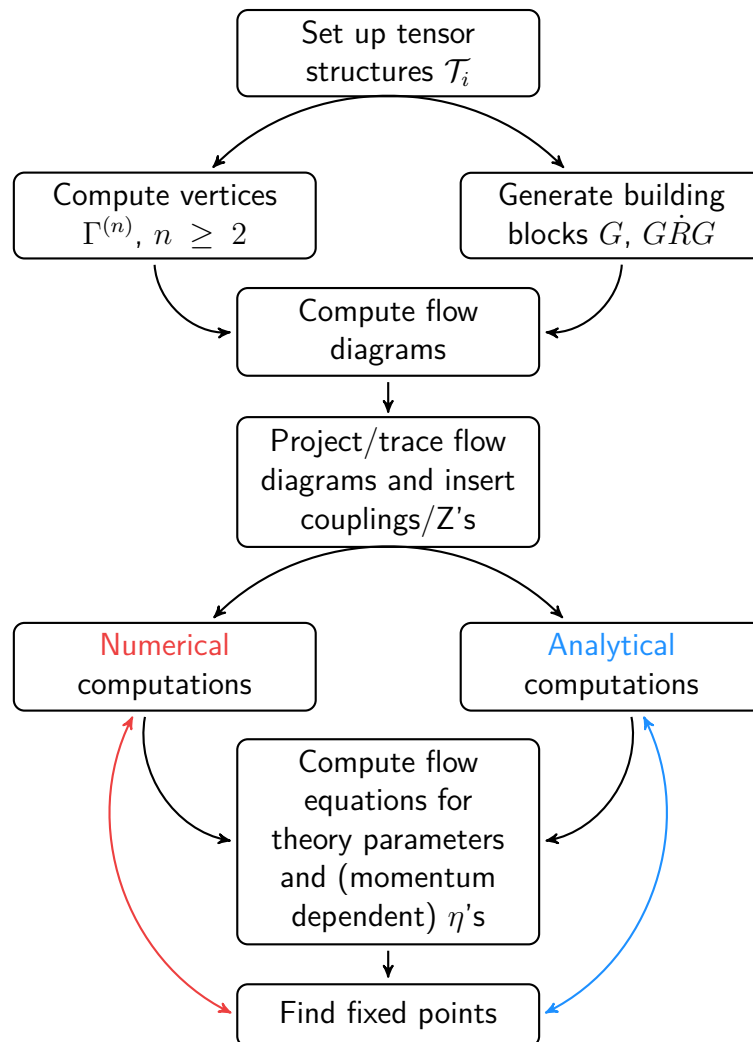
Unfortunately this is the point where the borders of computational feasibility couldn't be resolved. Hopefully this problem can be solved in future works. That is why no explicit flow equations for the higher order couplings at vertex level 3 are presented.

7 Computational details

For the sake of understanding basic ideas of the computations a few computational details are presented in this chapter. Since many different programs were used this is mainly done in symbolical rather than in technical language. At some points the discussion gets more detailed to provide successful methods for further work in the future.

7.1 General workflow

At first the whole workflow is presented below as a flow chart.



Computational steps

At first vertices are computed from a set of tensor structures. Therein one should use general and unspecific prefactors for the tensor structures to shorten the expressions which have to pass the tracing process. Then the propagators can be derived. With the vertices and building blocks by hand one can assemble the flow diagrams. Combining the latter with projectors and tracing over open indices leads to scalar quantities. Afterwards one can replace the general prefactors by concrete couplings and Z 's. It is only left to execute the integration over the loop momentum. Depending on the investigated theory parameter this is done either numerically or analytically. Repeating these steps for different flows and projectors yields a set of flow equations. This allows to search for fixed points. Furthermore the fixed point values can be used to investigate other aspects of the flows, e.g. their polynomial momentum dependence.

Number of terms

The biggest challenge in this work is to handle the enormous amount of terms due to the higher order curvature invariants. An overview of the number of terms in contrast to the Einstein-Hilbert case is presented in [Table 7.1](#) and [Figure 7.1](#).

Vertex order	Einstein-Hilbert	with higher orders	factor
3-graviton vertex	206 terms	1 156 terms	≈ 5.6
4-graviton vertex	3 597 terms	44 652 terms	≈ 12.4
5-graviton vertex	65 799 terms	1 554 546 terms	≈ 23.5

Table 7.1: Comparison of the number of terms for different graviton vertex orders in the case of Einstein-Hilbert and higher order vertices

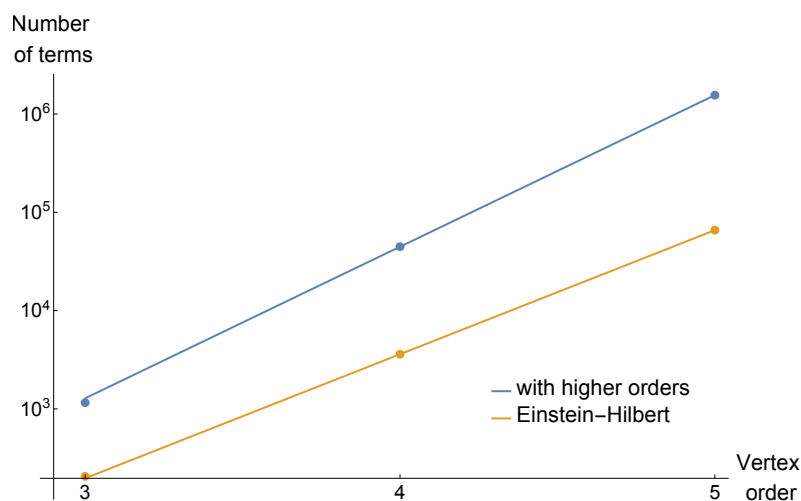


Figure 7.1: Number of terms for [Einstein-Hilbert](#) and [higher order](#) vertices at each order

Especially the plot reveals the difference to Einstein-Hilbert vertices: In both cases the number of terms (depicted by the colored dots) is approximately exponentially growing with the vertex order (denoted by the fitted straight lines in a logarithmic plot). But for higher order vertices this growth is slightly larger and the starting point is much bigger than for Einstein-Hilbert vertices.

Programs in use

Unsurprisingly the most important program for the whole work is *Mathematica* by Wolfram Research Inc. (version 11.2) [107]. But for some tasks other programs or packages for *Mathematica* turned out to be more suitable since the wide powerfulness of *Mathematica* can be its bottleneck if expressions are too complicated. In the case of quantum gravity this applies mainly to two computational steps: The derivation of vertices which is nothing but taking functional derivatives of very complicated objects and the tracing process of full diagrams in combination with several projectors. For both parts the *mathematica* package *TARDIS* (unpublished version) [108] is used. *TARDIS* itself uses the packages *VertEXpand* (unpublished version) [109] for the generation of vertices, *FORM* (version 4.2.0) [110, 111], the *xAct* packages *xPerm* (version 1.2.3) [112], *xTensor* (version 1.1.2) and *xPert* (version 1.0.5) [113], *DoFun* (version 2.0.3) [114] for symbolic flow equations and *FormTracer* (version 2.3.4) [115] for the tracing process. Only for the G-projected 3-graviton flow self-written *FORM* scripts were used instead (cf. [116]). A typical example of *FORM* code can be found in Appendix A of [116].

Spherical coordinate system

Another task is to execute the integration over the loop momentum 4-vector \vec{q} . In order to do that one has to stick to a specific coordinate system. Of course spherical coordinates are the best choice due to their symmetry properties. Generalizing the well-known expression for the three-dimensional spherical coordinates to a four-dimensional space leads to

$$\vec{q} = q \begin{pmatrix} \cos(\theta_1) \\ \sin(\theta_1) \cos(\theta_2) \\ \sin(\theta_1) \sin(\theta_2) \cos(\phi) \\ \sin(\theta_1) \sin(\theta_2) \sin(\phi) \end{pmatrix}. \quad (7.1)$$

Therein q denotes the absolute value of \vec{q} , the two θ_i are the azimuthal angles s.t. $\theta_i \in [0, \pi)$ for $i = 1, 2$ and ϕ is the radial angle s.t. $\phi \in [0, 2\pi)$. Calculating the Jacobian yields an expression for the four-dimensional volume element

$$d^4q = dq q^3 d\theta_1 \sin^2(\theta_1) d\theta_2 \sin(\theta_2) d\phi. \quad (7.2)$$

For actual computations it turns out to be advantageous to transform the two azimuthal angles θ_1 and θ_2 to real numbers x and y by defining

$$x := \cos(\theta_1), \quad (7.3)$$

$$y := \cos(\theta_2), \quad (7.4)$$

s.t. $x, y \in [-1, 1)$. Using $dx = -\sin(\theta_1) d\theta_1$, $dy = -\sin(\theta_2) d\theta_2$ and $\sin(\theta_1) = \sqrt{1-x^2}$ then gives

$$d^4 q = dq q^3 dx \sqrt{1-x^2} dy d\phi. \quad (7.5)$$

In this coordinates the integration is performed over the region $[0, \infty) \times [-1, 1) \times [-1, 1) \times [0, 2\pi)$.

It is left to say a word about the orientation of the momenta within the coordinate system. The two choices made so far (i.e. choosing a coordinate system in eq. (7.1) and a specific momentum configuration in eq. (6.93)) correspond to $\theta_1 \triangleleft (\vec{p}_1, \vec{q})$. For computations at 2-point flow level momentum conservation kills \vec{p}_2 , s.t. the y -integration can be evaluated directly which simply gives 2. Only at 3-point flow level \vec{p}_2 has to be respected (but again momentum conservation eliminates \vec{p}_3) and the y -integration becomes non-trivial. In addition mixed scalar products, i.e. scalar products of the loop momentum and one external momentum, can be evaluated using

$$\vec{p}_1 \cdot \vec{q} = pq \cos(\theta_1) = p_1 q x, \quad (7.6)$$

$$\begin{aligned} \vec{p}_2 \cdot \vec{q} &= \frac{pq}{2} \left(-\cos(\theta_1) + \sqrt{3} \sin(\theta_2) \cos(\theta_2) \right) \\ &= \frac{pq}{2} \left(-x + \sqrt{3} \sqrt{1-x^2} y \right). \end{aligned} \quad (7.7)$$

A formula for scalar products between two external momenta was already presented in eq. (6.94) s.t. all occurring scalar products are executable now.

7.2 Some more details

The 2nd part of this chapter is dedicated to those who want to redo some of the shown computations on their own. Having in mind the working routine from the previous section this mainly applies to the steps *generate building blocks*, *analytical computations* and *numerical computations*. For each step mentioned a simple example and some explanations are discussed. Additionally intermediate results are presented to provide a more deep understanding and to simplify a potential reconstruction.

7.2.1 Pure propagators and propagators with regulator insertions

Here the computations of the building blocks are discussed. The crucial parts are: 1st Representing the graviton 2-point function in a suitable basis, 2nd inverting 2-point function + regulator and 3rd taking the limit $\alpha \rightarrow 0$. Of course the situation for the gravity building blocks is much more complicated than for the ghost building blocks since the ghost and anti-ghost fields only have one index, i.e. c_μ, \bar{c}_μ , whereas the fluctuating metric in gravity has two ($h_{\mu\nu}$). The propagators follow by taking two functional derivatives, therefore this gets even worse: As one will see the ghost propagator can be represented as a 2×2 matrix while the graviton propagator needs a 4×4 matrix. Since this section will involve juggling around with indices all quantities are denoted with explicit indices henceforward.

Graviton propagator

As mentioned many times before the graviton propagator is constructed from the graviton 2-point function which follows from taking two functional derivatives of the appearing tensor structures and the gauge-fixing action S_{gf} (since $S_{\text{gf}} \propto h^2$) w.r.t. projected parts of the fluctuating metric $h_{\mu\nu}$ (the ghost action S_{gh} doesn't contribute) and dressing the result with suitable wavefunction renormalization constants $Z_{h_{\text{TT}}}$ and Z_{h_S} (cf. [section 6.2](#)). Therefore the graviton 2-point function has four open indices and so does the graviton propagator. Let's start with a general expression for the undressed graviton 2-function without respecting the different projections, i.e. just taking functional derivatives w.r.t. $h_{\mu\nu}$, to get a better understanding for the vertex construction presented in [section 6.2](#) and to justify it. Orienting at eq. (6.45) suggests

$$\bar{\Gamma}_{\mu\nu\gamma\sigma}^{(2h)} = \frac{\delta}{\delta h^{\mu\nu}} \frac{\delta}{\delta h^{\gamma\sigma}} \int d^4x \left[\sqrt{g} \left(\tilde{g}_\Lambda + \tilde{g}_R R + \tilde{g}_{R^2} R^2 + \tilde{g}_{R_{\mu\nu}^2} R_{\mu\nu}^2 \right) + \sqrt{\tilde{g}} \frac{1}{2\alpha} \tilde{g}_{\mu\nu} F^\mu F^\nu \right]. \quad (7.8)$$

Note that taking functional derivatives of a scalar quantity w.r.t. the fluctuating metric with upper indices will result in a quantity with lower indices. The explicit computation of eq. (7.8) can be done with *TARDIS*. It calculates the two functional derivatives generically, uses the resulting Dirac delta's to carry out the space-time integration in eq. (7.8) and to implement momentum conservation and transforms the result in momentum space using a Fourier transformation. Therefore the result only consists of Dirac delta's, one momentum vector p (only one instead of two due to momentum conservation) and scalar products of the same. Fortunately the graviton 2-point function is short enough to be written out here. The result is ordered w.r.t. the terms appearing in eq. (7.8)

$$\begin{aligned} \bar{\Gamma}_{\mu\nu\gamma\sigma}^{(2h)} &= \frac{1}{4} \left(\delta_{\mu\nu} \delta_{\gamma\sigma} - \delta_{\mu\sigma} \delta_{\nu\gamma} - \delta_{\mu\gamma} \delta_{\nu\sigma} \right) \tilde{g}_\Lambda && \sim (\sqrt{g})^{(2h)} \\ &+ \frac{1}{4} \left(p^2 (\delta_{\mu\sigma} \delta_{\nu\gamma} + \delta_{\mu\gamma} \delta_{\nu\sigma} - 2\delta_{\mu\nu} \delta_{\gamma\sigma}) \right. \\ &\quad \left. - \delta_{\nu\sigma} p_\mu p_\gamma - \delta_{\mu\sigma} p_\gamma p_\nu - \delta_{\gamma\nu} p_\mu p_\sigma - \delta_{\mu\gamma} p_\nu p_\sigma \right. \\ &\quad \left. + 2\delta_{\gamma\sigma} p_\mu p_\nu + 2\delta_{\mu\nu} p_\gamma p_\sigma \right) \tilde{g}_R && \sim (\sqrt{g}R)^{(2h)} \\ &+ 2 (\delta_{\mu\nu} p^2 - p_\mu p_\nu) (\delta_{\gamma\sigma} p^2 - p_\gamma p_\sigma) \tilde{g}_{R^2} && \sim (\sqrt{g}R^2)^{(2h)} \\ &+ \frac{1}{4} \left(p^4 (2\delta_{\mu\nu} \delta_{\gamma\sigma} + \delta_{\mu\gamma} \delta_{\nu\sigma} + \delta_{\mu\sigma} \delta_{\nu\gamma}) \right. \\ &\quad \left. - p^2 (2\delta_{\mu\nu} p_\gamma p_\sigma + \delta_{\mu\gamma} p_\nu p_\sigma + \delta_{\mu\sigma} p_\nu p_\gamma + \delta_{\nu\gamma} p_\mu p_\sigma \right. \\ &\quad \left. + \delta_{\nu\sigma} p_\mu p_\gamma + 2\delta_{\gamma\sigma} p_\mu p_\nu) + 4p_\mu p_\nu p_\gamma p_\sigma \right) \tilde{g}_{R_{\mu\nu}^2} && \sim (\sqrt{g}R_{\mu\nu}^2)^{(2h)} \\ &+ \frac{1}{4\alpha} \left(\delta_{\mu\nu} \delta_{\gamma\sigma} p^2 - 2\delta_{\mu\nu} p_\gamma p_\sigma - 2\delta_{\gamma\sigma} p_\mu p_\nu \right. \\ &\quad \left. + \delta_{\nu\sigma} p_\mu p_\gamma + \delta_{\mu\sigma} p_\gamma p_\nu + \delta_{\gamma\nu} p_\mu p_\sigma + \delta_{\mu\gamma} p_\nu p_\sigma \right). && \sim (\sqrt{g}F^\mu F_\mu)^{(2h)} \end{aligned} \quad (7.9)$$

From this representation one can learn four things: 1st The part which comes from the cosmological constant term is momentum independent, 2nd the part from the Ricci scalar goes like p^2 , 3rd the parts from the higher orders tensors have a p^4 behaviour and 4th there is a term $\propto \frac{1}{\alpha}$ from the gauge-fixing action S_{gf} , s.t. the limit $\alpha \rightarrow 0$ can't be taken here. Luckily the propagator is computed after inverting the dressed version of eq. (7.9) which prevents from any problems regarding $\alpha \rightarrow 0$.

The next step is to express the graviton 2-point function in a suitable basis. As said before this is the basis formed by the six Stelle projectors. With them one can write

$$\bar{\Gamma}_{\mu\nu\gamma\sigma}^{(2h)} = \sum_{i=1}^6 \bar{\Gamma}_i^{(2h)} \mathcal{P}_{\mu\nu\gamma\sigma}^i \quad (7.10)$$

in general. To represent this as a 4×4 matrix one has to map the six individual indices i to six other indices constructed from pairs of only four indices (j, k) with $j \wedge k \leq 4$. The first four indices are mapped equally, s.t. $i \rightarrow (i, i)$ holds for $i = 1, 2, 3, 4$, i.e. $i = \text{TT}, \text{V}, \text{S}_1, \text{S}_2$. In the resulting 4×4 matrix these are the four diagonal entries. The last two indices are mapped to the two off-diagonal elements in the lower-right 2×2 block matrix, s.t. 5 (i.e. S_3) $\rightarrow (3, 4)$ and 6 (i.e. S_4) $\rightarrow (4, 3)$ holds. Finally this yields

$$\bar{\Gamma}^{(2h)} = \begin{pmatrix} \bar{\Gamma}_{\text{TT}}^{(2h)} & 0 & 0 & 0 \\ 0 & \bar{\Gamma}_{\text{V}}^{(2h)} & 0 & 0 \\ 0 & 0 & \bar{\Gamma}_{\text{S}_1}^{(2h)} & \bar{\Gamma}_{\text{S}_3}^{(2h)} \\ 0 & 0 & \bar{\Gamma}_{\text{S}_4}^{(2h)} & \bar{\Gamma}_{\text{S}_2}^{(2h)} \end{pmatrix}. \quad (7.11)$$

Following this procedure for the explicit graviton 2-point function given in eq. (7.9), i.e. fully contracting it with each of the six Stelle projectors to get the matrix entries (note that the 1st Stelle projector has norm 5 and the 2nd has norm 3 while all others have norm 1, s.t. one has to divide the respective entries by 5 or 3), changes the involved couplings to their projected versions. Therefore one can use eq. (6.50) to assign the projected g'_{T_i, h_i^2} couplings and then the four identifications for vertex level 2 to include the real theory parameters. Please note that at this stage also V-projected couplings appear. One can include Z_{ϕ_i} and ends up with the dressed graviton 2-point function

$$\Gamma_{\text{TT}}^{(2h)} = \frac{Z_{h_{\text{TT}}}}{32\pi} \left(\mu_{h_{\text{TT}}} k^2 + p^2 + g_{R_{\mu\nu}, h_{\text{TT}}^2} \frac{p^4}{k^2} \right), \quad (7.12)$$

$$\Gamma_{\text{V}}^{(2h)} = Z_{h_{\text{V}}} \left(\frac{\mu_{h_{\text{V}}} k^2}{32\pi} + \frac{p^2}{2\alpha} \right), \quad (7.13)$$

$$\Gamma_{\text{S}_1}^{(2h)} = Z_{h_{\text{S}}} \left(-\frac{\mu_{h_{\text{S}}} k^2}{64\pi} - \frac{p^2}{16\pi} + \frac{3g_{R^2, h_{\text{S}}^2}}{8\pi} \frac{p^4}{k^2} + \frac{g_{R_{\mu\nu}, h_{\text{TT}}^2}}{8\pi} \frac{p^4}{k^2} + \frac{3p^2}{4\alpha} \right), \quad (7.14)$$

$$\Gamma_{\text{S}_2}^{(2h)} = Z_{h_{\text{S}}} \left(\frac{\mu_{h_{\text{S}}} k^2}{64\pi} + \frac{p^2}{4\alpha} \right), \quad (7.15)$$

$$\Gamma_{\text{S}_3}^{(2h)} = \Gamma_{\text{S}_4}^{(2h)} = -Z_{h_{\text{S}}} \left(\frac{\sqrt{3}\mu_{h_{\text{S}}} k^2}{64\pi} + \frac{\sqrt{3}p^2}{4\alpha} \right). \quad (7.16)$$

Now one is able to compute the graviton regulator. It is chosen to be

$$R_{\mu\nu\gamma\sigma}(p^2) = (\Gamma_{\mu\nu\gamma\sigma}^{(2h)}(k^2) - \Gamma_{\mu\nu\gamma\sigma}^{(2h)}(p^2))\Theta(k^2 - p^2). \quad (7.17)$$

When computing eq. (7.17) explicitly using eqs. (7.12)-(7.16) one will directly see that this choice for the graviton regulator cancels out the momentum independent part of the graviton 2-point function, i.e. the term proportional to the graviton mass parameter. Therefore the regulator carries no mass term which is independent of the momentum scale and only acts as a mass term for low momentum modes. For the further calculation one can use the exact same basis as before since $R \propto \Gamma^{(2h)}$ s.t.

$$R_i(p^2) = (\Gamma_i^{(2h)}(k^2) - \Gamma_i^{(2h)}(p^2))\Theta(k^2 - p^2) \quad \text{with } i = \{1, 2, 3, 4, 5, 6\} \quad (7.18)$$

and

$$R_{\mu\nu\gamma\sigma} = \sum_{i=1}^6 R_i \mathcal{P}_{\mu\nu\gamma\sigma}^i \quad (7.19)$$

holds. This feature is crucial if one wants to obtain the graviton propagator: Since both the graviton 2-point function and the graviton regulator can be expressed in the full Stelle basis the graviton propagator simply follows from inverting the sum of both in the Stelle basis. Therefore one can write

$$G_{h,\mu\nu\gamma\sigma} = \left(\sum_{i=1}^6 (\Gamma_i^{(2h)} + R_i) \mathcal{P}_{\mu\nu\gamma\sigma}^i \right)^{-1}. \quad (7.20)$$

The remaining task is a simple matrix inversion. Based on the general form of the propagator building blocks (cf. eq. (7.11)) one can deduce that the inverse graviton propagator is of the form

$$G_h^{-1} = \begin{pmatrix} a & 0 & 0 & 0 \\ 0 & b & 0 & 0 \\ 0 & 0 & c & e \\ 0 & 0 & f & d \end{pmatrix} \quad (7.21)$$

with general coefficients a, b, c, d, e, f . Matrix inversion of eq. (7.21) then leads to

$$G_h = \begin{pmatrix} \frac{1}{a} & 0 & 0 & 0 \\ 0 & \frac{1}{b} & 0 & 0 \\ 0 & 0 & \frac{d}{cd-ef} & \frac{e}{-cd+ef} \\ 0 & 0 & \frac{f}{-cd+ef} & \frac{c}{cd-ef} \end{pmatrix}. \quad (7.22)$$

As an example let's compute the V-component of the graviton propagator explicitly. Inserting eq. (7.13) gives an expression for the V-component of the graviton regulator

$$R_{h,V} = Z_{h_V} \left(\frac{k^2 - p^2}{2\alpha} \right) \Theta(k^2 - p^2), \quad (7.23)$$

s.t. the V-component of the graviton propagator reads (cf. eq. (7.20))

$$\begin{aligned} G_{h,V}(p^2) &= (\Gamma_V^{(2h)}(p^2) + R_{h,V}(p^2))^{-1} \\ &= \frac{1}{Z_{h_V} 16\pi(p^2 + (k^2 - p^2)\Theta(k^2 - p^2) + \alpha\mu_{h_V}k^2)}. \end{aligned} \quad (7.24)$$

Last but not least the limit $\alpha \rightarrow 0$ can be computed without further problems. For the V-component of the graviton propagator this leads to

$$\lim_{\alpha \rightarrow 0} G_{h,V}(p^2) = 0, \quad (7.25)$$

as promised before. Note that all other components are finite in this limit. Proceeding for all remaining components as shown in the example and putting everything together finally gives for the full graviton propagator

$$G_h = \begin{pmatrix} c_{TT} & 0 & 0 & 0 \\ 0 & 0 & 0 & 0 \\ 0 & 0 & c_S & \sqrt{3}c_S \\ 0 & 0 & \sqrt{3}c_S & 3c_S \end{pmatrix} \quad (7.26)$$

with

$$\begin{aligned} c_{TT} &= \frac{32\pi}{Z_{h_{TT}}} \left[\mu_{h_{TT}} k^2 + p^2 + g_{R_{\mu\nu}, h_{TT}^2} \frac{p^4}{k^2} \right. \\ &\quad \left. + \left(k^2(1 + g_{R_{\mu\nu}, h_{TT}^2}) - p^2 - g_{R_{\mu\nu}, h_{TT}^2} \frac{p^4}{k^2} \right) \Theta(k^2 - p^2) \right]^{-1}, \end{aligned} \quad (7.27)$$

$$\begin{aligned} c_S &= \frac{16\pi}{Z_{h_S}} \left[-\mu_{h_S} k^2 - p^2 + 2 \left(3g_{R^2, h_S^2} + g_{R_{\mu\nu}, h_{TT}^2} \right) \frac{p^4}{k^2} \right. \\ &\quad \left. + \left(k^2 \left(-1 + 2 \left(3g_{R^2, h_S^2} + g_{R_{\mu\nu}, h_{TT}^2} \right) \right) + p^2 \right. \right. \\ &\quad \left. \left. - 2 \left(3g_{R^2, h_S^2} + g_{R_{\mu\nu}, h_{TT}^2} \right) \frac{p^4}{k^2} \right) \Theta(k^2 - p^2) \right]^{-1}. \end{aligned} \quad (7.28)$$

At last the four scalar components in eq. (7.26) can be merged using the scalar projector $\mathcal{P}_{\mu\nu\alpha\beta}^S$ defined in eq. (6.38).

Graviton propagator with regulator insertion

The other building block in the gravity sector is $(G\dot{R}G)_h$. This quantity appears in all diagrams with a graviton loop and it's important to note that every regulator insertion has a propagator on its left and right side (cf. diagrams in eq. (6.17) where the orange dots for the propagators weren't dropped). To compute $(G\dot{R}G)_h$ one has to follow three steps: 1st Compute \dot{R}_h from R_h by taking a scale-derivative, 2nd do a matrix multiplication of all three quantities (propagators without $\alpha \rightarrow 0$ since $R_h \propto \frac{1}{\alpha}$) and 3rd take the limit $\alpha \rightarrow 0$. For the 1st step the full graviton regulator is needed. Each

of its six components can be calculated analogously to eq. (7.23). Taking a scale-derivative of this will especially produce \dot{Z}_{h_i} if hitting a Z_{h_i} term, $\dot{g}_{R^2, h_S^2}, \dot{g}_{R_{\mu\nu}^2, h_{\text{TT}}^2}$ terms if hitting the higher order couplings and $2k^2\delta(k^2 - p^2)$ if hitting a $\Theta(k^2 - p^2)$ term. The latter circumstance won't cause any problems since the whole term will be of the form $\sim (k^2 - p^2)\delta(k^2 - p^2)$ (cf. e.g. eq. (7.23)) s.t. momentum integration over the loop momentum kills this term. Therefore it is in principle possible to leave it out in actual computations. The full expression for \dot{R}_h will not be written out here since it is simply too long.

For the matrix multiplication one needs the graviton propagator without $\alpha \rightarrow 0$ which is also a very long expression. Therefore let's skip the explicit matrix multiplication and move forward to the 3rd and last step: The matrix $(G\dot{R}G)_h$ has the same structure as the propagator G_h , i.e. taking the limit $\alpha \rightarrow 0$ results again in a vanishing V-component. Also the scalar sector of $(G\dot{R}G)_h$ can be abbreviated as before using the scalar projector $\mathcal{P}_{\mu\nu\alpha\beta}^S$. Finally one gets

$$(G\dot{R}G)_h = \begin{pmatrix} d_{\text{TT}} & 0 & 0 & 0 \\ 0 & 0 & 0 & 0 \\ 0 & 0 & d_S & \sqrt{3}d_S \\ 0 & 0 & \sqrt{3}d_S & 3d_S \end{pmatrix} \quad (7.29)$$

with (using the graviton anomalous dimensions $\eta_{h_{\text{TT}}}$ and η_{h_S})

$$d_{\text{TT}} = \frac{32\pi k^2}{Z_{h_{\text{TT}}}} \left[\begin{aligned} & \left(2k^4 + (k^4 - p^4)\dot{g}_{R_{\mu\nu}^2, h_{\text{TT}}^2} - k^4\eta_{h_{\text{TT}}} + k^2p^2\eta_{h_{\text{TT}}} \right. \\ & \quad \left. + g_{R_{\mu\nu}^2, h_{\text{TT}}^2} (2(k^4 + p^4) + (p^4 - k^4)\eta_{h_{\text{TT}}}) \right) \\ & \cdot \left(k^2 (p^2 - \mu_{h_{\text{TT}}}k^2 + (k^2 - p^2)\Theta(k^2 - p^2)) \right) \\ & \quad \left. + g_{R_{\mu\nu}^2, h_{\text{TT}}^2} (p^4 + (k^4 - p^4)\Theta(k^2 - p^2)) \right)^{-2} \Theta(k^2 - p^2) \\ & \quad \left. + \delta(k^2 - p^2) \text{ term} \right], \quad (7.30) \end{aligned}$$

$$d_S = \frac{-16\pi k^2}{Z_{h_S}} \left[\begin{aligned} & \left(2k^4 - (k^4 - p^4)(6\dot{g}_{R^2, h_S^2} + 2\dot{g}_{R_{\mu\nu}^2, h_{\text{TT}}^2}) - k^4\eta_{h_S} + k^2p^2\eta_{h_S} \right. \\ & \quad \left. + (6g_{R^2, h_S^2} + 2g_{R_{\mu\nu}^2, h_{\text{TT}}^2}) (2(k^4 + p^4) + (p^4 - k^4)\eta_{h_S}) \right) \\ & \cdot \left(k^2 (p^2 - \mu_{h_S}k^2 + (k^2 - p^2)\Theta(k^2 - p^2)) \right) \\ & \quad \left. + (6g_{R^2, h_S^2} + 2g_{R_{\mu\nu}^2, h_{\text{TT}}^2}) (p^4 + (k^4 - p^4)\Theta(k^2 - p^2)) \right)^{-2} \Theta(k^2 - p^2) \\ & \quad \left. + \delta(k^2 - p^2) \text{ term} \right]. \quad (7.31) \end{aligned}$$

Ghost propagator

For the ghost propagator the approach is essentially the same. The only difference is that the ghost 2-point function has just two open indices which makes the whole computation dramatically less difficult. One can obtain the ghost 2-point function from taking two functional derivatives (one w.r.t. the ghost field c^μ and the other one w.r.t. the anti-ghost field \bar{c}^ν) of the ghost action S_{gh} since $S_{\text{gh}} \propto c\bar{c}$. All other input quantities (tensor structures or S_{gf}) don't contribute. Therefore one gets

$$\bar{\Gamma}_{\mu\nu}^{(c\bar{c})} = \frac{\delta}{\delta c^\mu} \frac{\delta}{\delta \bar{c}^\nu} \int d^4x \sqrt{g} \bar{c}^\alpha M_{\alpha\beta} c^\beta. \quad (7.32)$$

Computing this expression with *TARDIS* leads to the simple term

$$\bar{\Gamma}_{\mu\nu}^{(c\bar{c})} = \frac{1}{2} p^2 \delta_{\mu\nu}. \quad (7.33)$$

Obviously taking the limit $\alpha \rightarrow 0$ isn't necessary for the ghost sector at all. In principle it is possible to express the result in a basis formed by the transverse and longitudinal projectors and go on, but due to the simple form of $\bar{\Gamma}_{\mu\nu}^{(c\bar{c})}$ the computation should be done without changing the basis.

The next step is to implement the ghost wavefunction renormalization constant Z_c . Using the analog of eq. (6.50) for the ghost sector leads to

$$\Gamma_{\mu\nu}^{(c\bar{c})} = Z_c \bar{\Gamma}_{\mu\nu}^{(c\bar{c})} \stackrel{(7.33)}{=} \frac{Z_c}{2} p^2 \delta_{\mu\nu}. \quad (7.34)$$

From this one can directly obtain the ghost regulator

$$\begin{aligned} R_{c,\mu\nu} &= (\Gamma_{\mu\nu}^{(c\bar{c})}(k^2) - \Gamma_{\mu\nu}^{(c\bar{c})}(p^2)) \Theta(k^2 - p^2) \\ &= \frac{Z_c}{2} (k^2 - p^2) \Theta(k^2 - p^2) \delta_{\mu\nu}. \end{aligned} \quad (7.35)$$

The needed matrix inversion for the graviton propagator is particularly simple since the Kronecker delta is its own inverse. Therefore one ends up with

$$\begin{aligned} G_{c,\mu\nu} &= \frac{2}{Z_c} (p^2 + (k^2 - p^2) \Theta(k^2 - p^2) \delta_{\mu\nu})^{-1} \\ &= \frac{2}{Z_c (p^2 + (k^2 - p^2) \Theta(k^2 - p^2))} \delta_{\mu\nu}. \end{aligned} \quad (7.36)$$

Ghost propagator with regulator insertion

It is left to compute $(G\dot{R}G)_c$. Fortunately one can directly use the propagator in eq. (7.36) since $\alpha \rightarrow 0$ doesn't regard the ghost sector, s.t. only \dot{R}_c has to be computed. Straightforwardly one gets

$$\begin{aligned} \dot{R}_{c,\mu\nu} &= \frac{1}{2} \left((2k^2 Z_c + \dot{Z}_c (k^2 - p^2)) \Theta(k^2 - p^2) \right. \\ &\quad \left. + 2k^2 Z_c (k^2 - p^2) \delta(k^2 - p^2) \right) \delta_{\mu\nu}. \end{aligned} \quad (7.37)$$

Combining the latter two equations and inserting η_c finally yields

$$\begin{aligned}
 (G\dot{R}G)_{c,\mu\nu} &= G_{c,\mu\alpha}\dot{R}_c^{\alpha\beta}G_{c,\beta\nu} \\
 &= \left(\frac{2(2k^2 - \eta_c(k^2 - p^2))\Theta(k^2 - p^2)}{Z_c(p^2 + (k^2 - p^2)\Theta(k^2 - p^2))^2} \right. \\
 &\quad \left. + \frac{4k^2(k^2 - p^2)\delta(k^2 - p^2)}{Z_c(p^2 + (k^2 - p^2)\Theta(k^2 - p^2))^2} \right) \delta_{\mu\nu}.
 \end{aligned} \tag{7.38}$$

7.2.2 Momentum derivatives and analytical integrals

Some flows are computed by taking a 2nd derivative w.r.t. p evaluated at $p^2 = 0$. In an actual computation this step would be done before integrating analytically as the integrand isn't singular. The non-analytic behaviour of the Litim-regulator complicates the situation and somehow introduces a misbehaviour of *Mathematica*: Products of Heaviside theta's and Dirac delta's aren't treated well. In general this can be handled using [117]

$$\delta(x)f(x, \Theta(x)) = \delta(x) \int_0^1 du f(0, u). \tag{7.39}$$

A diagram with a loop has two loop contributions: A propagator with regulator insertion carrying the loop momentum q and a propagator with momentum $p + q$. Then each projected part of the full diagram has the following general form

$$\text{diagram} = \frac{f(p)\Theta(k^2 - q^2)}{m^2 + s^2 + zs^4 + (k^2 - s^2 - zs^4)\Theta(k^2 - s^2)}, \tag{7.40}$$

where $s^2 \equiv p^2 + 2pqx + q^2$ was introduced. The s -dependent Heaviside theta in the denominator can be pulled up using

$$\frac{1}{a^2 + (k^2 - a^2)\Theta(k^2 - a^2)} = \frac{\Theta(k^2 - a^2)}{k^2} + \frac{\Theta(a^2 - k^2)}{a^2}. \tag{7.41}$$

Taking a 2nd derivative w.r.t. p evaluated at $p^2 = 0$ gives only two contributions which don't vanish after integration (e.g. a term $\Theta(k^2 - q^2)\Theta(q^2 - k^2)$ appears which of course is zero after integrating over q). The 1st of them can be integrated in *Mathematica* without further problems. Only the 2nd contribution needs a careful treatment: At $p^2 = 0$ (which implicates $s^2|_{p^2=0} = q^2$) one finds

$$\begin{aligned}
 \frac{\partial^2}{\partial p^2} (\text{diagram}) \Big|_{p^2=0} &= f''(0)\Theta(k^2 - q^2) \left(\frac{\Theta(k^2 - q^2)}{m^2 + k^2 + zk^4} + \frac{\Theta(q^2 - k^2)}{m^2 + s^2 + zs^4} \right) \\
 &\quad - \frac{4f(0)(q^2x^2 + 2zq^4x^2)}{(m^2 + q^2 + zq^4)^2} \delta(q^2 - k^2)\Theta(k^2 - q^2).
 \end{aligned} \tag{7.42}$$

The 3rd term in eq. (7.42) can be resolved using eq. (7.39), in particular one gets

$$\delta(q^2 - k^2)\Theta(k^2 - q^2) \stackrel{(7.39)}{=} \delta(q^2 - k^2) \int_0^1 du u = \frac{1}{2}\delta(q^2 - k^2). \quad (7.43)$$

To simplify expressions like $\delta(f(x))$ one can use the formula

$$\delta(f(x)) = \sum_{i=1}^n \frac{\delta(x - x_i)}{|f'(x_i)|}, \quad (7.44)$$

where x_i are single roots of $f(x)$. In the present case this leads to

$$\delta(q^2 - k^2) = \frac{1}{|2k|} (\delta(q - k) + \delta(q + k)) = \frac{\delta(q - k)}{2k}, \quad (7.45)$$

since $k \geq 0$ and $q \geq 0$. Now all expressions can be integrated without further ambiguities. For a more detailed discussion cf. section 7.4 in [116].

7.2.3 Numerical checks of analytically performed integrals

In principle integrating analytically is technically much easier than integrating numerically and interpolating the result, but practically one should check analytical results with a short numerical computation. This applies especially to the flow equations of $\mu_{h_{\text{TT}}}$, μ_{h_S} and λ_3 , which are obtained by a projection at $p^2 = 0$ and to the analytical equations of g_{R,h_{TT}^3} and the anomalous dimensions, computed via a p^2 derivative at $p^2 = 0$.

Introducing the Fermi-Dirac distribution

A reasonable and also fast check can be done as follows: At the first the Heaviside function gets replaced by the mirror-inverted Fermi-Dirac distribution which exhibits a small parameter ϵ and is given by

$$f_\epsilon(x) := \frac{1}{\exp\left(\frac{-x}{\epsilon}\right) + 1}. \quad (7.46)$$

This function is analytical and has the property to converge to the Heaviside function in the limit $\epsilon \rightarrow 0$, i.e. $f_\epsilon(x) \rightarrow \Theta(x)$ for $\epsilon \rightarrow 0$. Figure 7.2 shows $f_\epsilon(x)$ for different values of ϵ . Therein one can clearly see how it converges to the Heaviside function for shrinking ϵ . Furthermore its derivative is suitable to replace Dirac delta functions s.t. $\partial_x f_\epsilon(x) \rightarrow \delta(x)$ holds for $\epsilon \rightarrow 0$, which is depicted in Figure 7.3. Both figures suggest that $\epsilon = 10^{-2}$ and $\epsilon = 10^{-3}$ should be sensible values for a numerical test s.t. an agreement up to several decimal digits should be achievable.

Numerical check procedure

Another nice feature for a test is the convergence property of $f_\epsilon(x)$ since this property is handed down to the full diagram. Consequently integrating a diagram numerically

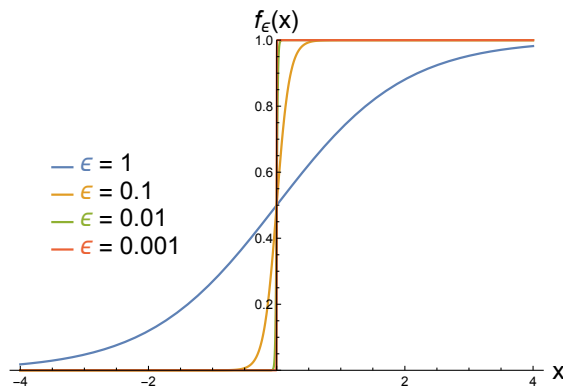


Figure 7.2: The analytical Fermi-Dirac function with four different values for ϵ

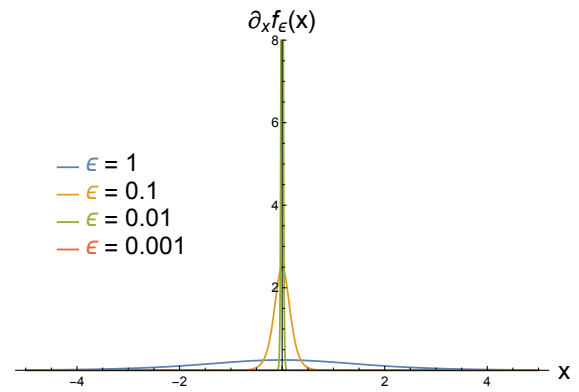


Figure 7.3: Derivative of the analytical Fermi-Dirac function with four different values for ϵ

for shrinking ϵ and plotting the resulting numerical values for each ϵ should give a converging curve where the result obtained with the smallest values of ϵ should be equal to the analytical result up to a given numerical precision. In practical computations a recommendable choice is to lower ϵ in logarithmic steps from 10^{-1} to 10^{-3} and to integrate a full diagram, s.t. one gets out 5 different points of the form (ϵ /numerical value of the diagram). It should be clear that a numerical integration can only be done without other parameters hanging around, i.e. all theory parameters have to be set to a specific numerical value. Therefore the whole procedure should be repeated with several distinct numerical values for the theory parameters. Plotting the results and building in the analytic value (obtained by using the same numerical values for the theory parameters) leads to charts like Figure 7.4. Therein the red line denotes the analytical

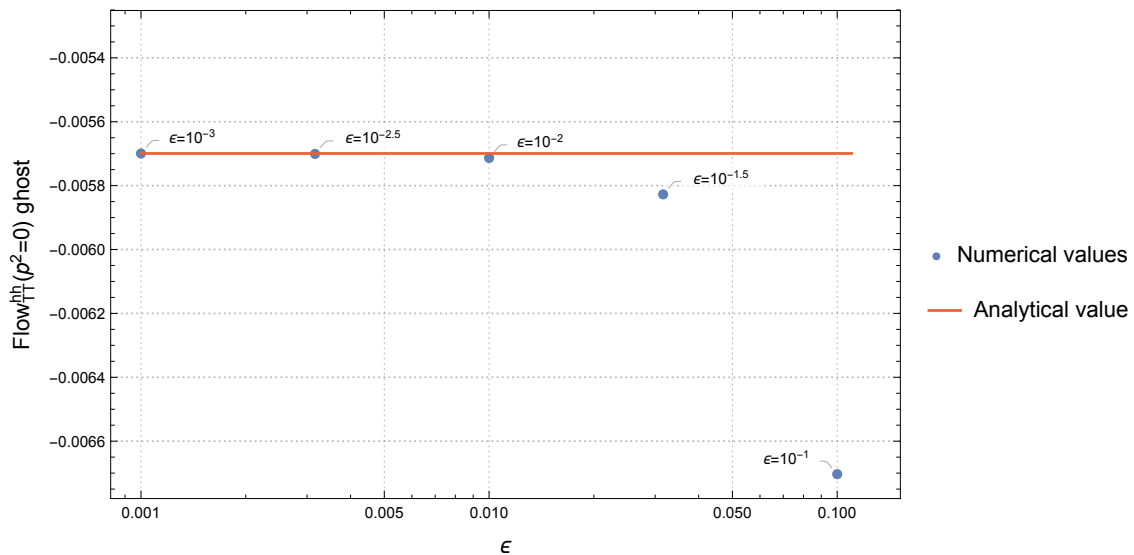


Figure 7.4: Numerical check of an analytically integrated flow diagram at $p^2 = 0$

result and the blue points have to be read from right to left, i.e. ϵ shrinks from right to left (beginning with $\epsilon = 10^{-1}$ and ending up with $\epsilon = 10^{-3}$ in logarithmic steps $10^{-0.5}$). The shown graph corresponds to the ghost diagram of the TT-projected flow of the graviton 2-point function at $p^2 = 0$ where all theory parameters were set to 1.

The procedure also works for the derivative projection up to 2nd derivatives of a flow diagram w.r.t. the external momentum p as pointed out in Figure 7.5 (same setup).

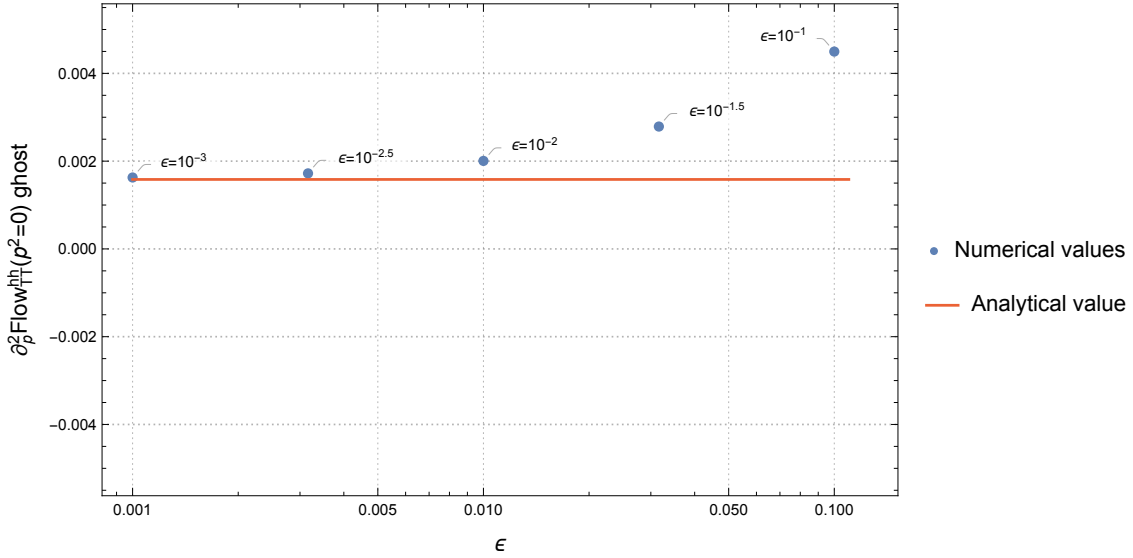


Figure 7.5: Numerical check of an analytically integrated flow diagram after taking a 2nd p -derivative at $p^2 = 0$

Unfortunately the non-analytic behaviour of the Litim-regulator destroys every numerical computation beyond 2nd derivatives. This concerns especially 4th derivatives, which would be necessary for a projection onto the higher order couplings within a derivative projection scheme.

7.2.4 Numerical integration and interpolation procedure

The bi-local and tri-local momentum projection requires a lot of numerical integration and subsequent interpolation. Before going into details remember that the flow of the graviton 2-point function has to be evaluated at four different points ($p^2 = 0, p^2 = \frac{k^2}{2}, p^2 = k^2$ and $p^2 = -\mu_{h_{TT|S}} k^2$).

Integrating diagrams analytically

In the case of $p^2 = 0$ the integration can and should always, i.e. for all diagrams, be performed analytically without any approximations. Furthermore the tadpole diagram (for each level there exists one unique tadpole diagram) should always be integrated analytically since the loop and therefore the whole denominator doesn't depend on the external momentum p . In all other cases the integration has to be performed numerically.

Integrating ghost loop diagrams numerically

In principle integrating a diagram with a ghost loop is much easier than integrating a diagram with a graviton loop, especially for a numerical integration. For $p^2 \neq -\mu_{h_{\text{TT}|S}} k^2$ the only appearing theory parameters are g_{R,h_{TT}^3} and $\eta_c(p^2)$. The general factored form is given by

$$\text{Flow}_{\text{TT}|S}^{(2h)} \Big|_{\text{ghost}} = \int_0^\infty dq q^3 \int_{-1}^1 dx \sqrt{1-x^2} g_{R,h_{\text{TT}}^3} \frac{f(p, q, x) - \eta_c(q^2) g(p, q, x)}{h(p, q, x)}, \quad (7.47)$$

with general functions f, g and h . To integrate such an object numerically one can do the following: First of all g_{R,h_{TT}^3} can simply be excluded since it's a total prefactor if its momentum dependence is neglected. As a next step the numerator can be written as a scalar product of 2D vectors where the 1st entry corresponds to η_c^0 and the 2nd entry corresponds to $\eta_c(q^2)$. The approximation $\eta_c(q^2) = \eta_c(k^2)$ allows to exclude the vector containing η_c^0 and $\eta_c(k^2)$ and one can write in total

$$\text{Flow}_{\text{TT}|S}^{(2h)} \Big|_{\text{ghost}} = g_{R,h_{\text{TT}}^3} (1, \eta_c(k^2)) \cdot \int_0^\infty dq q^3 \int_{-1}^1 dx \frac{\sqrt{1-x^2}}{h(p, q, x)} \underbrace{\begin{pmatrix} f(p, q, x) \\ -g(p, q, x) \end{pmatrix}}_{=\mathcal{T}_{\text{TP}}}. \quad (7.48)$$

For graviton loop diagrams the latter 2D vector will be a high dimensional tensor. Therefore it's generally called *theory parameter tensor* \mathcal{T}_{TP} . If n different theory parameters appear in a diagram the corresponding theory parameter tensor has dimension $d = n + 1$. The entries of \mathcal{T}_{TP} do only depend on the external momentum p , the loop momentum q and the angular coordinate x . To integrate both entries numerically it is only left to stick to a specific value for the external momentum. For practical computations it is also highly recommended to set $k = 1$, $\Theta(k^2 - q^2) = 1$ and integrate over q from 0 to 1. At last the integrated theory parameter tensor can be multiplied with the 1st vector to obtain the final result.

In the case of $p^2 = -\mu_{h_{\text{TT}|S}} k^2$ a new theory parameter appears, i.e. $\mu_{h_{\text{TT}}}$ or μ_{h_S} respectively. Unfortunately it is not possible to exclude this parameter since it is contained in all three functions f, g and h . The most common way to circumvent such a problem is to integrate the whole expressions numerically for many specific values of $\mu_{h_{\text{TT}}}$ or μ_{h_S} and to interpolate the result, i.e. integrating numerically on a *grid*. A reasonable range is $\mu_{h_{\text{TT}|S}} \in [-0.8, 0]$ with 0.05 steps s.t. one gets out 16 points in total. The result can then be interpolated with polynomials of order 3 (or even higher) since the grid is structured.

Integrating graviton loop diagrams numerically

Now things get more complicated: Firstly the graviton propagator introduces poles which depend on the specific approximation. In approximation 1 (only including the $R_{\mu\nu}^2$ tensor structure besides Einstein-Hilbert and identifying $\mu_{h_{\text{TT}}} \equiv \mu_{h_S}$, $\eta_{h_{\text{TT}}} \equiv \eta_{h_S}$) the factored

graviton loop diagram is of the form

$$\text{Flow}_{\text{TT}}^{(2h)}|_{3h}^{(1)} = \int_0^\infty dq q^3 \int_{-1}^1 dx \sqrt{1-x^2} \frac{g_{R,h_{\text{TT}}}^3}{(1-2g_{R_{\mu\nu},h_{\text{TT}}}^2 + \mu_{h_{\text{TT}}})^2 (1+g_{R_{\mu\nu},h_{\text{TT}}}^2 + \mu_{h_{\text{TT}}})^2} \cdot \frac{f(p, q, x, \eta_{h_{\text{TT}}}(q^2), \mu_{h_{\text{TT}}}, g_{R_{\mu\nu},h_{\text{TT}}}^2, \dot{g}_{R_{\mu\nu},h_{\text{TT}}}^2, \lambda_3)}{g(p, q, x, \mu_{h_{\text{TT}}}, g_{R_{\mu\nu},h_{\text{TT}}}^2)}, \quad (7.49)$$

with general functions f and g . Note that factorizing the diagram causes $f = f(\mu_{h_{\text{TT}}})$. The poles are explicitly included in the 2nd term in eq. (7.49) (cf. blue and green lines in Figure 7.6) and also implicitly contained in the function g . In general the numerical integration and interpolation procedure has to circumvent the poles but the final result should still include the behaviour of the poles in their neighborhood. This can be achieved by pulling the prefactor containing the poles out of the integral and excluding a small region around the poles in the numerical integration and interpolation procedure (cf. orange dashed lines and red points in Figure 7.6). Furthermore the theory

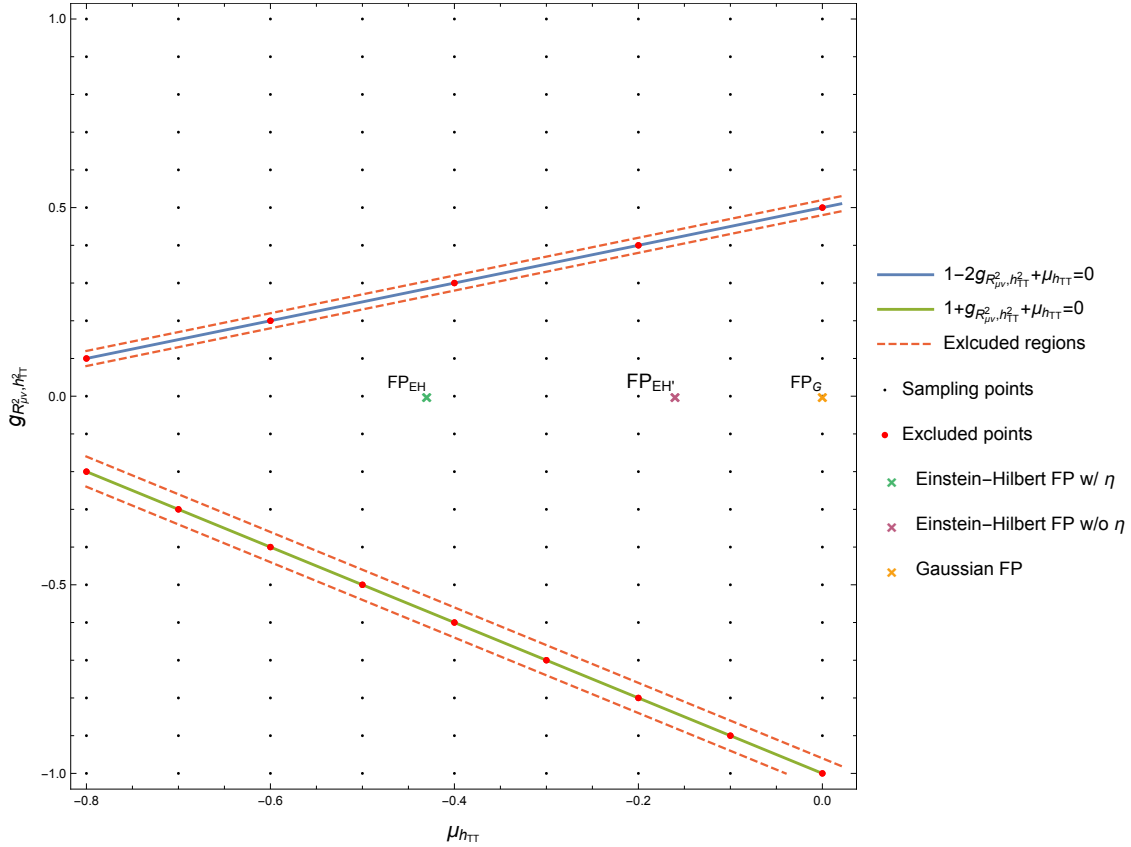


Figure 7.6: Sampling points, poles, excluded regions/points and trivial fixed points for the 1st approximation

parameter tensor \mathcal{T}_{TP} consists of much more entries: All theory parameters appearing

in the function f have to be pulled out the integral in all powers. The maximal power are $\eta_{h_{\text{TT}}}^1, \mu_{h_{\text{TT}}}^3, g_{R_{\mu\nu}, h_{\text{TT}}}^6, \dot{g}_{R_{\mu\nu}, h_{\text{TT}}}^1$ and λ_3^3 (the minimal powers are zero for all parameters). Therefore \mathcal{T}_{TP} has $2 \cdot 4 \cdot 7 \cdot 2 \cdot 4 = 448$ entries. Of course not all combinations exist, s.t. only 150 entries are non-zero and have to be integrated explicitly. Applying all this to eq. (7.49) gives (this step is fully analogous to the step eq. (7.47) to eq. (7.48))

$$\begin{aligned} \text{Flow}_{\text{TT}}^{(2h)} \Big|_{3h}^{(1)} &= \frac{g_{R, h_{\text{TT}}}^3}{(1 - 2g_{R_{\mu\nu}, h_{\text{TT}}}^2 + \mu_{h_{\text{TT}}})^2 (1 + g_{R_{\mu\nu}, h_{\text{TT}}}^2 + \mu_{h_{\text{TT}}})^2} \\ &\quad \sum_{i,j,k,l,m} \mu_{h_{\text{TT}}}^i \dot{g}_{R_{\mu\nu}, h_{\text{TT}}}^j g_{R_{\mu\nu}, h_{\text{TT}}}^k \lambda_3^l \eta_{h_{\text{TT}}}^m(k^2) \int_0^\infty dq q^3 \int_{-1}^1 dx \sqrt{1-x^2} \\ &\quad \cdot \mathcal{T}_{\text{TP}} \left(\frac{f_{(ijklm)}(p, q, x)}{g(p, q, x, \mu_{h_{\text{TT}}}, g_{R_{\mu\nu}, h_{\text{TT}}}^2)} \right), \end{aligned} \quad (7.50)$$

where each entry of \mathcal{T}_{TP} has the same denominator g (containing the two poles) and different numerators $f_{(ijklm)}$.

Now a word about the poles and how to handle them. Excluding small regions around the poles divides the theory parameter space in three regions (cf. Figure 7.6), where only one of them is physically relevant: The region surrounded by the two poles contains the Gaussian fixed point (yellow cross) and the fixed points for Einstein-Hilbert tensor structures with and without η 's found in [17] (purple and light green crosses). The Gaussian fixed point should be connectable to the fixed points of the full system via a flow trajectory and the Einstein-Hilbert fixed point via an adiabatic expansion of the higher order coupling. Therefore the found fixed points have to lie in the same region. Otherwise a trajectory would run into a pole.

Moreover one gets constraints from the graviton propagator: Comparing the TT-component (cf. eq. (7.27)) with the S-component (cf. eq. (7.28)) reveals that the $R_{\mu\nu}^2$ coupling ($\propto p^4$) appears with different signs. Therefore at least one of the two components will become negative for high momenta. Consequently the presented approximation is only valid for $p^2/k^2 \lesssim 1$. Otherwise unitarity would be lost.

In approximation 2 (now only $\mu_{h_{\text{TT}}} \equiv \mu_{h_S}$) the R^2 coupling comes into play. The calculation follows along the same lines but yet the poles are surfaces in a three dimensional theory subspace spanned by $\mu_{h_{\text{TT}}}, g_{R^2, h_S^2}$ and $g_{R_{\mu\nu}, h_{\text{TT}}}^2$ (cf. blue and red surfaces in Figure 7.7). The analog of eq. (7.49) reads

$$\begin{aligned} \text{Flow}_{\text{TT}}^{(2h)} \Big|_{3h}^{(2)} &= \int_0^\infty dq q^3 \int_{-1}^1 dx \sqrt{1-x^2} \\ &\quad \cdot \frac{g_{R, h_{\text{TT}}}^3}{(1 - 6g_{R^2, h_S^2} - 2g_{R_{\mu\nu}, h_{\text{TT}}}^2 + \mu_{h_{\text{TT}}})^2 (1 + g_{R_{\mu\nu}, h_{\text{TT}}}^2 + \mu_{h_{\text{TT}}})^2} \\ &\quad \cdot \frac{f(p, q, x, \eta_{h_{\text{TT}}}(q^2), \eta_{h_S}(q^2), \mu_{h_{\text{TT}}}, g_{R^2, h_S^2}, \dot{g}_{R^2, h_S^2}, g_{R_{\mu\nu}, h_{\text{TT}}}^2, \dot{g}_{R_{\mu\nu}, h_{\text{TT}}}^2, \lambda_3)}{g(p, q, x, \mu_{h_{\text{TT}}}, g_{R^2, h_S^2}, g_{R_{\mu\nu}, h_{\text{TT}}}^2)}. \end{aligned} \quad (7.51)$$

The logic is the same, but of course the theory parameter tensor grows again. The highest powers are now $\eta_{h_{TT}}^1, \eta_{h_S}^1, \mu_{h_{TT}}^3, g_{R^2, h_S^2}^4, \dot{g}_{R^2, h_S^2}^1, g_{R_{\mu\nu}^2, h_{TT}^2}^6, \dot{g}_{R_{\mu\nu}^2, h_{TT}^2}^1$ and λ_S^2 (the minimal powers are again zero for all parameters), s.t. \mathcal{T}_{TP} has $2 \cdot 2 \cdot 4 \cdot 5 \cdot 2 \cdot 7 \cdot 2 \cdot 3 = 6720$ entries, but fortunately only 640 of them are non-zero. Due to the high amount of terms and the additional theory parameters the density of the sampling points is lowered compared to approximation 1. However parallel computing is essential.

The poles (cf. blue and red surfaces in Figure 7.7) divide the theory subspace in four parts, where one part includes all previous fixed points (light green/purple/yellow dots, which are aligned on a grey dashed line). Here the setting is different: To pre-

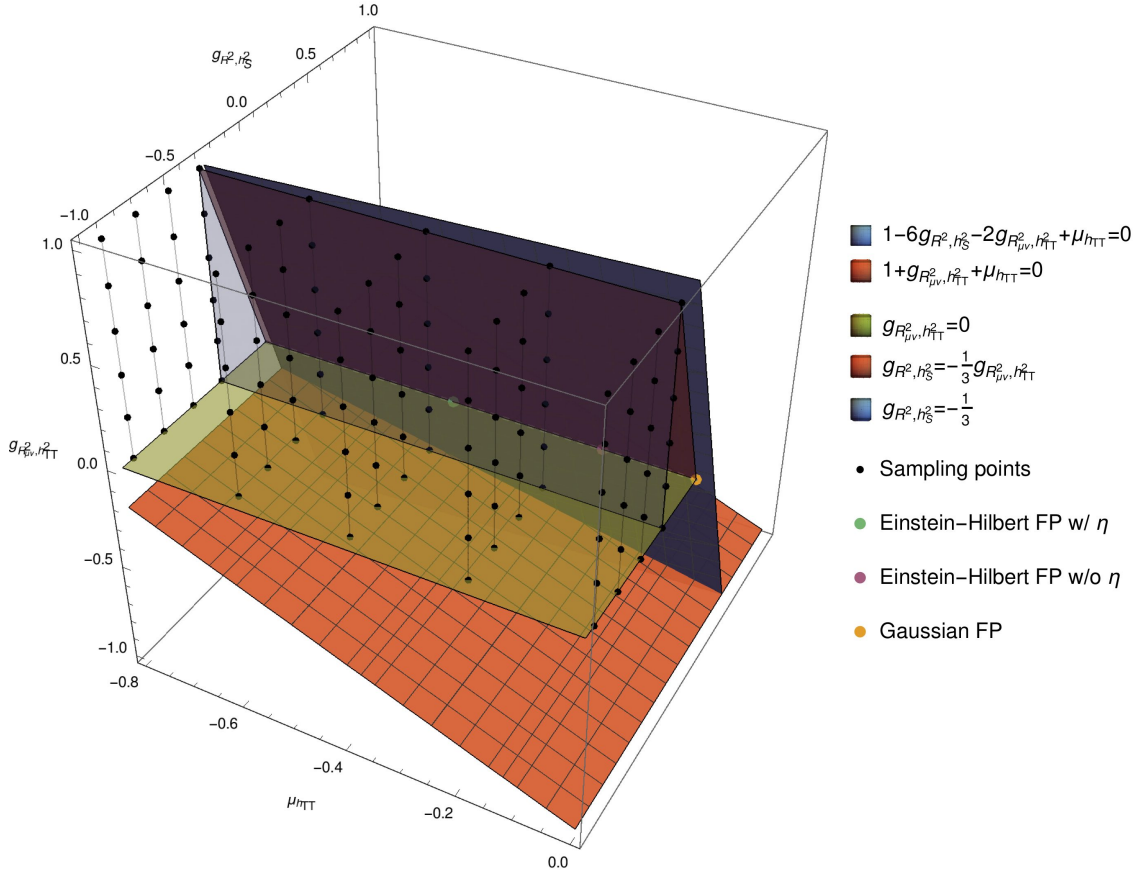


Figure 7.7: Sampling points, poles, included regions and trivial fixed points for the 2nd approximation

vent the graviton propagator components from becoming negative one has to demand that $g_{R_{\mu\nu}^2, h_{TT}^2} \geq 0$ (restricted by the light green plane obtained for an equal sign) and $-(3g_{R^2, h_S^2} + g_{R_{\mu\nu}^2, h_{TT}^2}) \geq 0$ (light red plane, also computed with an equal sign, which is connected to all three fixed points). The remaining subspace is no cuboid, which is impractical for an interpolation procedure based on a grid with low sampling point density. To change this the maximal absolute value of both higher order couplings is set to 1. Then $g_{R_{\mu\nu}^2, h_{TT}^2}$ is only computed in $[0, 1]$, s.t. g_{R^2, h_S^2} has to stay within $[-1, -\frac{1}{3}]$ to

fulfill the prior mentioned requirements. $g_{R^2, h_\xi^2} = -\frac{1}{3}$ is shown as a light blue plane in [Figure 7.7](#). Together with the light green plane it limits the cuboid computation grid.

Short summary

To get a quick overview how the three diagrams at the four momentum values are computed have a short look at [Table 7.2](#).

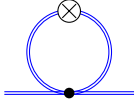
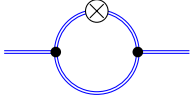
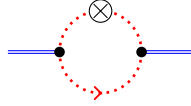
Momentum value			
$p^2 = 0$ $p^2 = \frac{k^2}{2}$	analytically analytically	analytically numerically (on grid w/ different poles in approx. 1 and 2)	analytically numerically (w/o poles)
$p^2 = k^2$	analytically	numerically (on grid w/ different poles in approx. 1 and 2)	numerically (w/o poles)
$p^2 = -\mu_{h_{\text{TPIS}}} k^2$	analytically	numerically (on grid w/ different poles in approx. 1 and 2)	numerically (on grid w/o poles)

Table 7.2: Overview of integrating procedures (analytically/numerically) for the three diagrams at all four momentum values

Moreover the characteristics of \mathcal{T}_{TP} including the maximal calculation time for the numerical integration and interpolation procedure (obtained for $p^2 = \frac{k^2}{2}$) for all three cases is presented in [Table 7.3](#). The calculation was done at the computing grid of the institute, which features parallel computing at 8 kernels and RAM up to 64 GB. The total calculation of approximation 2 (the S-projected flow doubles the time) took approximately 12 days.

Approximation	Total entries	Non-zero entries	Time
Einstein-Hilbert	8	6	$\leq 10\text{min}$
Approximation 1	448	150	$\leq 20\text{h}$
Approximation 2	6 720	640	$\leq 70\text{h}$

Table 7.3: Total number and number of non-zero entries of \mathcal{T}_{TP} together with the maximal calculation time for one diagram in each approximation

Part III

Results

8 Results and discussion

In this chapter all results are presented and discussed. The 1st section is dedicated to the Einstein-Hilbert level: All flow equations in this thesis can be considered as an upgrade of the Einstein-Hilbert truncation, therefore one should be able to reproduce the found flow equations and fixed points. Furthermore the Einstein-Hilbert truncation will be investigated with split TT- and S-projected graviton mass parameters and anomalous dimensions, which should give a feedback if their distinction (which is already implemented in the vertex construction) is reasonable or not.

In the 2nd section an important property of the graviton n -point functions is tested, namely momentum locality. This is done for the TT- and S-projected part of the graviton 2-point function and the G-projected part of the graviton 3-point function. To that end polynomial long division and power counting arguments are utilized to obtain analytical statements. In all cases also the split Einstein-Hilbert limit is tested and flows are plotted to exemplify the results.

Thereafter two approximations are investigated w.r.t. fixed point values and polynomial momentum dependence: The 1st approximation (Einstein-Hilbert and $R_{\mu\nu}^2$ tensor structures in the vertices) in the 3rd section and the 2nd approximation (Einstein Hilbert, R^2 and $R_{\mu\nu}^2$ tensor structures) in the 4th and last section.

8.1 Einstein-Hilbert truncation

The Einstein-Hilbert truncation was investigated several times before [16, 17, 18] (for analytic flow equations cf. the appendices of the three named publications) and should be regarded as a trivial check. This applies especially to the equations which stem from a numerical integration and interpolation procedure and hence are hard to compare. A comprehensive comparison w.r.t. fixed points is done in the 1st subsection. Afterwards the Einstein-Hilbert truncation is investigated without identifying TT- and S-projected couplings, i.e. without using $\mu_{h_{\text{TT}}} = \mu_{h_S}$ and $\eta_{h_{\text{TT}}} = \eta_{h_S}$.

8.1.1 Checking the Einstein-Hilbert limit

For this check all higher couplings which appear in the flows, i.e. after the numerical integration and interpolation procedure, are set to zero. Then several systems will be analyzed: g_{R,h_{TT}^3} (in previous works this coupling was named g_3) can be computed either analytically via a derivative projection at $p^2 = 0$ or numerically with a bi-local momentum projection and with or without anomalous dimensions, s.t. in addition four different systems can be tested. Note that the flow equations for $\mu_{h_{\text{TT}}}$ and λ_3 are always analytical. In all cases TT- and S-projected parameters are identified, i.e. $\mu_{h_{\text{TT}}} \equiv \mu_{h_S}$ and

$\eta_{h_{\text{TT}}} \equiv \eta_{h_5}$. In former works the couplings were extracted via the TT-projected flows and of course this approach will be adopted. In addition the TT-projected Einstein-Hilbert theory space is spanned by

$$\{\mu_{h_{\text{TT}}}, \lambda_3, g_{R,h_{\text{TT}}}^3\}, \quad (8.1)$$

with the momentum dependent anomalous dimensions $\eta_{h_{\text{TT}}}(p^2)$ and $\eta_c(p^2)$. In former language this reads $\{\mu_h, \lambda_3, g_3\}$, $\eta_h(p^2)$ and $\eta_c(p^2)$.

All fixed points have to fulfill certain physical requirements:

1. **Positive Newton coupling:** As the IR value of Newton's coupling is positive and the truncation forbids flow trajectories which correspond to a change of sign the Newton coupling has to be positive or zero, i.e. $g_{R,h_{\text{TT}}}^3 \geq 0$.
2. **Avoiding the graviton propagator's pole:** A flow trajectory can't cross a pole and there should be at least one trajectory connecting the UV fixed point with the Gaussian fixed point, s.t. only values $\mu_{h_{\text{TT}}} > -1$ are allowed.
3. **Fixed point with at least one attractive direction:** The UV fixed point should be fully attractive or metastable but not fully repulsive.
4. **Small anomalous dimensions at the fixed point:** Previous studies revealed that $\eta_{\Phi_i} < 2$ is a bound for all anomalous dimensions. This is due to the fact that anomalous dimensions are total prefactors in the regulator components which have to ensure the condition in eq. (4.16). As $\eta_{\Phi_i} \propto g_{R,h_{\text{TT}}}^3$ this translates directly to Newton's coupling.

The four conditions will play an even more important role in the case of higher order vertices: For Einstein-Hilbert vertices one needs only a handful sampling points in a *FindRoot* algorithm (numerical inaccuracies can cause artificial solutions, therefore a check is always indispensable) to find the fixed points and almost all found fixed points naturally fulfill the physical conditions. Higher order vertices behave more impractical: A very big range in the theory space has to be sampled (usually ≈ 1000 points) which produces ≈ 50 fixed point values whereof only ≈ 5 are physically relevant. To be sure the same algorithm was used in the Einstein-Hilbert case, with ≈ 10000 sampling points in all cases.

The full fixed point analysis is always done in two steps: At first all anomalous dimensions appearing in the flows are set to zero, i.e. $\eta_{\Phi_i} = 0$, which is of course an approximation. Then all dotted quantities are set to zero since the flows vanish at the fixed points. Note that some dotted quantities can appear on the RHS of another flow equation, e.g. $\dot{g}_{R,h_{\text{TT}}}^3$ in the flow equation for λ_3 (cf. eq. (6.97)), which are also zero at the fixed point. The resulting equations do only depend on theory parameters and can be solved for these using the *FindRoot* command. Although the anomalous dimensions were set to zero in the flows (which was an *approximation*) it is possible to compute their values at the fixed points by plugging in the fixed point values into their defining

equations. The 2nd step is essentially the same as before, but now the anomalous dimensions are already respected in the flows. Technically this is much more complicated because of the numerical behaviour of the anomalous dimensions which is transferred to all flow equations.

Fixed point analysis for analytical g_{R,h_{TT}^3}

Let's begin with the analytical flow equation for g_{R,h_{TT}^3} . The non-trivial UV fixed point values for flows with and without anomalous dimensions, together with the values of the anomalous dimensions and the eigenvalues at the fixed points are displayed in [Table 8.1](#).

Couplings	$\eta_{\phi_i} = 0$ in the flows	with η_{ϕ_i} in the flows
$\mu_{h_{\text{TT}}}^*$	-0.1645	-0.4387
λ_3^*	-0.1641	0.0251
$g_{R,h_{\text{TT}}^3}^*$	0.5702	0.5818
η_{ϕ_i} at FP		
$\eta_{h_{\text{TT}}}^*(0)$	0.81	1.03
$\eta_{h_{\text{TT}}}^*(k^2)$	0.29	0.31
$\eta_c^*(k^2)$	-0.49	-0.99
EV	$(-1.53 \pm 1.77i, 1.65)$	$(-1.25 \pm 4.72i, 6.02)$

Table 8.1: UV fixed point analysis in Einstein-Hilbert truncation for analytical g_{R,h_{TT}^3} with and without η_{ϕ_i} in the flows

The 1st column in [Table 8.1](#) has to be fully identical to previous results due to the analytical behaviour of the system, which is true. The 2nd column involves numerically computed quantities and therefore a small deviation is arguable. Compared to former results the deviation is always smaller than $\approx 15\%$ which is alright. Both fixed points have two attractive directions and fulfill the physical requirements. Besides the non-trivial fixed points one can find the so-called Gaussian fixed point located at

$$(\mu_{h_{\text{TT}}}^*, \lambda_3^*, g_{R,h_{\text{TT}}^3}^*) = (0, 0, 0). \quad (8.2)$$

Both systems contain this trivial fixed point and all anomalous dimensions are zero

$$(\eta_{h_{\text{TT}}}^*(0), \eta_{h_{\text{TT}}}^*(k^2), \eta_c^*(k^2)) = (0, 0, 0). \quad (8.3)$$

Furthermore the eigenvalues at the fixed point are

$$(-2, -2, 2), \quad (8.4)$$

s.t. the Gaussian fixed point has two attractive directions.

Fixed point analysis for numerical g_{R,h_{TT}^3}

The same analysis can be repeated for a numerically computed g_{R,h_{TT}^3} . As against to all other flow equations the corresponding flow equation was calculated in the Einstein-Hilbert limit only due to technical feasibility. The results are presented in [Table 8.2](#).

Couplings	$\eta_{\phi_i} = 0$ in the flows	with η_{ϕ_i} in the flows
$\mu_{h_{\text{TT}}}^*$	-0.3475	-0.5657
λ_3^*	-0.023	0.0932
$g_{R,h_{\text{TT}}^3}^*$	0.9688	0.6333
η_{ϕ_i} at FP		
$\eta_{h_{\text{TT}}}^*(0)$	1.47	1.43
$\eta_{h_{\text{TT}}}^*(k^2)$	0.48	0.44
$\eta_c^*(k^2)$	-1.26	-1.67
EV	$(-2.14 \pm 2.48i, 5.85)$	$(-0.49 \pm 4.03i, 12.12)$

Table 8.2: UV fixed point analysis in Einstein-Hilbert truncation for numerical g_{R,h_{TT}^3} with and without η_{ϕ_i} in the flows

Compared to previous works the deviation of the fixed point values and the values of the anomalous dimensions is again at most $\approx 15\%$. Besides the non-trivial UV fixed point for η_{ϕ_i} shown on [Table 8.2](#) one can find another non-trivial UV fixed point which is fully attractive. Its coordinates are

$$(\mu_{h_{\text{TT}}}^*, \lambda_3^*, g_{R,h_{\text{TT}}^3}^*) = (-0.3276, 0.2985, 1.0011) \quad (8.5)$$

and the corresponding eigenvalues read

$$(-4.28 \pm 1.28i, -2.83), \quad (8.6)$$

which lies once more within the 15% range. Furthermore the trivial Gaussian fixed point appears in both cases with the same properties as before (cf. eqs. (8.2), (8.3) and (8.4)).

Short summary

This section can be recapitulated in only one succinct sentence: Everything is fine. Nothing unexpected happened and all former results could be reproduced. The flow equations passed the trivial but meaningful test which implies that especially the numerical integration and interpolation procedure appears to be reasonable. Due to a comparatively low sampling point density limited by technical feasibility in the theory space this is a very promising result for the inclusion of higher order tensor structures in the vertices.

8.1.2 Einstein-Hilbert truncation with diverse TT- and S-projected couplings and anomalous dimensions

The vertex construction presented in this work is build upon the assumption that a distinction of TT- and S-projected parameters appearing in the graviton propagator, i.e. $\mu_{h_{\text{TT}}} \neq \mu_{h_{\text{S}}}$ and $\eta_{h_{\text{TT}}} \neq \eta_{h_{\text{S}}}$ is sensible. Before moving on to higher order tensor structures in the vertices this distinction is investigated in the Einstein-Hilbert case. To keep the computation as simple as possible g_{R,h_{TT}^3} is computed analytically via a derivative projection at $p^2 = 0$ and the η_{ϕ_i} appearing in the flows are set to zero for the fixed point search. The corresponding fixed point values for identified parameters can be found in the 1st column of [Table 8.1](#). In total one can discover four UV fixed points: Two of them are unphysical ($\mu_{h_{\text{S}}} < -1$ in both cases), one is a non-trivial and physically valid UV fixed point (cf. [Table 8.3](#)) and the remaining one is the Gaussian fixed point, where $\mu_{h_{\text{S}}}$ introduces an additional attractive direction with the eigenvalue -2 .

Couplings	$\eta_{\phi_i} = 0$ in the flows
$\mu_{h_{\text{TT}}}^*$	-0.2444
$\mu_{h_{\text{S}}}^*$	-0.3781
λ_3^*	0.0837
$g_{R,h_{\text{TT}}^3}^*$	0.5813
η_{ϕ_i} at FP	
$\eta_{h_{\text{TT}}}^*(0)$	0.67
$\eta_{h_{\text{TT}}}^*(k^2)$	0.22
$\eta_{h_{\text{S}}}^*(0)$	-0.22
$\eta_{h_{\text{S}}}^*(k^2)$	-0.99
$\eta_c^*(k^2)$	-0.43
EV	$(-1.33 \pm 2.74i, -3.43, 2.83)$

Table 8.3: UV fixed point analysis in split Einstein-Hilbert truncation for analytical g_{R,h_{TT}^3} without η_{ϕ_i} in the flows

Obviously $\mu_{h_{\text{TT}}}$ and $\mu_{h_{\text{S}}}$ take completely different fixed point values and none of them is approximately equal to the value of $\mu_{h_{\text{TT}}}$ for identified parameters (before: $\mu_{h_{\text{TT}}}^* = -0.1645$). Furthermore $g_{R,h_{\text{TT}}^3}^*$ is almost equal to before (before: $g_{R,h_{\text{TT}}^3}^* = 0.5702$) and λ_3^* even changed the sign (before: $\lambda_3^* = -0.1641$). The values of $\eta_{h_{\text{TT}}}$ and η_c at the fixed point don't change a lot, but both values of $\eta_{h_{\text{S}}}$ are negative and therefore far away. Combined the fixed point values of TT- and S-projected parameters are totally different.

As one can read from the eigenvalues $\mu_{h_{\text{S}}}$ introduces a new attractive direction. Analyzing the eigenvector which belongs to the only positive eigenvalue reveals that it's

mainly pointing in the λ_3 direction, which was already the case for identified parameters.

A more comprehensive method for a comparison is to compute the fully momentum dependent graviton anomalous dimensions at the fixed point via an iterative computation. Such a solution can be constructed as follows: At first take the defining equations for all anomalous dimensions and set the anomalous dimensions appearing in the flows to zero. Then the loop integrals can be executed to obtain a level 0 approximation for each anomalous dimension (cf. blue curves in [Figure 8.1](#) and [Figure 8.2](#), the plot for η_c isn't shown here). Afterwards these solutions are used for the anomalous dimensions in the flows, which leads to a system of coupled equations. The loop integration in this system can be executed and one will receive the level 1 approximation. Repeating the last step yields a converging series. A criterion for interrupting the iteration procedure has to be set by hand. In this work a relative deviation of 2% between two consecutive levels was chosen. Conveniently already a few iteration steps are enough to achieve this precision: In the plots the green curve (= level 2) already fully covers the yellow curve (= level 1).

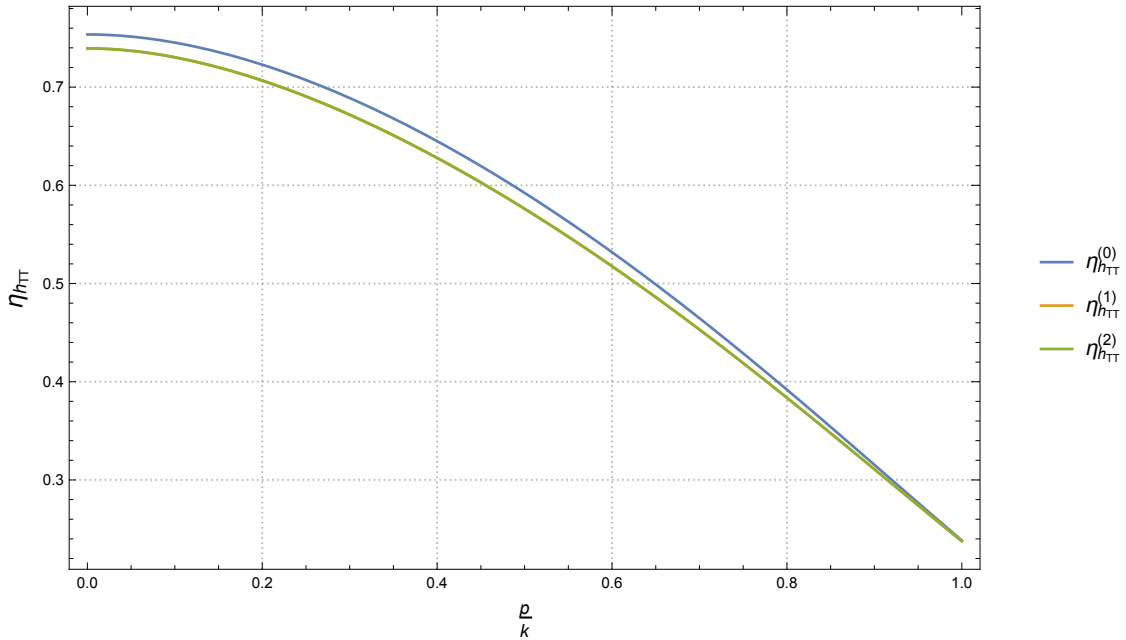


Figure 8.1: Fully momentum dependent $\eta_{h_{TT}}$ for the first three iteration levels in the momentum range $p \in [0, k]$

Please note that the values in [Table 8.3](#) do *not* have to match the corresponding values in [Figure 8.1](#) and [Figure 8.2](#) *exactly* due to the approximation $\eta_{\phi_i}(q^2) \approx \eta_{\phi_i}(k^2)$ in case of bi-locally computed anomalous dimensions.

[Figure 8.1](#) and [Figure 8.2](#) illustrate what already the values of both graviton anomalous dimensions at the fixed point implied: $\eta_{h_{TT}}$ and η_{h_S} behave totally different, not even the signs coincide. Therefore distinct TT- and S-projected theory parameters and especially anomalous dimensions have to be investigated further w.r.t. physical implications.

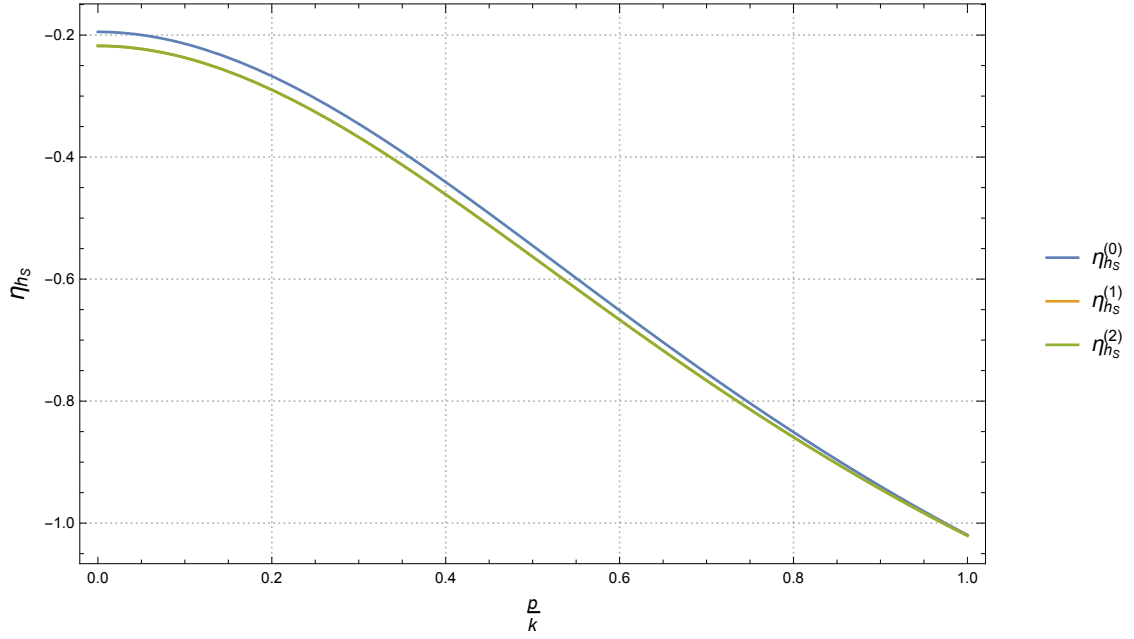


Figure 8.2: Fully momentum dependent η_{h_s} for the first three iteration levels in the momentum range $p \in [0, k]$

8.2 Momentum locality of the graviton flows

Every physical reliable QFT is a local theory in position space. Having in mind the perception of Wilson's renormalization procedure, i.e. integrating out small momentum shells at a specific scale k , allows to translate this key property in momentum space: An RG step at some scale k shouldn't be able to change the physics, i.e. correlation functions, at some other scale k' . This applies in particular to the following situation: Integrating out momentum shells at $k = 0$ in the IR shouldn't influence the UV. As the vertex expansion scheme approximates the scale-dependent effective action in terms of low-order vertices this requirement has to be fulfilled by all considered flows of the vertices, i.e. for the graviton 2-point and 3-point function. Since both of them are tensors the easiest way to check this is to investigate the components separately. In addition demanding momentum locality in terms of formulas yields

$$\lim_{p_j \rightarrow \infty} \frac{\partial_t \Gamma_i^{(nh)}(\vec{p})}{\Gamma_i^{(nh)}(\vec{p})} \stackrel{!}{=} 0 \quad \text{with } j = 1, \dots, n, \quad (8.7)$$

where i denotes a particular tensor component and $\vec{p} = (p_1, \dots, p_n)$ is the momentum vector of all n external momenta.

In the context of a renormalizable QFT in four space-time dimensions (Abelian or even non-Abelian) momentum locality is trivially fulfilled, which can be checked by usual power-counting. For non-renormalizable QFT's it's the other way round: Power-counting implies that non-local flows exist, s.t. only a non-trivial behaviour of the flows can ensure

momentum locality. It is believed that in quantum gravity diffeomorphism invariance is in charge of this actual cancellations of high momentum powers [17].

Previous studies confirmed momentum locality of the TT-projected graviton 2-point function [16, 20] and the G-projected graviton 3-point function [17] (even for an unfixed angle between the two open momenta) in the Einstein-Hilbert truncation.

Therefore the setup presented in this thesis may also feature momentum locality of the flows. At least it should be possible to find conditions for the higher order couplings s.t. momentum locality can be achieved. In the next two sections the flows of the graviton 2-point and 3-point functions will be investigated w.r.t. momentum locality.

8.2.1 Locality of the graviton 2-point function

The present setup allows to analyze two components of the graviton 2-point function, in particular the TT- and S-component given by the eqs. (6.59) and (6.79). In both cases one has two external momenta, but of course one of them is determined by the remaining one due to momentum conservation, s.t. in total eq. (8.7) in this case reads

$$\lim_{p \rightarrow \infty} \frac{\partial_t \Gamma_{k, \text{TT|S}}^{(2h)}(p)}{\Gamma_{k, \text{TT|S}}^{(2h)}(p)} \stackrel{!}{=} 0. \quad (8.8)$$

To examine the momentum locality condition one should at first think about the polynomial behaviour of the involved quantities since the limit $p \rightarrow \infty$ can be shifted to both parts of the fraction. The two components of the graviton 2-point function scale with p^4 for high momenta because of the higher order terms. Furthermore, before integrating over the loop momentum, the graviton 2-point flows are in general of the form

$$\text{Flow}_{\text{TT|S}}^{(2h)} = \int d^4 q \frac{\text{polynomial}_1(p^2)}{\text{polynomial}_2(p^2)}. \quad (8.9)$$

To get an exact polynomial expression plus rest one can do a polynomial long division. Technically this is possible for the graviton 2-point flows, but unfortunately not for the graviton 3-point flow. One gets out

$$\text{Flow}_{\text{TT|S}}^{(2h)} = \int d^4 q \left(c_0 p^4 + c_1 p^2 + c_2 + \frac{c_3}{\text{polynomial}(p^2)} \right), \quad (8.10)$$

where $c_i = c_i(q, x, \Theta(p^2))$ are functions of the theory parameters, the loop momentum and Heaviside theta functions which can possess p^2 as argument.

Obviously the flows also scale with p^4 for high external momenta, s.t. only the p^4 contributions have to be investigated in the context of momentum locality. A similar behaviour was discovered in the Einstein-Hilbert truncation, but there the highest power was p^2 . Momentum locality was found after integrating over the loop momentum (i.e. the contributions of all diagrams added up to zero), which is an open task here.

To execute the loop integration one has to implement $p \rightarrow \infty$ in the c_0 coefficient: There exist Heaviside theta functions like $\Theta(k^2 - (p+q)^2)$, which stem from the graviton

propagator, but for $p \rightarrow \infty$ these terms are zero. After having handled this problem one can integrate over q and x as usual. The results for the TT- and S-projected parts are presented separately below.

TT-projected graviton 2-point function

One finds that the p^4 coefficient of the TT-projected flow of the graviton 2-point function after the loop integration is of the form

$$\text{Flow}_{\text{TT}}^{(2h)} \Big|_{p^4} = \frac{g_{R,h_{\text{TT}}}^3 g_{R^2,\mu\nu,h_{\text{TT}}}^2}{(3g_{R^2,h_{\text{S}}}^2 + g_{R^2,\mu\nu,h_{\text{TT}}}^2)(1 - 6g_{R^2,h_{\text{S}}}^2 - 2g_{R^2,\mu\nu,h_{\text{TT}}}^2 + \mu_{h_{\text{S}}})^2} \cdot \frac{f(\mu_{h_{\text{TT}}}, \mu_{h_{\text{S}}}, \eta_{h_{\text{TT}}}, \eta_{h_{\text{S}}}, g_{R^2,\mu\nu,h_{\text{TT}}}^2, \dot{g}_{R^2,\mu\nu,h_{\text{TT}}}^2, g_{R^2,h_{\text{S}}}^2, \dot{g}_{R^2,h_{\text{S}}}^2)}{(1 + g_{R^2,\mu\nu,h_{\text{TT}}}^2 + \mu_{h_{\text{TT}}})^2}, \quad (8.11)$$

wherein f is a complicated polynomial of its displayed arguments. From eq. (8.11) one can directly deduce that a vanishing p^4 coefficient is

1. not achieved *in general*,
2. accomplished for $g_{R^2,\mu\nu,h_{\text{TT}}}^2 = 0$,
3. maybe obtained for a non-trivial condition which is an implication of $f = 0$.

Please note that $g_{R,h_{\text{TT}}}^3 = 0$ does *not* correspond to momentum locality since all flows are proportional to certain powers of $g_{R,h_{\text{TT}}}^3$ (cf. prefactor in eq. (6.50)). Statement no. 3 requires a more detailed investigation: Searching for roots of f with the two higher order couplings as variables leads to five solutions which depend on the other theory parameters. Three of them are imaginary and therefore unphysical. The remaining two are simple relations for both higher order couplings. To evaluate their physical meaning one can simplify them further by only regarding fixed points. There the flows of the higher order couplings vanish, i.e. $\dot{g}_{R^2,h_{\text{S}}}^2 = \dot{g}_{R^2,\mu\nu,h_{\text{TT}}}^2 = 0$. Then the two doublets of relations read

$$g_{R^2,h_{\text{S}}}^2 = \frac{23}{204} \cdot \frac{(-12 + 2\eta_{h_{\text{TT}}})}{(-8 + \eta_{h_{\text{TT}}})}, \quad (8.12)$$

$$g_{R^2,\mu\nu,h_{\text{TT}}}^2 = -\frac{68}{23} g_{R^2,h_{\text{S}}}^2 = -\frac{1}{3} \cdot \frac{(-12 + 2\eta_{h_{\text{TT}}})}{(-8 + \eta_{h_{\text{TT}}})} \quad (8.13)$$

and

$$g_{R^2,h_{\text{S}}}^2 = \frac{144 - 20\eta_{h_{\text{S}}} - 22\eta_{h_{\text{TT}}} + 3\eta_{h_{\text{TT}}}\eta_{h_{\text{S}}}}{9(-8 + \eta_{h_{\text{TT}}})(-8 + \eta_{h_{\text{S}}})}, \quad (8.14)$$

$$g_{R^2,\mu\nu,h_{\text{TT}}}^2 = -\frac{1}{3} \cdot \frac{(-12 + 2\eta_{h_{\text{TT}}})}{(-8 + \eta_{h_{\text{TT}}})}. \quad (8.15)$$

The 1st real solution doublet is displayed in Figure 8.3 (denoted by the blue and yellow graphs) together with the physical/technical bounds for the higher order couplings

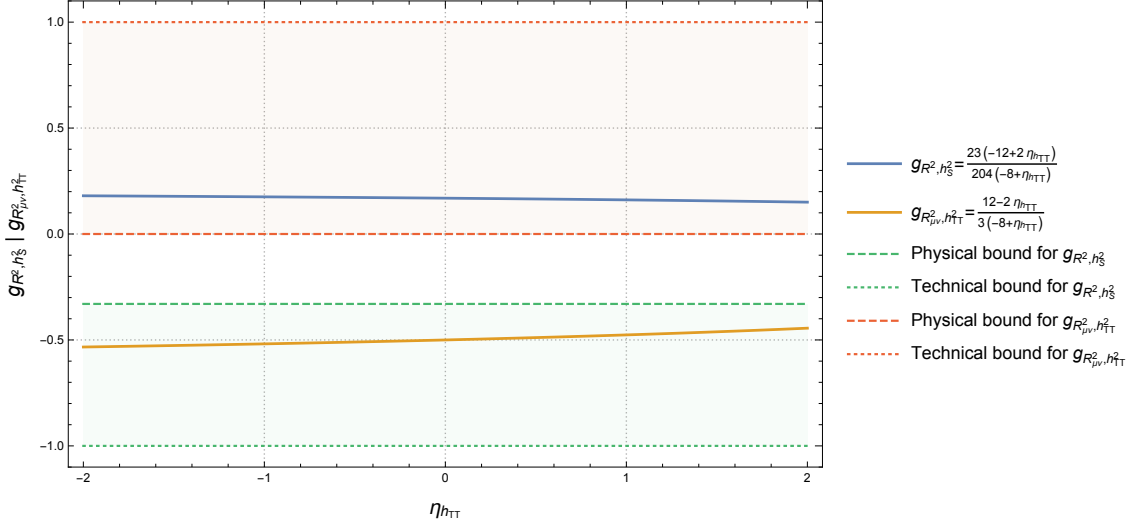


Figure 8.3: 1st real solution doublet of $f = 0$ (blue and yellow graphs) and physical/technical bounds for the higher order couplings (dashed/dotted green and red lines) in the physically relevant range $|\eta_{h_{TT}}| < 2$

(dashed/dotted red and green lines) in the physically relevant range defined by $|\eta_{h_{TT}}| < 2$. Therein one can see that both graphs process outside of their corresponding physical bound. In particular holds

$$g_{R^2, h_S^2} = \frac{23}{204} \cdot \frac{(-12 + 2\eta_{h_{TT}})}{(-8 + \eta_{h_{TT}})} > -\frac{1}{3} \quad \text{for } |\eta_{h_{TT}}| < 2, \quad (8.16)$$

$$g_{R^2_{\mu\nu}, h_{TT}^2} = -\frac{1}{3} \cdot \frac{(-12 + 2\eta_{h_{TT}})}{(-8 + \eta_{h_{TT}})} < 0 \quad \text{for } |\eta_{h_{TT}}| < 2. \quad (8.17)$$

Thus this solution doublet is unphysical, at least at the fixed point. Though momentum locality should be achieved at all scales and thus specifically in the UV. Consequently it is sufficient that the solution violates physical criteria at a sole scale to refuse it.

Let's move on to the 2nd solution doublet: The equation for g_{R^2, h_S^2} contains not only $\eta_{h_{TT}}$, but also η_{h_S} , s.t. the corresponding plot is three-dimensional (cf. Figure 8.4). Essentially Figure 8.4 is a three-dimensional version of Figure 8.2 and again both graphs correspond to unphysical situations. Therefore holds

$$g_{R^2, h_S^2} = \frac{144 - 20\eta_{h_S} - 22\eta_{h_{TT}} + 3\eta_{h_{TT}}\eta_{h_S}}{9(-8 + \eta_{h_{TT}})(-8 + \eta_{h_S})} > -\frac{1}{3} \quad \text{for } |\eta_{h_{TT}}|, |\eta_{h_S}| < 2, \quad (8.18)$$

$$g_{R^2_{\mu\nu}, h_{TT}^2} = -\frac{1}{3} \cdot \frac{(-12 + 2\eta_{h_{TT}})}{(-8 + \eta_{h_{TT}})} < 0 \quad \text{for } |\eta_{h_{TT}}| < 2. \quad (8.19)$$

In addition $f = 0$ does *not* lead to physical solutions which ensure momentum locality. Therefore the only solution for the TT-part of the flow which corresponds to a vanishing p^4 coefficient is $g_{R^2_{\mu\nu}, h_{TT}^2} = 0$. But does this situation really correspond to a momentum local flow? To answer this question let's have a look on the TT-projected graviton

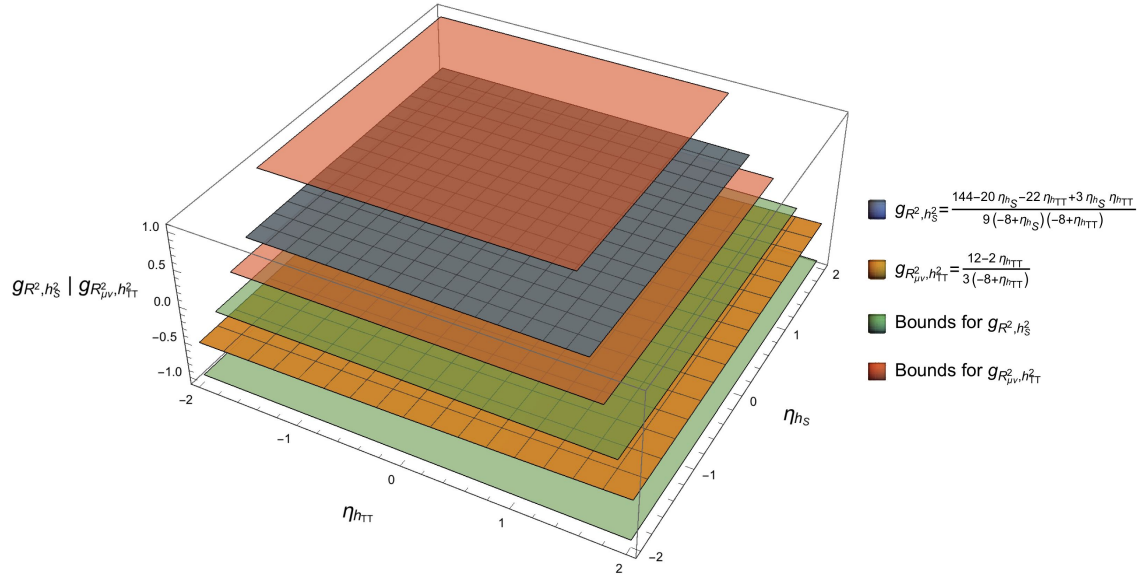


Figure 8.4: 2nd real solution doublet of $f = 0$ and $g = 0$ (blue and yellow surfaces) and bounds for the higher order couplings (semitransparent green and red planes) in the physically relevant range $|\eta_{h_{TT}}| < 2$ and $|\eta_{h_S}| < 2$

2-point function (cf. eq. (6.59)) again: Imposing $g_{R^2_{\mu\nu}, h_{TT}^2} = 0$ implies that the p^4 coefficient vanishes, which reduces the highest order in the denominator of eq. (8.9) to p^2 . Hence the nominator must also have a vanishing p^2 coefficient in order to achieve momentum locality. Combined $g_{R^2_{\mu\nu}, h_{TT}^2} = 0$ indeed kills the p^4 coefficient of the flow, but at the same time kills the p^4 coefficient of the correlation function, s.t. the whole analysis has to be transferred to the p^2 coefficient of the flow.

Since the two operations polynomial long division and $g_{R^2_{\mu\nu}, h_{TT}^2} = 0$ don't commute one has to start with the flow again and implement $g_{R^2_{\mu\nu}, h_{TT}^2} = 0$ at first. Note that as $g_{R^2_{\mu\nu}, h_{TT}^2} = 0$ holds at *all* scales one can directly conclude that $\dot{g}_{R^2_{\mu\nu}, h_{TT}^2} = 0$ is valid at all scales. Repeating the polynomial long division leads to an expression which scales as p^2 for high momenta, as expected. It reads

$$\text{Flow}_{TT}^{(2h)}(g_{R^2_{\mu\nu}, h_{TT}^2} = 0) \Big|_{p^2} = \frac{g_{R, h_{TT}^3} f'(\mu_{h_{TT}}, \mu_{h_S}, \eta_{h_{TT}}, \eta_{h_S}, g_{R^2, h_S^2}, \dot{g}_{R^2, h_S^2})}{(1 - 3g_{R^2, h_{TT}^2} + \mu_{h_S})^2 (1 + \mu_{h_S})^2}, \quad (8.20)$$

where once more f' is a complicated polynomial. Searching for roots of f' w.r.t. the remaining higher order coupling leads to three solutions which are all complex. Even the limit $g_{R^2, h_S^2} = 0$ and $\dot{g}_{R^2, h_S^2} = 0$ doesn't lead to a vanishing p^2 coefficient. Therefore there exists no solution which cancels the p^2 coefficient.

At this stage one can ask if this statement is a contradiction of the well-known momentum local behaviour of the TT-projected graviton 2-point function on Einstein-Hilbert level, because there the terms proportional to p^2 canceled each other after the x -integration. The crucial argument against this perception is again the behaviour of a polynomial long division: Although some higher order terms were killed by setting

$g_{R^2, h_{\text{TT}}^2} = 0$ before the polynomial long division one gets contributions to the p^2 coefficient from the remaining ones (e.g. the S-part of the graviton propagator still scales with p^4 in the denominator). Thus one can only retrieve Einstein-Hilbert results by setting all higher order couplings to zero at first and doing a polynomial long division afterwards. Compared to the latter analysis this is a trivial task. Due to the fact that previous works only checked flows where the identifications $\mu_{h_{\text{TT}}} = \mu_{h_S}$ and $\eta_{h_{\text{TT}}} = \eta_{h_S}$ were made, an analysis without performing these identifications is presented in the following to exclude their missing as a reason for the absence of momentum locality in case of higher order flows.

Setting all higher order couplings to zero and doing a polynomial long division reveals that the two graviton loop diagrams scale with p^2 while the ghost loop diagram is already constant. After the x -integration one finds that (note that the graviton loop diagrams have the same overall prefactor which is left out here and that k was set to one)

$$\begin{array}{c}
 -\frac{1}{2} \text{ (diagram)} \\
 \left. \begin{array}{l} \text{EH} \\ \text{TT}, p^2 \end{array} \right\} \propto -6 - 20\mu_{h_S} - 10\mu_{h_S}^2 - 5(-1 + q^2)\eta_{h_{\text{TT}}}(1 + \mu_{h_S})^2 \\
 \qquad \qquad \qquad + 8\mu_{h_{\text{TT}}} + 4\mu_{h_{\text{TT}}}^2 + 2(-1 + q^2)\eta_{h_S}(1 + \mu_{h_{\text{TT}}})^2, \quad (8.21)
 \end{array}$$

$$\begin{array}{c}
 \text{(diagram)} \\
 \left. \begin{array}{l} \text{EH} \\ \text{TT}, p^2 \end{array} \right\} \propto +6 + 20\mu_{h_S} + 10\mu_{h_S}^2 + 5(-1 + q^2)\eta_{h_{\text{TT}}}(1 + \mu_{h_S})^2 \\
 \qquad \qquad \qquad - 8\mu_{h_{\text{TT}}} - 4\mu_{h_{\text{TT}}}^2 - 2(-1 + q^2)\eta_{h_S}(1 + \mu_{h_{\text{TT}}})^2, \quad (8.22)
 \end{array}$$

$$\begin{array}{c}
 -2 \text{ (diagram)} \\
 \left. \begin{array}{l} \text{EH} \\ \text{TT}, p^2 \end{array} \right\} \propto 0. \quad (8.23)
 \end{array}$$

One can directly see that all terms cancel out and hence momentum locality is confirmed for split Einstein-Hilbert flows. Another nice method to present such a result is to take the unintegrated flows, set all contained theory parameters to a numerical value and integrate this expression numerically for several specific values of the external momentum p^2 (a reasonable choice is $p^2/k^2 \in [0, 10]$ with 0.05 steps). The result can be interpolated to obtain a smooth curve. [Figure 8.5](#) shows the outcome of such a computation: The chosen values for the theory parameters are $\mu_{h_{\text{TT}}} = -0.01$, $\mu_{h_S} = -0.02$, $\lambda_3 = 0.1$, $g_{R, h_{\text{TT}}^3} = 0.5$, $\eta_{h_{\text{TT}}} = 0.5$, $\eta_{h_S} = -0.5$, $\eta_c = -1$. Note that the anomalous dimensions are handled as momentum independent objects and that the TT- and S-projected parameters are intentionally set to different values. [Figure 8.5](#) illustrates not only the flow of the graviton 2-point function (blue curve), which tends to a constant value depicted by a horizontal asymptote (dashed red line), but also the flow divided by the 2-point function (green curve), which tends to zero (thick dashed gray line).

In summary momentum locality is achieved for distinct TT- and S-projected parameters in an Einstein-Hilbert truncation, but not for higher order vertices. Neither exists a combination of higher order theory parameters to cure this, nor does the distinction of TT- and S-projected parameters destroy the observed momentum locality on Einstein-Hilbert level.

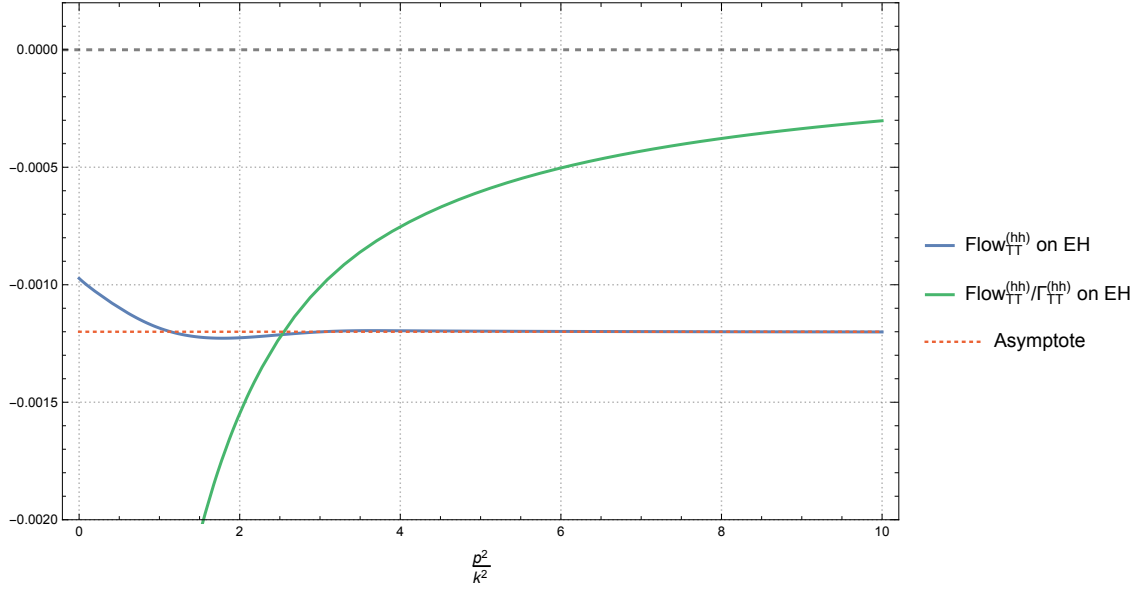


Figure 8.5: Flow of the TT-projected graviton 2-point function on Einstein-Hilbert (blue curve) together with its horizontal asymptote (red dashed line) for high momenta and the flow divided by the TT-projected graviton 2-point function on Einstein-Hilbert (green curve). Both curves are rescaled.

S-projected graviton 2-point function

All steps from the TT-part can be repeated without further ambiguities. The analog of eq. (8.11) for the S-projected part reads

$$\text{Flow}_S^{(2h)} \Big|_{p^4} = \frac{g_{R,h_{\text{TT}}}^3 (3g_{R^2,h_S^2} + g_{R_{\mu\nu},h_{\text{TT}}^2})}{g_{R_{\mu\nu},h_{\text{TT}}^2} (1 - 6g_{R^2,h_S^2} - 2g_{R_{\mu\nu},h_{\text{TT}}^2} + \mu_{h_S})^2} \cdot \frac{g(\mu_{h_{\text{TT}}}, \mu_{h_S}, \eta_{h_{\text{TT}}}, \eta_{h_S}, g_{R_{\mu\nu},h_{\text{TT}}^2}, \dot{g}_{R_{\mu\nu},h_{\text{TT}}^2}, g_{R^2,h_S^2}, \dot{g}_{R^2,h_S^2})}{(1 + g_{R_{\mu\nu},h_{\text{TT}}^2} + \mu_{h_{\text{TT}}})^2}, \quad (8.24)$$

where again g is a complex polynomial. Note that in comparison to eq. (8.11) the overall prefactor $(3g_{R^2,h_S^2} + g_{R_{\mu\nu},h_{\text{TT}}^2})^{-1}(g_{R_{\mu\nu},h_{\text{TT}}^2})$ got inverted. Therefore a vanishing p^4 coefficient is

1. also not achieved *in general*,
2. accomplished for $g_{R_{\mu\nu},h_{\text{TT}}^2} = -3g_{R^2,h_S^2}$,
3. maybe obtained for a non-trivial condition which is an implication of $g = 0$.

Demanding $g = 0$ and solving for the two higher order couplings at the fixed point yields

$$g_{R^2,h_S^2} = \frac{5}{24} \cdot \frac{(-12 + 2\eta_{h_{\text{TT}}})}{(-8 + \eta_{h_{\text{TT}}})}, \quad (8.25)$$

$$g_{R_{\mu\nu},h_{\text{TT}}^2} = -\frac{8}{5} g_{R^2,h_S^2} = -\frac{1}{3} \cdot \frac{(-12 + 2\eta_{h_{\text{TT}}})}{(-8 + \eta_{h_{\text{TT}}})} \quad (8.26)$$

and

$$g_{R^2, h_S^2} = \frac{144 - 20\eta_{h_S} - 22\eta_{h_{TT}} + 3\eta_{h_{TT}}\eta_{h_S}}{9(-8 + \eta_{h_{TT}})(-8 + \eta_{h_S})}, \quad (8.27)$$

$$g_{R_{\mu\nu}^2, h_{TT}^2} = -\frac{1}{3} \cdot \frac{(-12 + 2\eta_{h_{TT}})}{(-8 + \eta_{h_{TT}})}, \quad (8.28)$$

which are the only real solutions. Obviously the eqs. (8.26), (8.27) and (8.28) are fully identical to the eqs. (8.13), (8.14) and (8.20), only eq. (8.25) differs from eq. (8.12) by a factor of $\frac{46}{85} \approx 0.541 > 0$. To ensure a physical solution this ratio has to be negative. Nevertheless the 1st solution doublet is presented in Figure 8.6.

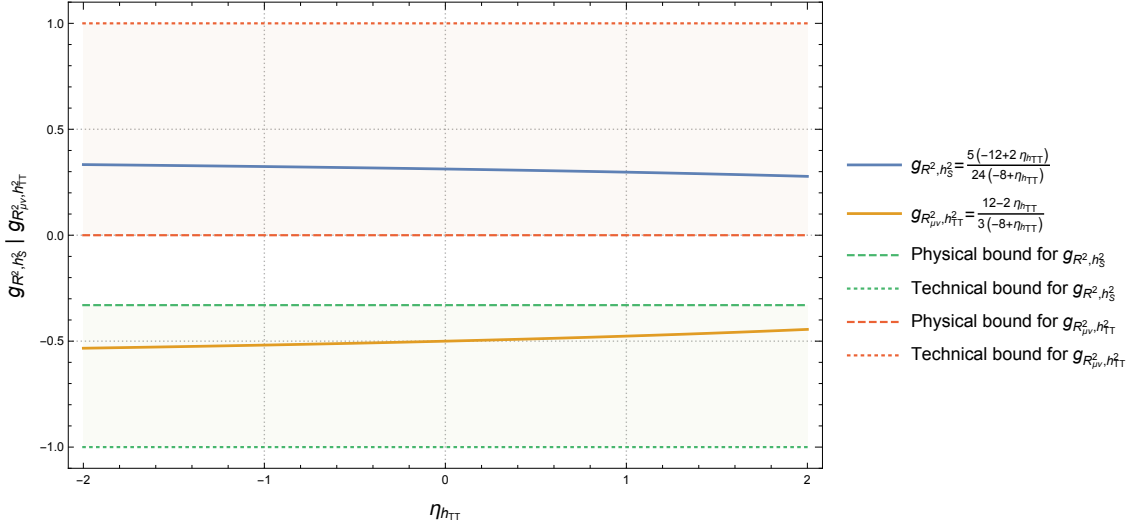


Figure 8.6: 1st real solution doublet of $g = 0$ (blue and yellow graphs) and physical/technical bounds for the higher order couplings (dashed/dotted green and red lines) in the physically relevant range $|\eta_{h_{TT}}| < 2$

Obviously the solution doublet is unphysical as

$$g_{R^2, h_S^2} = \frac{5}{24} \cdot \frac{(-12 + 2\eta_{h_{TT}})}{(-8 + \eta_{h_{TT}})} > -\frac{1}{3} \quad \text{for } |\eta_{h_{TT}}| < 2, \quad (8.29)$$

$$g_{R_{\mu\nu}^2, h_{TT}^2} = -\frac{1}{3} \cdot \frac{(-12 + 2\eta_{h_{TT}})}{(-8 + \eta_{h_{TT}})} < 0 \quad \text{for } |\eta_{h_{TT}}| < 2. \quad (8.30)$$

The 2nd solution doublet was already shown in Figure 8.4 and proven to be unphysical. Finally one can conclude that the only solution for a vanishing p^4 coefficient in the S-projected sector is given by $g_{R_{\mu\nu}^2, h_{TT}^2} = -3g_{R^2, h_S^2}$ and unfortunately the situation is exactly the same as in case of the TT-projected flow: $g_{R_{\mu\nu}^2, h_{TT}^2} = -3g_{R^2, h_S^2}$ kills also the p^4 coefficient of the S-projected graviton 2-point function (cf. eq. (6.79)), s.t. the analysis has to be repeated for the p^2 coefficient of the flow after imposing $g_{R_{\mu\nu}^2, h_{TT}^2} = -3g_{R^2, h_S^2}$

(again this conditions produces zeros in the flows s.t. polynomial long division has to be redone). As expected the p^4 coefficient vanishes and the p^2 coefficient turns out to be

$$\text{Flow}_S^{(2h)}(g_{R^2, \mu\nu, h_{\text{TT}}}^2 = -3g_{R^2, h_S^2}) \Big|_{p^2} = g'(\mu_{h_{\text{TT}}}, \mu_{h_S}, \eta_{h_{\text{TT}}}, \eta_{h_S}, g_{R^2, h_S^2}, \dot{g}_{R^2, h_S^2}, \dot{g}_{R^2, \mu\nu, h_{\text{TT}}}^2) \cdot \frac{g_{R, h_{\text{TT}}}^3}{(1 - 6g_{R^2, h_S^2} + \mu_{h_S})^2(1 + \mu_{h_{\text{TT}}})^2}. \quad (8.31)$$

Therein g' is a complicated polynomial which can now also depend on $\dot{g}_{R^2, \mu\nu, h_{\text{TT}}}^2$. Searching for roots of g' produces two solutions which are both complex and hence unphysical. Moreover setting the higher order couplings and their scale derivatives to zero doesn't lead to a vanishing p^2 coefficient, s.t. a subsequent analysis of the Einstein-Hilbert system without identified TT- and S-projected parameters is necessary. It is worth to mention that the S-projected graviton 2-point function wasn't investigated before at all within the presented approximations and methods.

As expected the graviton loop diagrams scale with p^2 and the ghost loop diagram is again constant after a polynomial long division without higher order tensor structures in the flows. Executing the x -integration gives (an overall prefactor is omitted and $k = 1$)

$$-\frac{1}{2} \left[\text{EH} \right. \left. \begin{array}{l} \propto +6 + 20\mu_{h_S} + 10\mu_{h_S}^2 + 5(-1 + q^2)\eta_{h_{\text{TT}}}(1 + \mu_{h_S})^2 \\ - 8\mu_{h_{\text{TT}}} - 4\mu_{h_{\text{TT}}}^2 - 2(-1 + q^2)\eta_{h_S}(1 + \mu_{h_{\text{TT}}})^2, \end{array} \right]_{S, p^2} \quad (8.32)$$

$$\left[\text{EH} \right. \left. \begin{array}{l} \propto +6 + \frac{20}{3}\mu_{h_S} + \frac{10}{3}\mu_{h_S}^2 + \frac{5}{3}(-1 + q^2)\eta_{h_{\text{TT}}}(1 + \mu_{h_S})^2 \\ + \frac{16}{3}\mu_{h_{\text{TT}}} + \frac{8}{3}\mu_{h_{\text{TT}}}^2 + \frac{4}{3}(-1 + q^2)\eta_{h_S}(1 + \mu_{h_{\text{TT}}})^2, \end{array} \right]_{S, p^2} \quad (8.33)$$

$$-2 \left[\text{EH} \right. \left. \begin{array}{l} \propto 0. \end{array} \right]_{S, p^2} \quad (8.34)$$

Surprisingly the two graviton loop contributions do *not* cancel each other as it was the case for the TT-projected flow. Even more interestingly eq. (8.32) is exactly the same as eq. (8.22). Also for identified TT- and S-projected parameters a cancellation is *not* observable: Both diagrams then read $3(2 + (-1 + q^2))\eta_{h_{\text{TT}}}(1 + \mu_{h_{\text{TT}}})^2$.

To highlight the found non-trivial behaviour the S-projected flow is computed numerically and interpolated in the momentum range $p^2/k^2 \in [0, 30]$ for both cases, i.e. for distinct (cf. Figure 8.7) and identified parameters (cf. Figure 8.8). The theory parameters and anomalous dimensions are chosen to be the same as for the TT-projected flow analysis. For identified parameters the S-projected parameters are set to the values of the TT-projected parameters. One can clearly see that both flows behave like p^2 for high momenta (red dashed fits) and that the ratio of the flows divided by the respective 2-point function tends to a non-zero constant (yellow dashed horizontal lines).

Centralized momentum locality is *not* accomplished for any of the investigated versions of the S-projected graviton 2-point function.

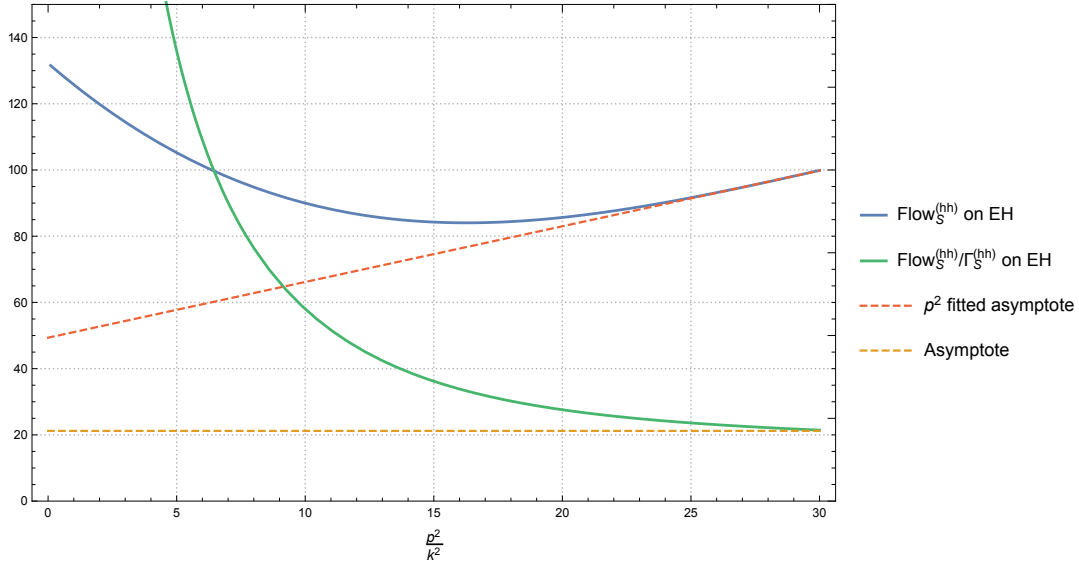


Figure 8.7: Flow of the S-projected graviton 2-point function on Einstein-Hilbert (blue curve) together with its p^2 fitted asymptote (red dashed line) and the flow divided by the S-projected graviton 2-point function on Einstein-Hilbert (green curve) accompanied with its horizontal and non-zero asymptote (yellow dashed line). TT- and S-projected couplings are *not* identified.

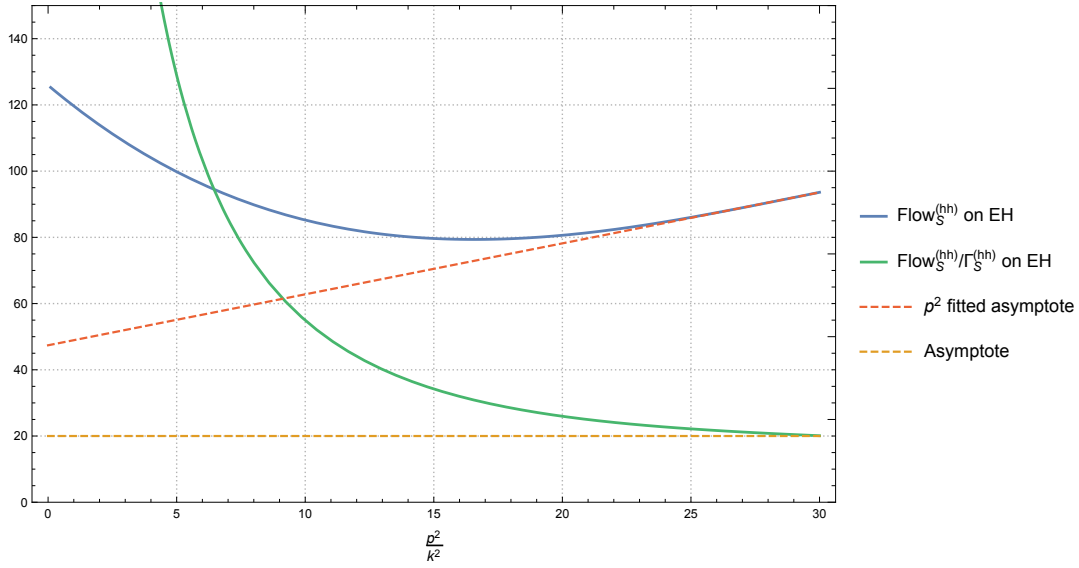


Figure 8.8: Flow of the S-projected graviton 2-point function on Einstein-Hilbert (blue curve) together with its p^2 fitted asymptote (red dashed line) and the flow divided by the S-projected graviton 2-point function on Einstein-Hilbert (green curve) accompanied with its horizontal and non-zero asymptote (yellow dashed line). TT- and S-projected couplings are identified.

8.2.2 Locality of the graviton 3-point function

The only momentum dependent scalar quantity extracted of the graviton 3-point function is its G-projected counterpart (cf. eq. (6.98)). In this case one has three external momenta where only one of them is killed by momentum conservation. For a rigorous analysis none of the two open momenta can be fixed. Unfortunately technical feasibility is again *the* limitation, s.t. only the symmetric momentum configuration defined in eq. (6.93) and shown in Figure 6.1 can be investigated. Applying all this to eq. (8.7) yields

$$\lim_{p \rightarrow \infty} \frac{\partial_t \Gamma_{\mathbb{G}}^{(3h)}(p)}{\Gamma_{\mathbb{G}}^{(3h)}(p)} \stackrel{!}{=} 0. \quad (8.35)$$

As the graviton 3-point function is constructed from a projector which has mass dimension p^2 it scales with p^6 instead of p^4 for high momenta (cf. eq. (6.94)). Note that in some papers this prefactor is directly excluded. A polynomial long division of the whole flow is too expensive at graviton level 3 (more precisely factoring the star diagram seems to be impossible within a few days), rather a simple power counting argumentation is used to construct the highest resulting power of p^2 appearing in the flow directly from the building blocks. One finds that the highest coefficient is indeed p^6 before and after the integration over the loop momentum. It reads

$$\text{Flow}_{\mathbb{G}}^{(3h)} \Big|_{p^6} = \frac{g_{R, h_{\text{TT}}}^2 g_{R_{\mu\nu}, h_{\text{TT}}}^2}{(3g_{R^2, h_{\text{S}}}^2 + g_{R_{\mu\nu}, h_{\text{TT}}}^2)^2 (1 - 6g_{R^2, h_{\text{S}}}^2 - 2g_{R_{\mu\nu}, h_{\text{TT}}}^2 + \mu_{h_{\text{S}}})^2} \cdot \frac{h(\mu_{h_{\text{TT}}}, \mu_{h_{\text{S}}}, \eta_{h_{\text{TT}}}, \eta_{h_{\text{S}}}, g_{R_{\mu\nu}, h_{\text{TT}}}^2, \dot{g}_{R_{\mu\nu}, h_{\text{TT}}}^2, g_{R^2, h_{\text{S}}}^2, \dot{g}_{R^2, h_{\text{S}}}^2)}{(1 + g_{R_{\mu\nu}, h_{\text{TT}}}^2 + \mu_{h_{\text{TT}}})^2}, \quad (8.36)$$

where h is a complex polynomial. The general form of eq. (8.36) is very similar to the form of eq. (8.11), which is not surprising since both stem from a fully TT-projected flow. Moreover eq. (8.36) reveals that the p^6 coefficient

1. does not vanish *in general*,
2. disappears for $g_{R_{\mu\nu}, h_{\text{TT}}}^2 = 0$,
3. may vanish for a non-trivial constraint implied by $h = 0$.

Demanding $h = 0$ leads to three solutions: One of them is imaginary and the remaining two read

$$g_{R_{\mu\nu}, h_{\text{TT}}}^2 = \frac{2}{55} \left(-233 \pm \sqrt{201865} \right) g_{R^2, h_{\text{S}}}^2. \quad (8.37)$$

A plot of eq. (8.37) together with the physical bounds for the higher order theory parameters ($\mu_{h_{\text{TT}}}$ and $\mu_{h_{\text{S}}}$ are chosen s.t. the allowed theory space is as large as possible) is presented in Figure 8.9. Therein the physical allowed area is restricted by the green and red dashed lines: Only the light green area left of the red border is admissible.

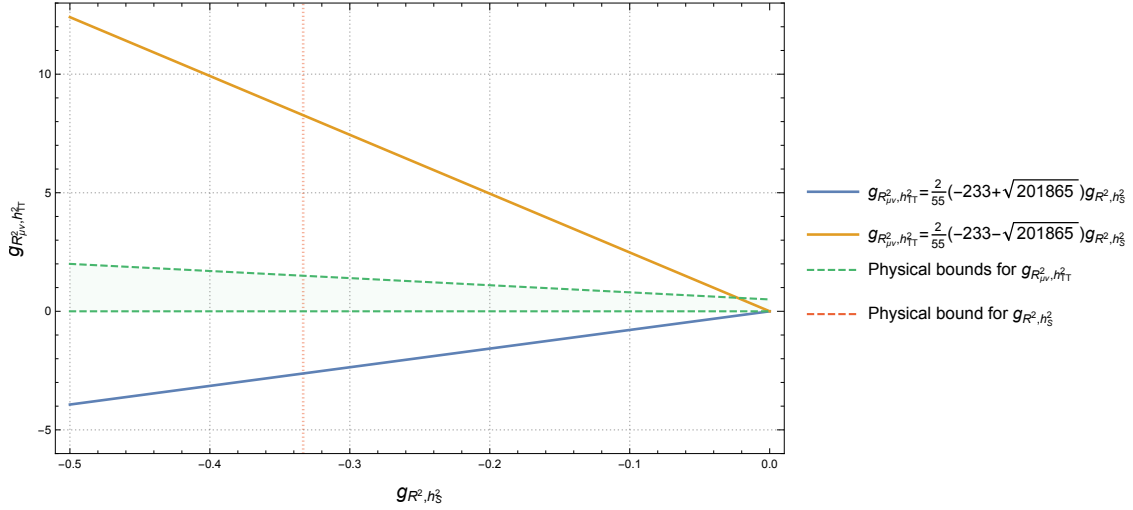


Figure 8.9: Real solutions of $h = 0$ (blue and yellow lines) and bounds for the higher order couplings (red and green dashed lines)

Obviously both solutions proceed outside of this area and hence are unphysical. Therefore the only solution is $g_{R_{\mu\nu}^2, h_{\text{TT}}^2} = 0$, but once more this solution ensures not only a vanishing p^6 coefficient of the flow, but also of the G-projected graviton 3-point function itself. Unfortunately an analysis of the next to leading order coefficient, i.e. p^4 , after implementing $g_{R_{\mu\nu}^2, h_{\text{TT}}^2} = 0$, is technically too expensive.

For completeness the flow is quickly investigated in an Einstein-Hilbert truncation without identified TT- and S-projected parameters. The integration over the loop momentum is fully executed (to reduce the number of terms) and as expected the highest power is p^4 . When skipping an overall prefactor and setting $k = 1$ the contributions of the different diagrams read

$$\begin{aligned}
 & -\frac{1}{2} \left[\text{Diagram: A circle with a cross inside, two external lines on the left, and two on the right. A vertical line with a dot is on the right side.} \right] \begin{array}{l} \text{EH} \\ \text{G}, p^4 \end{array} \propto 6(-423 - 2650\mu_{h_S} - 1325\mu_{h_S}^2 + 1804\mu_{h_{\text{TT}}} + 902\mu_{h_{\text{TT}}}^2) \\
 & \quad + 1325\eta_{h_{\text{TT}}}(1 + \mu_{h_S})^2 - 902\eta_{h_S}(1 + \mu_{h_{\text{TT}}})^2, \quad (8.38)
 \end{aligned}$$

$$\begin{aligned}
 & +3 \left[\text{Diagram: A circle with a cross inside, two external lines on the left, and two on the right. A vertical line with a dot is on the right side.} \right] \begin{array}{l} \text{EH} \\ \text{G}, p^4 \end{array} \propto 6(-270 + 2820\mu_{h_S} + 1410\mu_{h_S}^2 - 3360\mu_{h_{\text{TT}}} - 1680\mu_{h_{\text{TT}}}^2) \\
 & \quad - 1410\eta_{h_{\text{TT}}}(1 + \mu_{h_S})^2 + 1680\eta_{h_S}(1 + \mu_{h_{\text{TT}}})^2, \quad (8.39)
 \end{aligned}$$

$$\begin{aligned}
 & -3 \left[\text{Diagram: A circle with a cross inside, two external lines on the left, and two on the right. A vertical line with a dot is on the right side.} \right] \begin{array}{l} \text{EH} \\ \text{G}, p^4 \end{array} \propto 6(693 - 170\mu_{h_S} - 85\mu_{h_S}^2 + 1556\mu_{h_{\text{TT}}} + 778\mu_{h_{\text{TT}}}^2) \\
 & \quad + 85\eta_{h_{\text{TT}}}(1 + \mu_{h_S})^2 - 778\eta_{h_S}(1 + \mu_{h_{\text{TT}}})^2, \quad (8.40)
 \end{aligned}$$



$$\propto 0. \quad (8.41)$$

The contributions from the three graviton loop diagrams add up to zero and momentum locality is achieved. A plot which exemplifies this behaviour, i.e. shows the momentum dependence of the flow (blue curve) and the flow divided by the G-projected graviton 3-point function (green curve) in the momentum range $p^2/k^2 \in [0, 10]$ can be found in Figure 8.10 (the theory parameters were set to the same values as before and TT- and S-projected parameters were not identified). Therein the p^2 fitted asymptote (red dashed line) indicates the p^2 behaviour of the flow for high momenta.

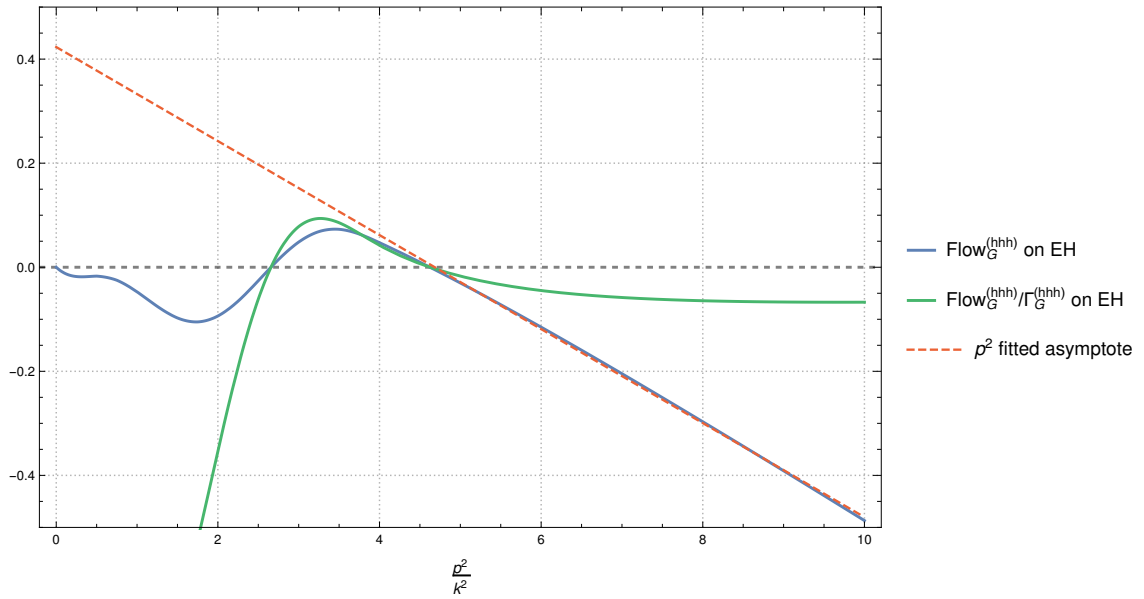


Figure 8.10: Flow of the G-projected graviton 3-point function on Einstein-Hilbert (blue curve) together with its p^2 fitted asymptote (red dashed line) and the flow divided by the G-projected graviton 3-point function on Einstein-Hilbert (green curve) approaching zero. TT- and S-projected couplings are *not* identified.

Finally one can conclude that momentum locality is reached in a split Einstein-Hilbert truncation and that in case of higher order vertices at least a vanishing p^6 coefficient is possible if and only if $g_{R_{\mu\nu}, h_{TT}^2} = 0$, but by mischance a comprehensive analysis including the p^4 coefficient was not possible. Moreover the presented breakdown included one specific momentum configuration, i.e. the symmetric one, s.t. further improvements are needed. Therefore a final statement regarding momentum locality is not feasible in the case of the graviton 3-point function.

8.2.3 Summary

Altogether the results seem to restrict momentum locality to TT-projected flows within an Einstein-Hilbert truncation. A survey of the analyzed systems is given in [Table 8.4](#).

n -point function	Higher orders	Split Einstein-Hilbert	Einstein-Hilbert
$\Gamma_{\text{TT}}^{(2h)}$	not found	found	confirmed
$\Gamma_{\text{S}}^{(2h)}$	not found	not found	not found
$\Gamma_{\text{G}}^{(3h)}$ (sym.)	unclear	found	confirmed

Table 8.4: Overview of the status of the investigated n -point functions w.r.t. momentum locality

Both previous known results could be confirmed and even upgraded with the split Einstein-Hilbert truncation. But all further upgrades failed: Neither the higher order system, nor the S-projected flow of the graviton 2-point function in an Einstein-Hilbert truncation feature momentum locality. This unexpected behaviour was shown within an analytical analysis of the highest coefficients in p^2 and visually substantiated with the help of several plots. The latter method is well suited especially for non-local flows since momentum locality should be attained in the whole theory space, s.t. one counterexample obtained at a specific point is sufficient to prove the converse.

Specifically that the S-projected graviton 2-point function is not momentum local, even in an Einstein-Hilbert truncation, privileges the TT-projection of the flows as the projection scheme of first class. This might be a further hint to the physical relevance of the TT-mode. It is very important to note that this statement also influences the relevance of the splitting of TT- and S-projected parameters in the graviton propagator. Consider e.g. the S-projected graviton mass parameter μ_{h_S} . Its flow can in general only be extracted from the S-projected flow of the graviton 2-point function, i.e. from a non-local correlation function. Therefore one can put S-projected couplings into question generally. In case of higher orders this gets particularly problematic as the R^2 tensor structure has no overlap with the TT-mode up to three derivatives w.r.t. the fluctuation metric $h_{\mu\nu}$. In this case one is forced to extract the running of the corresponding coupling via a S-projected quantity.

Nevertheless both components of the graviton 2-point function are not local in momentum space for higher order vertices, which is independent of the identifications $\mu_{h_{\text{TT}}} = \mu_{h_S}$ and $\eta_{h_{\text{TT}}} = \eta_{h_S}$. This raises the question if the presented vertex construction and the implemented approximations are physically reasonable, in particular if the higher order couplings in both propagator components can simply be identified with their counterparts at higher vertex levels. Already the appearance and physical meaning of *couplings* in the propagator can be scrutinized. Hopefully the analysis of the momentum dependence of the flows will reveal further insight to these questions.

8.3 Approximation 1: Einstein-Hilbert and $R_{\mu\nu}^2$

In the 1st approximation the R^2 tensor structure is excluded and the TT- and S-projected couplings are identified, i.e. $\mu_{h_{\text{TT}}} = \mu_{h_{\text{S}}}$ and $\eta_{h_{\text{TT}}} = \eta_{h_{\text{S}}}$. The main reason to investigate a system without R^2 at first is that in [18] it was found that only the R^2 tensor structure changes the polynomial behaviour of the flows, in particular all other higher orders besides R^2 were non-trivially suppressed. To observe the influence of R^2 it is therefore added to the Einstein-Hilbert system after $R_{\mu\nu}^2$.

8.3.1 Fixed points analysis

The momentum dependence of the flows somehow presumes a comprehensive fixed point analysis. Hence the system is at first investigated w.r.t. fixed points. The theory space is spanned by

$$\{\mu_{h_{\text{TT}}}, \lambda_3, g_{R, h_{\text{TT}}^3}, g_{R_{\mu\nu}^2, h_{\text{TT}}^2}\}, \quad (8.42)$$

with the momentum dependent anomalous dimensions $\eta_{h_{\text{TT}}}(p^2)$ and $\eta_c(p^2)$. Moreover the Einstein-Hilbert theory parameters are all calculated from analytical equations.

Some of the physical requirements for fixed points within an Einstein-Hilbert truncation, which were mentioned in subsection 8.1.1, have to be adjusted: The denominator of the graviton propagator includes two poles, which both depend on $g_{R_{\mu\nu}^2, h_{\text{TT}}^2}$. Consequently the fixed points should lie within a trapezium spanned by these two poles (cf. Figure 7.6). Moreover only the ghost anomalous dimension is still proportional to Newton's constant as higher order terms introduced additional canonical terms in the defining equation for $\eta_{h_{\text{TT}}}(p^2)$ (cf. eq. (6.65)). Therefore the bound $g_{R, h_{\text{TT}}^3} < 2$ remains valid, but it is possible that $\eta_{h_{\text{TT}}}(p^2)$ takes values larger than 2 for small values of g_{R, h_{TT}^3} . All other conditions keep their validity.

Setting $\eta_{\phi_i} = 0$ in the flows

Let's begin with the flows without η_{ϕ_i} . An area of 6 760 points in the theory space was sampled with a *FindRoot* algorithm. Including all conditions besides $\eta_{\phi_i} < 2$ leads to a total of 28 different fixed points. One of these is the trivial Gaussian fixed point, now located at

$$(\mu_{h_{\text{TT}}}^*, \lambda_3^*, g_{R, h_{\text{TT}}^3}^*, g_{R_{\mu\nu}^2, h_{\text{TT}}^2}^*) = (0, 0, 0, 0), \quad (8.43)$$

where all anomalous dimensions are zero. The eigenvalues read

$$(-2, -2, 2, 2), \quad (8.44)$$

s.t. compared to eq. (8.4) an irrelevant direction turned up. The eigenvector which belongs to the new positive eigenvalue points in the direction of g_{R, h_{TT}^3} .

Imposing the condition for the anomalous dimensions allows to reject 26 of the remaining 27 fixed points, s.t. exactly one fixed point persists. Its location in theory space,

Couplings	$\eta_{\phi_i} = 0$ in the flows
$\mu_{h_{\text{TT}}}^*$	-0.5784
λ_3^*	0.3152
$g_{R,h_{\text{TT}}^3}^*$	1.6499
$g_{R_{\mu\nu}^2,h_{\text{TT}}^2}^*$	0.1016
η_{ϕ_i} at FP	
$\eta_{h_{\text{TT}}}^*(0)$	-1.24
$\eta_{h_{\text{TT}}}^*(\frac{k^2}{2})$	-1.17
$\eta_{h_{\text{TT}}}^*(k^2)$	-0.66
$\eta_c^*(k^2)$	0.16
EV	$(-9.72 \pm 4.52i, -33.92, 35\ 359.9)$

Table 8.5: UV fixed point analysis in approximation 1 for analytical g_{R,h_{TT}^3} without η_{ϕ_i} in the flows

the values of the anomalous dimensions and the corresponding eigenvalues are presented in [Table 8.5](#).

The fixed point features three relevant directions and hence is UV attractive. The one positive eigenvalue is surprisingly large and the corresponding eigenvector mainly points into the $-g_{R,h_{\text{TT}}^3}$ direction. Therefore at least one trajectory of the flow should lead to the Gaussian fixed point.

It was explicitly checked if the flows approach an Einstein-Hilbert fixed point (where the higher order coupling is zero and the Einstein-Hilbert parameters attain their value from the Einstein-Hilbert fixed point (cf. 1st column in [Table 8.1](#))) or at least an Einstein-Hilbert similar fixed point with a small value for $g_{R_{\mu\nu}^2,h_{\text{TT}}^2}$, but none of the two mentioned fixed point types was found.

Including η_{ϕ_i} in the flows

Now to the physically more interesting system: The anomalous dimensions are included and computed at the three points $p^2 = 0$, $p^2 = \frac{k^2}{2}$ and $p^2 = k^2$ via a bi-local momentum projection (cf. eq. (6.65)). This system is technically much more complicated as in total four new numerically computed equations come into play. Furthermore the appearance of $\dot{g}_{R_{\mu\nu}^2,h_{\text{TT}}^2}$ in the flows couples all equations which again complicates things. Unfortunately this has two painful consequences: The scanned area has to be reduced (by a factor of ≈ 9 to 726 points) and the computation of eigenvalues gets impossible. Especially the latter circumstance is bad news for the fixed point analysis.

Nevertheless the system preserves enough non-trivial behaviour to be on the rebound: A total of 11 physically valid fixed points was found. These can be split into two groups: Those fixed points that feature non-trivial behaviour of the Einstein-Hilbert couplings

and those that are normal fixed points in this sense. The 1st group contains three fixed points which are listed in Table 8.6.

Couplings	EH	EH similar	EH $\rightarrow 0$
$\mu_{h_{\text{TT}}}^*$	-0.4387	-0.4300	0
λ_3^*	0.0251	0.0194	0
$g_{R,h_{\text{TT}}}^*$	0.5818	0.5911	0
$g_{R_{\mu\nu}^2,h_{\text{TT}}^2}^*$	0	0.0059	$c \in (-0.5, 0.5)$
η_{ϕ_i} at FP			
$\eta_{h_{\text{TT}}}^*(0)$	1.03	0.97	0
$\eta_{h_{\text{TT}}}^*(\frac{k^2}{2})$	0.60	0.61	$\frac{-2c}{2+c}$
$\eta_{h_{\text{TT}}}^*(k^2)$	0.31	0.24	$\frac{-2c}{1+c}$
$\eta_c^*(k^2)$	-0.99	-0.96	0

Table 8.6: UV fixed point analysis indicating non-trivial behaviour for Einstein-Hilbert couplings in approximation 1 for analytical $g_{R,h_{\text{TT}}}^3$ with η_{ϕ_i} in the flows

The 1st column of Table 8.6 contains the *exact same* Einstein-Hilbert fixed point which is known from the 2nd column in Table 8.1. The numerical calculations included many more digits (which aren't displayed here) that do all agree. Also the values of the anomalous dimensions are fully identical within the numerical precision. At this point one can ask why the corresponding fixed point didn't appear for the approximation $\eta_{\phi_i} = 0$ in the flows or why the appearance is non-trivial at all. The answer to both questions is hidden in the flow equation for $g_{R_{\mu\nu}^2,h_{\text{TT}}^2}$ (cf. eq. (6.78)): Setting the Einstein-Hilbert parameters to their respective fixed point value and setting a higher order parameter to zero at the same time ensures that the flow equations of the Einstein-Hilbert parameters are 0. But the flow equation for the higher order parameter does *not* necessarily need to be zero there. Only a non-trivial cancellation of the flows can ensure such a behaviour. In case of $\eta_{\phi_i} = 0$ this cancellation is prevented because the equations for the anomalous dimensions contain the needed counterparts.

A further interesting result is the 2nd column of Table 8.6: The values of the Einstein-Hilbert parameters and all anomalous dimensions are close to the pure Einstein-Hilbert fixed point values and $g_{R_{\mu\nu}^2,h_{\text{TT}}^2}$ is small (\sim factor 3 smaller than the smallest other coupling). This fixed point is consequently called an Einstein-Hilbert similar fixed point.

The 3rd column of Table 8.6 shows another non-trivial fixed point. The Einstein-Hilbert couplings are zero while $g_{R_{\mu\nu}^2,h_{\text{TT}}^2}$ can be set to an arbitrary constant value $c \in \mathbb{R}$. To understand the appearance of this fixed point let's go back to eq. (6.78) once more: Therein $g_{R,h_{\text{TT}}}^3 = 0$ causes all three flows evaluated at a specific external momentum to be zero since $\text{Flow}_{\text{TT}}^{(2h)} \propto g_{R,h_{\text{TT}}}^3$, s.t. only some of the canonical terms survive (also

$\mu_{h_{\text{TT}}} = 0$ kills three of them). The remaining terms include a graviton anomalous dimension. Plugging in the defining equation for the TT-projected graviton anomalous dimension (cf. eq. (6.65)) evaluated at $p^2 = \frac{k^2}{2}$ and $p^2 = k^2$ leads to (all terms which are zero at this fixed point are directly excluded)

$$\begin{aligned}
 \dot{g}_{R_{\mu\nu}^2, h_{\text{TT}}^2} &= 2g_{R_{\mu\nu}^2, h_{\text{TT}}^2} - \left(2 + g_{R_{\mu\nu}^2, h_{\text{TT}}^2}\right) \eta_{h_{\text{TT}}}\left(\frac{k^2}{2}\right) + 2\left(1 + g_{R_{\mu\nu}^2, h_{\text{TT}}^2}\right) \eta_{h_{\text{TT}}}(k^2) \\
 &= 2g_{R_{\mu\nu}^2, h_{\text{TT}}^2} - \left(2 + g_{R_{\mu\nu}^2, h_{\text{TT}}^2}\right) \cdot \frac{-2g_{R_{\mu\nu}^2, h_{\text{TT}}^2}}{2 + g_{R_{\mu\nu}^2, h_{\text{TT}}^2}} \\
 &\quad + 2\left(1 + g_{R_{\mu\nu}^2, h_{\text{TT}}^2}\right) \cdot \frac{-2g_{R_{\mu\nu}^2, h_{\text{TT}}^2}}{1 + g_{R_{\mu\nu}^2, h_{\text{TT}}^2}} \\
 &= 2g_{R_{\mu\nu}^2, h_{\text{TT}}^2} + 2g_{R_{\mu\nu}^2, h_{\text{TT}}^2} - 4g_{R_{\mu\nu}^2, h_{\text{TT}}^2} = 0.
 \end{aligned} \tag{8.45}$$

Thus the flow equation for $g_{R_{\mu\nu}^2, h_{\text{TT}}^2}$ is identical to zero if the Einstein-Hilbert parameters are zero and $g_{R_{\mu\nu}^2, h_{\text{TT}}^2} \equiv c$ itself can take every real value. But of course the physical requirements constrain this range: Having a quick look at Figure 7.6 reveals that $\mu_{h_{\text{TT}}} = 0$ causes $c \in (-1, 0.5)$. Another restriction comes from the anomalous dimensions. The ghost anomalous dimension is directly zero due to $\eta_c \propto g_R h_{\text{TT}}^3$. The graviton anomalous dimension evaluated at $p^2 = 0$ is zero, but c -dependent elsewhere. Figure 8.11 shows the dependence of $\eta_{h_{\text{TT}}}\left(\frac{k^2}{2}\right)$ (blue curve) and $\eta_{h_{\text{TT}}}(k^2)$ (green curve) on c at the fixed point. The limitation $\eta_{h_{\text{TT}}} < -2$ (red dashed horizontal line) obviously implies $c > -0.5$, s.t. in total follows $c \in (-0.5, 0.5)$ (black dashed vertical lines). Hence the Gaussian fixed point is included in this range with its normal properties (cf. eqs. (8.43) and (8.44)).

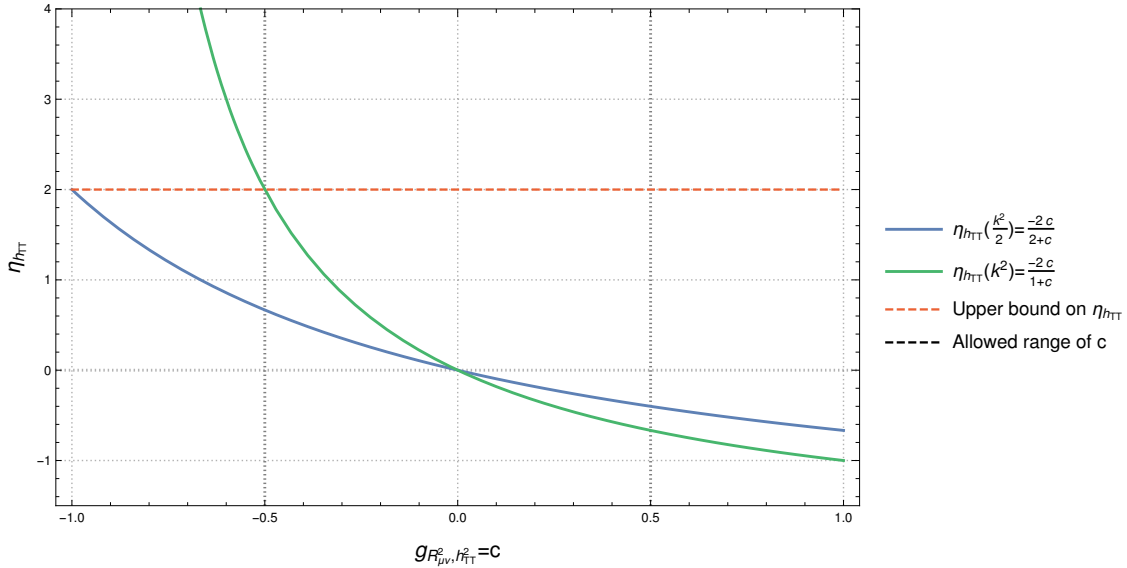


Figure 8.11: Behaviour of the graviton anomalous dimensions (blue and green green curve) at the EH $\rightarrow 0$ fixed point together their bound (red dashed horizontal line) and the range of c (black dashed vertical lines)

The 2nd group of fixed points contains the remaining 8 fixed points which are itemized in [Table A.1](#) together with the values of the anomalous dimensions. Unfortunately a further classification, in particular w.r.t. the number of relevant directions, is technically out of reach, but one can at least expect that some fixed points correspond to unphysical situations. It would of special interest which one of them can be connected to the Einstein-Hilbert fixed point via an adiabatic expansion of the higher order coupling. Moreover the analysis of the phase diagram would reveal further information about which fixed points are attained by a set of flow trajectories.

8.3.2 Polynomial behaviour of the flows

An important and non-trivial result in [\[18\]](#) was that the flows of the G-projected graviton 3- and 4-point functions divided by $-\frac{n}{2}\eta_h(p^2) - n + 2$ were essentially a polynomial in p^2 in the range $p^2 \in [0, k^2]$ for small couplings $|\lambda| \lesssim 1$, i.e.

$$\frac{\text{Flow}_G^{(3h)}(p^2)}{-\frac{3}{2}\eta_h(p^2) - 1} \approx a_0 + a_1 p^2, \quad (8.46)$$

$$\frac{\text{Flow}_G^{(4h)}(p^2)}{-2\eta_h(p^2) - 2} \approx b_0 + b_1 p^2 + b_2 p^4. \quad (8.47)$$

Furthermore eq. [\(8.46\)](#) suggests that a contribution from $R_{\mu\nu}^2$, which has a non-zero overlap with the G-projected graviton 3-point function, is non-trivially suppressed and eq. [\(8.47\)](#) indicates that only a R^2 contribution, which does *not* have an overlap with the G-projected graviton 3-point function but with the G-projected graviton 4-point function, appears due to the higher power of p^2 . As these statements follow from Einstein-Hilbert vertices an investigation for higher order vertices is required. For this one can expect that the highest order in p^2 will increase in some cases.

Please note again that here the G-projector has a mass dimension unequal to zero, s.t. the results in [\[18\]](#) have to be extended with one power of p^2 . Moreover the analysis w.r.t. momentum dependence is always done at or in the neighborhood of fixed points which were computed with anomalous dimensions in the flows. Therefore the two references for fixed points in this subsection are [Table 8.6](#) and especially [Table A.1](#).

TT-projected graviton 2-point flow

[Figure 8.12](#) shows the momentum dependence of the flow evaluated at four different fixed points in the momentum range $p^2 \in [0, k^2]$: The Einstein-Hilbert fixed point (blue curve), the Einstein-Hilbert similar fixed point (yellow curve) and exemplarily the two fixed points FP₂ (red curve) and FP₄ (green curve) from [Table A.1](#), which have different signs for the higher order coupling $g_{R_{\mu\nu}^2, h_{\text{TT}}^2}$. All flows are accompanied with p^4 fits (dashed curves with the same respective color), i.e. p^2 polynomial fits with p^4 as their highest power. One can clearly see that *all* four curves indeed behave like a p^4 polynomial. Specifically the curve which belongs to the Einstein-Hilbert fixed point behaves obviously *not* like p^2 , which would correspond to a straight line in a plot w.r.t. p^2 . This implies that the inclusion of a $R_{\mu\nu}^2$ tensor structure in the vertices does *not*

influence the highest power of the fitted polynomials at all, i.e. its effect is simply there in both cases.

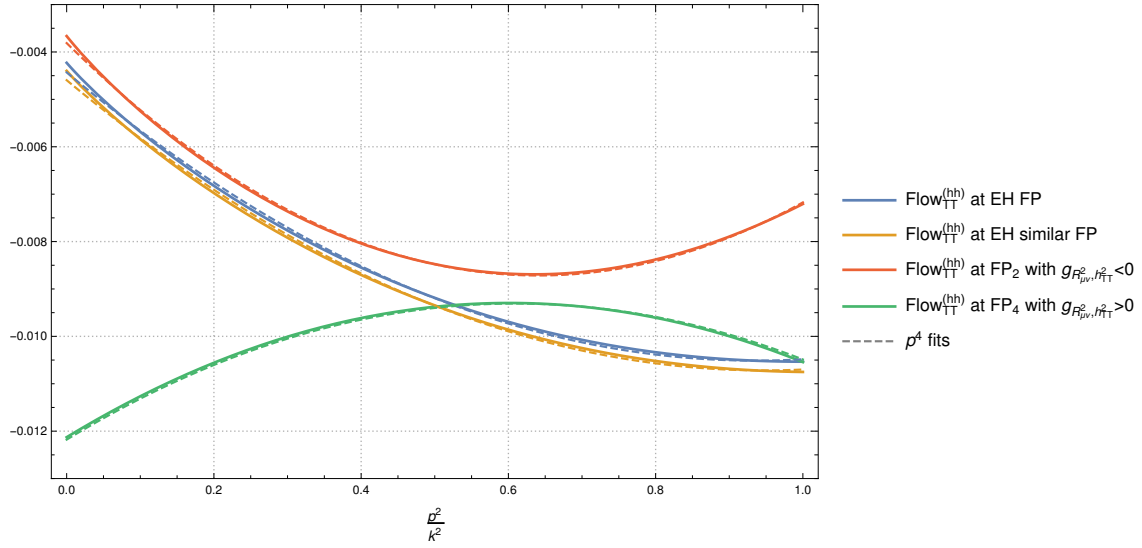


Figure 8.12: Momentum dependence of the TT-projected flow of the graviton 2-point function in approximation 1 in the range $p^2 \in [0, k^2]$ evaluated at different UV fixed points together with polynomial fits in p^2 where p^4 is the highest power (dashed curves)

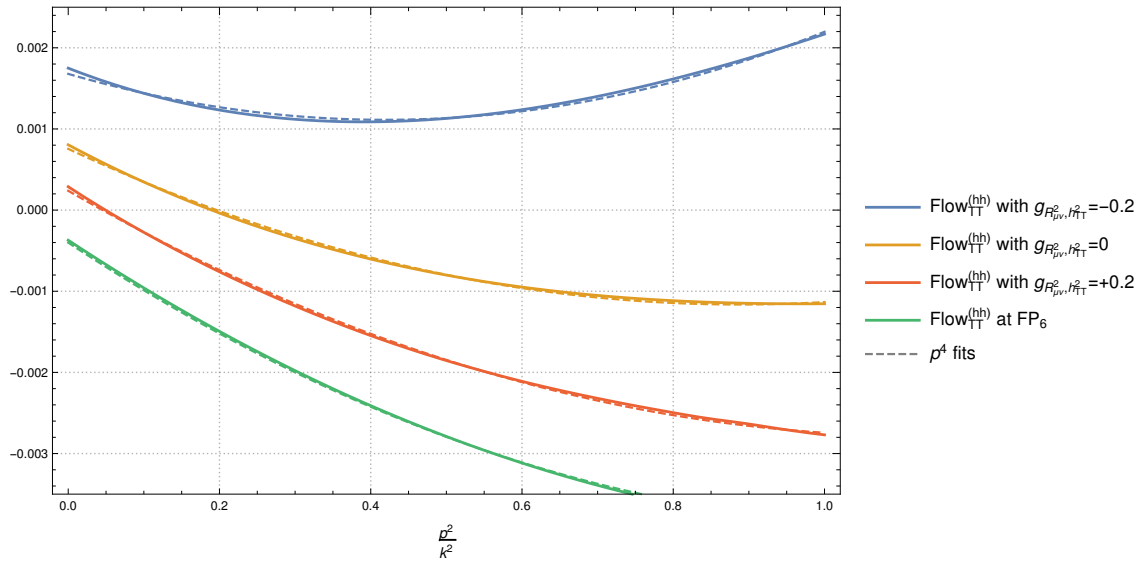


Figure 8.13: Momentum dependence of the TT-projected flow of the graviton 2-point function in approximation 1 in the range $p^2 \in [0, k^2]$ evaluated at UV fixed point number 6 with different values for $g_{R_{\mu\nu}^2, h_{TT}^2}$ together with polynomial fits in p^2 where p^4 is the highest power (dashed curves)

To substantiate this statement further the flow can be investigated at another fixed point (fixed point number 6 in Table A.1) with different values for the higher order coupling $g_{R_{\mu\nu}^2, h_{\text{TT}}^2}$ which is shown in Figure 8.13. Again all curves behave like p^4 (dashed curves with the respective color), even for the case $g_{R_{\mu\nu}^2, h_{\text{TT}}^2} = 0$ (yellow curve) which corresponds to Einstein-Hilbert. Furthermore the different signs of $g_{R_{\mu\nu}^2, h_{\text{TT}}^2}$ don't influence the orientation of the curves as it was the case in Figure 8.12, s.t. the orientation seems to depend not only on $g_{R_{\mu\nu}^2, h_{\text{TT}}^2}$, but also on other theory parameters.

In summary a p^4 contribution is there in all cases. When only allowing for low order and local curvature invariants this behaviour solely stems from $R_{\mu\nu}^2$, as a R^2 contribution could be excluded (no overlap with the TT-mode of the graviton 2-point function).

S-projected graviton 2-point flow

The same analysis can be repeated for the flow of the S-projected graviton 2-point function. Figure 8.14 shows the analogon of Figure 8.12, i.e. the momentum dependence of the S-projected flow of the graviton 2-point function in the range $p^2 \in [0, k^2]$ at different fixed points (FP₄ was excluded due to numerical integration problems) together with p^4 fits (dashed curves with the respective color). The behaviour is again approximately p^4 ,

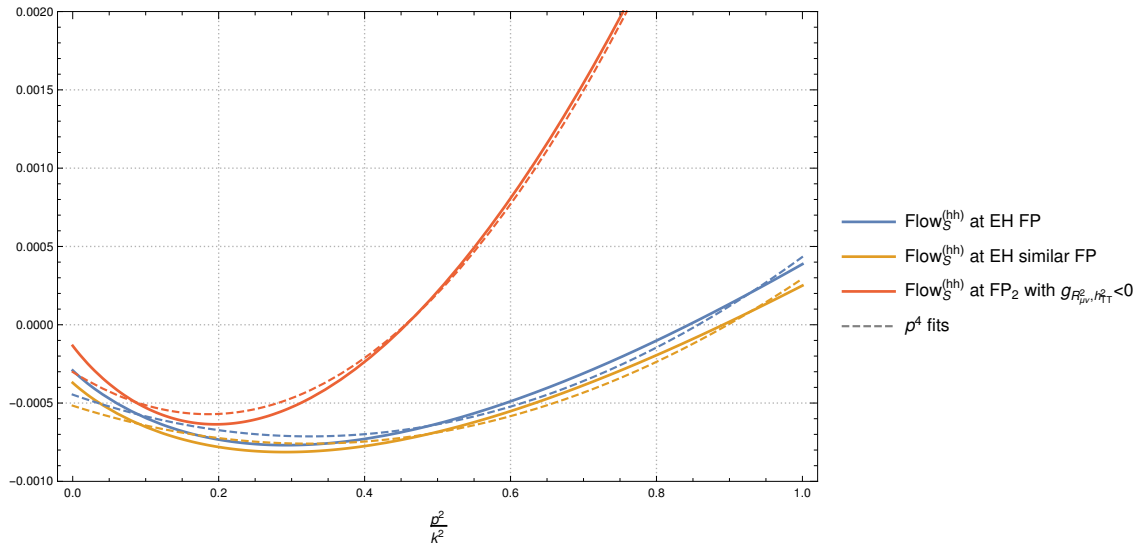


Figure 8.14: Momentum dependence of the S-projected flow of the graviton 2-point function in approximation 1 in the range $p^2 \in [0, k^2]$ evaluated at different UV fixed points together with polynomial fits in p^2 where p^4 is the highest power (dashed curves)

but with less precision: Especially around $p^2 = 0$ the accordance gets worse. The main difference to the TT-projected flow is that the overlap with a R^2 tensor structure is *not* zero anymore, s.t. the p^4 behaviour could stem from both higher order couplings. This applies already to the Einstein-Hilbert system, which behaves like p^4 as well (cf. blue curve in Figure 8.14). Therefore both parts of the graviton 2-point flow show the same characteristics, but the sources can be different.

G-projected graviton 3-point flow

Due to the larger numerical effort the G-projected graviton 3-point flow is only investigated at one single fixed point, in particular fixed point number 2 from Table A.1, which was used in both cases before. The resulting momentum dependence is presented in Figure 8.15. Keep in mind that one additional power of p^2 is caused by the G-projector and has to be excluded in the analysis.

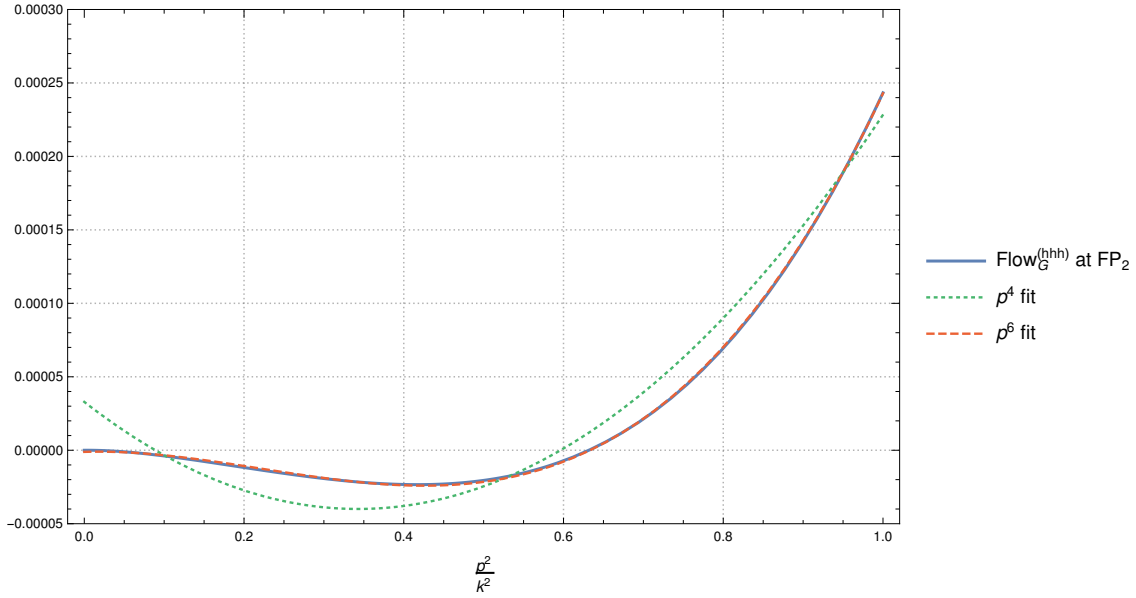


Figure 8.15: Momentum dependence of the G-projected flow of the graviton 3-point function in approximation 1 in the range $p^2 \in [0, k^2]$ evaluated at UV fixed point 2 (blue curve) together with polynomial fits in p^2 where p^4 (green dotted curve) or p^6 (red dashed curve) are the highest powers

Figure 8.15 reveals not only that the flow behaves like a polynomial with p^6 (red dashed curve), but also that a p^4 fit (green dotted curve) is simply insufficient. Compared to eq. (8.46), where contributions from higher order terms were suppressed, one can observe the opposite here: A $R_{\mu\nu}^2$ contribution appears (R^2 has no overlap with the G-projected graviton 3-point function), which was absent for Einstein-Hilbert vertices.

Short summary

The three presented cases have one thing in common: They all feature a contribution stemming from a $R_{\mu\nu}^2$ tensor structure, which is manifest due to the p^4 behaviour of the fitted polynomials and the non-zero overlap of the $R_{\mu\nu}^2$ tensor structure with the mentioned flows. Nevertheless a more detailed view reveals differences: At graviton level 2 the p^4 behaviour was already visible for the Einstein-Hilbert system, while graviton level 3 behaves differently. Although the flows were investigated at many points in theory space a restriction up to where the flows behave like polynomials in p^2 was not strictly quantifiable. However large absolute values for $g_{R_{\mu\nu}^2, h_{TT}^2}$ seem to destroy the polynomial behaviour, but it is not clear if this is a technical artefact.

8.4 Approximation 2: Einstein-Hilbert, R^2 and $R_{\mu\nu}^2$

Now the R^2 tensor structure is included in the vertices and the differently projected graviton anomalous dimensions are not identified, s.t. only $\mu_{h_{\text{TT}}} = \mu_{h_S}$ is implemented. Some aspects of the 2nd approximation were already investigated in [104] within a vertex expansion. The main differences to the present work are a different choice for the gauge parameter β (here: $\beta = 1$ instead of $\beta = -1$), a tri/bi-local projection rather than a derivative projection for the higher order couplings/anomalous dimensions and a Newton's coupling extracted from higher order vertices instead of a Newton coupling from Einstein-Hilbert vertices.

8.4.1 Fixed points analysis

The theory space is spanned by

$$\{\mu_{h_{\text{TT}}}, \lambda_3, g_{R, h_{\text{TT}}^3}, g_{R_{\mu\nu}^2, h_{\text{TT}}^2}, g_{R^2, h_S^2}\}, \quad (8.48)$$

together with the anomalous dimensions $\eta_{h_{\text{TT}}}(p^2)$, $\eta_{h_S}(p^2)$ and $\eta_c(p^2)$. Again all Einstein-Hilbert parameters are computed from analytical equations. The different pole structure and sign behaviour of the graviton propagator, which is displayed in Figure 7.7, changes the corresponding physical requirement for the fixed points another time. A possible fixed point has fulfill the conditions $g_{R_{\mu\nu}^2, h_{\text{TT}}^2} \geq 0$ and $g_{R^2, h_S^2} \leq -\frac{1}{3}g_{R_{\mu\nu}^2, h_{\text{TT}}^2}$, i.e. it has to be located between the light green and red planes in Figure 7.7.

The fixed point which was found in the latter mentioned paper exhibits the coordinates (note that the cosmological constant at level 3 was identified with the graviton mass parameter)

$$(\mu_{h_{\text{TT}}}^*, g_{R, h_{\text{TT}}^3}^*, g_{R_{\mu\nu}^2, h_{\text{TT}}^2}^*, g_{R^2, h_S^2}^*, \eta_{h_{\text{TT}}}^*) = (-0.34, 0.43, -0.41, 0.91, 0.77), \quad (8.49)$$

with the eigenvalues

$$(-1.5 \pm 2.7i, 2.4, 8.3). \quad (8.50)$$

Obviously this fixed point has only two relevant directions, i.e. as much as the Einstein-Hilbert fixed point. In [102] a similar system ($R_{\mu\nu}^2$ was traded for C^2) was investigated with background field flows and the found fixed point features three relevant directions. Therefore the number of relevant directions is of special interest.

Setting $\eta_{\phi_i} = 0$ in the flows

A total of 1 086 points was sampled with a *FindRoot* algorithm. The clearly increased complexity of the flow equations prohibited a sampling point density as high as for approximation 1. Before imposing the condition $\eta_{\phi_i} < -2$ the number of found fixed points is 7, where one of them is again the Gaussian fixed point. All other 6 fixed points feature at least one anomalous dimensions which violates the above mentioned condition. Therefore the fixed point analysis for $\eta_{\phi_i} = 0$ in the flows is over before it begun. Please

note that all trivial points, e.g. the Einstein-Hilbert fixed points or similar were checked and that nothing was found.

Including η_{ϕ_i} in the flows

The system which contains the anomalous dimensions in the flows shows a similar behaviour as its counterpart in approximation 1. After sampling 162 points one is left with 4 fixed points, which can be grouped as follows: Two of them violate the condition $g_{R^2, h_5^2} \leq -\frac{1}{3}g_{R_{\mu\nu}^2, h_{\text{TT}}^2}$ and can be excluded. One corresponds to the case where all Einstein-Hilbert parameters are zero and only the higher order couplings take non-zero values (cf. left column in Table 8.7) and the last one is a non-trivial UV fixed point (cf. right column in Table 8.7).

Couplings	EH \rightarrow 0	Non-trivial FP
$\mu_{h_{\text{TT}}}^*$	0	-0.5019
λ_3^*	0	0.3479
$g_{R, h_{\text{TT}}^3}^*$	0	1.2272
$g_{R_{\mu\nu}^2, h_{\text{TT}}^2}^*$	$c \geq 0$	-0.3298
$g_{R^2, h_5^2}^*$	$-\frac{1}{3}c$	0.8180
η_{ϕ_i} at FP		
$\eta_{h_{\text{TT}}}^*(0)$	0	-1.3906
$\eta_{h_{\text{TT}}}^*(\frac{k^2}{2})$	$\frac{-2}{2+c}$	-1.6298
$\eta_{h_{\text{TT}}}^*(k^2)$	$\frac{-2}{1+c}$	-1.4381
$\eta_{h_5}^*(0)$	0	0.4318
$\eta_{h_5}^*(\frac{k^2}{2})$	0	-0.0714
$\eta_{h_5}^*(k^2)$	0	-1.5719
$\eta_c^*(k^2)$	0	-0.4842

Table 8.7: UV fixed point analysis indicating non-trivial behaviour for Einstein-Hilbert couplings in approximation 2 for analytical g_{R, h_{TT}^3} with η_{ϕ_i} in the flows

Unfortunately computing the eigenvalues at the fixed points was not doable and hence a full comparison to the two mentioned papers remains to be seen. The EH \rightarrow 0 fixed point was already found in approximation 1 (cf. outer right column in Table 8.6). As the flow equation of $g_{R_{\mu\nu}^2, h_{\text{TT}}^2}$ was already checked and proven to be zero for vanishing Einstein-Hilbert couplings let's test the flow equation of g_{R^2, h_5^2} : Plugging in $g_{R_{\mu\nu}^2, h_{\text{TT}}^2} = c$ and the three equations for the S-projected graviton anomalous dimensions (cf. eq. (6.82)) evaluated at the three points $p^2 = 0$, $p^2 = \frac{k^2}{2}$ and $p^2 = k^2$) into the defining

equation for \dot{g}_{R^2, h_ξ^2} (cf. eq. (6.84)) leads to

$$\dot{g}_{R^2, h_\xi^2} = (3g_{R^2, h_\xi^2} + c) \cdot j(g_{R^2, h_\xi^2}, c), \quad (8.51)$$

wherein j is a rational function of the displayed arguments. The RHS of the latter equation is zero if and only if $g_{R^2, h_\xi^2} = -\frac{1}{3}c$ as j doesn't contain further roots. The found value for g_{R^2, h_ξ^2} is physically allowed, one only has to demand $c \geq 0$. Computing the anomalous dimensions at this fixed point doesn't lead to further limitations (cf. Figure 8.11: For $c \geq 0$ they behave well). Furthermore the Gaussian fixed point is contained in the range as it was the case in approximation 1.

The discovered non-trivial fixed point (cf. right column in Table 8.7) has a comparatively large value for Newton's constant, but all anomalous dimensions stay under their physical bound as they are not fully proportional to g_{R, h_{TT}^3} anymore. Compared to the fixed point found in [104] (cf. eq. (8.49)) the higher order couplings take at most similar values while the two Einstein-Hilbert couplings are more dissimilar.

At last a word about further fixed points: It was explicitly checked if the system features an Einstein-Hilbert or an Einstein-Hilbert similar fixed point, but the flow equations of the higher order couplings take non-zero values at the Einstein-Hilbert fixed point and no Einstein-Hilbert similar fixed point was found. Here one should note that both higher order flow equations are strongly coupled due to the appearance of \dot{g}_{R^2, h_ξ^2} and $\dot{g}_{R_{\mu\nu}^2, h_{\text{TT}}^2}$ in the nominator of the propagator with a regulator insertion.

8.4.2 Polynomial behaviour of the flows

The foreword to this subsection is essentially the same as in approximation 1, so let's start with the analysis. As the search for fixed point with η_{ϕ_i} in the flows led to only one fixed point all flows are simply evaluated at this fixed point.

TT-projected graviton 2-point flow

The momentum dependence of the TT-projected graviton 2-point flow in approximation 2 evaluated at the UV fixed point in the range $p^2 \in [0, k^2]$ is displayed in Figure 8.16 as a blue curve. One can see that a fitted polynomial with p^4 as highest power of p^2 (green dotted curve) is insufficient and that only a p^6 fit can reproduce the momentum dependence of the flow. This is a very interesting result, especially in comparison to approximation 1 (cf. Figure 8.12) where all flows were well described by a p^4 polynomial. A p^6 behaviour can not be generated by the two lowest order curvature invariants R^2 and $R_{\mu\nu}^2$, also not by R^3 as it has no overlap with the TT-mode of the graviton 2-point function. If restricting the analysis to diffeomorphism invariant tensor structures only more complicated combinations can cause such a behaviour, e.g. expressions which feature additional covariant derivatives or are build of a non-trivial contraction of three Ricci tensors. The observed result becomes even more interesting if one varies the higher order coupling which corresponds to R^2 at the fixed point (cf. Figure 8.17). For the values $g_{R^2, h_\xi^2} = -1$ (blue curve) and -0.8 (yellow curve) a p^4 (dotted curves with the respective colors) fit catches almost the momentum dependence of the flows while all

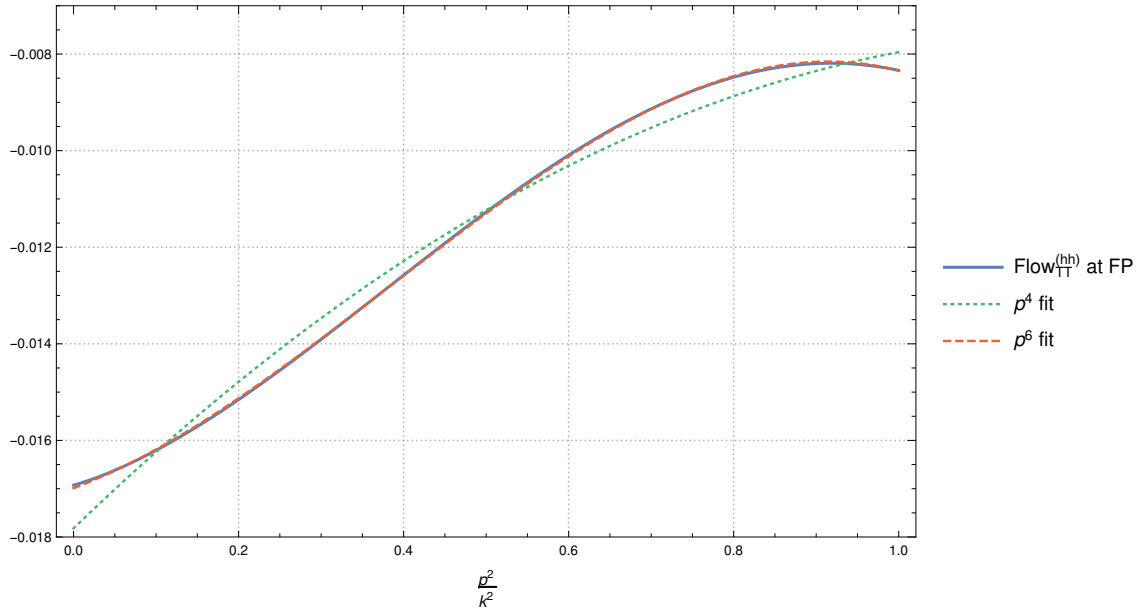


Figure 8.16: Momentum dependence of the TT-projected flow of the graviton 2-point function in approximation 2 in the range $p^2 \in [0, k^2]$ evaluated at the UV fixed point (blue curve) together with polynomial fits in p^2 where p^4 (green dotted curve) or p^6 (red dashed curve) are the highest powers

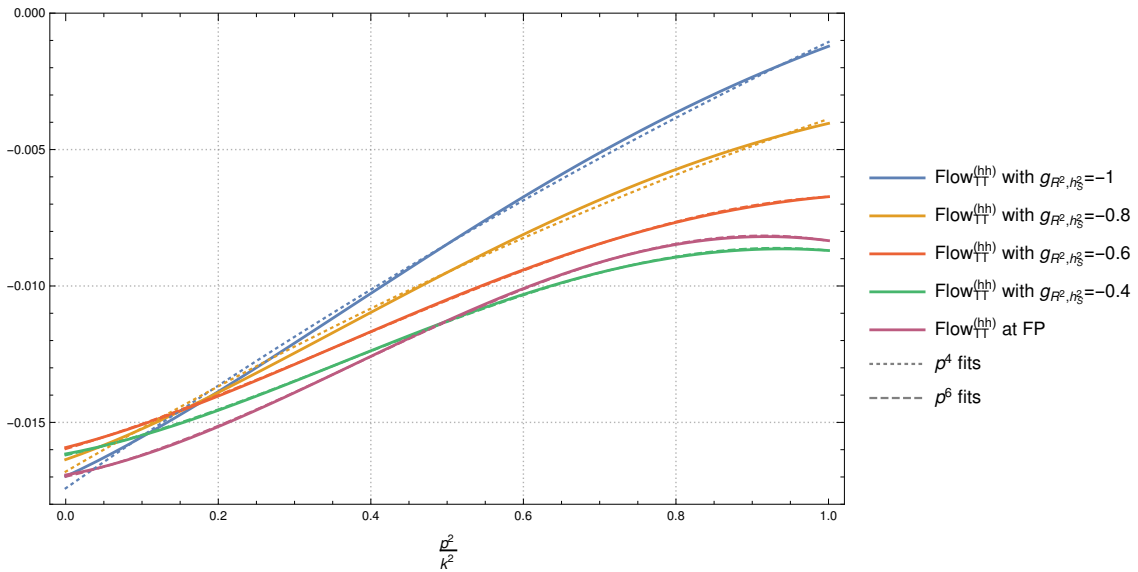


Figure 8.17: Momentum dependence of the TT-projected flow of the graviton 2-point function in approximation 2 in the range $p^2 \in [0, k^2]$ evaluated at the UV fixed point with different values for g_{R^2, h_s^2} together with polynomial fits in p^2 where p^4 (blue and yellow dotted curves) and p^6 (red, green and purple dashed curves) are the highest powers

larger values of g_{R^2, h_ξ^2} need a p^6 fit (dashed curves with the corresponding colors). The two latter plots indicate that the polynomial behaviour of the flow strongly depends on the evaluation point in theory space. At some points the p^6 contributions are approximately vanishing while at other points they are definitely not negligible. A quantitative version of this statement, i.e. a precise range where the p^6 coefficient plays a role, can not be given here.

S-projected graviton 2-point flow

The S-projected version of the graviton 2-point flow evaluated at the fixed point is shown in Figure 8.18. The blue curve denotes the flow, while the p^4/p^6 fits are marked by dot-

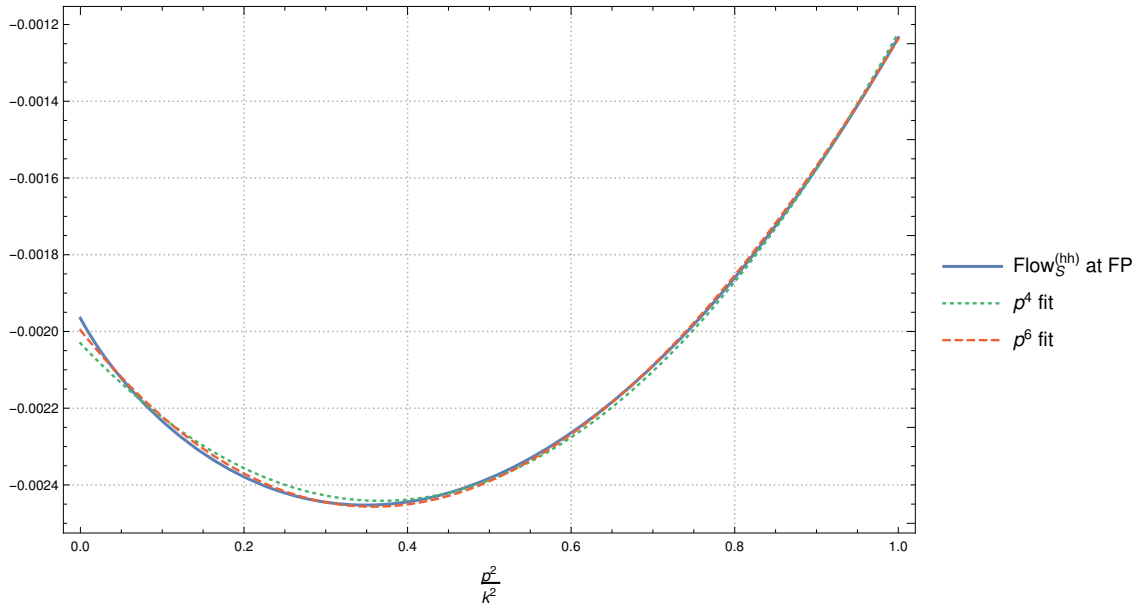


Figure 8.18: Momentum dependence of the S-projected flow of the graviton 2-point function in approximation 2 in the range $p^2 \in [0, k^2]$ evaluated at the UV fixed point (blue curve) together with polynomial fits in p^2 where p^4 (green dotted curve) or p^6 (red dashed curve) are the highest powers

ted/dashed green/red curves. Although a p^4 fit is reasonable and a p^6 fit doesn't offer a significant improvement this result does *not* contradict the findings for the TT-projected graviton 2-point flow (cf. Figure 8.16): It is not clear if the S-projected flow behaves like p^4 for all accessible points in theory space. Consequently it is possible that the regions where it eventually behaves like p^6 are not identical to those of the TT-projected flow. Nevertheless the very non-trivial behaviour of the flows is enlarged once more and a quantitative statement seems to be out of reach.

G-projected graviton 3-point flow

At last some words about the graviton 3-point function contracted with a G-projector. The analog of Figure 8.15 is shown on the next page (cf. Figure 8.19). As for approximation 1 the flow behaves almost like a fitted polynomial with p^6 as its highest power.

Around $p^2 = 0$ the accordance is less accurate but overall the p^6 fit is nevertheless

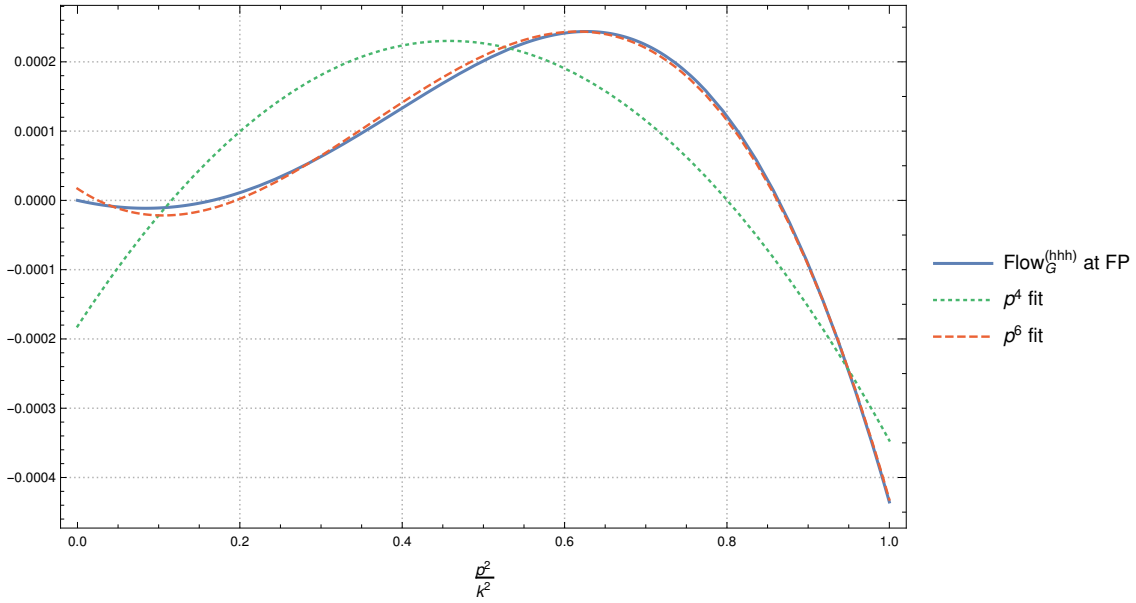


Figure 8.19: Momentum dependence of the G-projected flow of the graviton 3-point function in approximation 2 in the range $p^2 \in [0, k^2]$ evaluated at the UV fixed point (blue curve) together with polynomial fits in p^2 where p^4 (green dotted curve) or p^6 (red dashed curve) are the highest powers

reasonable. Interestingly the inclusion of a R^2 tensor structure does *not* change the behaviour of the graviton 3-point flow (cf. p^6 fit in Figure 8.15).

Short summary

In approximation 2 almost all flows behave like a polynomial with p^6 as its highest power. Such a contribution must stem from more complicated tensor structures. Furthermore in the most cases it is the inclusion of the R^2 tensor structures in the vertices which changes the behaviour from p^4 to p^6 . Together with the results from [18] this suggests that in principle at most these terms appear, which are associated to the tensor structures in the vertices with the *next highest order*. All higher contributions are definitely suppressed. Moreover there seems to be a non-trivial interplay between the TT- and S-projected flows: The highest power differs and may further depend on the specific point in theory space, where the flows are evaluated. Summarized in formulas this reads

$$\text{Flow}_i^{(nh)}(\mathcal{T}_1, \dots, \mathcal{T}_j(p^{2l})) \approx \sum_{m=0}^{l+1} c_{i,j,m} p^{2m}, \quad (8.52)$$

where $c_{i,j,m}$ are real numbers and in some cases holds $c_{l+1,j,m} \approx 0$ depending on the projection scheme i and the point in theory space.

9 Conclusion and outlook

The influence of the higher order tensor structures R^2 and $R_{\mu\nu}^2$ appearing in the vertices within a vertex expansion in an asymptotically safe theory of quantum gravity was investigated w.r.t. several physical properties. This included a clear distinction of the TT- and S-modes of the graviton propagator to decouple the effects of the higher order tensor structures. Furthermore the flows of the higher order couplings were extracted via a tri-local momentum projection scheme from the TT- and S-projection graviton 2-point function, while the flow of Newton's coupling was deduced via a derivative projection scheme at $p^2 = 0$ from the graviton 3-point function in the symmetric momentum configuration. Moreover the momentum dependence of the anomalous dimensions was taken into account.

At first the Einstein-Hilbert truncation was revisited: All former results could be reproduced and the influence of distinct TT- and S-projection parameters, which appear in the respective components of the graviton propagator, was investigated. It was shown that an identification of the latter mentioned parameters is *not* a reasonable approximation as they behave totally different. Nevertheless technical limitations can enforce these identification, especially when it comes to a numerical integration with a subsequent interpolation.

The 2nd extensive physical question concerned locality in momentum space. While TT-projected flows in an Einstein-Hilbert truncation exhibit the desired properties to achieve momentum local correlation functions all other flows, in particular S-projected or higher order flows, do *not* possess these properties. As a consequence theory parameters, which can only be extracted from S-projected flows, e.g. the coupling of R^2 on graviton level 2, stem from non-local flows, which reveals a distinction of TT- and S-projected parameters in the flows in a different light: On one side a distinction turned out to be reasonable, but on the other hand S-projected parameters result from non-local flows. Besides the higher order flows did *not* showed the desired momentum local behaviour. This statement is even independent of the projection scheme. Thus at least the way of evaluating momentum locality could be questioned.

Thereafter two systems were scanned for UV fixed points, in particular a system which contained Einstein-Hilbert and $R_{\mu\nu}^2$ tensor structures in the vertices (approximation 1) and a system which additionally included R^2 (approximation 2). To respect unitarity and to avoid the poles of the graviton propagator which became more complicated due to the inclusion of the higher order tensor structures physical conditions on the higher order parameters were imposed. These restricted the validity of the presented approximations to the momentum range $p^2 \lesssim k^2$. The anomalous dimensions appearing in the flows were excluded as a start and respected afterwards. Both systems featured several non-trivial UV fixed points which satisfy all physical requirements: Approximation 1 showed

the well-known Einstein-Hilbert fixed point, an Einstein-Hilbert similar fixed point, a fixed point which allowed several values for $g_{R_{\mu\nu}, h_{TT^2}}$ and required the Einstein-Hilbert parameters to be zero and 8 non-trivial UV fixed points. Approximation 2 contained a similar fixed point as approximation 1. One of the higher order couplings could be chosen, the other one was determined by the first one via a simple and physically allowed relation while the Einstein-Hilbert parameters were zero. Additionally a non-trivial UV fixed point showed up, but no Einstein-Hilbert similar fixed point was found. All fixed points which were computed from flows that included the anomalous dimensions were not classifiable w.r.t. the number of relevant directions due to technical limitations which prohibited the full computation of the stability matrix. This is a point where definitely some improvements are necessary to conclude the fixed point analysis and to especially answer the question how many relevant or irrelevant directions are introduced by the two higher order couplings which are accompanied by marginal couplings.

At last the momentum dependence of the flows in the range $p^2 \in [0, k^2]$ was investigated in both latter mentioned approximations. To that end the flows were evaluated at some fixed point values or in their neighborhood and numerically integrated. Roughly speaking the flows behaved very messy: In all cases they could be well described by low order polynomials in p^2 , but the highest order of the respective fits differed a lot. The findings indicate that the highest power depends on the projection scheme, the included tensor structures in the flows and the evaluation point in theory space. But nevertheless the highest order was at most one order higher than the highest order stemming from tensor structures which were included in the vertices. Therefore a non-trivial suppression of even higher contributions could be confirmed.

The investigated systems beg several questions which require further investigations. First of all it is generally *not* clear if the inclusion of higher order couplings in the graviton propagator is physically reasonable or even allowed. This step causes many problems at once: The pole structure of the propagator gets much more complicated which affects the physical meaning of the on-shell condition. Furthermore unitarity, which is in general a problem in four-derivative gravity theories, is spoiled, at least for some momenta. Already the appearance of couplings in the propagator, which are not associated with the mass of the described particle, seems to be doubtful. On top of that another question mark comes in when identifying the higher order couplings at graviton level 2 with those from graviton level 3 or even higher levels. In general the avatars of couplings at different levels are related via complicated Slavnov-Taylor identities but it is *not* clear if these simplify s.t. couplings appearing in the graviton propagator can be reasonably approximated with those stemming from graviton vertices, i.e. building blocks which represent the interacting part of the underlying theory.

An ansatz to resolve some of these questions is to handle the higher order terms appearing in the graviton propagator as expansion coefficients of the momentum dependence of the graviton wave function renormalization constants. In this case one gets either additional graviton anomalous dimensions or rescaled versions of the previous anomalous dimensions, which feature a better resolved momentum dependence. Somehow or other the p^4 contributions would be associated with the anomalous dimensions and not with additional couplings. Consequently the flows of the higher order couplings have to be

extracted from the graviton 3-point function, which is another point for improvements. The inclusion of higher order tensor structures expands the complexity of the graviton vertices tremendously and already tracing the flow diagrams was an extremely challenging task. Handling the graviton 3-point flow requires even more profoundly solutions: Either a momentum derivative w.r.t. p^4 at $p^2 = 0$ or a tri-local momentum projection are required to extract the runnings of the higher order couplings. The 1st option is not only technically challenging but also known to produce inaccurate results, especially for momentum dependent couplings. Unfortunately the 2nd option is simply out of reach in the near future. In general a numerical computation beyond graviton level 2 shouldn't be touched. It is more important to improve the approximations which were necessary due to technical feasibility, e.g. a clear distinction of the TT- and S-projected graviton mass parameters or a higher sampling point density for both, but especially for the 2nd approximations.

Part IV
Appendix

A Fixed point solutions for approximation 1 with η_{ϕ_i}

Couplings	FP ₁	FP ₂	FP ₃	FP ₄	FP ₅	FP ₆	FP ₇	FP ₈
$\mu_{h_{\text{TT}}}^*$	-0.5214	-0.4369	-0.4113	-0.4106	-0.0481	-0.0129	≈ 0	≈ 0
λ_3^*	0.3037	0.0469	-0.0025	0.2763	-0.3796	-0.5317	-0.4665	-0.5124
$g_{R,h_{\text{TT}}}^*$	1.7477	0.6317	0.6039	1.0699	0.3474	0.1790	0.3273	0.2487
$g_{R^2,h_{\text{TT}}}^*$	0.1008	-0.1040	0.0716	0.1360	0.1517	0.3064	-0.00002	0.2000
η_{ϕ_i} at FP								
$\eta_{h_{\text{TT}}}^*(0)$	-1.07	1.16	0.78	-0.86	0.07	0.30	-0.01	0.13
$\eta_{h_{\text{TT}}}^*(\frac{k^2}{2})$	-0.42	0.64	0.39	-0.81	0.13	-0.33	0.44	0.34
$\eta_{h_{\text{TT}}}^*(k^2)$	0.24	0.12	-0.01	-0.77	-0.20	-0.97	0.27	-0.17
$\eta_c^*(k^2)$	-1.05	-1.67	0.66	-0.51	-0.17	-0.11	-0.21	-0.12

Table A.1: UV fixed point analysis in approximation 1 for analytical $g_{R,h_{\text{TT}}}^*$ with η_{ϕ_i} in the flows. Therein ≈ 0 denotes values $< 10^{-6}$.

B Lists

B.1 List of Figures

2.1	Movement of a classical particle	12
2.2	Movement of a quantum particle	12
2.3	Paths away from the classical path: Amplitudes cancel each other out; from [61, p. 9]	12
2.4	Paths near the classical path: Amplitudes get added up; from [61, p. 9] .	12
2.5	Wick rotation	14
2.6	Electric field $\vec{E}(\vec{r})$ of an electron	17
2.7	Electric potential $V(r)$ of an electron with a gauge parameter a	17
2.8	Integration over one representation per gauge orbit	19
4.1	RG trajectories in the theory space $\{c_1, \dots, c_n\}$ with the starting point $\Gamma_{k=\Lambda} = S_{\text{bare}}$ and the endpoint $\Gamma_{k=0} = \Gamma$ for several regulators	39
4.2	Litim Regulator $R_{k,\text{Litim}}(q)$ and its scale derivative $\partial_t R_{k,\text{Litim}}(q)$	41
4.3	Exponential Regulator $R_{k,\text{exp}}(q)$ and its scale derivative $\partial_t R_{k,\text{exp}}(q)$	42
5.1	UV critical surface in a Theory Space with attractive and repulsive flows; from [94]	47
5.2	Phase diagram of the two dimensional theory space within the Einstein- Hilbert truncation. The arrows point along the RG flow, i.e. in the IR; from [88, p. 32]	51
6.1	Symmetric momentum configuration in the (p^0, p^1) plane	77
7.1	Number of terms for Einstein-Hilbert and higher order vertices at each order	81
7.2	The analytical Fermi-Dirac function with four different values for ϵ	92
7.3	Derivative of the analytical Fermi-Dirac function with four different values for ϵ	92
7.4	Numerical check of an analytically integrated flow diagram at $p^2 = 0$	92
7.5	Numerical check of an analytically integrated flow diagram after taking a 2 nd p -derivative at $p^2 = 0$	93
7.6	Sampling points, poles, excluded regions/points and trivial fixed points for the 1 st approximation	95
7.7	Sampling points, poles, included regions and trivial fixed points for the 2 nd approximation	97

8.1	Fully momentum dependent $\eta_{h_{\text{TT}}}$ for the first three iteration levels in the momentum range $p \in [0, k]$	105
8.2	Fully momentum dependent η_{h_s} for the first three iteration levels in the momentum range $p \in [0, k]$	106
8.3	1 st real solution doublet of $f = 0$ (blue and yellow graphs) and physical/technical bounds for the higher order couplings (dashed/dotted green and red lines) in the physically relevant range $ \eta_{h_{\text{TT}}} < 2$	109
8.4	2 nd real solution doublet of $f = 0$ and $g = 0$ (blue and yellow surfaces) and bounds for the higher order couplings (semitransparent green and red planes) in the physically relevant range $ \eta_{h_{\text{TT}}} < 2$ and $ \eta_{h_s} < 2$	110
8.5	Flow of the TT-projected graviton 2-point function on Einstein-Hilbert (blue curve) together with its horizontal asymptote (red dashed line) for high momenta and the flow divided by the TT-projected graviton 2-point function on Einstein-Hilbert (green curve). Both curves are rescaled.	112
8.6	1 st real solution doublet of $g = 0$ (blue and yellow graphs) and physical/technical bounds for the higher order couplings (dashed/dotted green and red lines) in the physically relevant range $ \eta_{h_{\text{TT}}} < 2$	113
8.7	Flow of the S-projected graviton 2-point function on Einstein-Hilbert (blue curve) together with its p^2 fitted asymptote (red dashed line) and the flow divided by the S-projected graviton 2-point function on Einstein-Hilbert (green curve) accompanied with its horizontal and non-zero asymptote (yellow dashed line). TT- and S-projected couplings are <i>not</i> identified.	115
8.8	Flow of the S-projected graviton 2-point function on Einstein-Hilbert (blue curve) together with its p^2 fitted asymptote (red dashed line) and the flow divided by the S-projected graviton 2-point function on Einstein-Hilbert (green curve) accompanied with its horizontal and non-zero asymptote (yellow dashed line). TT- and S-projected couplings are identified.	115
8.9	Real solutions of $h = 0$ (blue and yellow lines) and bounds for the higher order couplings (red and green dashed lines)	117
8.10	Flow of the G-projected graviton 3-point function on Einstein-Hilbert (blue curve) together with its p^2 fitted asymptote (red dashed line) and the flow divided by the G-projected graviton 3-point function on Einstein-Hilbert (green curve) approaching zero. TT- and S-projected couplings are <i>not</i> identified.	118
8.11	Behaviour of the graviton anomalous dimensions (blue and green green curve) at the EH $\rightarrow 0$ fixed point together their bound (red dashed horizontal line) and the range of c (black dashed vertical lines)	123
8.12	Momentum dependence of the TT-projected flow of the graviton 2-point function in approximation 1 in the range $p^2 \in [0, k^2]$ evaluated at different UV fixed points together with polynomial fits in p^2 where p^4 is the highest power (dashed curves)	125

8.13 Momentum dependence of the TT-projected flow of the graviton 2-point function in approximation 1 in the range $p^2 \in [0, k^2]$ evaluated at UV fixed point number 6 with different values for g_{R^2, h_{TT}^2} together with polynomial fits in p^2 where p^4 is the highest power (dashed curves) . . . 125

8.14 Momentum dependence of the S-projected flow of the graviton 2-point function in approximation 1 in the range $p^2 \in [0, k^2]$ evaluated at different UV fixed points together with polynomial fits in p^2 where p^4 is the highest power (dashed curves) 126

8.15 Momentum dependence of the G-projected flow of the graviton 3-point function in approximation 1 in the range $p^2 \in [0, k^2]$ evaluated at UV fixed point 2 (blue curve) together with polynomial fits in p^2 where p^4 (green dotted curve) or p^6 (red dashed curve) are the highest powers . . 127

8.16 Momentum dependence of the TT-projected flow of the graviton 2-point function in approximation 2 in the range $p^2 \in [0, k^2]$ evaluated at the UV fixed point (blue curve) together with polynomial fits in p^2 where p^4 (green dotted curve) or p^6 (red dashed curve) are the highest powers . . 131

8.17 Momentum dependence of the TT-projected flow of the graviton 2-point function in approximation 2 in the range $p^2 \in [0, k^2]$ evaluated at the UV fixed point with different values for g_{R^2, h_{ξ}^2} together with polynomial fits in p^2 where p^4 (blue and yellow dotted curves) and p^6 (red, green and purple dashed curves) are the highest powers 131

8.18 Momentum dependence of the S-projected flow of the graviton 2-point function in approximation 2 in the range $p^2 \in [0, k^2]$ evaluated at the UV fixed point (blue curve) together with polynomial fits in p^2 where p^4 (green dotted curve) or p^6 (red dashed curve) are the highest powers . . 132

8.19 Momentum dependence of the G-projected flow of the graviton 3-point function in approximation 2 in the range $p^2 \in [0, k^2]$ evaluated at the UV fixed point (blue curve) together with polynomial fits in p^2 where p^4 (green dotted curve) or p^6 (red dashed curve) are the highest powers . . 133

B.2 List of Tables

4.1 Three classes of theories concerning their renormalizability 32

4.2 Three classes of operators under RG transformations 33

5.1 Two types of fixed points (gaussian and non-gaussian) and their key properties 45

5.2 Three types of signs of $\text{Re}(b_k)$ 46

5.3 Three cases for the stability of a fixed point 47

6.1 Building blocks of flow diagrams 55

7.1 Comparison of the number of terms for different graviton vertex orders in the case of Einstein-Hilbert and higher order vertices 81

7.2	Overview of integrating procedures (analytically / numerically) for the three diagrams at all four momentum values	98
7.3	Total number and number of non-zero entries of \mathcal{T}_{TP} together with the maximal calculation time for one diagram in each approximation	98
8.1	UV fixed point analysis in Einstein-Hilbert truncation for analytical g_{R,h_{TT}^3} with and without η_{ϕ_i} in the flows	102
8.2	UV fixed point analysis in Einstein-Hilbert truncation for numerical g_{R,h_{TT}^3} with and without η_{ϕ_i} in the flows	103
8.3	UV fixed point analysis in split Einstein-Hilbert truncation for analytical g_{R,h_{TT}^3} without η_{ϕ_i} in the flows	104
8.4	Overview of the status of the investigated n -point functions w.r.t. momentum locality	119
8.5	UV fixed point analysis in approximation 1 for analytical g_{R,h_{TT}^3} without η_{ϕ_i} in the flows	121
8.6	UV fixed point analysis indicating non-trivial behaviour for Einstein-Hilbert couplings in approximation 1 for analytical g_{R,h_{TT}^3} with η_{ϕ_i} in the flows . .	122
8.7	UV fixed point analysis indicating non-trivial behaviour for Einstein-Hilbert couplings in approximation 2 for analytical g_{R,h_{TT}^3} with η_{ϕ_i} in the flows . .	129
A.1	UV fixed point analysis in approximation 1 for analytical g_{R,h_{TT}^3} with η_{ϕ_i} in the flows. Therein ≈ 0 denotes values $< 10^{-6}$	138

C Bibliography

- [1] Albert Einstein. Die Feldgleichungen der Gravitation. *Sitzungsberichte der Preußischen Akademie der Wissenschaften*, pages 844–847, 1915. URL: <http://echo.mpiwg-berlin.mpg.de/ECHOdocuView?url=/permanent/echo/einstein/sitzungsberichte/6E3MAXK4/index.meta&pn=1>.
- [2] Albert Einstein. Die Grundlage der allgemeinen Relativitätstheorie. *Annalen der Physik*, 354(7):769–822, 1916. DOI: [10.1002/andp.19163540702](https://doi.org/10.1002/andp.19163540702).
- [3] Albert Einstein. Über den Einfluß der Schwerkraft auf die Ausbreitung des Lichtes. *Annalen der Physik*, 340(10):898–908, 1911. DOI: [10.1002/andp.19113401005](https://doi.org/10.1002/andp.19113401005).
- [4] LIGO Scientific Collaboration and Virgo Collaboration, Benjamin P. Abbott *et al.* Observation of Gravitational Waves from a Binary Black Hole Merger. *Physical Review Letters*, 116(6), 2016. DOI: [10.1103/PhysRevLett.116.061102](https://doi.org/10.1103/PhysRevLett.116.061102).
- [5] Cian O’Luanaigh. New results indicate that new particle is a Higgs boson, 2013. URL: <https://home.cern/about/updates/2013/03/new-results-indicate-new-particle-higgs-boson>.
- [6] Gerardus ’t Hooft and Martinus J. Veltman. One-loop divergencies in the theory of gravitation. *Annales de l’I.H.P. Physique théorique*, 20(1):69–94, 1974. URL: http://www.numdam.org/item?id=AIHPA_1974__20_1_69_0.
- [7] Kenneth G. Wilson. Renormalization Group and Critical Phenomena. I. Renormalization Group and the Kadanoff Scaling Picture. *Physical Review B*, 4(9):3174–3183, 1971. DOI: [10.1103/PhysRevB.4.3174](https://doi.org/10.1103/PhysRevB.4.3174).
- [8] Steven Weinberg. Ultraviolet Divergences In Quantum Theories Of Gravitation. In Stephen William Hawking and Werner Israel, editors, *General Relativity: An Einstein centenary survey*, pages 790–831. Cambridge University Press, 1979. ISBN: 0521222850.
- [9] Christof Wetterich. Exact evolution equation for the effective potential. *Physics Letters B*, 301(1):90–94, 1993. DOI: [10.1016/0370-2693\(93\)90726-X](https://doi.org/10.1016/0370-2693(93)90726-X).
- [10] Martin Reuter. Nonperturbative evolution equation for quantum gravity. *Physical Review D*, 57(2):971–985, 1998. DOI: [10.1103/PhysRevD.57.971](https://doi.org/10.1103/PhysRevD.57.971).
- [11] Wataru Souma. Non-Trivial Ultraviolet Fixed Point in Quantum Gravity. *Progress of Theoretical Physics*, 102(1):181–195, 1999. DOI: [10.1143/PTP.102.181](https://doi.org/10.1143/PTP.102.181).

- [12] Max Niedermaier and Martin Reuter. The Asymptotic Safety Scenario in Quantum Gravity. *Living Reviews in Relativity*, 9(5), 2006. : DOI: [10.12942/lrr-2006-5](https://doi.org/10.12942/lrr-2006-5).
- [13] Max Niedermaier. The asymptotic safety scenario in quantum gravity: an introduction. *Classical and Quantum Gravity*, 24(18):R171, 2007. DOI: [10.1088/0264-9381/24/18/R01](https://doi.org/10.1088/0264-9381/24/18/R01).
- [14] Alessandro Codello, Roberto Peracci and Christoph Rahmede. Investigating the Ultraviolet Properties of Gravity with a Wilsonian Renormalization Group Equation. *Annals of Physics*, 324(2):414–469, 2009. DOI: [10.1016/j.aop.2008.08.008](https://doi.org/10.1016/j.aop.2008.08.008).
- [15] Ivan Donkin and Jan M. Pawłowski. The phase diagram of quantum gravity from diffeomorphism-invariant RG-flows. 2012. arXiv: [1203.4207](https://arxiv.org/abs/1203.4207).
- [16] Nicolai Christiansen, Benjamin Knorr, Jan M. Pawłowski and Andreas Rodigast. Global flows in quantum gravity. *Physical Review D*, 93(4):044036, 2016. DOI: [10.1103/PhysRevD.93.044036](https://doi.org/10.1103/PhysRevD.93.044036).
- [17] Nicolai Christiansen, Benjamin Knorr, Jan Meibohm, Jan M. Pawłowski and Manuel Reichert. Local quantum gravity. *Physical Review D*, 92(12):121501, 2015. DOI: [10.1103/PhysRevD.92.121501](https://doi.org/10.1103/PhysRevD.92.121501).
- [18] Tobias Denz, Jan M. Pawłowski and Manuel Reichert. Towards apparent convergence in asymptotically safe quantum gravity. *The European Physics Journal C*, 78:336, 2018. DOI: [10.1140/epjc/s10052-018-5806-0](https://doi.org/10.1140/epjc/s10052-018-5806-0).
- [19] Kellogg S. Stelle. Renormalization of higher derivative quantum gravity. *Physical Review D*, 16(4):953–969, 1977. DOI: [10.1103/PhysRevD.16.953](https://doi.org/10.1103/PhysRevD.16.953).
- [20] Nicolai Christiansen, Daniel F. Litm, Jan M. Pawłowski and Andreas Rodigast. Fixed points and infrared completion of quantum gravity. *Physics Letters B*, 728:114–117, 2014. DOI: [10.1016/j.physletb.2013.11.025](https://doi.org/10.1016/j.physletb.2013.11.025).
- [21] Paul A. M. Dirac. The Quantum Theory of the Emission and Absorption of Radioation. *Proceedings of the Royal Society of London, Series A*, 114(767):243–265, 1927. DOI: [10.1098/rspa.1927.0039](https://doi.org/10.1098/rspa.1927.0039).
- [22] Wolfgang E. Pauli and Pascal Jordan. Zur Quantenelektrodynamik ladungsfreier Felder. *Zeitschrift für Physik*, 47(3-4):151–173, 1928. DOI: [10.1007/BF02055793](https://doi.org/10.1007/BF02055793).
- [23] Paul A. M. Dirac. The Quantum Theory of the Electron. *Proceedings of the Royal Society of London, Series A*, 117(778):610–624, 1928. DOI: [10.1098/rspa.1928.0023](https://doi.org/10.1098/rspa.1928.0023).
- [24] Enrico Fermi. Versuch einer Theorie der β -Strahlen. *Zeitschrift für Physik*, 88(3-4):161–177, 1934. DOI: [10.1007/BF01351864](https://doi.org/10.1007/BF01351864).
- [25] Richard P. Feynman. Space-Time Approach to Non-Relativistic Quantum Mechanics. *Reviews of Modern Physics*, 20(2):367–387, 1948. DOI: [10.1103/RevModPhys.20.367](https://doi.org/10.1103/RevModPhys.20.367).

- [26] Richard P. Feynman. A Relativistic Cut-Off for Classical Electrodynamics. *Physical Review*, 74(8):939–946, 1948. DOI: [10.1103/PhysRev.74.939](https://doi.org/10.1103/PhysRev.74.939).
- [27] Richard P. Feynman. Relativistic Cut-Off for Quantum Electrodynamics. *Physical Review*, 74(10):1430–1438, 1948. DOI: [10.1103/PhysRev.74.1430](https://doi.org/10.1103/PhysRev.74.1430).
- [28] Julian Schwinger. On Quantum-Electrodynamics and the Magnetic Moment of the Electron. *Physical Review*, 73(4):416–417, 1949. DOI: [10.1103/PhysRev.73.416](https://doi.org/10.1103/PhysRev.73.416).
- [29] Julian Schwinger. Quantum Electrodynamics. I. A Covariant Formulation. *Physical Review*, 74(10):1439–1461, 1948. DOI: [10.1103/PhysRev.74.1439](https://doi.org/10.1103/PhysRev.74.1439).
- [30] Julian Schwinger. Quantum Electrodynamics. II. Vacuum Polarization and Self-Energy. *Physical Review*, 75(4):651–679, 1949. DOI: [10.1103/PhysRev.75.651](https://doi.org/10.1103/PhysRev.75.651).
- [31] Julian Schwinger. Quantum Electrodynamics. III. The Electromagnetic Properties of the Electron—Radiative Corrections to Scattering. *Physical Review*, 76(6):790–817, 1949. DOI: [10.1103/PhysRev.76.790](https://doi.org/10.1103/PhysRev.76.790).
- [32] Nobel Foundation. The Nobel Prize in Physics 1965, 1965. URL: https://www.nobelprize.org/nobel_prizes/physics/laureates/1965/index.html.
- [33] Shin'ichirō Tomonaga. On a Relativistically Invariant Formulation of the Quantum Theory of Wave Fields. *Progress of Theoretical Physics*, 1(2):27–42, 1946. DOI: [10.1143/PTP.1.27](https://doi.org/10.1143/PTP.1.27).
- [34] Zirô Koba, Takao Tati, and Shin'ichirō Tomonaga. On a Relativistically Invariant Formulation of the Quantum Theory of Wave Fields. II: Case of Interacting Electromagnetic and Electron Fields. *Progress of Theoretical Physics*, 2(3):101–116, 1947. DOI: [10.1143/ptp/2.3.101](https://doi.org/10.1143/ptp/2.3.101).
- [35] Zirô Koba, Takao Tati, and Shin'ichirō Tomonaga. On a Relativistically Invariant Formulation of the Quantum Theory of Wave Fields. III: Case of Interacting Electromagnetic and Electron Fields. *Progress of Theoretical Physics*, 2(4):198–208, 1947. DOI: [10.1143/ptp/2.4.198](https://doi.org/10.1143/ptp/2.4.198).
- [36] Sueto Kanesawa and Shin'ichirō Tomonaga. On a Relativistically Invariant Formulation of the Quantum Theory of Wave Fields. IV. *Progress of Theoretical Physics*, 3(1):1–13, 1948. DOI: [10.1143/ptp/3.1.1](https://doi.org/10.1143/ptp/3.1.1).
- [37] Sueto Kanesawa and Shin'ichirō Tomonaga. On a Relativistically Invariant Formulation of the Quantum Theory of Wave Fields. V. *Progress of Theoretical Physics*, 3(2):101–113, 1948. DOI: [10.1143/ptp/3.2.101](https://doi.org/10.1143/ptp/3.2.101).
- [38] Zirô Koba and Shin'ichirō Tomonaga. On Radiation Reactions in Collision Processes. I: Application of the “Self-Consistent” Subtraction Method to the Elastic Scattering of an Electron. *Progress of Theoretical Physics*, 3(3):290–303, 1948. DOI: [10.1143/ptp/3.3.290](https://doi.org/10.1143/ptp/3.3.290).

- [39] Shin'ichirō Tomonaga and Julius Robert Oppenheimer. On Infinite Field Reactions in Quantum Field Theory. *Physical Review*, 74(2):224–225, 1948. DOI: [10.1103/PhysRev.74.224](https://doi.org/10.1103/PhysRev.74.224).
- [40] Chen-Ning Yang and Robert Mills. Conservation of Isotopic Spin and Isotopic Gauge Invariance. *Physical Review*, 96(1):191–195, 1954. DOI: [10.1103/PhysRev.96.191](https://doi.org/10.1103/PhysRev.96.191).
- [41] Nobel Foundation. The Nobel Prize in Physics 2008, 2008. URL: https://www.nobelprize.org/nobel_prizes/physics/laureates/2008/index.html.
- [42] Yōichirō Nambu. Quasiparticles and Gauge Invariance in the Theory of Superconductivity. *Physical Review*, 117(3):648–663, 1960. DOI: [10.1103/PhysRev.117.648](https://doi.org/10.1103/PhysRev.117.648).
- [43] François Englert and Robert Brout. Broken Symmetry and the Mass of Gauge Vector Mesons. *Physical Review Letters*, 13(9):321–323, 1964. DOI: [PhysRevLett.13.321](https://doi.org/10.1103/PhysRevLett.13.321).
- [44] Peter Higgs. Broken Symmetries and the Masses of Gauge Bosons. *Physical Review Letters*, 13(16):508–509, 1964. DOI: [10.1103/PhysRevLett.13.508](https://doi.org/10.1103/PhysRevLett.13.508).
- [45] Nobel Foundation. The Nobel Prize in Physics 2013, 2013. URL: https://www.nobelprize.org/nobel_prizes/physics/laureates/2013/index.html.
- [46] Sheldon Lee Glashow. The renormalizability of vector meson interactions. *Nuclear Physics*, 10:107–117, 1959. DOI: [10.1016/0029-5582\(59\)90196-8](https://doi.org/10.1016/0029-5582(59)90196-8).
- [47] Abdus Salam and John Clive Ward. Weak and electromagnetic interactions. *Nuovo Cimento*, 11(4):568–577, 1959. DOI: [10.1007/BF02726525](https://doi.org/10.1007/BF02726525).
- [48] Nobel Foundation. The Nobel Prize in Physics 1979, 1979. URL: https://www.nobelprize.org/nobel_prizes/physics/laureates/1979/index.html.
- [49] Steven Weinberg. A Model of Leptons. *Physical Review Letters*, 19(21):1264–1266, 1967. DOI: [10.1103/PhysRevLett.19.1264](https://doi.org/10.1103/PhysRevLett.19.1264).
- [50] Nobel Foundation. The Nobel Prize in Physics 1969, 1969. URL: https://www.nobelprize.org/nobel_prizes/physics/laureates/1969/index.html.
- [51] Murray Gell-Mann. The Eightfold Way: A Theory of strong interaction symmetry. Technical report, California Institute of Technology, 1961. DOI: [10.2172/4008239](https://doi.org/10.2172/4008239).
- [52] Murray Gell-Mann. A schematic model of baryons and mesons. *Physical Letters*, 8(3):214–215, 1964. DOI: [10.1016/S0031-9163\(64\)92001-3](https://doi.org/10.1016/S0031-9163(64)92001-3).
- [53] David Jonathan Gross and Frank Wilczek. Ultraviolet Behavior of Non-Abelian Gauge Theories. *Physical Review Letters*, 30(26):1343–1346, 1973. DOI: [10.1103/PhysRevLett.30.1343](https://doi.org/10.1103/PhysRevLett.30.1343).

- [54] Nobel Foundation. The Nobel Prize in Physics 2004, 2004. URL: https://www.nobelprize.org/nobel_prizes/physics/laureates/2004/index.html.
- [55] Hugh David Politzer. Reliable Perturbative Results for Strong Interactions? *Physical Review Letters*, 30(26):1346–1349, 1973. DOI: [10.1103/PhysRevLett.30.1346](https://doi.org/10.1103/PhysRevLett.30.1346).
- [56] Steven Weinberg. *The Quantum Theory of Fields. Volume I. Foundations*. Cambridge University Press, 1995. ISBN: 0-521-55001-7.
- [57] Gerardus 't Hooft. Chapter 1: The Evolution of Quantum Field Theory: From QED to Grand Unification. *The Standard Theory of Particle Physics*, pages 1–27, 2016. DOI: [10.1142/9789814733519_0001](https://doi.org/10.1142/9789814733519_0001).
- [58] Michael E. Peskin and Daniel V. Schroeder. *An Introduction to Quantum Field Theory*. Westview Press, 1995. ISBN: 0-201-50397-2.
- [59] Taichiro Kugo. *Eichtheorie*. Springer-Verlag Berlin Heidelberg, 1997. ISBN: 978-3-540-62063-1.
- [60] Timo Weigand. Quantum Field Theory I + II, Lecture Notes, 2014. URL: <http://www.thphys.uni-heidelberg.de/weigand/QFT2-14/SkriptQFT2.pdf>.
- [61] Daniel D. Baumann. Concepts in Theoretical Physics, Lecture Notes, 2012. URL: <http://www.damtp.cam.ac.uk/user/db275/concepts/Lectures.pdf>.
- [62] Vladimir Naumovich Gribov. Quantization of non-Abelian gauge theories. *Nuclear Physics B*, 139(1-2):1–19, 1975. DOI: [10.1016/0550-3213\(78\)90175-X](https://doi.org/10.1016/0550-3213(78)90175-X).
- [63] Albert Einstein. Über das Relativitätsprinzip und die aus demselben gezogenen Folgerungen. *Jahrbuch der Radioaktivität und Elektronik*, 4:411–462, 1908. URL: https://www.itp.kit.edu/~slava/Einstein_Ueber_das_Relativitaetsprinzip.pdf.
- [64] Albert Einstein and Marcel Grossmann. Entwurf einer verallgemeinerten Relativitätstheorie und einer Theorie der Gravitation. *Zeitschrift für Mathematik und Physik*, 62:225–261, 1913.
- [65] Albert Einstein. Erklärung der Perihelbewegung des Merkur aus der allgemeinen Relativitätstheorie. *Sitzungsberichte der Preußischen Akademie der Wissenschaften*, pages 831–839, 1915. URL: http://articles.adsabs.harvard.edu/cgi-bin/get_file?pdfs/SPAW./1915/1915SPAW.....831E.pdf.
- [66] Leo Corry, Jürgen Renn and John Stachel. Belated Decision in the Hilbert-Einstein Priority Dispute. *Science*, 278(5341):1270–1273, 1997. DOI: [10.1126/science.278.5341.1270](https://doi.org/10.1126/science.278.5341.1270).
- [67] Friedwardt Winterberg. On "Belated Decision in the Hilbert-Einstein Priority Dispute", published by L. Corry, J. Renn, and J. Stachel. *Zeitschrift für Naturforschung*, 59(10):715–719, 2004. DOI: [10.1515/zna-2004-1016](https://doi.org/10.1515/zna-2004-1016).

- [68] Robert M. Wald. *General Relativity*. The University of Chicago Press, 1984. ISBN: 0-226-87033-2.
- [69] Torsten Fließbach. *Allgemeine Relativitätstheorie*. Springer Spektrum, 2016. ISBN: 978-3-662-53106-8, DOI: [10.1007/978-3-662-53106-8](https://doi.org/10.1007/978-3-662-53106-8).
- [70] Sean M. Carroll. Lecture Notes on General Relativity, 1997. URL: <https://arxiv.org/pdf/gr-qc/9712019.pdf>.
- [71] Edmund Bertschinger. Symmetry Transformations, the Einstein-Hilbert Action, and Gauge Invariance, Lecture Notes, 2002. URL: <https://dspace.mit.edu/bitstream/handle/1721.1/36859/8-962Spring2002/NR/rdonlyres/Physics/8-962Spring2002/6D03860E-9C15-4EB8-B96A-8B720D68EFE8/0/gr5.pdf>.
- [72] Matthias Bartelmann. General Relativity, Lecture Notes, 2014. URL: <http://www.ita.uni-heidelberg.de/research/bartelmann/files/relativity.pdf>.
- [73] Albert Einstein. Prinzipielles zur allgemeinen Relativitätstheorie. *Annalen der Physik*, 360(4):241–244, 1918. DOI: [10.1002/andp.19183600402](https://doi.org/10.1002/andp.19183600402).
- [74] Michael Esfeld (Ed.). *Philosophie der Physik*. Suhrkamp Taschenbuch Wissenschaft, 2012. ISBN: 978-3518296332.
- [75] David Lovelock. The Einstein Tensor and Its Generalizations. *Journal of Mathematical Physics*, 12(3):498–501, 1971. DOI: [10.1063/1.1665613](https://doi.org/10.1063/1.1665613).
- [76] Jan M. Pawłowski. Chapter 7.1: Wilson’s renormalisation group, Lecture Notes in Quantum Field Theory, 2017. URL: http://www.thphys.uni-heidelberg.de/pawlowski/qftII_17/script/QFTII-7-1-WilsonRenormalisationGroup.pdf.
- [77] Holger Gies. Introduction to the functional RG and applications to gauge theories, Lecture Notes, 2006. arXiv: [hep-ph/0611146](https://arxiv.org/abs/hep-ph/0611146).
- [78] Joshua Ellis. TikZ-Feynman: Feynman diagrams with TikZ, 2016. arXiv: [1601.0543](https://arxiv.org/abs/1601.0543).
- [79] Nobel Foundation. The Nobel Prize in Physics 1982, 1982. URL: https://www.nobelprize.org/nobel_prizes/physics/laureates/1982/index.html.
- [80] Kenneth G. Wilson. Renormalization Group and Critical Phenomena. II. Phase-Space Cell Analysis of Critical Behavior. *Physical Review B*, 4(9):3184–3205, 1971. DOI: [10.1103/PhysRevB.4.3184](https://doi.org/10.1103/PhysRevB.4.3184).
- [81] Kenneth G. Wilson and Michael E. Fisher. Critical Exponents in 3.99 Dimensions. *Physical Review Letters*, 28(4):240–243, 1972. DOI: [10.1103/PhysRevLett.28.240](https://doi.org/10.1103/PhysRevLett.28.240).
- [82] Kenneth G. Wilson. Critical phenomena in 3.99 dimensions. *Physica*, 73(1):119–128, 1974. DOI: [10.1016/0031-8914\(74\)90229-8](https://doi.org/10.1016/0031-8914(74)90229-8).

- [83] Kenneth G. Wilson. The renormalization group and the ϵ expansion. *Physics Reports*, 12(2):75–199, 1974. DOI: [10.1016/0370-1573\(74\)90023-4](https://doi.org/10.1016/0370-1573(74)90023-4).
- [84] Kenneth G. Wilson. The renormalization group: Critical phenomena and the Kondo problem. *Reviews of Modern Physics*, 47(4):773–840, 1975. DOI: [10.1103/RevModPhys.47.773](https://doi.org/10.1103/RevModPhys.47.773).
- [85] Kenneth G. Wilson. Renormalization group methods. *Advances in Mathematics*, 16(2):170–186, 1975. DOI: [10.1016/0001-8708\(75\)90149-8](https://doi.org/10.1016/0001-8708(75)90149-8).
- [86] Kenneth G. Wilson. The renormalization group and critical phenomena. *Reviews of Modern Physics*, 55(3):583–600, 1983. DOI: [10.1103/RevModPhys.55.583](https://doi.org/10.1103/RevModPhys.55.583).
- [87] Daniel F. Litim. Optimisation of the exact renormalisation group. *Physics Letters B*, 486(1):92–99, 2000. DOI: [10.1016/S0370-2693\(00\)00748-6](https://doi.org/10.1016/S0370-2693(00)00748-6).
- [88] Martin Reuter and Frank Saueressig. Renormalization group flow of quantum gravity in the Einstein-Hilbert truncation. *Physical Review D*, 65(6):065016, 2002. DOI: [10.1103/PhysRevD.65.065016](https://doi.org/10.1103/PhysRevD.65.065016).
- [89] Astrid Eichhorn. Status of the Asymptotic Safety Paradigm for Quantum Gravity and Matter. *Foundations of Physics*, 48(10):1407–1429, 2018. DOI: [10.1007/s10701-018-0196-6](https://doi.org/10.1007/s10701-018-0196-6).
- [90] Roberto Peracci. A short introduction to asymptotic safety, 2011. arXiv: [1110.6389](https://arxiv.org/abs/1110.6389).
- [91] Gerardus 't Hooft. Perturbative QUANTUM GRAVITY. In *From Quarks and Gluons to Quantum Gravity*, pages 249–269, 2003. DOI: [10.1142/9789812796653_0007](https://doi.org/10.1142/9789812796653_0007).
- [92] Ralph Blumenhagen, Dieter Lüst and Stefan Theisen. *Basic Concepts of String Theory*. Theoretical and Mathematical Physics. Springer-Verlag Berlin Heidelberg, 2012. ISBN: 978-3-642-29497-6.
- [93] Carlo Rovelli. Quantum Gravity, 2003. URL: <http://www.cpt.univ-mrs.fr/roveli/book.pdf>.
- [94] Andreas Nink. UV critical surface and flow trajectories, 2013. URL: <https://upload.wikimedia.org/wikipedia/commons/thumb/0/02/UVCriticalSurfaceInTheorySpace.png/760px-UVCriticalSurfaceInTheorySpace.png>.
- [95] Astrid Eichhorn and Aaron Held. Top mass from asymptotic safety. *Physics Letters B*, 777:217–221, 2018. DOI: [10.1016/j.physletb.2017.12.040](https://doi.org/10.1016/j.physletb.2017.12.040).
- [96] Mikhail Shaposhnikov and Christof Wetterich. Asymptotic safety of gravity and the Higgs boson mass. *Physics Letters B*, 683(2-3):196–200, 2010. DOI: [10.1016/j.physletb.2009.12.022](https://doi.org/10.1016/j.physletb.2009.12.022).

- [97] Daniel F. Litim and Jan M. Pawłowski. On general axial gauges for QCD. *Nuclear Physics B - Proceedings Supplements*, 74(1-3):329–332, 1999. DOI: [10.1016/S0920-5632\(99\)00188-7](https://doi.org/10.1016/S0920-5632(99)00188-7).
- [98] Elisa Manrique and Martin Reuter. Bimetric truncations for quantum Einstein gravity and asymptotic safety. *Annals of Physics*, 325(4):785–815, 2010. DOI: [10.1016/j.aop.2009.11.009](https://doi.org/10.1016/j.aop.2009.11.009).
- [99] Elisa Manrique, Stefan Rechenberger and Frank Saueressig. Asymptotically Safe Lorentzian Gravity. *Physical Review Letters*, 106(25):251–302, 2011. DOI: [10.1103/PhysRevLett.106.251302](https://doi.org/10.1103/PhysRevLett.106.251302).
- [100] Alessandro Codello and Roberto Peracci. Fixed Points of Higher-Derivative Gravity. *Physical Review Letters*, 97(22):221301, 2006. DOI: [10.1103/PhysRevLett.97.221301](https://doi.org/10.1103/PhysRevLett.97.221301).
- [101] Max Niedermaier. Gravitational Fixed Points from Perturbation Theory. *Physical Review Letters*, 103(10):101303, 2009. DOI: [10.1103/PhysRevLett.103.101303](https://doi.org/10.1103/PhysRevLett.103.101303).
- [102] Dario Benedetti, Pedro F. Machado and Frank Saueressig. Asymptotic safety in higher-derivative gravity. *Modern Physics Letters A*, 24(28):2233–2241, 2009. DOI: [10.1142/S0217732309031521](https://doi.org/10.1142/S0217732309031521).
- [103] Astrid Eichhorn, Peter Labus, Jan M. Pawłowski and Manuel Reichert. Effective universality in quantum gravity, 2018. arXiv: [1804.00012v2](https://arxiv.org/abs/1804.00012v2).
- [104] Nicolai Christiansen. Four-Derivative Quantum Gravity Beyond Perturbation Theory, 2016. arXiv: [1612.06223](https://arxiv.org/abs/1612.06223).
- [105] James W. York Jr. Conformally invariant orthogonal decomposition of symmetric tensors on Riemannian manifolds and the initial value problem of general relativity. *Journal of Mathematical Physics*, 14(4):456–464, 1973. DOI: [10.1063/1.1666338](https://doi.org/10.1063/1.1666338).
- [106] Nicolai Christiansen, Daniel F. Litim, Jan M. Pawłowski and Manuel Reichert. Asymptotic safety of gravity with matter. *Physical Review D*, 97(10):106012, 2018. DOI: [10.1103/PhysRevD.97.106012](https://doi.org/10.1103/PhysRevD.97.106012).
- [107] Wolfram Research Inc. Mathematica 11.2, 2017. URL: <http://www.wolfram.com/mathematica/>.
- [108] Tobias Denz, Aaron Held, Jan M. Pawłowski and Andreas Rodigast. *TARDIS*.
- [109] Andreas Rodigast. *VertEXpand*.
- [110] Jos A. M. Vermaseren. New features of *FORM*, 2000. arXiv: [math-ph/0010025](https://arxiv.org/abs/math-ph/0010025).
- [111] Jan Kuipers, Takahiro Ueda, Jos A. M. Vermaseren and Jens Vollinga. *FORM* version 4.0. *Computer Physics Communications*, 184(5):1453–1467, 2013. DOI: [10.1016/j.cpc.2012.12.028](https://doi.org/10.1016/j.cpc.2012.12.028).

-
- [112] Jose M. Martin-Garcia. *xPerm*: fast index canonicalization for tensor computer algebra. *Computer Physics Communications*, 179(8):597–603, 2008. DOI: [10.1016/j.cpc.2008.05.009](https://doi.org/10.1016/j.cpc.2008.05.009).
- [113] David Brizuela, Jose M. Martin-Garcia and Guillermo A. Mena Marugan. *xPert*: computer algebra for metric perturbation theory. *General Relativity and Gravitation*, 41:2415, 2009. DOI: [10.1007/s10714-009-0773-2](https://doi.org/10.1007/s10714-009-0773-2).
- [114] Markus Q. Huber and Jens Braun. Algorithmic derivation of functional renormalization group equations and Dyson–Schwinger equations. *Computer Physics Communications*, 183(6):1290–1320, 2012. DOI: [10.1016/j.cpc.2012.01.014](https://doi.org/10.1016/j.cpc.2012.01.014).
- [115] Anton K. Cyrol, Mario Mitter and Nils Strodthoff. Formtracer - A Mathematica Tracing Package Using FORM. *Computer Physics Communications*, 219:346–352, 2017. DOI: [10.1016/j.cpc.2017.05.024](https://doi.org/10.1016/j.cpc.2017.05.024).
- [116] Shahryar Ghaed Sharaf. Higher derivative operators in quantum gravity. Master's thesis, Heidelberg University, 2018.
- [117] Tim R. Morris. The exact renormalization group and approximate solutions. *International Journal of Modern Physics A*, 9(14):2411–2449, 1994. DOI: [10.1142/S0217751X94000972](https://doi.org/10.1142/S0217751X94000972).

Acknowledgments

First of all I want to thank Prof. Jan Pawłowski for giving me the opportunity to be a part of his Quantum Gravity group and to work on asymptotically safe quantum gravity. I learned a lot during this master thesis year. Secondly I would like to thank Prof. Tilman Plehn for immediately accepting the 2nd correction of this master thesis.

A special thanks goes to Manuel for several long and patient discussions concerning physical and also technical questions and simply for being around and helping out whenever needed. Another special thanks to Tobias for sharing his knowledge about *TARDIS* and *FormTracer* and explaining several technically very deep details. Moreover I want to thank my colleague and very good friend Shahryar Ghaed Sharaf for the great teamwork during the whole year. I believe that this was essential for passing the technical problems. Moreover I would like to thank him for proofreading my thesis and of course for fantastic Fortnite nights. Next I would like to thank Kim for tolerating the sometimes heated discussions between me and Shah and providing a nice and pleasant working atmosphere.

Most importantly I thank the love of my life, Bella. For all her love, patience, understanding and never ending support from the first day we met. In my personal point of view I'm nothing without you and your Penne al Arrabiata. The same thanks goes to my family, especially my brother, my dad and my mum, for always being there and letting me pursue my way. Every step I make is a step for the family. Last but not least I want to thank my aunt Dr. Angela Vogel for her constant and unconditional financial support. Without her my studies would not have been possible.

Erklärung:

Ich versichere, dass ich diese Arbeit selbstständig verfasst habe und keine anderen als die angegebenen Quellen und Hilfsmittel benutzt habe.

Heidelberg, den 25.10.2018

.....